Implementation and Application of Light Induced Orthogonal Ligation Protocols in Polymer Chemistry

Zur Erlangung des akademischen Grades eines
DOKTORS DER NATURWISSENSCHAFTEN
(Dr. rer. nat.)

von der KIT-Fakultät für Chemie und Biowissenschaften
des Karlsruher Instituts für Technologie (KIT)

genehmigte
DISSERTATION
von

Dipl.-Chem. Kai Uwe Hiltebrandt

aus
Heilbronn, Deutschland

Dekan: Prof. Dr. Willem Klopper
Referent: Prof. Dr. Christopher Barner-Kowollik
Korreferent: Prof. Dr. Manfred Wilhelm
Tag der mündlichen Prüfung: 21.10.2016

Die vorliegende Arbeit wurde von Oktober 2013 bis September 2016 unter Anleitung von Prof. Dr. Christopher Barner-Kowollik am Karlsruher Institut für Technologie (KIT) – Universitätsbereich angefertigt.

Erklärung

Ich erkläre hiermit, dass ich die vorliegende Arbeit im Rahmen der Betreuung durch Prof. Dr. Christopher Barner-Kowollik selbstständig verfasst und keine anderen als die angegebenen Quellen und Hilfsmittel verwendet habe. Wörtlich oder inhaltlich übernommene Stellen sind als solche kenntlich gemacht und die Satzung des Karlsruher Instituts für Technologie (KIT) zur Sicherung guter wissenschaftlicher Praxis wurde beachtet.
Desweiteren erkläre ich, dass ich mich derzeit in keinem weiteren laufenden Promotionsverfahren befinde und auch keine vorausgegangenen Promotionsversuche unternommen habe.

Karlsruhe, den 31.08.2016

_____

Kai Hiltebrandt

Most people say that it is the intellect which makes a great scientist. They are wrong: it is character.

-Albert Einstein-

By all means, marry! If you get a good wife, you'll be happy. If you get a bad wife, you'll become a philosopher.

-Socrates-

Tell me what you can hear
And then tell me what you see
Everybody has a different way
To view the world
I would like you to know
When you see the simple things
To appreciate this life
It's not to late to learn

-Iron Maiden: "Different World" (A Matter of Life and Death, 2006)-

PUBLICATIONS ARISING FROM THIS THESIS

[1a] **λ-Orthogonal Pericyclic Macromolecular Photoligation**

K. Hiltebrandt, T. Pauloehrl, J. P. Blinco, K. Linkert, H. G. Börner, C. Barner-Kowollik, *Angew. Chem. Int. Ed.* **2015**, 54, 2838-2843.

[1b] **λ-Orthogonale Photochemie: Lichtinduzierte pericyclische Reaktionen an Makromolekülen**

K. Hiltebrandt, T. Pauloehrl, J. P. Blinco, K. Linkert, H. G. Börner, C. Barner-Kowollik, *Angew. Chem. Int. Ed.* **2015**, 127, 2880-2885.

[2] **Wavelength Selective Polymer Network Formation of End-Functional Star Polymers**

M. Kaupp, K. Hiltebrandt, V. Trouillet, P. Mueller, A. S. Quick, M. Wegener, C. Barner-Kowollik, *Chem. Comm.* **2016**, 52, 1975-1978.

[3] **A Light Activated Reaction Manifold**

K. Hiltebrandt, K. Elies, D. R. D'hooge, J. P. Blinco, C. Barner-Kowollik, *J. Am. Chem. Soc.* **2016**, 138, 7048-7054.

[4] **Star Polymer Synthesis via λ-Orthogonal Photochemistry**

K. Hiltebrandt, M. Kaupp, E. Molle, J. P. Menzel, J. P. Blinco, C. Barner-Kowollik, *Chem. Comm.* **2016**, 52, 9426-9429.

ADDITIONAL PUBLICATIONS

[1] **UV-Triggered Endgroup Conversion of Photo-Initiated Poly(Methyl Methacrylate)**

D. Voll, D. Neshchadin, K. Hiltebrandt, G. Gescheidt, C. Barner-Kowollik, *Macromolecules* **2012**, 45, 5850–5858.

[2] **Global trends for k_p? Expanding the Frontier of Ester Side Chain Topography in Acrylates and Methacrylates**

A. Haehnel, M. Schneider-Baumann, K. U. Hiltebrandt, A. M. Misske, C. Barner-Kowollik, *Macromolecules* **2013**, 46, 15–28.

[3] **Polymer-Fullerene Network Formation via Light-induced Crosslinking**

Y. Sugawara, K. Hiltebrandt, E. Blasco, C. Barner-Kowollik, *Macromol. Rapid Commun.* **2016**, 37, 1466–1471.

ABSTRACT

The design and the synthesis of novel polymer systems play a dominant role in the domain of advanced soft matter materials. In this context, photochemical reactions offer an ecologically friendly, economical and often straightforward reaction path that can be readily applied by a diverse set of disciplines. A system containing a photoactive compound that can undergo an exclusive photoreaction in the presence of another (photoactive) species, which remains unreacted, and vice versa offers wavelength dependent control over a one-pot reaction. Furthermore, such wavelength dependent light induced systems extend significantly our abilities for intramolecular end group transformations as well as intermolecular ligations in an orthogonal fashion, in addition to offering the inherent advantages of a photochemical system.

The present thesis introduces the concept of orthogonal pericyclic light induced ligation protocols, which are explored in three different projects demonstrating the generation as well as the modification of complex polymer architectures.

The first project addresses a light activated reaction manifold exploiting two reaction paths of *o*-methyl benzaldehyde to introduce – for the first time – chemical selectivity in a photonic field: The photoreaction of the light induced *o*-methyl benzaldehyde species (photoenol) with electron-poor enes and a non-irradiative transformation of the *o*-methyl benzaldehyde into an imine with hexylamine. The manifold shows a solvent dependent behaviour of the photoreaction kinetics, which can be exploited in variable applications. In non-polar solvents, the photoreaction kinetics exceed only slightly the imine formation kinetics.

In this case, the manifold shows a concentration dependent behaviour, whereby an efficient selectivity for the photoreaction under irradiation conditions can be established, while the imine formation virtually ceases. This behaviour is based on the fact that the equilibrium between *o*-methyl benzaldehyde and its photo-induced state can be influenced to obtain pathway selectivity. As polar solvents lead to a strong

acceleration of the photoreaction, orthogonal block copolymer formations are performed either via a photochemical ligation or via an imine ligation in the dark. In the second project, a ***λ***-orthogonal reaction principle featuring the wavelength dependent activation of *o*-methyl benzaldehyde and tetrazole is evidenced via the end group modifications of polymers. The employed tetrazole absorbs light in the range between 200-340 nm, whereas *o*-methyl benzaldehyde absorbs light up to 360 nm. Thus, maleimides are attached initially to *o*-methyl benzaldehyde at $\lambda > 340$ nm and subsequently to tetrazole with more energetic UV light in a one-pot system. Hereby, it is demonstrated that *o*-methyl benzaldehyde is able to undergo an exclusive photochemical reaction in the presence of the tetrazole with light of an appropriate wavelength. Furthermore, various enes carrying different functionalities such as an acid group and a fluorescent dye are added selectively to an oligomeric bilinker with an *o*-methyl benzaldehyde and a tetrazole end group. ***λ***-Orthogonal triblock copolymers are synthesised by adding maleimide terminated macromolecules such as polylactides and peptides to the central oligomer bilinker building block. Subsequently, the previously presented ***λ***-orthogonal principle able to operate in one direction is extended by the reverse reaction path leading to a complete orthogonal light induced ligation. Hereby, the reversible photochemical deactivation of the *o*-methyl benzaldehyde species with hexylamine yielding an imine allows the initial tetrazole activation enabling the second orthogonal reaction path. Both photoreaction paths are employed as a synthetic tool for the formation of star polymers in an orthogonal fashion. In this context, either the *o*-methyl benzaldehyde or the tetrazol end group of the oligomer bilinker are attached selectively to a trifunctional maleimide centre, followed by the subsequent ligation of a maleimide terminated polymer to the remaining photoactive compound of the bilinker.

The third project addresses the selective network formation using the ***λ***-orthogonal principle in one direction. Herein, four arm shaped star polymers carrying either *o*-methyl benzaldehyde or tetrazole end groups as well as a trifunctional maleimide are cross-linked selectively by irradiating the solution with a specific light source. Furthermore, the design and the generation of novel ***λ***-orthogonal photoresists for Direct Laser writing are explored.

ZUSAMMENFASSUNG

Die Entwicklung und die Synthese neuartiger polymerer Systeme spielen eine beherrschende Rolle im Bereich angewandter weicher Materialien. In diesem Zusammenhang ermöglichen photochemische Reaktionen einen umweltfreundlichen, wirtschaftlichen und oftmals unkomplizierten Reaktionspfad, der von vielfältigen Fachrichtungen einfach zu handhaben ist. Ein System, das eine photoaktive Verbindung enthält, die eine alleinige Photoreaktion in Gegenwart einer anderen (photoaktiven) Substanz durchläuft, welche zwischenzeitlich nicht reagiert und umgekehrt, eröffnet eine wellenlängenabhängige Kontrolle über die Eintopfreaktion. Desweiteren erweitern derartige wellenlängenabhängige lichtinduzierte Systeme enorm die Möglichkeiten zu intramolekularen Endgruppenumwandlungen, als auch zu intermolekularen Verknüpfungen auf orthogonale Weise, während zusätzlich die Vorteile photochemischer Systeme genutzt werden können.

Die vorliegende Arbeit stellt ein Konzept zu lichtinduzierten, pericyclischen, chemischen Verknüpfungen vor, die in drei Projekten untersucht werden und den Aufbau als auch die Modifizierung von komplexen polymeren Architekturen aufzeigen.

Das erste Projekt behandelt einen durch Licht aktivierbaren Reaktionskanal, welcher zwei verschiedene Reaktionspfade eröffnet und zum ersten Mal chemische Selektivität in einem photonischen Feld einführt: Die Photoreaktion eines photoinduzierten *o*-Methylbenzaldehyds (Photoenol) mit elektronenarmen Alkenen und eine bestrahlungsfreie Umwandlung des *o*-Methylbenzaldehyds mittels Hexylamin in ein Imin. Der Zweiwegereaktionskanal zeigt für die Reaktionsgeschwindigkeit der Photoreaktion ein lösungsmittelabhängiges Verhalten auf, was unterschiedliche Anwendungen ermöglicht. In unpolaren Lösungsmitteln übersteigt die Photoreaktionsrate nur leicht die Iminbildungsrate.

Auf diese Weise zeigt der Zweiwegekanal ein konzentrationsabhängiges Verhalten, wobei eine effiziente Selektivität der Photoreaktion unter Bestrahlung erreicht

werden kann, während die Iminbildung nahezu unterbleibt. Dieses Verhalten basiert darauf, dass das Gleichgewicht zwischen dem *o*-Methylbenzaldehyd und seinem lichtinduzierten Zustand beeinflusst wird, wodurch eine hohe Selektivität der Reaktionspfade erreicht werden kann.

Da polare Lösungsmittel zu einer enormen Beschleunigung der Photoreaktion führen, werden orthogonale Blockcopolymerbildungen entweder durch eine photochemische Verknüpfung oder durch eine Iminbildung im Dunkeln durchgeführt.

Im zweiten Projekt wird ein ***λ***-orthogonales Reaktionsprinzip, welches durch die wellenlängenabhängige Aktivierung eines *o*-Methylbenzaldehyds und eines Tetrazols gekennzeichnet ist, anhand von Endgruppenmodifizierungen an Polymeren implementiert. Ein spezifisches Tetrazol absorbiert Licht im Bereich zwischen 200-340 nm wobei *o*-Methylbenzaldehyd Licht bis zu 360 nm absorbiert. Daher werden Maleimide zunächst an *o*-Methylbenzaldehyd bei $\lambda > 340$ nm und anschließend an ein Tetrazol durch höherenergetisches UV Licht in einem Eintopfsystem gebunden. Auf diese Weise wird demonstriert, dass *o*-Methylbenzaldehyd durch Licht einer passenden Wellenlänge in Gegenwart von Tetrazol ausschließliche eine photochemische Reaktion eingehen kann. Desweiteren werden vielfältige Alkene, die verschiedene Funktionalitäten wie eine Säuregruppe und einen fluoreszierenden Farbstoff enthalten, selektiv an einen oligomeren Bilinker, der eine *o*-Methylbenzaldehyd- und eine Tetrazolendgruppe trägt, eingebaut. ***λ***-Orthogonale Triblockcopolymere werden durch den Einbau von maleimidterminalen Makromolekülen wie Polylactiden und Peptiden an den oligomeren Bilinkerbaustein synthetisiert. Anschließend wird das zuvor beschriebene ***λ***-orthogonale Reaktionsprinzip durch den umgekehrten Reaktionspfad erweitert, was zu einer komplett orthogonalen, lichtinduzierten Verknüpfung führt. Auf diese Weise erlaubt die reversible photochemische Deaktivierung der *o*-Methylbenzaldehydspezies mit Hexylamin – über eine Iminbildung – die anfängliche Tetrazolaktivierung, wodurch der zweite orthogonale Reaktionspfad ermöglicht wird. Beide Photoreaktionspfade werden als synthetisches Werkzeug verwendet um Sternpolymere auf orthogonale Weise herzustellen. In diesem Zusammenhang wird entweder die *o*-Methylbenzaldehyd- oder die Tetrazolendgruppe des oligomeren Bilinkermoleküls selektiv an ein trifunktionales Maleimidzentrum gebunden, gefolgt von dem anschließenden Einbau eines maleimidterminalen Polymers an die verbleibende photoaktive Bilinkergruppe.

Das dritte Projekt beschäftigt sich mit der selektiven Netzwerkbildung unter Anwendung des $\boldsymbol{\lambda}$-orthogonalen Prinzips. Hierbei werden Vierarmsternpolymere, die entweder *o*-Methylbenzaldehyd- oder Tetrazolendgruppen tragen als auch ein trifunktionales Maleimid durch die Bestrahlung mit einer spezifischen Lichtquelle selektiv quervernetzt. Außerdem wird die Konzeption und Entwicklung neuartiger $\boldsymbol{\lambda}$-orthogonaler Photolacke für Direktes Laserschreiben beschrieben.

TABLE OF CONTENTS

1

1. Introduction and Motivation

Materials showing advanced and highly sophisticated properties have always been the key driving force for human development. Therefore, superior materials are still increasingly important in science and industrial applications in order to address future challenges that are relevant to society and the public. Polymers with tailored material properties and specific architectures meet sophisticated requirements in various areas whereby examples of consideration are provided in the following. For example, blends of biodegradable polymers are nowadays utilised in packagings,[1] detergents and cosmetics,[2] as well as medical applications.[3],[4] Another key field for superior polymer systems are self-healing materials[5] which feature predetermined response mechanisms.[6] In addition, polymers are, e.g. implemented as matrix displays in organic electronics[7] and as semiconductors in voltaic cells.[8] Electronically conducting polymers can even be used in areas such as energy storage.[9],[10] The large field of nanotechnology is also critically influenced by polymers.[11] Semiconducting nanoparticles used as photoacoustic agents for *in vivo* photoacoustic molecular imaging,[12] and nanocomposites as flexible high-temperature dielectric materials[13],[14] are a versatile example for polymers applied in nanotechnology. Further, advanced classes of polymers such as supramolecular polymers are frequently discussed in the scientific community.[15]

The development of such highly sophisticated polymeric materials will drive their application and handling. In any case, easy and straightforward synthesis routes towards complex soft matter materials as well as their molecular transformations play a predominant role. The modification of soft matter materials into materials with sophisticated properties relies on the insertion of specific structures or functionalities. Post-modification reactions are often difficult and require subsequent purification steps. In this context, the implementation of a synthetic reaction protocol enabling the orthogonal modification of materials in a one-pot system would be a breakthrough in material science. Such a system should contain at least two compounds, whereby each compound is able to undergo an exclusive ligation in the presence of the other compound via a distinct trigger such as light of a certain wavelength. In this regard, photochemical reactions offer an ecologically friendly, mild, economic, and straightforward protocol that can be easily applied by scientists from many fields.[16] Furthermore, photoinduced approaches offer spatial and temporal control over both covalent bond forming and molecular cleavage reaction.[17] Nevertheless, most photoactive compounds have a broad absorption range preventing the exclusive activation of one photoactive compound in the presence of another photoactive species. Therefore, the present thesis aims to implement a λ-orthogonal system which is defined by progressing independently of other light triggered processes via the selection of chemical functionalities that can be activated within specific light wavelength regimes[18] (refer to Figure 1).

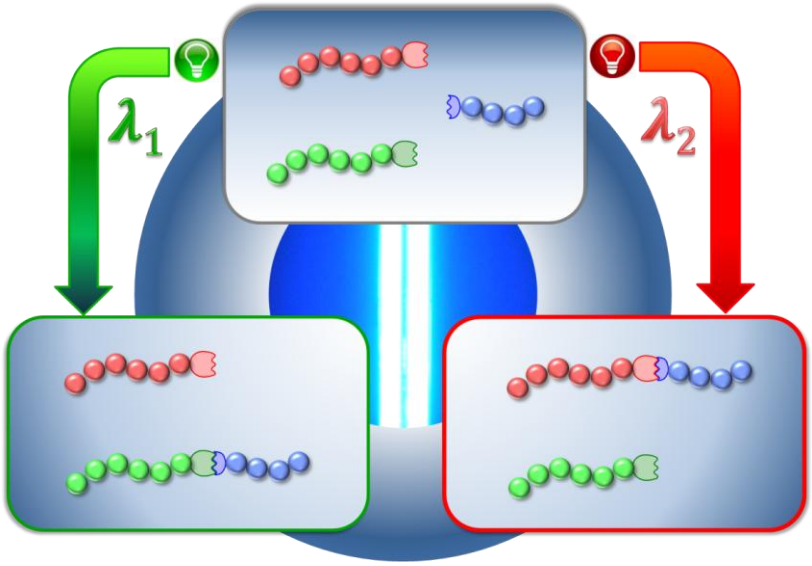

Figure 1: *Overview of an ideal λ-orthogonal system. The one-pot system offers two independent reaction paths. Each orthogonal reaction path is activated by light of a specific wavelength.*

The herein introduced ***λ***-orthogonal photoligation protocol combines the concepts of modular ligation chemistry (*click* chemistry) and photochemistry, making it an interesting application for orthogonal post-polymerisation modifications. An ideal ***λ***-orthogonal system enables the wavelength selective incorporation of a specific chemical functionality with a distinct physical property into a polymer. For instance, a polymer could be modified by either hydrophobic groups at low energetic UV light (high wavelengths) making the polymer insoluble in water or by hydrophilic groups at high energetic UV light (low wavelengths) yielding a water soluble structure.

Moreover, the ***λ***-orthogonal principle can be employed for the wavelength selective design of complex polymer architectures. Thus, the present thesis introduces the synthesis of one-dimensional, two-dimensional and three-dimensional polymer architectures in a ***λ***-orthogonal fashion. An outline of all investigations addressed in this thesis is depicted in Scheme 1.

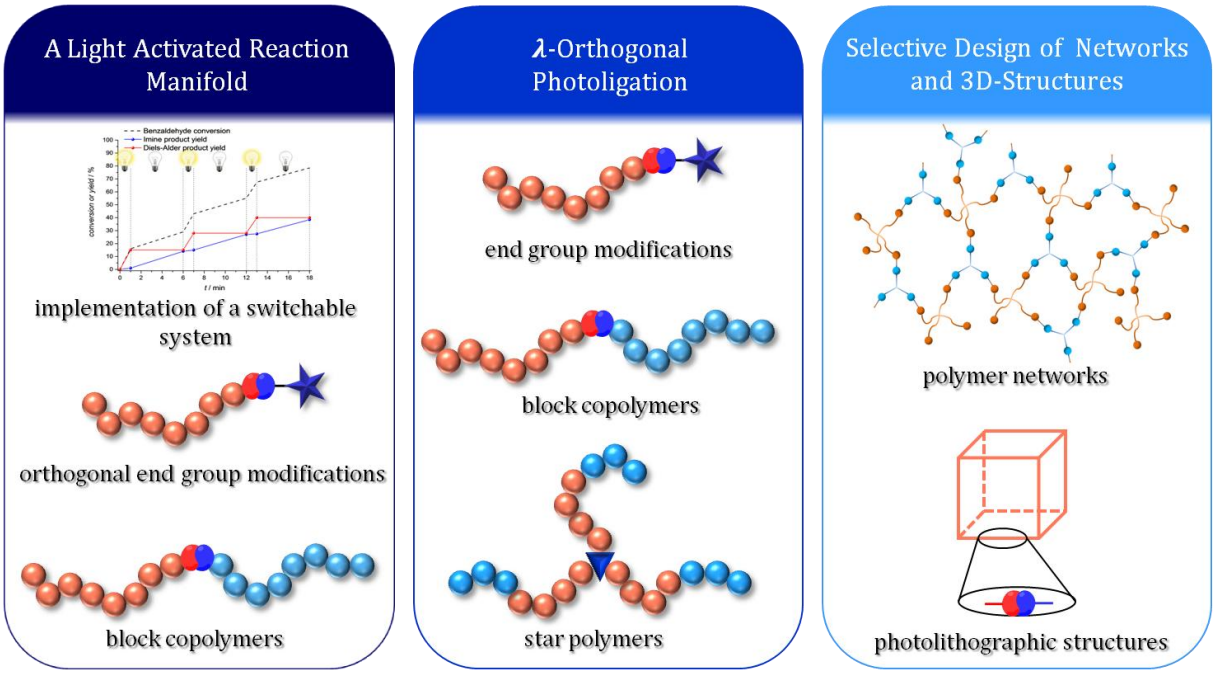

Scheme 1: *Overview of all projects in the present dissertation.*

Hereby, different systems consisting of *o*-methyl benzaldehyde, diphenyl tetrazole, and electron-poor enes such as maleimides were selectively activated in the wavelength range of 310-350 nm leading to the exclusive conjugation between the light induced photoenol species of *o*-methyl benzaldehyde and the ene. The diphenyl tetrazole functionality is able to undergo a subsequent ligation reaction by activating the system in the wavelength range of 270-310 nm. The various polymer structures were

constructed by either irradiation procedures with commercially available light sources such as lamps and LEDs in a custom-built photoreactor or by a two-photon absorption via direct laser writing (DLW).

Furthermore, the orthogonal modification of soft matter materials can also be realised by a reaction manifold based on two orthogonal reaction paths of one compound. In this context, each reaction channel is initiated by a certain trigger enabling orthogonality. Therefore, a novel highly effective switchable reaction manifold was implemented on the basis of the *o*-methyl benzaldehyde species whereby an orthogonal reaction path is activated by either irradiation or non-irradiation of the system.

2

2. Theoretical Background

The present chapter provides an overview of all theoretical topics and aspects that are relevant for this dissertation. Hereby the main focus lies on polymer chemistry including advanced synthetic procedures and state-of-the-art mechanisms, the concept of modular ligation chemistry as well as photochemistry. The content of the present chapter is designed to provide the reader with all necessary information that form the basis of the scientific output in the present thesis. Thus, the reader is able to follow the subsequent scientific discussion. The main topics (polymer chemistry, modular ligation chemistry, photochemistry including photoenol and tetrazole chemistry, DLW, and mass spectrometry) are outlined whereas important subitems relying on inherent aspects in this dissertation are presented in detail.

.

2.1. Polymer Chemistry

The term "polymer" was first introduced by Berzelius in 1833 but the actual meaning was associated with isomerism and had nothing to do with large molecules.[19] The present meaning of polymer describes a (large) molecule that consists of repeating units of the same nature called monomers. The term "polymer" derives from the Greek words "poly" meaning many and "méros" meaning part.[20] In 1920, the German chemist Staudinger first proposed that all kind of polymers are long chains of short molecular repeating units linked by covalent bonds,[21] although the majority of the scientific community questioned the existence of polymers. Nowadays, it is commonly accepted that the number of the repeating units in a polymer can reach 10^5 and even more. The term "macromolecule" was initially mentioned as well by Staudinger in 1922[22] and describes all molecules with high molar masses whereby the necessity of equal repeating units is not essential. Polymers can be either artificially synthesised or naturally occurring in plants and animals.[23] The most important natural polymers are carbohydrates such as starch, polypeptides such as proteins, and polynucleotids such as deoxyribonucleic acid (DNA). All of these biopolymers enable life on earth and are omnipresent in every living system.[24] Synthetic polymers are of critical importance for the functionality of our modern world, underpinned by the fact that mankind is currently using 260 million tons of polymers per year.[25] Hereby, these polymers are mostly mixed with a wide range of other materials such as plasticizers, flame retardants, fillers, blowing agents, pigments, stabilizers or other polymers in order to improve the processability as well as the physical and mechanical material properties.[26],[27],[28],[29] The emerging material is commonly named "plastic".[30] Due to their low price, low weight and manifold features, plastics can be found in nearly all areas of everyday applications and modern technology, often replacing other materials such as metals, wood, glass and ceramics.

The physical properties of a polymer are determined by the degree of polymerisation, the polydispersity, the constitution, the configuration, and the topology of the sample. The degree of polymerisation DP_n is defined as the number n of monomeric repeating units M_0 in a polymer.

$$DP_n = \frac{M_n}{M_0}$$

The polydispersity $Đ$ determines the molar mass distribution of a polymeric sample and is therefore a benchmark for the heterogeneity of the size of the molecules.[31] The polydispersity is defined as the ratio between the weight average mass M_w and the number average molecular weight M_n.

The constitution is defined as the chemical structure of the individual polymer chain.[32] Polymers consisting of only a single type of monomers are termed homopolymers. Polymers containing two or more different monomer units are called copolymers. The configuration describes the spatial arrangement of substituents and therefore leads to the effect of stereo isomerism in the polymer backbone.[33] A particular stereo isomerism is known as tacticity. Polymers have either an isotactic, a syndiotactic or an atactic configuration.[34] In an isotactic arrangement, all the substituents are located on one side of the polymer chain. In syndiotactic polymers, the asymmetric side groups alternate in their position along the backbone. In atactic polymers, the substituents are randomly arranged (refer to Scheme 2).

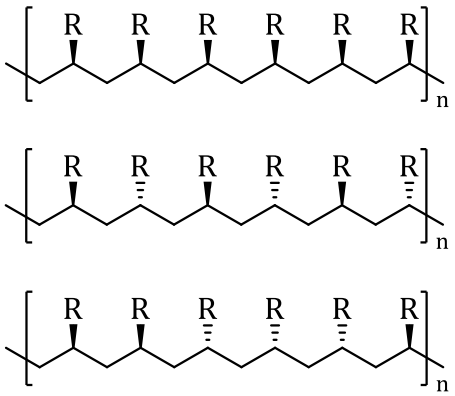

Polymer with isotactic configuration

Polymer with syndiotactic configuration

Polymer with atactic configuration

Scheme 2: *The side groups in isotactic polymers are arranged on the same side of the polymer chain, the substituents in syndiotactic polymers alternate along the backbone and the side groups in atactic polymers are located randomly along the polymeric chain.*

The topology is also known as the overall polymer architecture whereby polymers can be divided into linear polymers, networks, star polymers among other structures.[35]

The polymerisation process can be classified as either step-growth polymerisation or chain-growth polymerisation. In this regard, step-growth polymerisations require functionalised monomers which undergo a stepwise conjugation reaction resulting in the initial formation of oligomers. Hence, the polymerisation rate is relatively slow and polymers with high molecular weights are only obtained with high yields.[36] Polyaddition and polycondensation reactions are typical examples for step-growth polymerisations.[37] In contrast, chain-growth polymerisations require unsaturated

monomers bearing a double bond as well as an initiator which is able to generate a highly reactive centre. The monomers are perpetually linked towards the reactive centre resulting in a growing chain whereby the reactive centre is shifted to the chain end after each propagation step until termination events stop the propagation. Therefore, the polymerisation rate is relatively high in contrast to the step-growth polymerisation. For instance, chain-growth polymerisation methods are subdivided into free radical polymerisation, anionic polymerisation, cationic polymerisation, and coordination polymerisation.[38]

Moreover, polymers are classified into three main groups: thermoplastic polymers, thermosetting polymers, and elastomeric polymers. Thermoplastic polymers consist of linear, non-branched chains which are coiled in one another.[39] The mentioned entanglement affects the physical behaviour.[40] The polymer chains show mutual interactions leading to either disordered amorphous or compact and ordered crystalline regions. Polymers with predominant crystalline regions are more stable and brittle, whereas amorphous polymers show elastic behaviour.[41] The simultaneous presence of amorphous and crystalline regions also determines the thermal properties in such a way that thermoplastics show a glass transition temperature T_G among a melting point T_m. Glass transition describes a temperature range causing the transition of amorphous and semi-crystalline materials from a hard and brittle state into a molten rubber-like state.[42],[43] In most cases, thermoplastic polymers find only applications below the glass transition range due to the significant change of physical properties. The second group of polymers is represented by thermosetting polymers. Thermosets are three-dimensional polymer networks, in which the individual polymer chains are close-meshed cross-linked. This class of polymers is rigid, brittle, and shows mechanical and thermal stability.[44] Thermosets do not have a melting point or a glass transition range and decompose at high temperature exposure due to the chemical linkage between the polymer chains.[45] The third group of polymers are elastomers. Elastomers can be classified into thermoset elastomers consisting of long chains that are widely cross-linked and thermoplastic elastomers which are block copolymers.[46] Elastomers show a flexible, viscoelastic behaviour and are therefore also known as rubber. The rubber-like property of thermoset elastomers derives from the reconfiguration and recovery ability of the polymer chains after applied stress.[47] Thermoplastic elastomers are always two-phase systems consisting of a block copolymer with hard and soft segments that

undergo a phase separation. Hereby thermoplastic elastomers are physically cross-linked in contrast to the chemical linkage of thermoset elastomers[48]

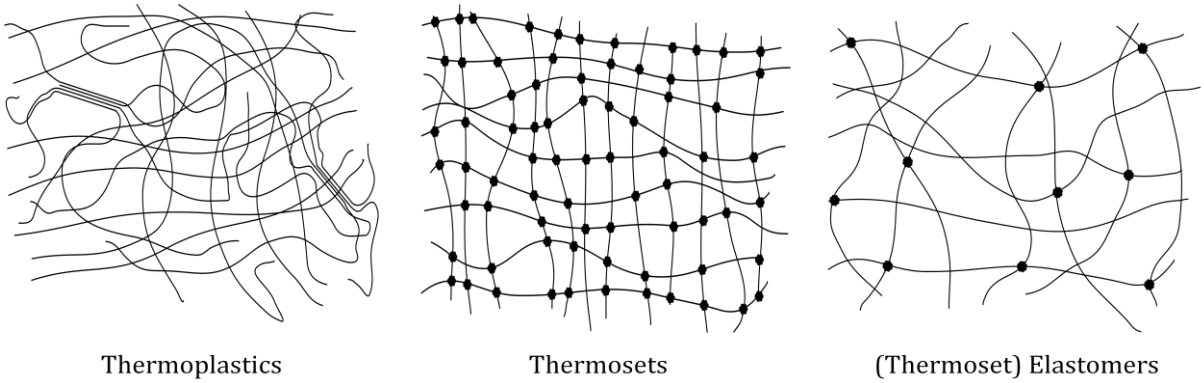

Figure 2: *A thermoplastic polymer consists of entangled chains forming either amorphous or crystalline areas (left-hand side). A thermosetting polymer is a three-dimensional network with a high cross-linking rate (middle). An elastomer is widely cross-linked allowing viscoelasticity (right-hand side).*

2.2. Free Radical Polymerisation

Free radical polymerisation (FRP) represents one of the most employed polymerisation techniques in science and in industrial applications.[49],[50] Generally, FRP has a high industrial significance due to the fact that this polymerisation method features mild reaction conditions, tolerates various chemical functionalities, and thus can be utilised for a large range of monomers.[51] Nevertheless, FRP faces some significant drawbacks in its practical application due to its inherent mechanism.[52] Polymers obtained via FRP show several limitations such as the hard to control end group functionality and the lack of control over the dispersity of the molecular weight. The four basic reaction steps[53] of FRP are summarised below:

I) Initiation

II) Propagation

II) Termination

IV) Chain Transfer

The initiation step is characterised, e.g., by the homolytic fission of an initiator into two radicals. The radical formation via dissociation can be triggered by irradiation in the presence of a photoinitiator,[54] a temperature increase in the presence of a thermally decaying species,[55],[56] or redox reactions.[57] Furthermore the first step also includes the addition of the initiator radical I· to a monomer molecule M.[58] The rate coefficient k_{diss} of the dissociation varies between 10^{-5} and 10^{-1} s^{-1}, depending on the employed initiator.

$$\text{I-I} \xrightarrow{k_{diss}} 2\ \text{I}\bullet$$

$$\text{I}\bullet + \text{M} \xrightarrow{k_{I}} \text{I-M}\bullet$$

Scheme 3: *The initiation step consisting of the initiator dissociation and the primary propagation step.*

The propagation process consists of the subsequent addition of monomer units to the radical. In this context, the growing polymer chain always entails a radical end group functionality.[59],[60] The propagation is chemically controlled meaning that the rate coefficient k_p is highly depending on the monomer because its reactivity is influenced by

the character of the chemical functionality next to the double bond. Typical values of k_p are in the range between 10^2 and $5 \cdot 10^4$ L·mol·s^{-1} at 60°C, with an activation energy of approximately 20-40 kJ·mol^{-1}.[61],[62],[63]

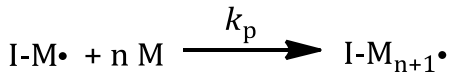

Scheme 4: *The propagation step leads to the consecutive addition of monomer units to the radical species formed in the initiation step.*

The subsequent termination reaction step leads to the limitation of the polymer growth. The statistically occurring bimolecular termination process results in the reaction of two radical functionalities[64] and is the main reason for the broad chain length distributions detected in polymerisations.

The termination reaction can be classified in either disproportionation or recombination. Recombination occurs if two radical end groups meet each other and form a saturated molecule via a single bond.[65] Hereby, diffusion is the rate determining step because both macromolecular radicals are relatively large. In this regard, an increase in the monomer to polymer conversion increases both the chain length and the viscosity of the polymerisation mixture resulting in the deceleration of the termination reaction.[66] Disproportionation describes the second possible termination mechanism. Herewith a hydrogen atom is abstracted from one polymer chain radical to another polymer radical leading to the formation of an unsaturated double bond at the end of the first polymer chain. The disproportionation product carrying a terminal double bond functionality is sometimes reported to function as macromonomer for further polymerisation procedures.[67] The rate coefficient k_t of the termination varies between 10^6 and 10^8 L·mol·s^{-1}, with a negligible activation energy.[68],[69]

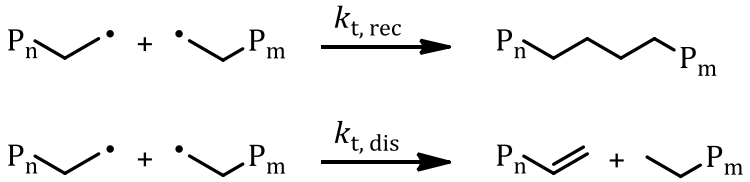

Scheme 5: *The statistically occurring termination step includes recombination and disproportionation leading to the stop of the polymer propagation.*

Chain transfer is a possible side reaction that can occur during polymerisation[70] and leads to a limitation of the maximum molecular weight that may be maximally obtained. The growing macromolecular radical, which is chain extended during the propagation

step, is able to transfer the active centre – the radical functionality – to a transfer agent. In this context, the transfer agent abstracts a hydrogen atom that is added subsequently to the polymer radical. As a result, the former polymer radical $P_n\cdot$ is transformed into the inactive saturated polymer P_n and the transfer agent HX is turned into the radical species X· due to the hydrogen abstraction.[71],[72] Chain transfer does not alter the radical concentration in contrast to the termination process, which leads to a decrease of radicals in the system. As such, the obtained radical X· is able to reinitiate a polymerisation cascade. Chain transfer can be induced by different molecules, such as solvents,[70] monomers,[73] polymer chains generated during the polymerisation[74] or deliberately added compounds (e.g. thioles).[75],[76] Chain transfer towards the polymer backbone, either intra- or intermolecularly, represents a very important mechanism for the formation of branched polymers.[77]

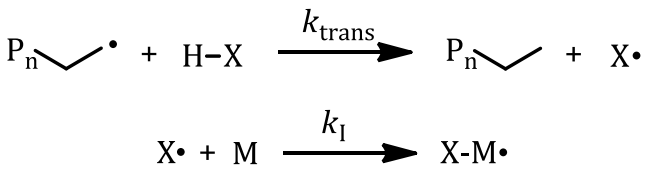

Scheme 6: *The chain transfer step is described by the hydrogen shift of a transfer agent to a polymer radical resulting in the formation of a saturated polymer chain and a radical species which is able to initiate a new propagation step.*

2.3. Reversible Deactivation Polymerisation

As mentioned above, free radical polymerisation shows certain significant drawbacks such as the broad molar mass distribution, the lack of control over the molecular weight, and the chemically often poor end group functionality devoid of synthetic handles. The predominant reason for the described disadvantages is due to the termination step which statistically stops the propagation step in the polymerisation process.[78]

In this case, the reversible deactivation polymerisation is a versatile possibility in order to overcome the drawbacks of conventional FRP. The basic characteristic of the reversible deactivation polymerisation is the limitation of any chain transfer or termination reactions.[79],[80] A formerly used term for reversible deactivation polymerisation was living or controlled polymerisation.[81],[82] Key features of this polymerisation technique are a fast and thorough initiation process, a linear evolution of the molecular weight regarding monomer to polymer conversion, a narrow molar mass distribution (i.e. $M_w/M_n \leq 1.2$), and a high end group fidelity.[83],[84],[85] In consequence, the suppression of the termination events during polymerisation results in the control over the FRP process.

In general, reversible deactivation polymerisations can be divided according to their underpinning mechanistic processes. The initial and first developed mechanism is characterised by a reduction of the radical concentration during the polymerisation process.[79],[85],[86] Consequently, the polymerisation rate of the propagation step decelerates linearly with a decrease of the radical species.[87] The termination step is described as a quadratic function of the radical concentration, evidencing that the termination step is very strongly regulated by the radical concentration. Main approaches of this mechanism are the nitroxide mediated polymerisation (NMP)[88] and the atom transfer radical polymerisation (ATRP)[78],[89].

An alternative mechanism utilises the reversible activation and deactivation of propagating radical species during polymerisation in order to decrease the amount of terminated chains.[85],[90]. Hereby, the radical concentration maintains constant which involves a non-reduced polymerisation rate comparable to conventional FRP. A main representative of this mechanism is the reversible addition-fragmentation chain transfer polymerisation (RAFT). In the following, ATRP and RAFT will be described in more detail.

2.3.1. Atom Transfer Radical Polymerisation

Atom transfer radical polymerisation (ATRP) was first reported by Matyjaszewski and Sawamoto in 1995.[78],[89] The basic feature of the ATRP process can be described by an equilibrium switching between an active and a dormant state of the polymeric chain end.

The initial homolytic cleavage of the alkyl halide initiator R-X by the transition metal complex $M^{[n]}$-Lig leads to the formation of the corresponding complex X-$M^{[n+1]}$-Lig and the radical R·.[91] During the initiation, the metal atom in the metal complex $M^{[n]}$-Lig is oxidized. The obtained radical R· is able to initiate the polymerisation.[92],[93] However, the propagating polymer radical can also undergo a termination reaction or is reversibly deactivated by the coordination complex X-$M^{[n+1]}$-Lig. The ATRP principle relies on the fact that the oxidized transition metal complex acquires the character of a persistent radical (refer to Scheme 7).

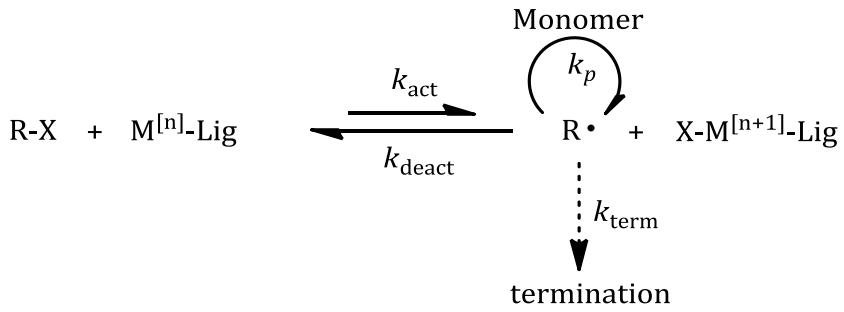

Scheme 7: *General mechanism of ATRP.*

The possible termination of the radical species is reduced due to the metal complex which works as a deactivator. The deactivation of the propagating radical chain shifts the equilibrium in such a way that the dormant species R-X becomes dominant, provided that the deactivation rate coefficient k_{deact} is much larger than the activation rate coefficient k_{act}. The equilibrium constant $K_{ATRP} = k_{act}/k_{deact}$ is in the range between 10^{-11} and 10^{-6} in order to obtain control over the molar mass and the polydispersity. In addition, K_{ATRP} is highly dependent on reaction conditions such as the ligand structure, the solvent, temperature, and pressure.[94],[95]

Moreover, ATRP can be mediated by various transition metals such as iridium[96] and iron[97] whereby copper species are most commonly used. As already mentioned before, ligands do not only improve the solubility of the metal ion, but also have an important

effect on the catalyzing properties of the active ATRP complex.[95] In general, nitrogen containing ligands are used for copper mediated ATRP reactions (refer to Figure 3).[98]

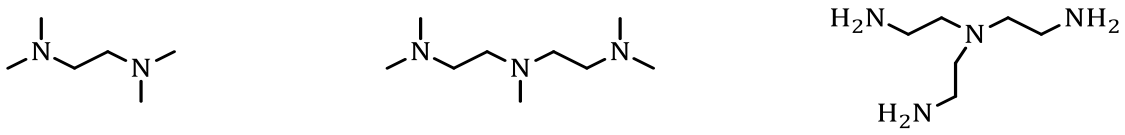

Figure 3: *Typical ligands for copper mediated ATRP; TMEDA: N,N,N',N'-tetramethylethane-1,2-diamine; PMDETA: N,N,N',N',N''-pentamethyldiethylenetriamine; TREN: tris(2-aminoethyl)amine.*

The ATRP process can be initiated by a large variety of alkyl halides.[99] The basic structure of these compounds essentially contains a halogen end group, which is activated by α-carbonyl, phenyl, vinyl or also cyano functionalities (refer to Figure 4) and promotes the cleavage of a halogen radical.

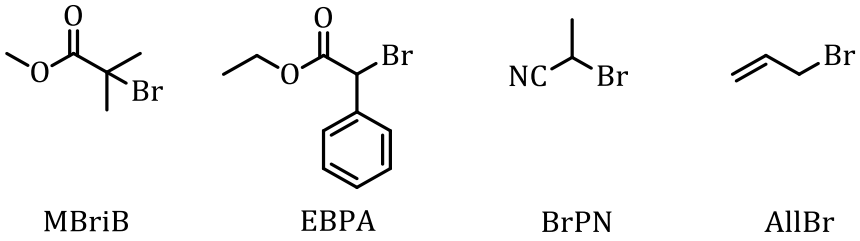

Figure 4: *Classes of possible ATRP initiators; MBriB: methyl α-bromoisobutyrate; EBPA: ethyl α-bromophenylacetate; BrBN: 2-bromopropionitrile; AllBr: allyl bromide.*

ATRP has several advantages such as soft reaction conditions, a well defined end group functionality in terms of the halide moiety at the polymer chain, and a wide range of functional initiators. The halide end groups of the obtained polymers offer a versatile and broad range of various post-polymerisation modifications on the basis of nucleophilic substitution reactions.[100],[101] An important post-modification step is the exchange of an azide moiety with the bromine end group of the polymer. However, ATRP is very sensitive to oxygen and the utilised copper has a toxic potential which requires a post-polymerisation purification of the polymer.[102] Additionally, the number of the employed monomers is strongly limited on structures without nitrogen due to a possible interaction of nitrogen containing species with the ATRP active metal complex.

2.3.2. Activator Generated by Electron Transfer ATRP

The activator generated by electron transfer (AGET) atom transfer polymerisation (ATRP) was first introduced by Matyjaszweski in 2005.[103] The fundamental characteristic of AGET ATRP can be delineated by an *in situ* activation/initiation process leading to an oxidatively stable catalyst complex in combination with an atom transfer polymerisation.[104],[105]

AGET ATRP starts with alkyl halides as initiator and transition metal complexes in their oxidatively stable state. In most cases a system consisting of copper(II) bromide and typical ATRP ligands is chosen but systems with other transition metals are also well known.[103] The crucial step in the AGET ATRP mechanism is that a non-radical forming reducing agent undergoes a reaction with the stable copper(II) complex and therefore rapidly generates the activated copper(I) complex. The copper(I) species is now able to initiate an atom transfer polymerisation (refer to Scheme 8).

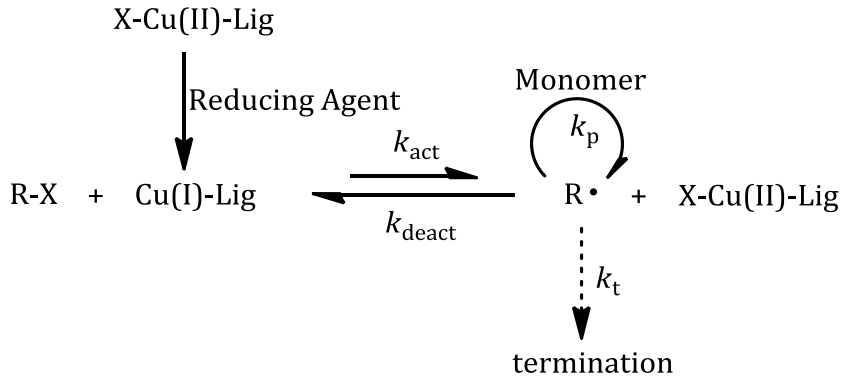

Scheme 8: *General mechanism of AGET ATRP.*

Possible reducing agents are tin(II) 2-ethylhexanoate,[104] ascorbic acid,[106] methylaluminoxane (MAO),[107] triethylamine,[108] copper[109] or even nitrogen containing monomers[110] (refer to Figure 5).

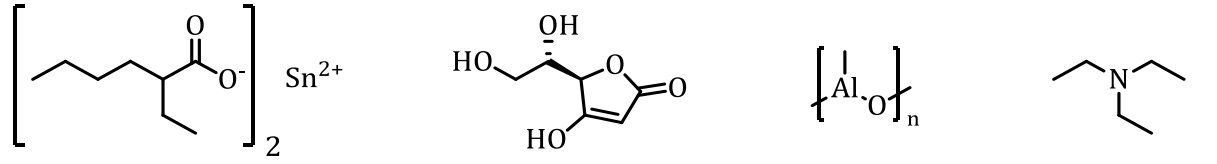

Tin(II) 2-ethylhexanoate | Ascorbic acid | MAO | Triethylamine

Figure 5: *Classes of possible AGET ATRP reducing agents; tin(II) 2-ethylhexanoate; ascorbic acid; MAO: methylaluminoxane; triethylamine.*

AGET ATRP provides similar benefits as basic ATRP. Furthermore, this procedure generates a more oxidatively stable catalyst complex in the polymerisation mixture because the reducing agent removes remaining oxygen. Therefore AGET ATRP is an efficient tool for the synthesis and attachment of polymer on surfaces in the presence of air.[111],[112] Moreover, AGET ATRP can also be carried out successfully in miniemulsion reactions[113],[114] and for the synthesis of polymers in a homogeneous aqueous environment.[115]

2.3.3. Activators Regenerated by Electron Transfer ATRP

The major drawback of classic ATRP procedures is the use of high amounts of copper containing catalysts.[78] Copper and copper containing compounds show a severe cyctotoxic behaviour.[116],[117] The biological applications of polymers generated by ATRP are still limited though there are several purification methods for its removal.[118],[119],[120] In this case, the activators regenerated by electron transfer (ARGET) atom transfer polymerisation method is a controlled polymerisation technique that overcomes this drawback by utilising a new initiation process compared to ATRP. The mechanism of ARGET ATRP is based on the continuous regeneration of the active copper(I) species out of the copper (II) deactivator (refer to Scheme 9).[121]

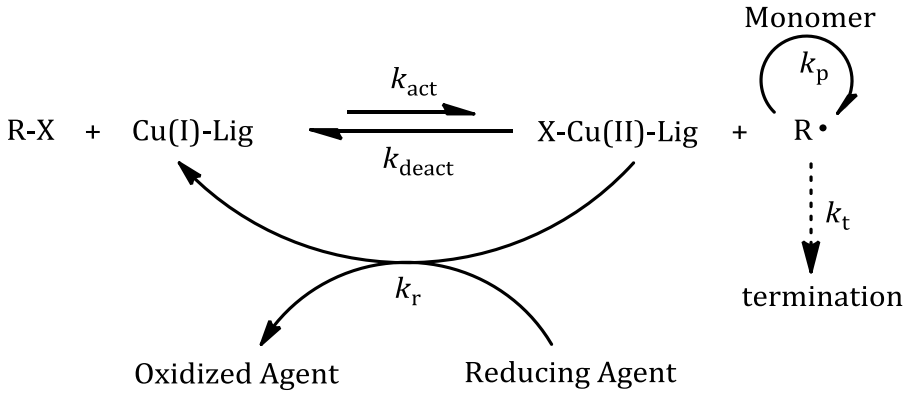

Scheme 9: *General mechanism of ARGET ATRP.*

In contrast to AGET ATRP, ARGET ATRP relies on a slow and steady regeneration of copper(I) species.[122] The amount of copper catalyst can be reduced to a significantly lower concentration of 10 ppm or even less. The value of the equilibrium coefficients k_{act}

and k_{deact}, as well as the reduction rate coefficient k_r are crucial for a controlled ARGET ATRP.[123] Typical ligands in this process are PMDETA or TPMA (refer to Figure 6).

PMDETA TPMA

Figure 6: *Typical ligands for ARGET ATRP; PMDETA: N,N,N',N'',N''-pentamethyldiethylenetriamine; TPMA: tris(2-pyridylmethyl)amine.*

Possible reducing agents are tin(II) 2-ethylhexanoate, ascorbic acid,[122] glucose, hydrazine and copper (refer to Figure 7).

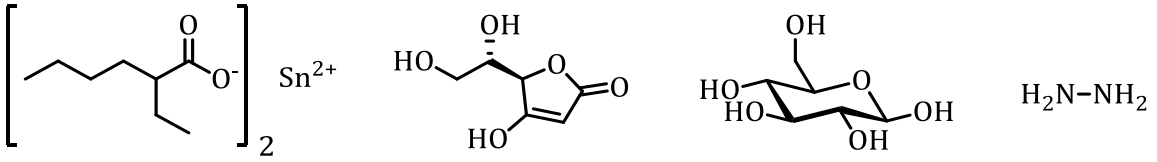

Tin(II) 2-ethylhexanoate Ascorbic acid Glucose Hydrazine

Figure 7: *Classes of possible ARGET ATRP reducing agents: tin(II) 2-ethylhexanoate, ascorbic acid, glucose, hydrazine.*

2.3.4. Reversible Addition-Fragmentation Chain Transfer Polymerisation

The reversible addition-fragmentation chain transfer (RAFT) process was developed by a group of the Commonwealth Scientific and Industrial Research Organization (CSIRO) in 1998.[124] At the same time, a French scientists reported independently of the Australian researchers about a procedure which based on the same mechanism and named it macromolecular design by interchange of xanthates (MADIX).[125],[126] The basic principle of the RAFT process is premised on degenerative chain transfers[127] which are embedded in an array of addition-fragmentation equilibria in the presence of a RAFT agent. The momentarily accepted mechanism of the RAFT process with dithiobenzoate as RAFT agent is depicted in Scheme 10.[126],[128]

Initiation

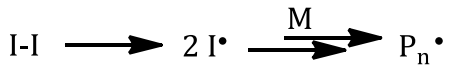

Reversible chain transfer/propagation

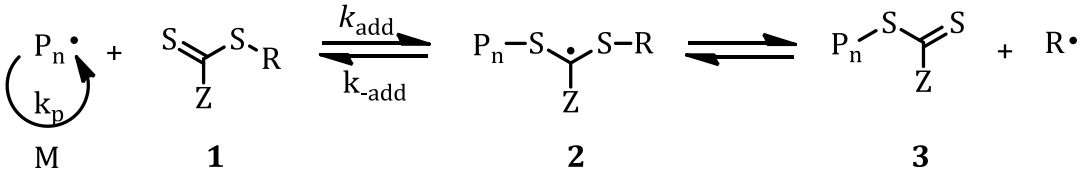

Reinitiation

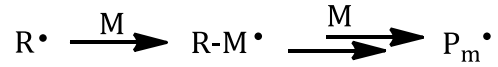

Reversible chain transfer/propagation

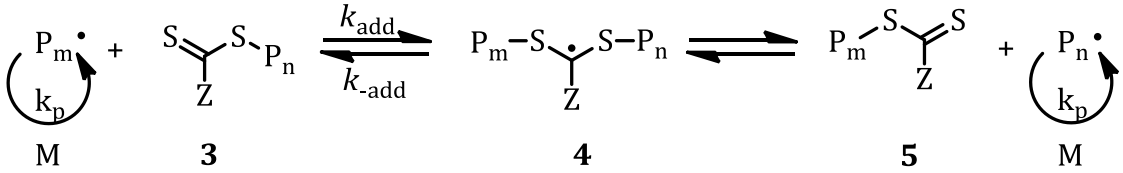

Termination

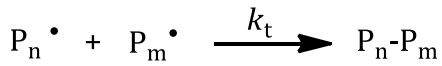

Scheme 10: *The basic mechanism of the RAFT process.*

Initially, the initiation and the propagation steps are started by conventional initiators under free radical polymerisation conditions. At the beginning of the process, the growing radical chain P_n· attaches reversibly to the dithiocarbonyl compound **1** working as the RAFT agent in the system. Afterwards, the intermediate radical **2** decomposes into the macromolecular dithiocarbonyl compound **3** and the radical species R· deriving from the RAFT agent. The radical R· is now able to reinitiate the polymerisation. The growing polymer chains P_n· and P_m· as well as the dormant molecule **3** are in a rapid equilibrium leading to an equal propagation probability for all chains and results in a narrow molar mass distribution.[129],[130],[131] Therefore, the radical concentration maintains constant throughout the entire polymerisation. As a result no inherent retardation of the polymerisation rate is expected according to theory.[132]

The essential parts of a RAFT agent are represented by the R group and the Z group. The R group is supposed to stabilize a radical in such a way that the formation of

compound **3** is favoured over compound **2**. The Z group affects the stability of the C=S bond as well as the intermediate radicals **2** and **4**.[133] Therefore, the RAFT agent needs to be individually adapted to the monomer and the polymerisation system. Dithioesters, dithiobenzoates, trithiocarbonates, xanthates or dithiocarbamates have demonstrated to be appropriate substances for the RAFT process[134] and are depicted in Figure 8.

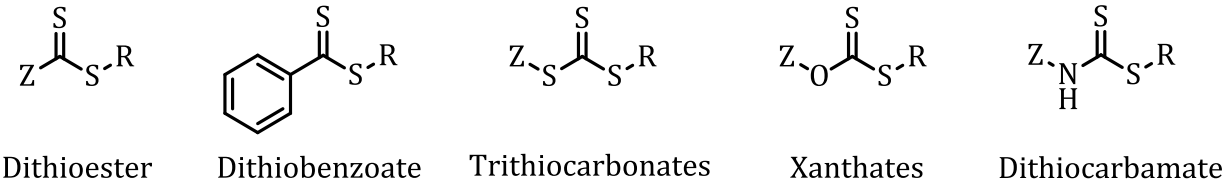

Figure 8: *Possible RAFT agents.*

The basic chemical structure of a RAFT agent contains a C=S functionality which can be activated by radicals which guarantees a high addition rate coefficient k_{add}. RAFT agents are able to mediate the polymerisation due to the afore mentioned reversible chain transfer process. In addition, the intermediate radicals **2** and **4** (refer to Scheme 10) have to fragment rapidly whereas the expelled radical R· undergoes subsequently a new polymerisation cycle.

The chain equilibrium between the dormant and the active species is established after the consumption of the RAFT agent. In theory, the propagating rate, which relies on the number of the propagating species, is supposed to be independent from the presence of the RAFT agent. Nevertheless, experiments have shown the existence of the rate retardation for some RAFT agents when the RAFT agent concentration is ceased.[135] In this regard, it became obvious that the main reason for the retardation derives from the decrease of the propagating radical concentration[136] leading to the formation of two opposing theories that try to explain the kinetic mechanism. In this context, the slow fragmentation (SL) theory states the significant stability of **4** resulting in a slow fragmentation procedure.[137] This theory is able to explain the obtained large equilibrium constant but the predicted concentrations of **4** higher than the ones determined by experiments.[138] The second theory which is known as the radical termination (IRT) theory proposes the termination of **4** yielding a small amount of a dead star polymer.[139] The predicted overall radical concentration of this theory is in good agreement with the experimental data whereas the predicted equilibrium constant is too low,

The procedure of RAFT polymerisation features many advantages in order to design well-defined polymer architectures and allows a large range of monomers and solvents.[125] Moreover, RAFT offers fast polymerisation kinetics, the reaction conditions include a wide temperature range and do not necessarily require a complete absence of oxygen. Polymers obtained via the RAFT process can be modified by various post-polymerisation procedures.[140],[141] However, it has to be considered that RAFT polymerisation shows also certain disadvantages, such as the necessary usage of individually designed RAFT agents depending on the monomer and the possible instability of the obtained polymers while being stored under laboratory conditions[142] or while being processed.[143]

RAFT has been employed for the synthesis of star polymers carrying photoactive end groups which were selectively cross-linked in order to form networks.[144] Furthermore, a RAFT-mediated *ab initio* emulsion copolymerisation using acrylonitrile and 1,3-butadiene as monomers was successfully performed.[145] In addition, the RAFT mechanism was used in order to graft polymers onto cellulose resulting in hybrid materials.[146]

2.4. Photochemistry

The term photochemistry describes a set of chemical reactions, isomerisations as well as physical phenomena occurring in the presence of light in the ultraviolet (200-380 nm), the visible (380-780 nm) or the infrared (780 nm-1 mm) wavelength range. As early as 1500 BC, the people of ancient Canaan used a photochemical reaction in order to prepare a purple dye from a local mollusk.[147] The discovery of photochemical transformations by Trommsdorff[148] in 1834 and the photodimerisation of anthracene by Fritsche[149] in 1866 established the modern era of organic photochemistry. At the beginning of the 20th century, Ciamician addressed to chemical transformations of organic molecules during irradiation.[150],[151] The revolutionary work of Planck on black body irradiation[152] in 1900 and the groundbreaking work of Einstein on the photoelectric effect[153] in 1905 prepared the ground for a better theoretical view of light. According to theory, light consists of quanta (photons) whereas the energy of a photon depends on the inherent wavelength: $E = h \cdot c \cdot \lambda^{-1}$. Albert Einstein was awarded with the Nobel Prize in physics for his services to theoretical physics and his discovery of the law of the photoelectric effect in 1921.[154] Max Planck was awarded with the Nobel Prize for the services he rendered to the advancement of physics by his discovery of energy quanta in 1918.[155] Nowadays, photochemistry and processes that are related to light induced reactions play an important role in chemistry, physics, biology, and technology.[156]

In general, photochemical transformations are combined into two fundamental principles. The first principle is called Grotthus-Draper law and states that a reactant has to absorb light in order to undergo a photochemical process.[157] Einstein and Stark formulated independently of each other the second law of photochemistry.[158],[159] The so-called photo-equivalence law states that for every absorbed photon, one molecule of the irradiated compound triggers a subsequent reaction. Furthermore, the efficiency of a photochemical process is determined by its quantum yield $\boldsymbol{\phi}$ and it is defined as the number of photochemical events per number of absorbed photons.[160]

A schematic description of general photochemical processes was initially introduced by Jablonski in 1935.[161] A Jablonski diagram illustrates the electronic states and their associated relative energies of an excited molecule considering inherent spin orientations like singlet and triplet states. Furthermore the Jablonski diagram

exemplifies photochemical events as transitions between these different electronic states.[162] In general, a Jablonski diagram focuses only on electronical and vibrational transitions leading to a simplified but nonetheless effective depiction of photochemical processes. The initial absorption of a photon leads directly to the promotion of an electron of the activated molecule from the (singlet) ground state to an excited (singlet) state. Subsequently, radiative and non-radiative transitions can occur based on the excited state. Radiative transitions always result in the emission of photons whereas non-radiative processes are defined as transitions that do not involve the emission of light. In this context non-radiative transitions proceed according to the Franck-Condon principle stating that electronic shifts are much faster than any atomic movement.[163] Moreover, this principle elucidates that an electronic transition will be more probable to happen when the vibrational wave functions of two different states overlap significantly. The following photochemical processes are depicted in Scheme 11. It is stated that radiative transitions are featured by straight arrows and non-radiative processes are portrayed by dashed arrows, respectively.

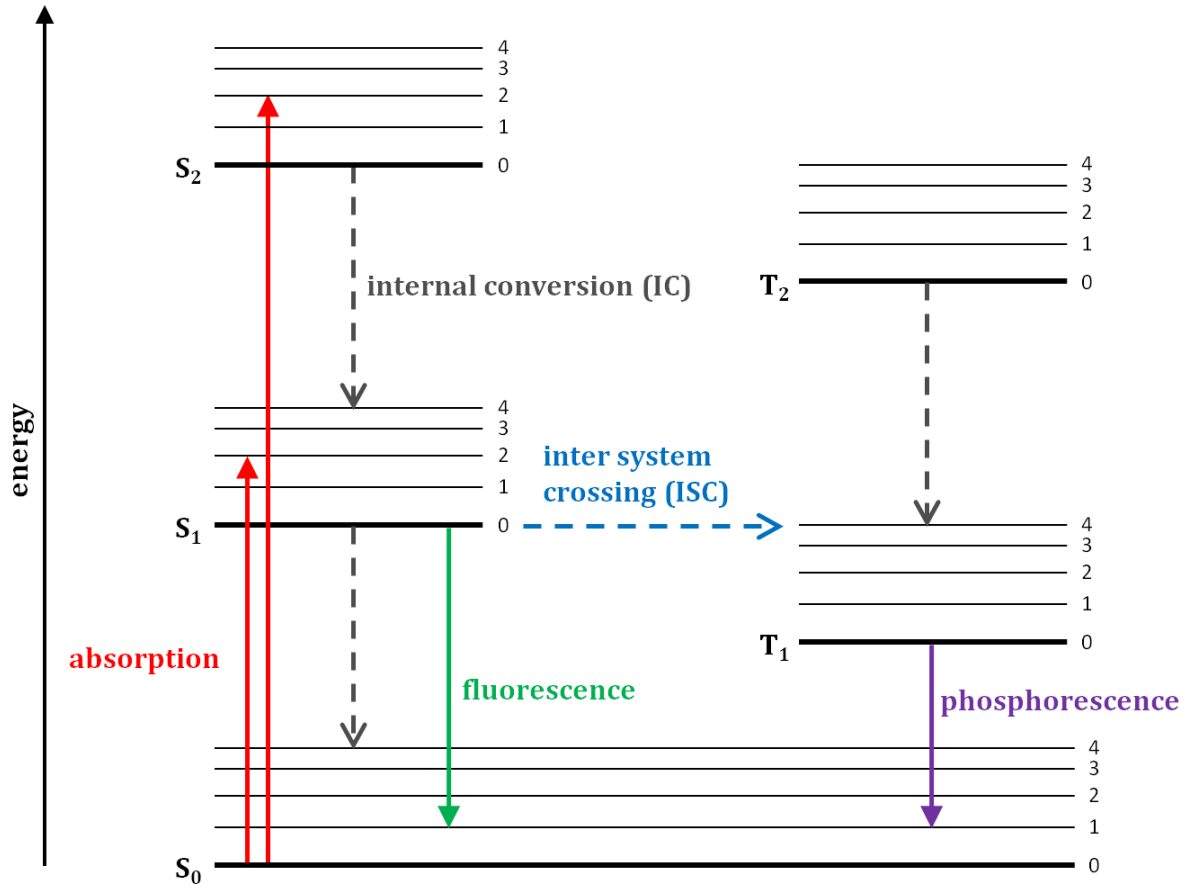

Scheme 11: *Jablonski diagram showing radiative and non-radiative photochemical transitions. Possible processes are absorption, fluorescence, inter system crossing (ISC), phosphorescence, and internal conversion (IC).*

- Internal conversion (IC) lowers the energy states of the same multiplicity and can be described as a fast, non-radiative, and spin allowed relaxation (loss of heat energy) from an excited state to the ground state. Hereby, the electronic energy is transformed into vibrational energy.
- Inter system crossing (ISC) is slower than IC and is defined as a spin-forbidden, radiationless electron transfer between two electronic states that differ in their spin multiplicity such as singlet and triplet states.[164] This means that the activated molecule undergoes a non-radiative spin inversion. Efficient ISC occurs when the energy gap is small between these two states. In general, carbonyl functionalities like ketones tend to have enhanced ISC rates.[165]
- Fluorescence is a form of photoluminescence which occurs when an electron relaxes to the electronic singlet ground state after being promoted to an excited singlet state.[166] Electromagnetic radiation is emitted in this process. In general, the emitted light has a longer wavelength and therefore less energy than the absorbed light known as the Stokes Shift.[167] The lifetime of fluorescence is relatively short (0.5-20 ns) due to the allowed transition between two singlet states.
- Phosphorescence is a different type of photoluminescence. It occurs when an electron undergoes ISC to the triplet state T_1 and relaxes subsequently to the electronic singlet ground state after being excited to a higher energetic singlet state.[168] The lifetime of phosphorescence is relatively long (up to several hours) because the quantum mechanical forbidden transition between a triplet and a singlet state inhibits the radiative relaxation of an electron to the ground state.[169]

A further important topic of photochemistry deals with the photochemical cleavage of carbonyl functionalities like ketones and aldehydes. In this context, Norrish and coworkers reported initially about the photodecomposition of aldehydes and ketones after an $n \rightarrow \pi^*$ excitation.[170],[171] Norrish reactions can be divided into two groups: Norrish type I and Norrish type II reactions. The Norrish type I process is a carbon-carbon bond fission via an α-cleavage from either the singlet or more common the triplet state.[172]

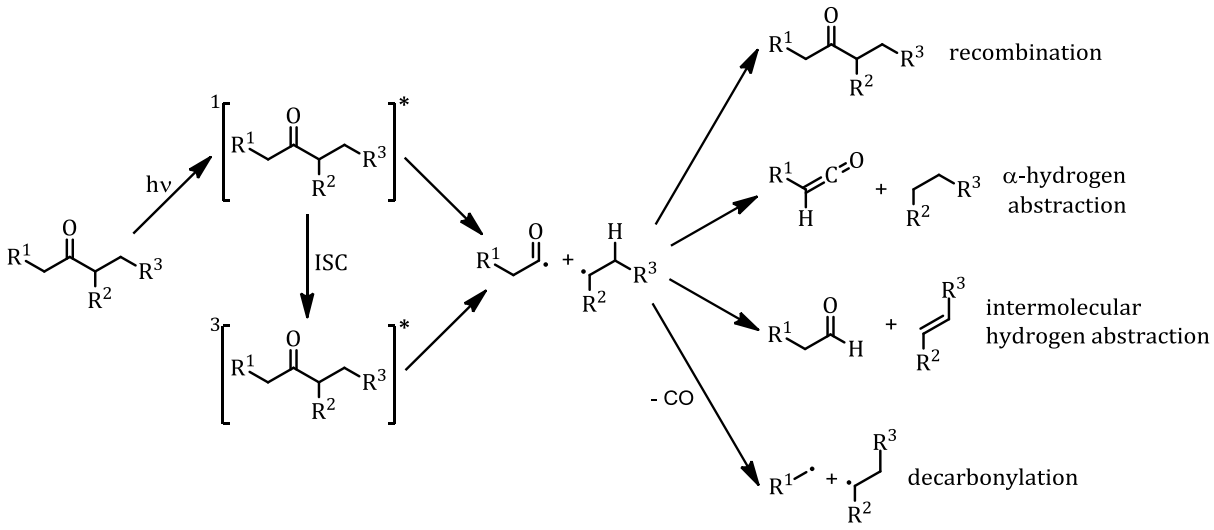

Scheme 12: *The Norrish Type I reaction proceeds via an α-cleavage of carbonyl functionalities like aldehydes and ketones. The process results in highly reactive alkyl and acyl radicals which are able to undergo various subsequent reactions.*

The cleavage results in the formation of highly reactive alkyl and acyl radicals, respectively. Subsequently, the formed radicals are able to undergo recombination, hydrogen abstraction, intermolecular hydrogen abstraction, and decarbonylation. In this context the light triggered decomposition of benzoin and its derivatives via Norrish type I mechanism is investigated and established as initiator system for radical polymerisation.[173],[174],[175]

The Norrish type II reaction involves a light triggered intramolecular [1,5]-H shift of carbonyl functionalities deriving from either a singlet or a triplet state and leading to a biradical intermediate.[176],[177] The presence of the biradical species was determined by photo racemisation and quenching experiments.[178] The formed biradical molecule is able to undergo cyclisation and elimination.[179]

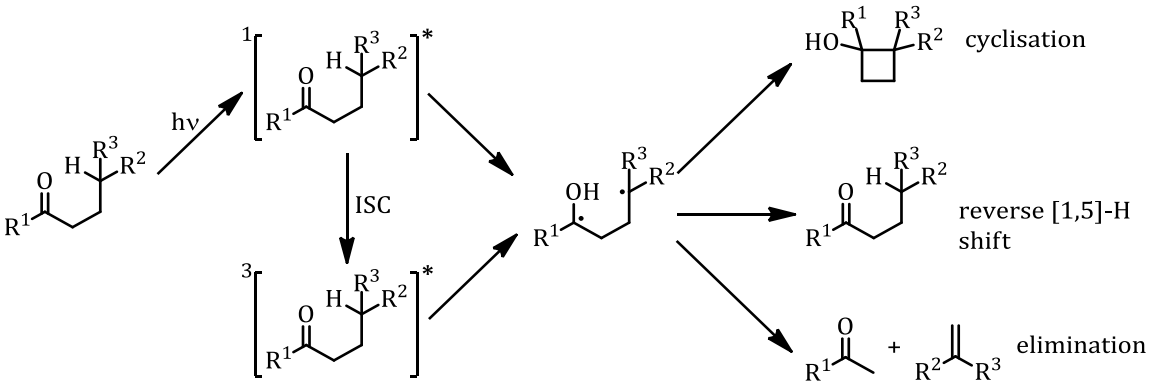

Scheme 13: *The Norrish type II reaction proceeds via an intramolecular [1,5]-H shift resulting in the formation of a biradical molecule. The biradical species is able to undergo several subsequent reactions.*

2.4.1. Photoenol Chemistry

Photo sensitive carbonyl groups which are able to undergo light triggered reactions have been known for a long time. In this case, efficient photochemical reactions of benzophenones were initially reported by Hammond *et al.*[180] and by Martin *et al.*[181] in 1959. The studies of Yang *et al.*[182] and the subsequent implementation of photoenolisation by Sammes[183] finally led to the development of *o*-methyl benzaldehydes and their versatile application in photochemical reaction protocols with maleimides by Barner-Kowollik and co-workers.[184],[185]

After irradiation with light of an appropriate wavelength the *o*-methyl benzaldehyde forms a highly reactive diene – also known as *o*-quinodimethane (photoenol) – that is able to undergo an irreversible [4+2]-cycloaddition with electron-poor dienophiles such as maleimides as well as fumarates. The mechanistic details of photoenol formation were initially determined by Tchir and Porter. Hereby the lifetimes of every involved molecular species were detected by flash photolysis experiments in degassed cyclohexane.[186],[187] The currently established mechanism is depicted in Scheme 14.

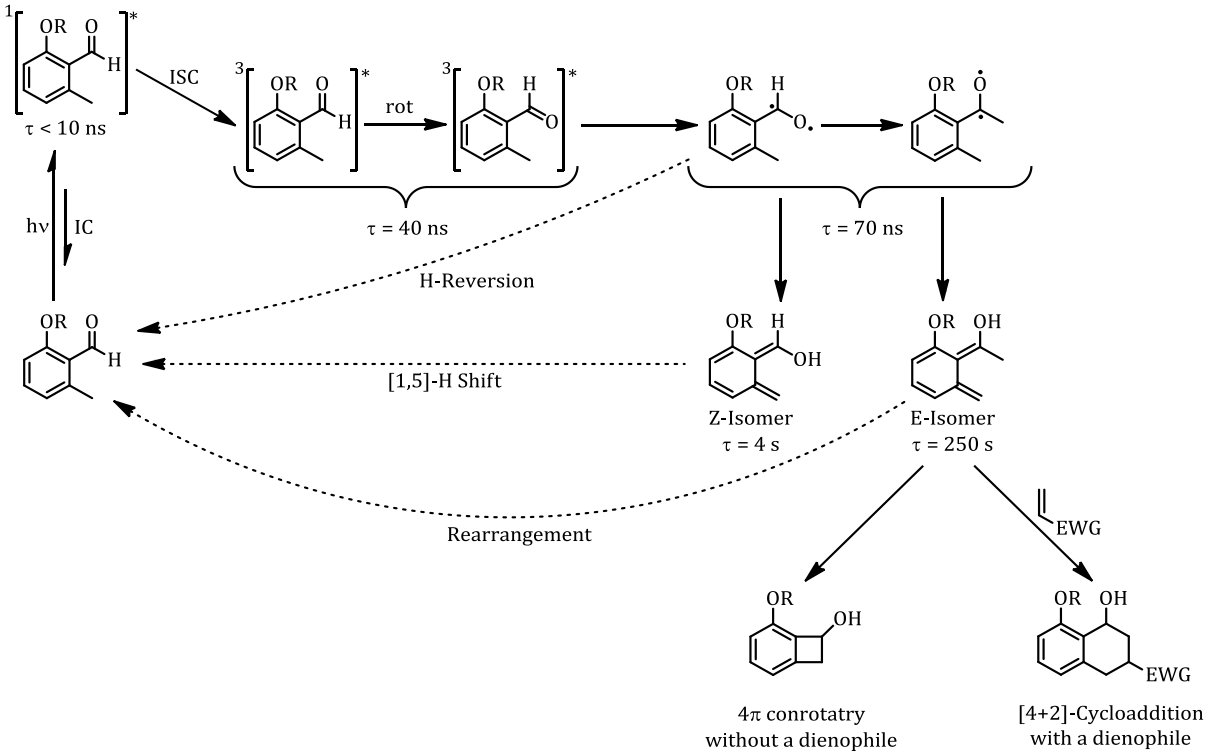

Scheme 14: *The currently accepted mechanism of photoenol chemistry.*

Firstly, the *o*-methyl benzaldehyde is excited towards a short-lived singlet state by photon absorption via an n → π* transition of the carbonyl moiety. Then the activated *o*-

methyl benzaldehyde undergoes inter system crossing (ISC) leading to a triplet state of the molecule. Thus, the carbonyl functionality of the triplet state species is able to rotate about the axis formed by the benzylic centre. Therefore a subsequent Norrish type II γ-hydrogen abstraction induces the formation of two biradical conformational isomers. The biradical species are able to either rearrange into the diene state which is obtained as an conformational E/Z mixture or the formed species may drop back into the ground state.[188] The E and Z isomers differ dramatically in their reactivity. The Z isomer forms a short lived state and is unlikely to undergo a cycloaddition with dienophiles.[189] Instead, the Z isomer of photoenol is transformed into the singlet ground state via a sigmatropic [1,5]-H shift. In contrast, the long lived E isomer is not able to undergo a H shift and is therefore able to undergo thermally allowed reactions such as the [4+2]-cycloaddition in the presence of a dienophile or the conrotatory ring closure without dienophiles.[190],[191]

Photoenol chemistry offers many advantages such as selectivity and orthogonality. A very important advantage of photoenol chemistry is the fact that *in vitro* generated reactive precursors do not have to be deactivated after the irradiation procedure. The formation of the excited photoenol species is reversible and can be thus transformed into the electronic ground state. Hereby, partially converted photoenol moieties will not leave behind reactive dienes after irradiation. In this context, *o*-methyl benzaldehyde can be combined with other photosensitive compounds such as tetrazoles in order to create selectively more complex structures via photochemical reactions.[18],[192] Besides, *o*-methyl benzaldehyde has been used as a fast and highly efficient tool in spatially resolved surface modifications,[193],[194] light triggered block copolymer formations,[185] and the light induced modification of silver nanoparticles with functional polymers.[195] Besides, it is also possible to combine *o*-methyl benzaldehyde with thermal *click* reactions in order to synthesise triblock copolymers at ambient temperature.[196]

As shown before, the photoenolisation process requires a toluene species which carries a carbonyl functionality in *ortho*-position. In this regard, the phototriggered photoenolisation is not only restricted towards *o*-methyl benzaldehydes. For instance, *o*-methyl benzophenone fulfils the structural requirements due to its chemical similarity compared to *o*-methyl benzaldehyde. The phototriggered reaction of *o*-methyl benzophenone is also based on the *in situ* trapping of the intermediate diene form by electron-poor alkynes[182] which is in good agreement to the mechanistic details of the *o*-

methyl benzaldehyde reaction. The obtained Diels-Alder product of the *o*-methyl benzophenone reaction is able to form a naphthalene species via an aromatisation process (refer to Scheme 15).

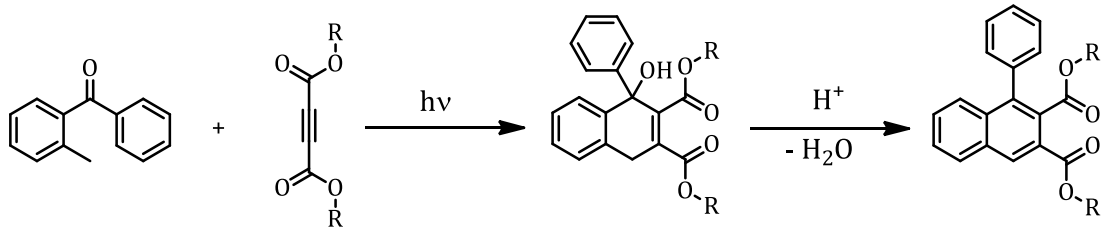

Scheme 15: *The light triggered photoenolisation of o-methyl benzophenone leads to a Diels-Alder reaction with electron-poor dienes. The obtained product is able to undergo an aromatisation yielding a naphthalene derivative.*

Furthermore, it has been demonstrated that 3-(hydroxymethyl)-2-naphtol derivatives are able to undergo facile a Hetero-Diels-Alder reaction with dienophiles in aqueous solution, too (refer to Scheme 16).[197] The interesting aspect of this reaction is the fact that the photoactive compound is a diol in contrast to the carbonyl functionality of *o*-methyl benzaldehyde and *o*-methyl benzophenone.

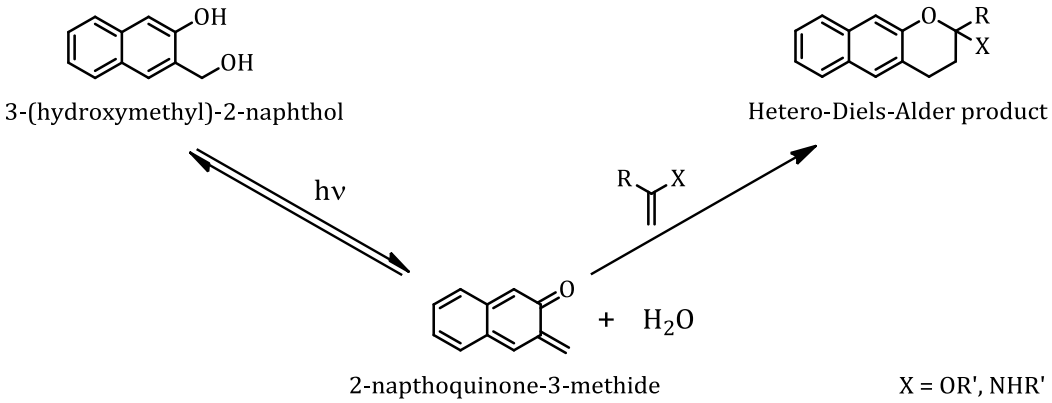

Scheme 16: *The mechanism of Hetero-Diels Alder reaction of 3-(hydroxymethyl)-2-naphthol is based on the light triggered formation of the 2-napthoquinone-3-methide species carrying a carbonyl functionality. The intermediate species can be either retransformed with water into 3-(hydroxymethyl)-2-naphthol or it can be converted into the Hetero-Diels-Alder product. The [4+2]-cycloaddition shows a high selectivity in water as only vinyl ethers as well as enamines yield the respective Hetero-Diels-Alder product.*

The mechanism relies on the light induced water abstraction of the 3-(hydroxymethyl)-2-naphtol leads to the transformation of a 2-napthoquinone-3-methide intermediate species which is able to undergo an irreversible [4+2]-cycloaddition with dienophiles. Water induces again the rapid retransformation of the unreacted intermediate into the 3-(hydroxymethyl)-2-naphtol. In this context, the Hetero-Diels-Alder reaction and the hydration are two competing reactions for the light induced 2-napthoquinone-3-

methide species. The Hetero-Diels-Alder reaction is substantially preferred with reactive dienophiles such as vinyl ethers and enamines whereas other alkenes do not yield the [4+2]-cycloadduct in water. Therefore, the 2-napthoquinone-3-methide intermediate is a highly selective diene regarding dienophiles.

2.4.2. Tetrazole Chemistry

The thermal decomposition of tetrazole derivatives under release of nitrogen was initially reported in 1959.[198] In 1967, Huisgen and co-workers developed the light triggered cycloaddition of 2,5-diphenyltetrazole.[199] The irradiation of a tetrazole compound in the range between 280 and 320 nm leads towards the formation of a nitrile imine under the release of nitrogen. The nitrile imine was detected as an intermediate of the light triggered process in several studies[199],[200],[201] and is a highly reactive 1,3-dipole that can be categorized to the propargyl-allyl type. The formed dipole structure is able to undergo a [3+2]-cycloaddition with a huge range of electron-poor enes comparable to the light induced photoenol reaction (refer to chapter 2.4.1). The product of the cycloaddition is a fluorescent 4,5-dihydro pyrazole derivative. The phototriggered cycloaddition of tetrazoles is also known as nitrile imine-mediated tetrazole ene cycloaddition (NITEC) due to the appearance of the 1.3-dipole intermediate.[202] The mechanism of the NITEC reaction is depicted in Scheme 17.

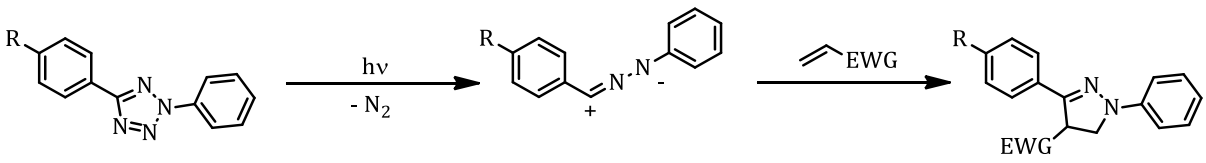

tetrazole nitrile imine 4,5-dihydro pyrazole

Scheme 17: *The mechanism of the NITEC process.*

Tetrazole chemistry offers an efficient, fast, and modular ligation technique.[203],[204],[205] Moreover, the NITEC mediated ligation of tetrazoles is not inevitably limited to electron-poor enes such as maleimide. In contrast to the light induced photoenol reaction, the addition of electron-rich alkenes such as 1-pentene was reported to a dilinker carrying two tetrazole end groups (refer to Scheme 18).[206]

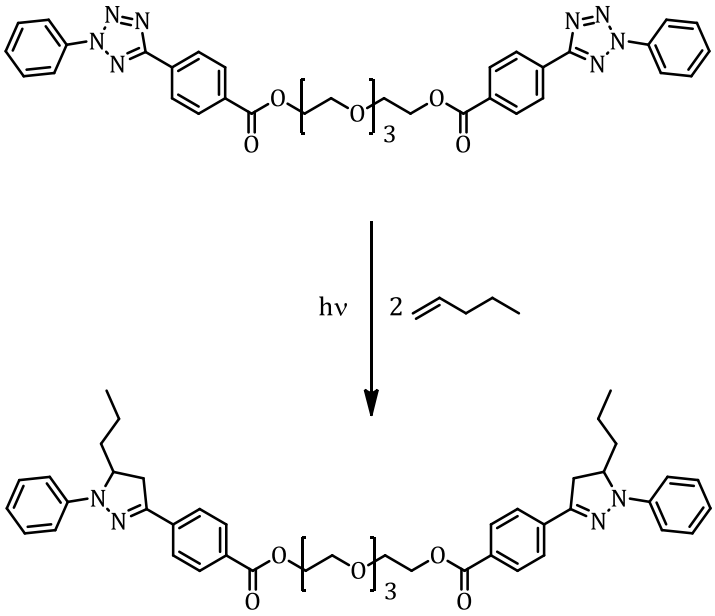

Scheme 18: *A dilinker carrying two tetrazole end groups and 1-penten yield a 4,5-diydro pyrazole after irradiation. The reaction demonstrates that the NITEC reaction can also be performed with electron-rich alkenes such as 1-pentene.*

Subsequently, the photoactive dilinker was additionally employed for the phototriggered cross-linking with the double bonds in polymer backbone of 1,2-polybutadienes. A further NITEC reaction featuring electron-rich double bonds was performed by the phototriggered conjugation of a tetrazole moiety with fullerenes.[207] Tetrazole can be handled easily since both the synthesis and the implementation in other systems is very facile and straightforward. NITEC systems offer the possibility to tune selectively the absorption range between 254-365 nm by introducing functionalities with various adequate electronic structures at the terminal N-phenyl ring.[208] The utilisation of push-pull substituted diaryltetrazoles results in the red-shifting of the absorption because the delocalisation of the tetrazole π-electrons is amplified.[209] As a result, a more delocalised π-system requires less energy for its excitation. In this context, the red-shifting of a tetrazole moiety into the visible light range has been reported via the substitution of the N-phenyl ring by a pyrene ring.[210] The structure of the obtained pyrene functional tetrazole is depicted in Figure 19.

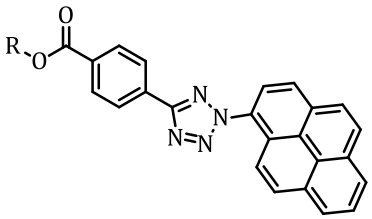

Scheme 19: *The structure of the pyrene functional tetrazole allowing NITEC photoreactions in the visible light range.*

The pyrene functional tetrazole species can be activated at λ = 410-460 nm under catalyst free conditions. For instance, a pyrene functional tetrazole terminated polymer was employed for end group modifications as well as the formation of block copolymers using the visible light induced NITEC reaction as ligation tool.[210]

In general, the NITEC reaction featuring tetrazoles shows a huge biocompatibility deriving from the absence of metal catalysts. In contrast, especially copper catalysed ligation protocols such as the azide alkyne Huisgen cycloaddition show a severe cytotoxic behaviour (refer to chapter 2.5.1). Therefore, phototriggered reactions between tetrazole and enes were applied in areas like protein modification,[203],[211] and the attachment of enzymes on artificial vesicles called polymersomes.[212] In addition, the NITEC method was also classified as a bioorthogonal reaction.[211] Since bioorthogonal reactions are supposed to be performed in living systems, bioorthogonality requires a chemoselective and very efficient ligation procedure in combination with the absence of any interactions of the reactant with other biological structures. For instance, it has been demonstrated that the postsynthetic modification of nucleic acids carrying reactive functional groups was successfully performed using in a bioorthogonal fashion using NITEC photoreactions.[209],[213] Nevertheless, the question still remains if tetrazole is able to undergo a bioorthogonal photoreaction with all kinds of functionalities in biological systems. Therefore, the reaction of tetrazole and as set of different biological nucleophiles was investigated in a 1:1 mixture of acetonitrile and phosphate buffered saline (PBS) (refer to Scheme 20).[214] In this case, the photoreaction between tetrazole and an excess of 100 eq. pent-4-enoic acid resulted in the nucleophilic attack of the carboxylic acid towards the nitrile imine intermediate (71 % yield). The expected [3+2]-cycloaddition between the nitrile imine and the double bond of pent-4-enoic acid, yielding the 4,5-dihydro pyrazole conjugated product, could not be detected (reaction I). Furthermore, the photoreaction of tetrazole, but-3-en-1-ol, and acetic acid yielded exclusively the nucleophilic addition product (75 % yield) (reaction II). In addition, the irradiation of the tetrazole compound and but-3-en-1-ol resulted in a mixture of the expected NITEC product and the product derived from of the addition of acetonitrile towards the nitrile imine species (reaction III). Next, the photoreaction of a tetrazole and L-alanine yielded again the nucleophilic addition of L-alanine towards the nitrile imine intermediate (reaction IV).

As a result, the bioorthogonal application of tetrazole is limited as it is able to undergo potential reactions with nucleophiles which are present in biological systems.

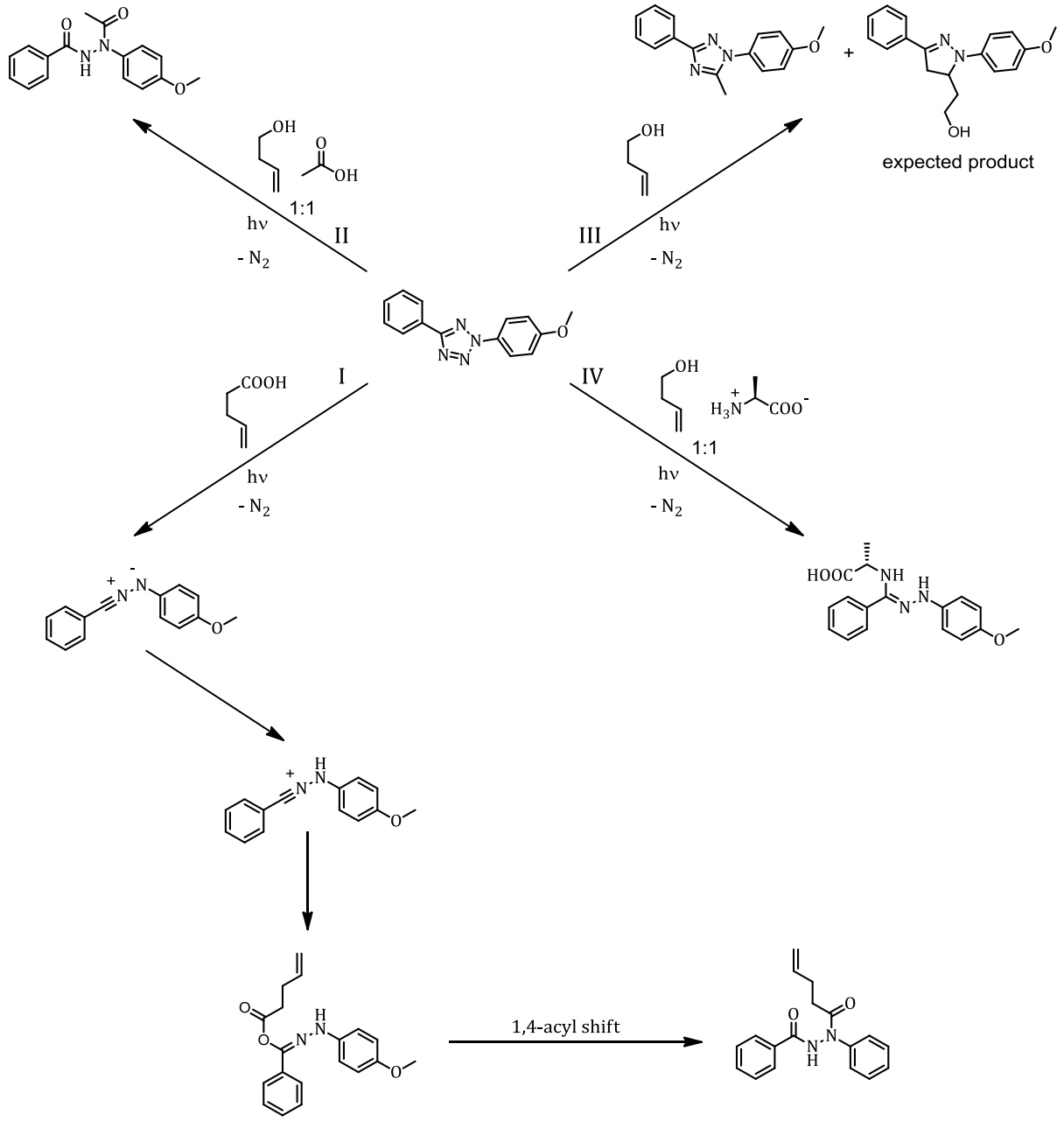

Scheme 20: *An overview of the light triggered reactions of a tetrazole moiety with a functionalised ene and a competing nucleophile in a 1:1 mixture of acetonitrile and phosphate buffered saline (PBS). The tetrazole compound is irradiated with the ene moiety pent-4-enoic acid (reaction I), the ene moiety but-3-en-1-ol in the presence of the nucleophile acetic acid (reaction II), the ene moiety but-3-en-1-ol (reaction III), and the ene moiety but-3-en-1-ol in the presence of the nucleophile L-alanine (reaction IV). The expected 4,5-dihydro pyrazole formation, resulting from the NITEC reaction, only occurs as a side product in reaction III. In addition, the tetrazole also undergoes a [3+2]-cycloaddition with acetonitrile(reaction III). The other reactions demonstrate that the reaction between the tetrazole and the additionally added nucleophiles is preferred over the NITEC reaction (reactions II + IV). The reaction between the tetrazole moiety and the acidic ene results in the initial protonation of the nitrile imine intermediate and a subsequent nucleophilic attachment of the obtained carboxylate moiety(reaction I).*

Furthermore, NITEC reactions find widespread applications in either grafting-to or grafting-from surface conjugations of polymers,[202],[215],[216] and photoresponsive compounds[217] on various substrates like cellulose, silicon or poly(dopamine) interfaces. An additional advantage of NITEC chemistry is the before mentioned yielding of fluorescent products out of non-fluorescent starting materials at ambient temperature. In this regard, the NITEC photoreaction has been applied for the phototriggered step growth polymerisation of non-fluorescent monomers yielding fluorescent polymers.[218] Besides, the NITEC reaction was used for the photochemical design of fluorescent single-chain nanoparticles starting from non-fluorescent side-chain functionalised polymers.[219]

Nevertheless, the profluorescent behaviour of the obtained NITEC products can be employed by the use of nitroxide containing tetrazole as versatile scaffolds for the sensoring of radical and redox systems.[220] The efficiency of the sensors relies on its ability to quench fluorescence in the absence of radicals and to start fluorescence in the presence of radicals. A set of nitroxide containing tetrazoles and maleimides were irradiated in a NITEC reaction yielding nitroxide capped 4,5-dihydro pyrazoles. Although 4,5-dihydro pyrazoles are profluorescent as mentioned before, the obtained nitroxide containing 4,5-dihydro pyrazole is non-fluorescent (refer to Scheme 21).

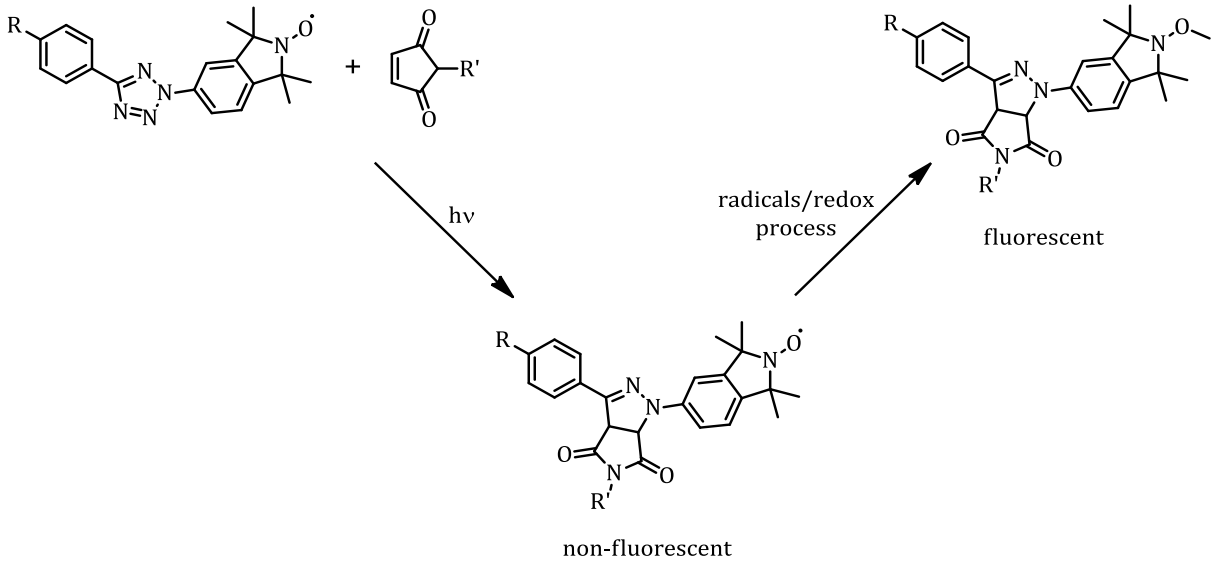

Scheme 21: *The NITEC photoreaction of a nitroxide containing tetrazole and maleimide results in the formation of a non-fluorescent 4,5-diydropyrazole. In this regard, the paramagnetic nitroxide radical accelerates ISC from the excited states to the triplet state with lower energy, increases the lifetime of triplet state and thus the non-irradiative relaxation is substantially preferred. Radicals or redox systems lead to a conversion of the nitroxide into a saturated diamagnetic molecule which is no longer able to inhibit fluorescence.*

The suppression of the fluorescence can be explained by paramagnetic character of the nitroxide species. After excitation, the fluorophore relaxes from its excited state to the excited state with the lowest energy S_1.[221] The subsequent ISC towards a lower energy triplet state is considerably accelerated by the nitroxide moiety. Hereby, non-irradiative relaxation is substantially preferred because the relaxation from the triplet state to the ground state is spin-forbidden and the lifetime of the triplet state is increased. In contrast, fluorescence occurs by the radiative relaxation from the excited singlet state to the singlet ground state (refer to chapter 2.4).

2.5. Modular Ligation Chemistry

The concept of *click* chemistry was first introduced by Sharpless and co-workers in 2001.[222] The idea of the present modular ligation principle was initially inspired by chemical processes in nature such as *in vivo* protein formations.[223] In this case the term *click* chemistry is defined by a modular ligation approach that uses the most practical and reliable chemical transformations of small building blocks in order to form new structures.[224] In general, *click* reactions have to fulfill certain requirements and criteria:[222],[225]

- Orthogonality and wide in scope reaction paths
- Simple reaction conditions including ambient temperature and no sensitivity to oxygen or water
- Stereoselectivity of the reaction
- Equimolarity and availability of all starting materials
- Quantitative yield as well as easy isolation steps for the products
- Fast reaction kinetics

The presented modular ligation principle has undoubtedly led to a paradigm shift in synthetic chemistry.[226] The unique character of *click* reactions allows the easy synthesis of complex molecular structures because it overcomes sequential synthesis steps used in classic organic chemistry. The huge variety of organic reaction classes that fulfill the given *click* criteria are listed below:

- the Diels-Alder reaction
- the thiol-ene reaction as well as the thiol-yne reaction
- the azide alkyne Huisgen cycloaddition
- Nucleophilic substitution reactions such as the ring-opening of epoxides

Besides, the modular ligation principle was also employed in order to simplify and advance the field of polymer chemistry. In this context, functionalised polymers are used as building blocks for the design of complex polymer architectures[227] such as block copolymers,[196] star polymers,[228] and dendrimers.[229] Since polymers do not require

stereospecifity in contrast to natural products, the *click* criteria were adjusted for polymers highlighting equimolarity, short timescales as wells as large-scale purification.[230] Additionally, *click* chemistry was also combined with polymerisation techniques such as ATRP.[231],[232]

2.5.1. Azide Alkyne Huisgen Cycloaddition

The thermal 1,3-dipolar cycloaddition of an azide and an alkyne yielding a 1,2,3-triazole was initially developed by Huisgen in 1963 and the reaction was finally named after him.[233],[234] The formation of the five-membered heterocycle is performed by a concerted pericyclic shift of the four electrons of the azide and two π-electrons of the alkyne. The thermal azide alkyne Huisgen cycloaddition requires high temperatures in order to trigger the reaction whereby the formed 1,2,3-triazole occurs as a mixture of two regioisomers (refer to Scheme 22).

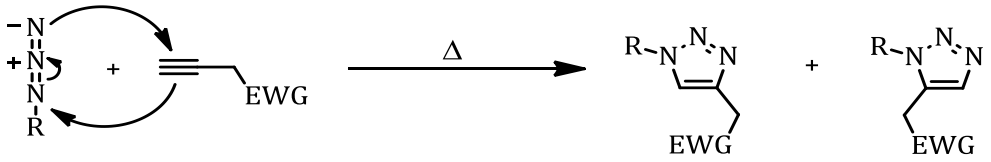

Scheme 22: *The mechanism of the thermal azide alkyne Huisgen cycloaddition.*

An important modification of the azide alkyne Huisgen reaction is the copper(I)-catalysed 1,3-dipolar cycloaddition between an alkyne and an azide which was introduced by Meldal[235] and Fokin[236] in 2002 (refer to Scheme 23). A main advantage of the copper(I)-catalysed 1,3-dipolar cycloaddition is the exclusive formation of the 1,4-regioisomer at ambient temperature.

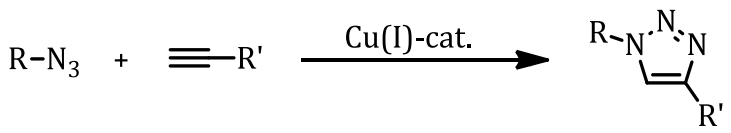

Scheme 23: *Overview of the copper(I)-catalysed azide alkyne cycloaddition.*

The mechanism of this reaction proposes the initial reaction of the terminal alkyne with the copper(I) complex. Afterwards the azide is attached to the copper terminus of the

alkyne and introduced subsequently via an intramolecular reaction under exclusion of the copper catalyst[237] (refer to Scheme 24).

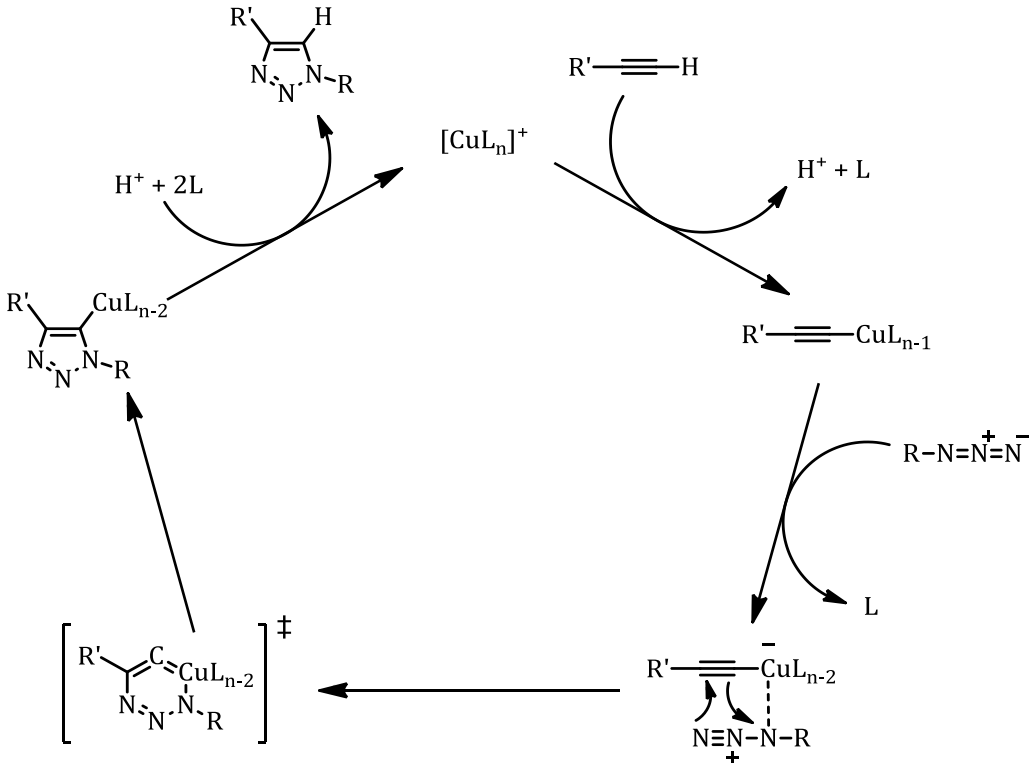

Scheme 24: *General mechanism of the copper(I)-catalysed azide alkyne cycloaddition.*

Moreover, it is reported that the 1,3-dipolar azide alkyne cycloaddition can also be catalysed by silver(I) salts[238] and ruthenium complexes.[239] The cytotoxic potential of these metal catalysed reactions is the main disadvantage and prevents possible applications in biological as well as living systems. In this context, the metal-free 1,3-dipolar cycloaddition variant using an azide and a fluorinated cyclooctyne species was initially implemented by Bertozzi in 2007.[240],[241] The copper-free azide alkyne cycloaddition (refer to Scheme 25) does not interfere with biochemical processes in living systems[242] and is classified as *click* reaction due to mild reaction conditions as well as a rapid reactivity of the starting materials. Consequently, this reaction is also termed bioorthogonal chemistry. The reaction takes place without catalyst or elevated temperature because the linear geometry of the sp hybridised carbon atoms in the ring leads to highly strained structures resulting in an activated triple bond.

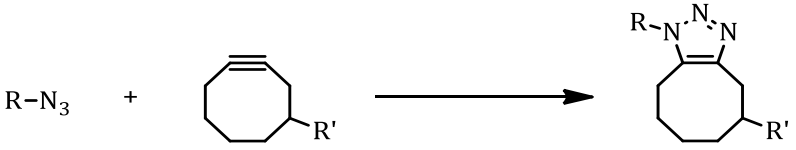

Scheme 25: *Overview of the bioorthogonal copper-free azide alkyne cycloaddition.*

2.5.2. Diels-Alder Reaction

The Diels-Alder reaction is a [4+2]-cycloaddition that was initially reported by the German researchers Diels and Alder in 1928[243] and both scientists were awarded the Nobel Prize in 1950. The concerted pericyclic reaction is thermally allowed and involves the four π-electrons of a conjugated diene moiety and the two π-electrons of a dienophile which can be either a substituted ene or a substituted alkyne. According to Woodward-Hoffmann rules, the four π-electrons of the diene and the two π-electrons of the dienophile undergo a suprafacial-suprafacial interaction.[244] A close mechanistic investigation prompts that the cycloaddition occurs without intermediates, instead the presence of one single cyclic transition state is presumed.[245] The driving force of the Diels-Alder reaction lies in the transformation of the π-bonds of the starting materials into the energetically more stable σ-bonds of the product. The general mechanism of the concerted pericyclic Diels-Alder reaction is depicted in Scheme 26.

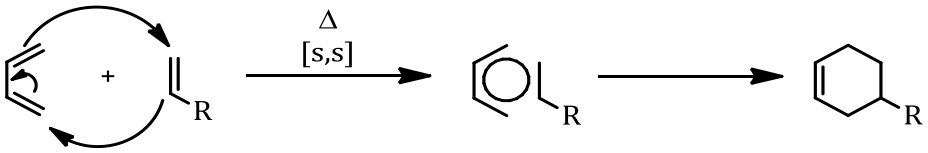

Scheme 26: *The mechanism of the Diels-Alder reaction featuring a diene and a dienophile.*

The reaction between mono-substituted dienes and mono-substituted dienophiles leads to the formation of predominant regioisomers. The formation depends on the position of the diene substituent which influences the diene frontier orbital coefficients as well as their energy.[246] Dienes with a substituent in 1-position yield the *ortho*-cyclohexene whereas dienes with a substituent in 2-position yield the respective *para*-product[247] (refer to Scheme 27).

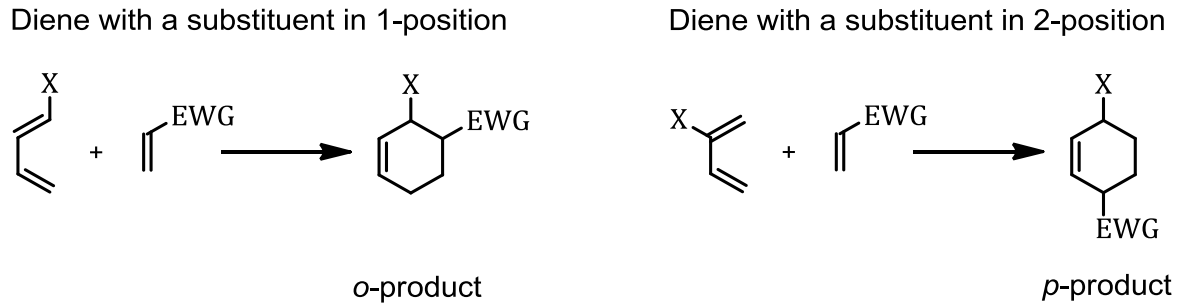

Scheme 27: *Dienes with a substituent in 1-position and a mono-substituted dienophile form a product that carries both substituents in ortho position. Instead, dienes with a substituent in 2-position and a mono-substituted dienophile form a product with both substituents in para position.*

Besides, the Diels-Alder reaction shows also a high stereoselective behaviour.[248] In particular, the product of cyclic dienes such as cyclopentadiene and substituted dienophiles are able to form two different stereoisomers: an endo or an exo-product. The endo product is usually sterically hindered but it is kinetically favoured because the energy of the transition state is lowered due to secondary orbital interactions. Therefore, the endo-product is formed preferentially at low temperature. Instead, the formation of the exo-product is preferred by thermodynamics and occurs at elevated temperatures (refer to Scheme 28).[249]

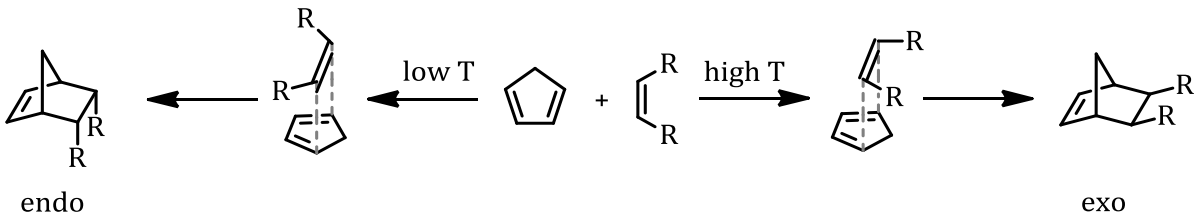

Scheme 28: *The endo product is kinetically favoured and is formed at low temperature whereas the exo product is regulated by thermodynamics and is formed at high temperatures.*

The yield and the reaction kinetics of a Diels-Alder reaction is highly dependent on the electronic structure of both the diene and the dienophile. Experimental data prompt that the efficiency of Diels-Alder reactions can be improved significantly when the starting materials have an opposing electronic structure.[250] The basic reaction between a diene and dienophile is described by the frontier molecular orbital (FMO) theory which considers the interaction of the highest occupied molecular orbital (HOMO) of one compound with the lowest unoccupied molecular orbital (LUMO) of the second compound.[251] Hereof, Diels-Alder reactions are classified as neutral, normal or inverse according to the electron demand of the diene and the dienophile. The diene and the dienophile of neutral Diels-Alder reactions show similar electronic structures leading to relatively large and equal energy distances between the HOMOs and the LUMOs.[252] Diels-Alder reactions with normal electron demand such as the photoenol reaction (refer to chapter 2.4.1) are performed with electron-rich dienes as well as electron-poor dienophiles whereas Diels-Alder reactions with inverse electron demand are performed with electron-poor dienes and electron-rich dienophiles. Electron-donating substituents such as alkyl functionalities decrease the relative FMO energy. On the contrary, electron-withdrawing groups such as carboxylic functionalities increase the FMO energy.[253],[254] Diels-Alder reactions featuring normal electron demand are characterised by the interaction of the lowered dienophile LUMO with the elevated diene HOMO leading to a

narrowed energy gap. In contrast, the lowered diene LUMO with the elevated dienophile HOMO overlap with each other leading to a narrowed energy gap for the inverse electron demand Diels-Alder reactions. The FMO interactions of the three possible Diels-Alder reaction variants are depicted in Scheme 29.

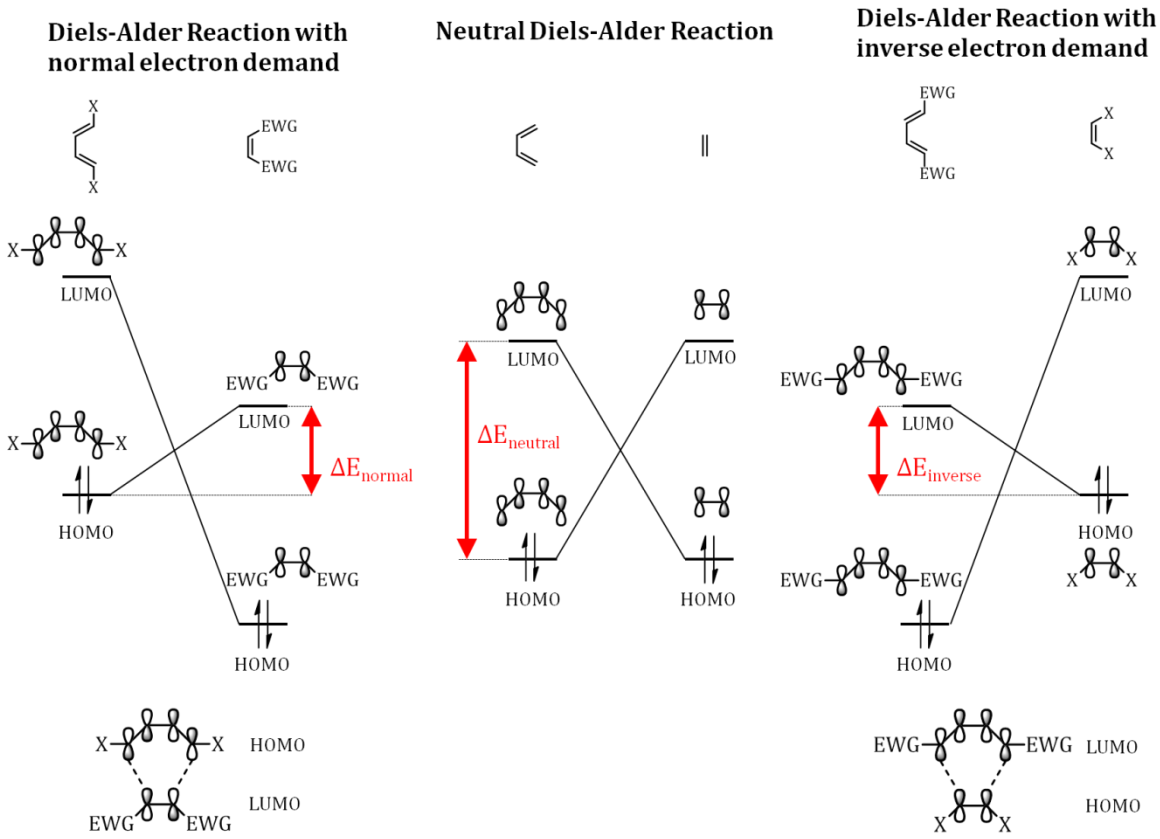

Scheme 29: *Overview of the possible Diels-Alder reactions according to FMO. The normal electron demand Diels-Alder reaction involves an electron-rich diene as well as an electron-poor dienophile. In this case, the HOMO of the diene and the LUMO of the dienophile overlap with each other because the electron-withdrawing group of the dienophile lowers the energy of the LUMO whereas the electron-releasing group of the diene increases the energy of the HOMO (left). The neutral Diels-Alder reaction involves a diene and a dienophile whose electron demand is similar leading to equal HOMO-LUMO gaps between both compounds (centre). The inverse electron demand Diels-Alder reaction employs an electron-poor diene as well as an electron-rich dienophile. The LUMO of the diene and the HOMO of the dienophile overlap with each other because the electron-releasing group of the dienophile increases the energy of the HOMO whereas the electron-withdrawing group of the diene lowers the energy of the LUMO (right).*

2.6. Direct Laser Writing

Direct Laser Writing (DLW) depicts a multiphoton lithography method for the design of three-dimensional microscopic structures. Hereof, DLW allows the creation of structures with a resolution of less than 100 nm[255] and has been applied for the design of photonic metamaterials,[256],[257] micro-supercapacitors,[258] and the microstructuring of graphene oxide nanosheets.[259] The basic principle of this lithographic method rests on non-linear multiphoton absorption.[260] The most important physical process in the context of DLW is the two-photon absorption (TPA) which was theoretically predicted by Göppert-Mayer in 1931[261] and initially demonstrated in an experiment in 1961.[262]

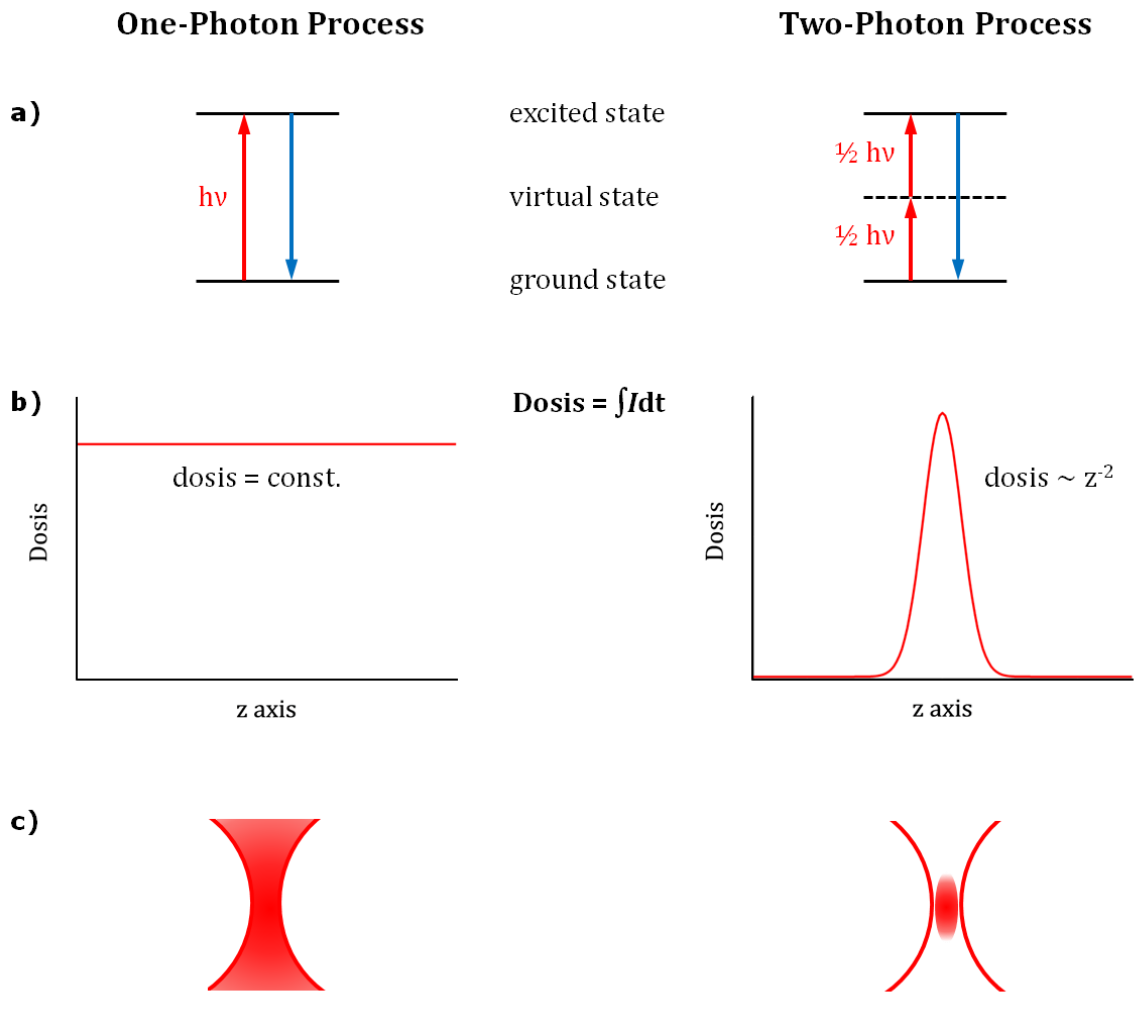

Figure 9: *a) The absorption of one photon from the ground state to the promoted state is the classic example of a light induced excitation (left). The simultaneous absorption of two photons by a molecule is called two photon-absorption. b) A one-photon process has got a constant intensity profile (left). A two-photon process shows a non-linear intensity profile (right). c) A focused laser beam generated by a one-photon process is still consistent (left). A focused laser beam generated by a two-photon process leads to the creation of a voxel (right).*

TPA is defined as the contemporaneous absorption of two photons with different or identical energies by the same molecule resulting in the excitation from its ground state via a virtual state to a higher electronic state (refer to Figure 9a). TPA is a second-order process in which the probability of its occurrence is dependent on the square of the applied light intensity in contrast to a linear (one photon) absorption (refer to Figure 9b).[263] Therefore a two-photon process can only be triggered by a very short laser pulse enabling a high photon density and is able to dominate the linear absorption process at high light intensities.[264] The key step of the DLW process is the very tight focussing of femtosecond laser pulses. In general, the focussing of a collimated laser beam to a spot depends on the lens aperture and the wavelength.[265],[266] Hereby, the light intensity of the laser is only significant in the central region of the focus in order to enable a non-linear two-photon absorption. The resulting absorption and thus the DLW process in the focus is limited to a sharp three-dimensional volume element which is called voxel. The voxel allows the spatial resolved activation of a photoresist leading to a three-dimensional structures of any kind. In contrast, a linear absorption in the focus would generate to a tight light stream along the laser beam path (refer to Figure 9c).

A basic DLW setup consists of a laser source emitting ultrashort pulses, an intensity tuning device, an objective, a device enabling the relative motion between the focus and the substrate as well as a computer for data acquisition.[267]

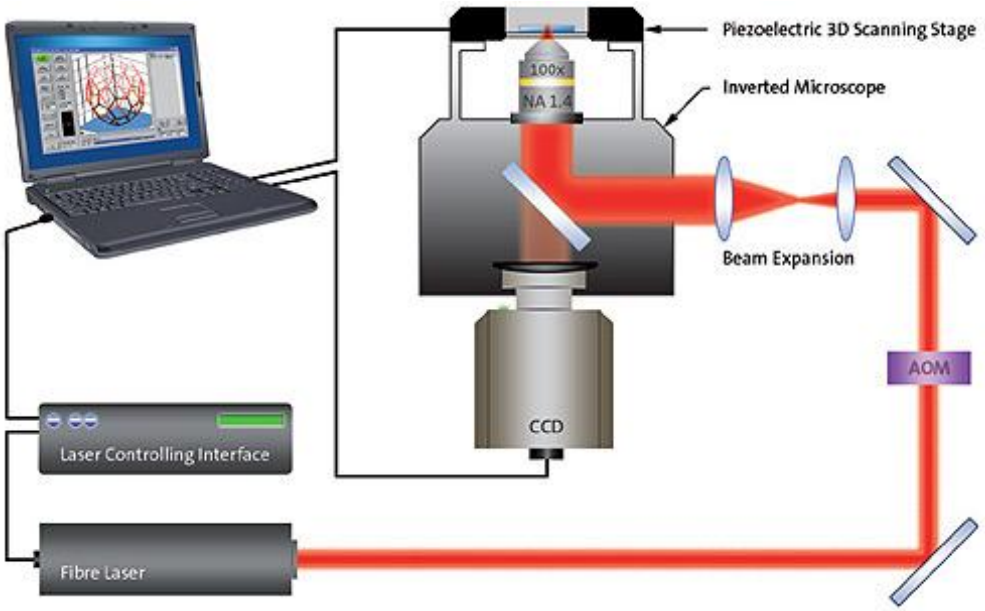

Figure 10: *Basic setup for DLW. Reproduced with permission from nanoscribe.*

2.7. Mass Spectrometry

Mass spectrometry is a sensitive and widespread analytic method which detects the exact mass of substances. Basically, a mass spectrometer converts uncharged substrates into ions which are separated and detected subsequently according to their mass-to-charge ratio m/z.[268] The most important parameter of a mass spectrometer is the resolution R. The resolution determines the resolving power of the device and compares the distance between the theoretical and the experimental m/z value (refer to Figure 11).[269] Therefore, the resolution allows the distinction of two ions with similar mass-to-charge ratios. The larger the resolution the better is the ion separation.

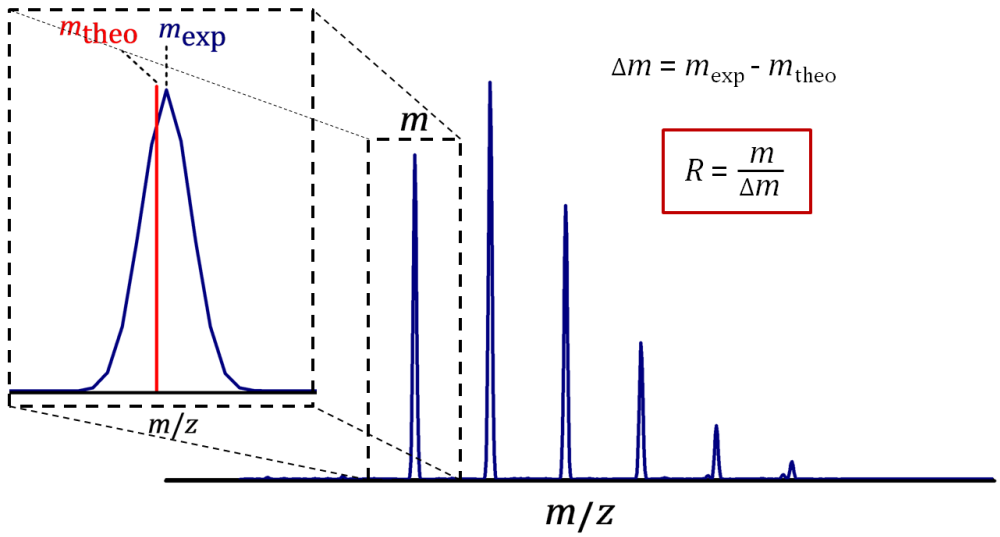

Figure 11: *The definition of the resolution R.*

The general setup of a mass spectrometer is depicted in Figure 12. At the beginning, the sample is injected into the inlet system. The molecules of the sample are subsequently ionised in an ion source because uncharged molecules cannot be detected by the mass spectrometer. All components of the device are under high vacuum in order to prevent inadvertent collisions of the ionised molecules with gas molecules of the atmosphere. In general, ionisation techniques can be categorised into hard or soft. Hard ionisation techniques such electron impact ionisation (EI) lead to fragmentation of the analyte during the ionisation procedure.[270] In contrast, soft ionisation methods prevent any fragmentation of the sample. The most common soft ionisation methods are matrix assisted laser desorption ionisation (MALDI) in which the matrix embedded analyte is vaporised by a laser,[271] chemical ionisation in which the analyte collides softly with an

ionised reagent gas (CI),[272] as well as electrospray ionisation (ESI)[273] which is presented in detail in Chapter 2.7.1. After the generation of ions, the charged molecules are separated in the mass analyser. The most common mass analysers are the quadrupole which constrains the generated ions on oscillating motions,[274] the quadrupole ion trap which is able to hold the ions within a three-dimensional electrical field,[275] the time-of-flight (ToF) mass analyser which separates ions according to their velocity[276], the Orbitrap analyser which traps ions on helical trajectories due to electrostatic attraction[277] as well as the fourier transform ion cyclotron resonance (FT-ICR) spectrometer which separates ions according to their orbital frequency in a strong homogeneous magnetic field.[278] Subsequently, the separated ions reach the detector where they are counted and converted into electrical signals. Detectors are subdivided into time or position dependent types. Time dependent instruments contain one electrical amplifier generating a cascade of electrons on the surface of an electrode and detect the ion beam successively.[279] These detectors are the most common ones and are designed as electron multipliers, faraday cups and scintillation counters. Position dependent components are photographic plates as well as array detectors and detect simultaneously distracted ions.[280] Afterwards the digital data reach the signal processor which processes and interprets the obtained data in order to produce a mass spectrum.

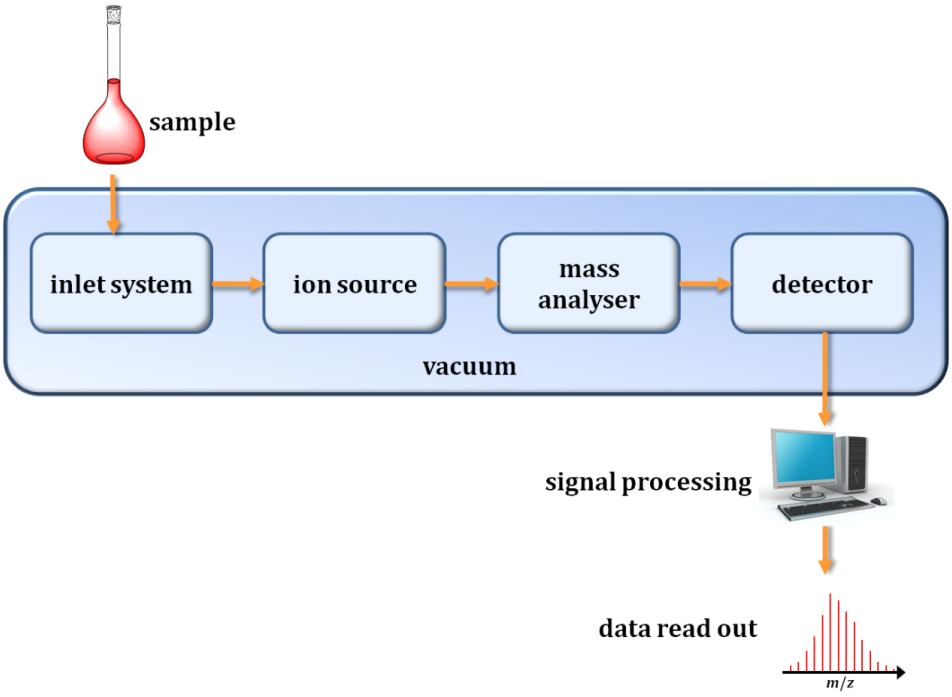

Figure 12: *The general setup of a mass spectrometer.*

2.7.1. Electrospray Ionisation Mass Spectrometry

In the late 1960's, Dole and co-workers have initially dealt with experiments on the electrospraying behaviour of diluted polymer solutions.[281] Their work laid the foundation for the term electrospray ionisation (ESI). The ESI process was established by Yamashita and Fenn in 1984.[282] In 2002, Fenn was awarded the Nobel Prize in Chemistry for the development of the ESI technique in mass spectrometry. Starting from its beginning as ionisation source for polymeric materials, the ESI was also employed for the analysis of small molecules. Nowadays, electrospray ionisation mass spectrometry (ESI-MS) is one of the most applied and most versatile soft ionisation techniques in analytics.[283],[284]

The basic procedure requires the complete solvation of the analyte with a salt. In polymer chemistry a solution of sodium trifluoracetate in THF and methanol has been shown to be a good system. ESI-MS is based on the physical phenomenon that liquids can be dispersed as fine and highly charged droplets by a strong electric potential. The potential is applied between the tip of the spray capillary and the counter electrode (cone). The high electric field in the tip of the capillary separates cations and anions within the solution whereby the positively charged ions are concentrated at the tip. Charge repulsion at the tip of the capillary leads to the formation of a Taylor cone[285] (refer to Figure 13).

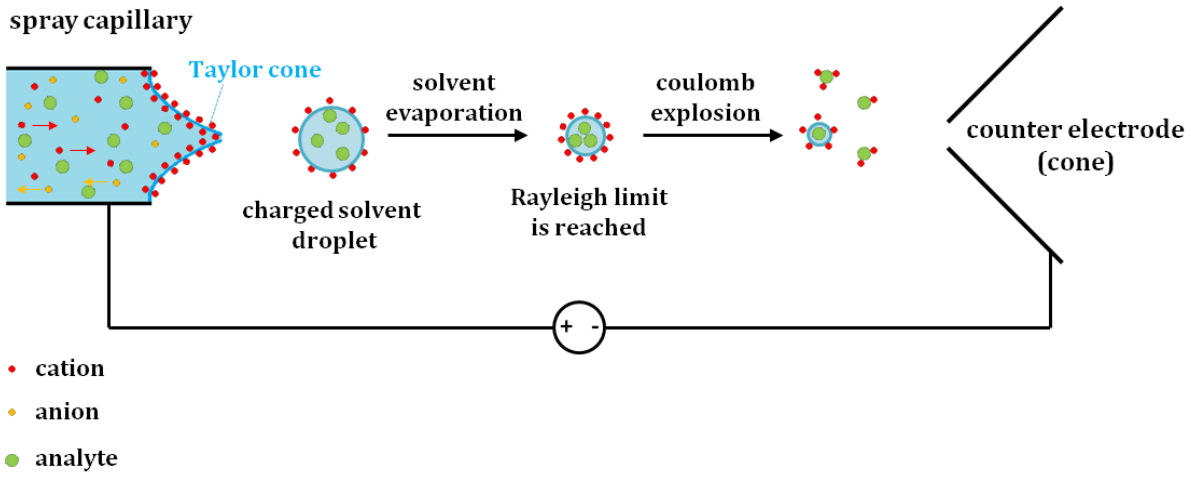

Figure 13: *Overview of the ESI process. The image was modified from ref.[286] with permission from the Hindawi Publishing corporation, 2016.*

A jet of nitrogen is sprayed from the capillary tip and carries the analyte containing droplets towards the counter electrode. The formed droplets shrink step by step due to

continued solvent evaporation until they reach the Rayleigh limit.[287] As far as the concentration of equally charged ions on the surface of the droplets approaches an upper level, a so-called coulomb explosion is initiated.[288] After the explosive decay, single gas-phase ions are generated from the analyte molecules. In contrast to MALDI, multiple charged ions can be formed via the ESI process.[289] The magnitude of multiple charged ions largely depends on the size of the polymer, its chemical nature as well as its conformation. However, the presence of multiple charged ions in the mass spectrum can also be a disadvantage, especially when the peaks of multiple charged signals overlap with each other. The quantitative size-exclusion chromatography electrospray ionization mass spectrometry (SEC-ESI-MS) provides a solution for this issue, as it enables the separation of differently charged fragments.

3

3. A Light Activated Reaction Manifold

The kinetic analysis in Chapter 3.3.2 was performed by D. D'Hooge (Department of Chemical Engineering and Technical Chemistry, Ghent University). Parts of the present chapter were reproduced with permission from K. Hiltebrandt, K. Elies, D. R. D'hooge, J. P. Blinco, C. Barner-Kowollik, *J. Am. Chem. Soc.*, **2016**, 138, 7048-7054. (DOI: 10.1021/jacs.6b01805). Copyright ACS 2016.

3.1. Motivation

In general, the simultaneous use of more than one reaction in a one-pot system can lead to the interference of the reaction processes with each other. Accordingly, the formation of unsolicited side-products, poor reaction yields, and restraints of the reactivity are possible consequences. A system including a molecule which enables two or more reaction paths that proceed independent from each other can overcome these mentioned disadvantages. In this respect, a reaction manifold is represented by one compound which can undergo at least two orthogonal reaction pathways depending on external trigger signals or – in a wider sense – on the employed reaction conditions.

A set of various methods that allow chemical selectivity have been reported.[290] In this regard, selectivity relies on a sequence of successive reaction steps yielding a target structure[291] or orthogonal reaction paths which are initiated due to distinct reactivities. For example, orthogonal polymerisation techniques for the design of nanocontainers,[292] the orthogonal design of covalent organic frameworks,[293] and a cascade of orthogonal photoconjugation as well as photocleavage reactions allowing hydrogels to tune in their properties[294] rely on systems featuring orthogonal reactivities. Furthermore, an orthogonal coupling strategy for the synthesis of dendrimers[295] and the bioorthogonal sequential immobilisation of polymers on defined surfaces have been introduced.[296] Nevertheless, the previously mentioned examples cannot be classified as reaction manifold because they require a compound for every reaction path.

The present chapter introduces a reaction manifold based on two orthogonal reaction paths of *o*-methyl benzaldehyde in a one-pot system: a light induced Diels-Alder reaction with maleimides on the one hand and a thermal imine formation with hexylamine during periods of non-irradiation on the other hand. Both reaction paths are depicted in Figure 14. Hereby, the orthogonal behaviour of both reaction paths is predominantly based on the structural disparity of the *o*-methyl benzaldehyde and its photoinduced *o*-quinodimethane (photoenol) state during irradiation.[297] In this regard, the reactive group in the dark is an aldehyde functionality whereas the reactive group of the photoenol state is a diene. The following section introduces a novel reaction pathway for the *o*-methyl benzaldehyde exploiting the electrophilic behaviour of aldehydes to add hexylamine yielding a stable imine. Furthermore, the photoinduced state of *o*-methyl

benzaldehyde – i.e. the photoenol – has been reported to react with electron-poor alkenes such as dithioesters,[184] maleimides[298] or diphenylcarbenes.[299] Since the photoreaction kinetics of the *o*-methyl benzaldehyde species are highly solvent dependent,[300],[301] the reaction manifold behaves differently in polar or non-polar solvents. The combination of the novel imine formation path with the basic photoreaction path of *o*-methyl benzaldehyde in dichloromethane as well as acetonitrile is presented in the following.

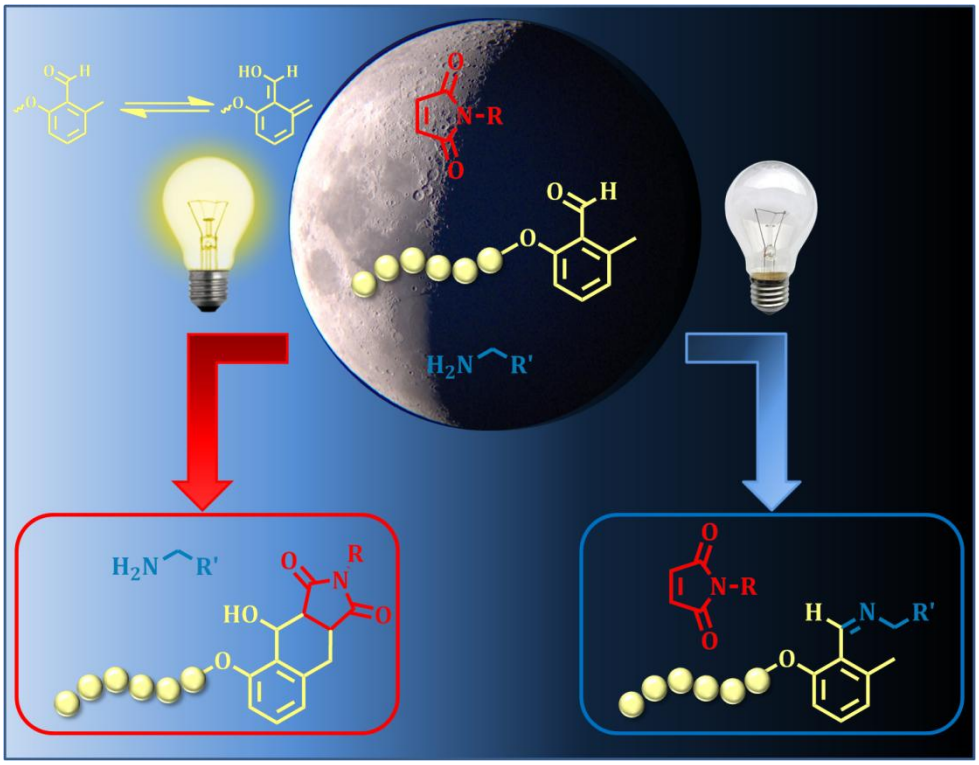

Figure 14: *A light induced reaction manifold consisting of a maleimide, hexylamine as well as o-methyl benzaldehyde. The o-methyl benzaldehyde functionality is able to undergo two independent reaction paths: an irreversible photoreaction with the maleimide and a non-irradiative imine formation with hexylamine. The image was modified from ref.*[297] *with permission from the American Chemical Society (ACS), 2016.*

3.2. The Imine Formation as a Novel Thermal Reaction Path for *o*-Methyl Benzaldehydes

The present section introduces the novel non-irradiative reaction pathway for the photoactive *o*-methyl benzaldehyde with hexylamine reversibly yielding an imine species as well as the behaviour of the imine during irradiation.

3.2.1. Investigation of the Imine Formation Procedure

The typical reaction path of an *o*-methyl benzaldehyde species is its photo triggered activation towards a diene (photoenol) compound, which undergoes a subsequent Diels-Alder reaction with electron-poor alkenes such as maleimides. The light induced reaction has been applied in many cases as an elaborate photochemical tool in order to perform functionalisation or ligation protocols. The detailed theoretical aspects of the light induced photoenol reaction is summarised in Chapter 2.4.1.

The alternative reaction path for *o*-methyl benzaldehyde is performed under non-irradiative conditions. Hereby, the aldehyde functionality of the *o*-methyl benzaldehyde species can be readily transformed with hexylamine into an imine (refer to Scheme 30).

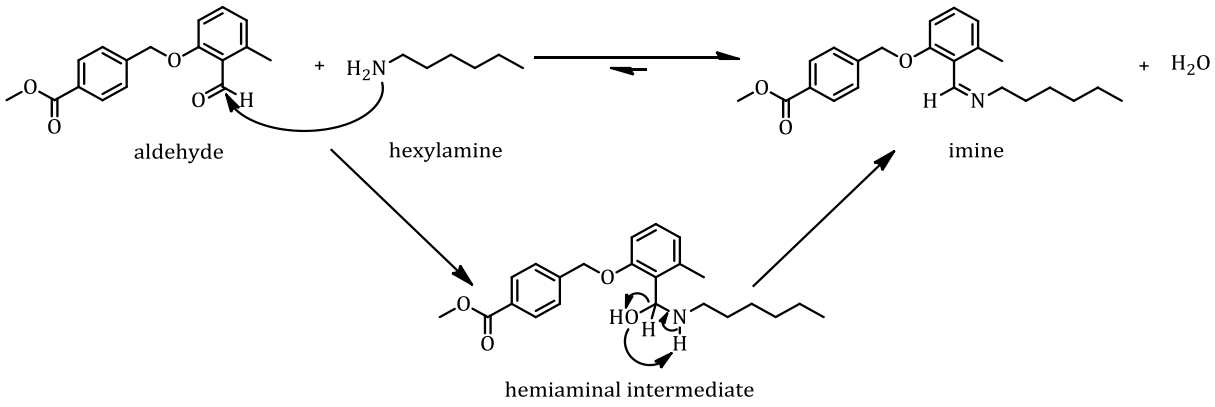

Scheme 30: *General mechanism of the thermal reaction between an o-methyl benzaldehyde compound and hexylamine leading to the initial formation of a hemiaminal intermediate which forms the imine species and water. The formation of the stable imine is favoured.*

The crucial aspect of this alternative reaction path is that it does not require light in order to induce a reaction for *o*-methyl benzaldehyde. Instead, this thermal process is a typical second-order reaction of the *o*-methyl benzaldehyde featuring several *click* criteria. In this regard, the reaction is catalyst-free and leads to a quantitative yield. The driving force of the imine formation rests on the nucleophilic addition of hexylamine onto the electron-rich aldehyde. Although, most imines are unstable and tend to undergo spontaneous hydrolysis,[302] the benzylic imine can be isolated and is stable under laboratory conditions. However, certain hydrolysis conditions still induce the re-formation of the aldehyde species. This versatile imine formation can be traced via ^{1}H NMR spectroscopy due to a distinct shift of the aldehyde signal (10.69 ppm) to the imine signal (8.63 ppm). The ^{1}H NMR study of the exemplary reaction between 4-((2-formyl-3-methylphenoxy)methyl)benzoate **1** and hexylamine **2** is depicted in Figure 15.

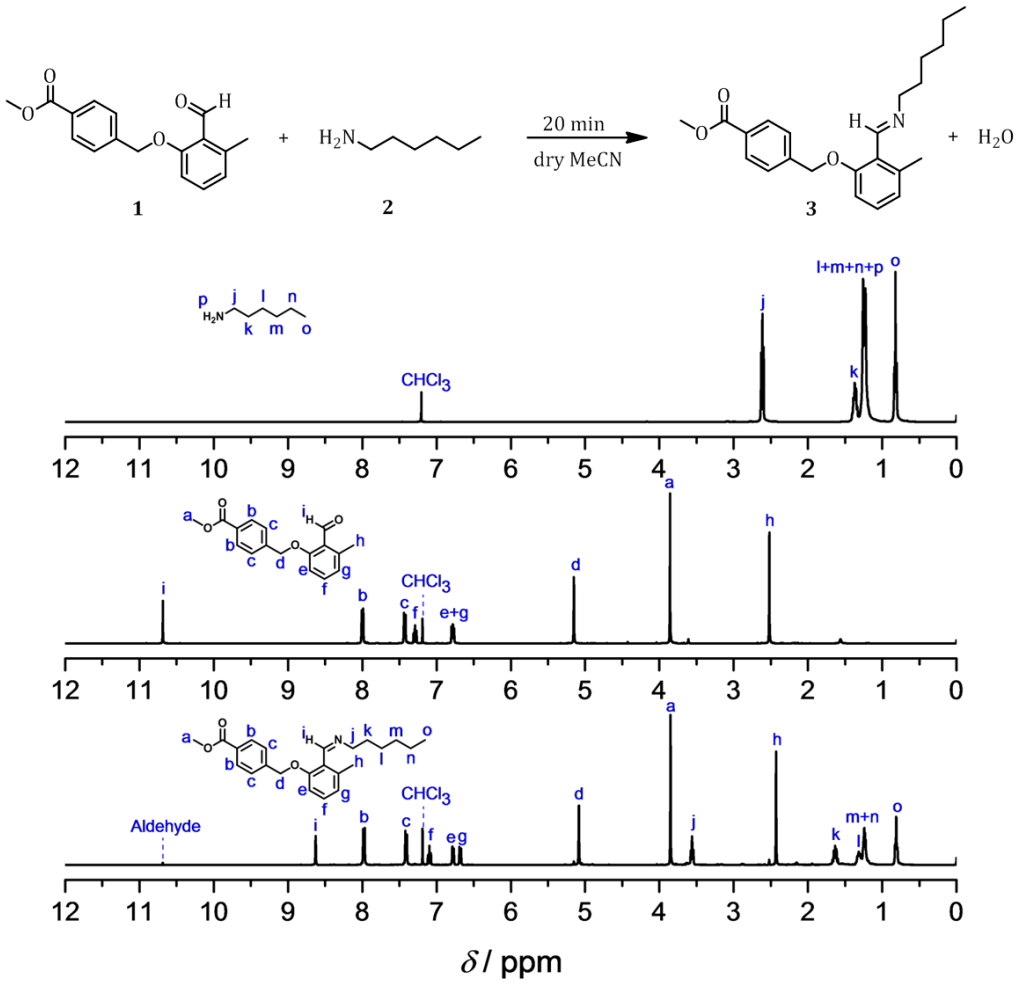

Figure 15: *^{1}H NMR study of the imine formation using methyl 4-((2-formyl-3-methylphenoxy)methyl)benzoate **1** (1.0 eq.) and hexylamine **2** (1.1 eq.) in $CDCl_3$. A clear shift of the arylic methyl resonance (h) and the aldehyde resonance (i) of the benzaldehyde species towards higher fields is displayed. The image was modified from ref.*[297] *with permission from the American Chemical Society (ACS), 2016.*

3.2.2. Photochemical Properties of the Benzylic Imine

The structural modification of the formed benzylic imine species compared to the *o*-methyl benzaldehyde moiety does not only lead to different spectroscopic resonances, as depicted in the previous section, but also to an altered interaction with light. In this context, the imine product shows a distinct blue shift of approximately 20 nm towards higher energetic UV-light in the UV/vis absorption spectrum (refer to Figure 16).

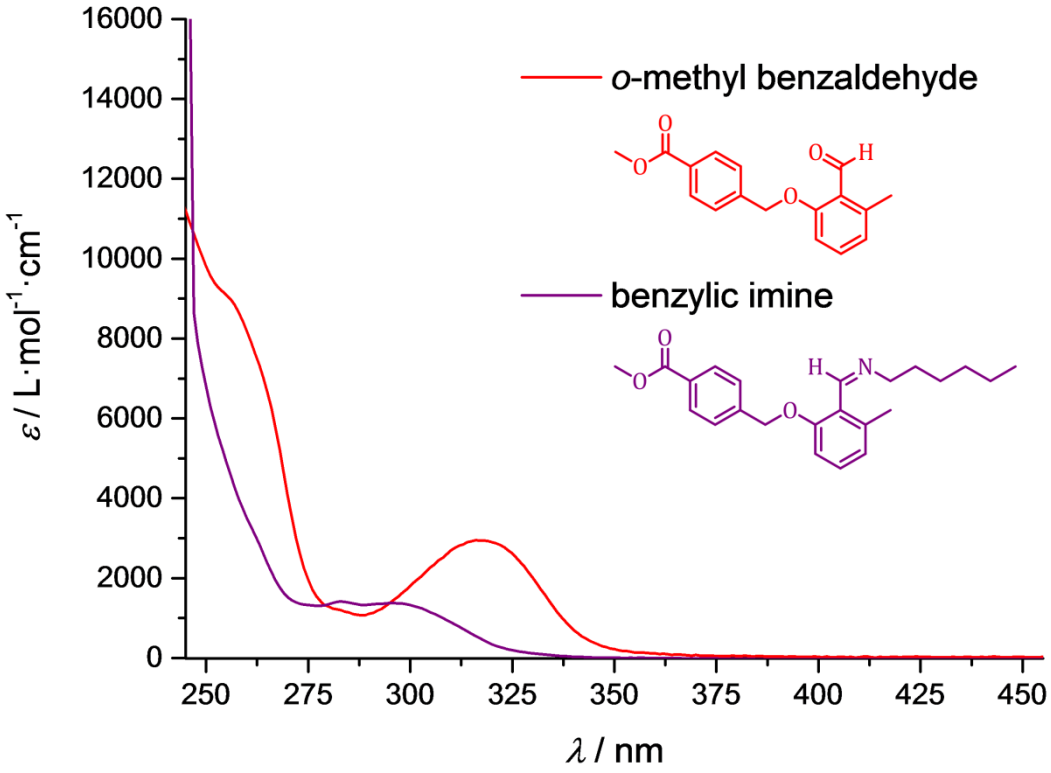

Figure 16: *Comparison of the UV/vis spectra between an o-methyl benzaldehyde species and a benzylic imine moiety whereby the imine absorption is noticeably blue-shifted. The image was modified from ref.*[297] *with permission from the American Chemical Society (ACS), 2016.*

In addition, from a different light absorption, *o*-methyl benzaldehyde and the thereof resulting imine species show an opposing photochemical behaviour. Hereby, *o*-methyl benzaldehyde is a versatile photoactive compound which undergoes photoenolisation resulting in a highly reactive diene in the presence of an appropriate light source. It is not sure if the obtained imine species, derived from *o*-methyl benzaldehyde and hexylamine, is able to undergo a similar photoenolisation process. Nevertheless, irradiation experiments illustrate that the benzylic imine is no longer a photoactive compound.[303] Hence, the benzylic imine is not able to undergo light induced reactions with maleimides.

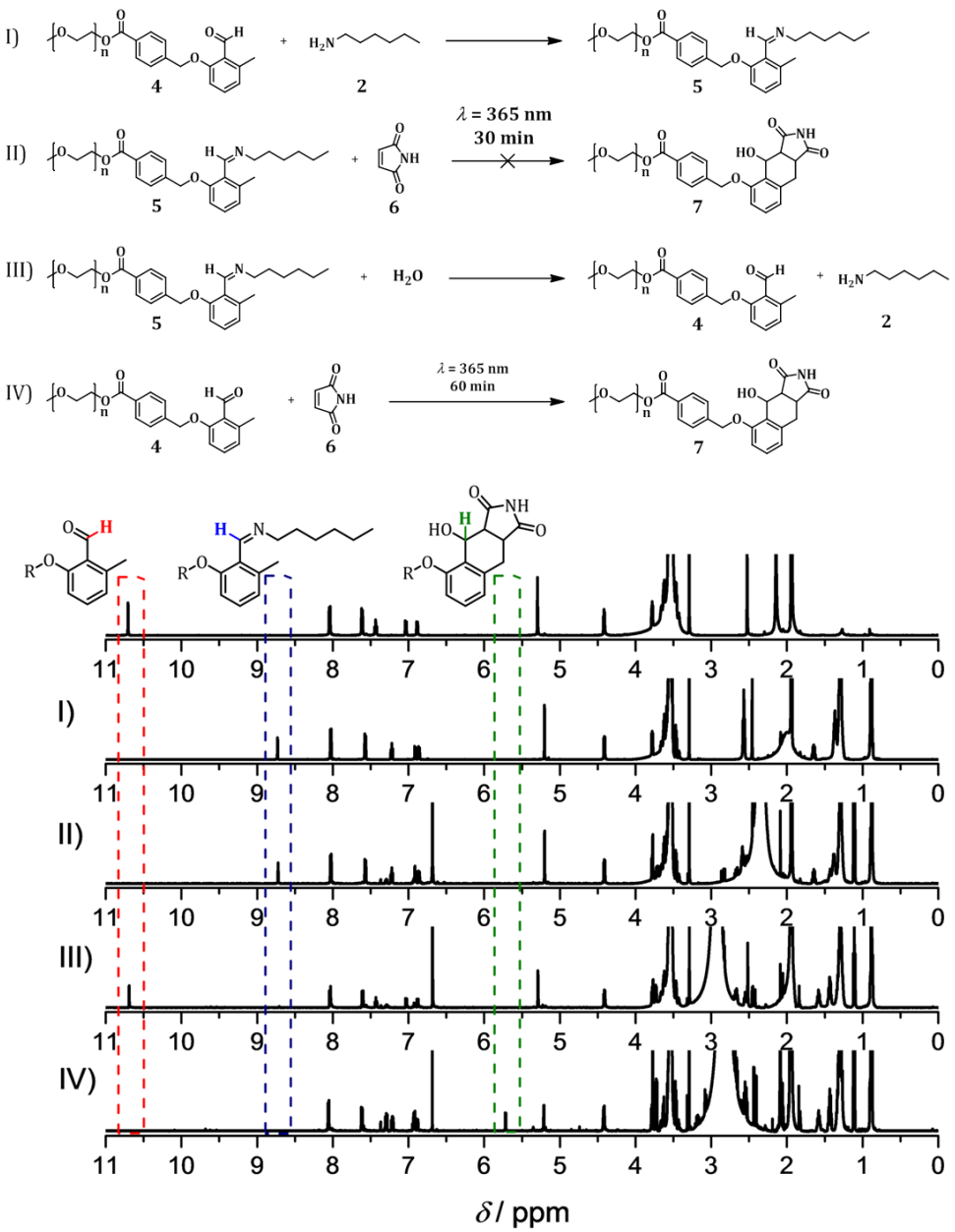

Figure 17: *^{1}H NMR analysis of the imine protection group during irradiation in CD_3CN. The aldehyde signal (**δ** = 10.71 ppm) indicates the presence of the photoactive benzaldehyde **4** (top row). The imine transformation of the benzaldehyde with hexylamine **2**, yielding the imine **5** is traced by the occurrence of the imine signal at **δ** = 8.72 ppm (I). The irradiation of **5** with the maleimide **6** does not result in the Diels-Alder product **7**. The imine signal (**δ** = 8.72 ppm) remains unchanged (II). The hydrolysis of the imine **5** with D_2O and acetic acid results in the back formation of the photoactive aldehyde moiety, which can be traced by the presence of the aldehyde signal (**δ** = 10.71 ppm) and the absence of the imine signal (III). The subsequent irradiation of the obtained benzaldehyde **4** with **6** leads to the formation of the Diels-Alder product **7**, which can be verified by the ring formation (**δ** = 5.72 ppm) and the absence of the aldehyde signal (IV). The picture was modified from ref.*[303] *with permission from the Royal Society of Chemistry (RSC), 2016.*

The implementation of the imine functionality as a reversible and versatile photochemical protection group for *o*-methyl benzaldehyde was evidenced via a ^{1}H NMR analysis of a one-pot system containing *o*-methyl benzaldehyde terminated poly(ethylene glycol) **4** (benzaldehyde terminated PEG), hexylamine **2**, and maleimide **6** (refer to Figure 17). Initially, **4** and **2** were dissolved for 24 h in deuterated acetonitrile (step I). Then, **6** was added to the solution of step I and the system was irradiated with the PL-L lamp ($\boldsymbol{\lambda}$ = 310-440 nm; $\boldsymbol{\lambda}_{max}$ = 365 nm; 36 W). However, irradiation of the solution did not result in the formation of the Diels-Alder product **7** (step II). As a result, the experimental data of step II proves unambiguously the efficiency of the imine protection group for *o*-methyl benzaldehydes. Subsequently, hydrolysis of **5** was performed by the addition of an excess of deuterated water (250 eq.) as well as acetic acid to the solution, which led to the re-formation of the *o*-methyl benzaldehyde terminated PEG **4** (step III). The previously mentioned step illustrates the plain reversibility of the imine protection group. Although, the benzylic imine is stable while being dissolved, the addition of extensive amounts of water induce an immediate hydrolysis of the imine functionality. The solution of step III was irradiated at $\boldsymbol{\lambda}_{max}$ = 365 nm leading to the irreversible formation the Diels-Alder product **7**. The last step demonstrates that the removal of the imine functionality re-generates the photoactive *o*-methyl benzaldehyde group which is again able to undergo a light induced Diels-Alder reaction with maleimides.

3.3. Kinetic Competition between the Imine Formation and the Photoreaction

In non-polar solvents such as dichloromethane (DCM), the kinetics of the photoreaction between *o*-methyl benzaldehyde and a maleimide moiety only slightly exceed the kinetics of the darktime imine formation between *o*-methyl benzaldehyde and hexylamine. Hence, a mixture of *o*-methyl benzaldehyde terminated **4** and ethyl maleimide **8** in dichloromethane was irradiated with the PL-L lamp (λ = 310-440 nm; λ_{max} = 365 nm; 36 W) for several time intervals to determine the photoreaction kinetics. The experimental data of the kinetics and the emission spectra of the light sources are presented in chapter 7. Furthermore, a mixture of **4** and **2** in dichloromethane was stirred for preset time periods in order to determine the imine formation kinetics. The evolution of both products was analysed via high resolution mass spectrometry. The Diels-Alder product was obtained after 7.5 min whereas the imine formation took 90 min (refer to Figure 18).

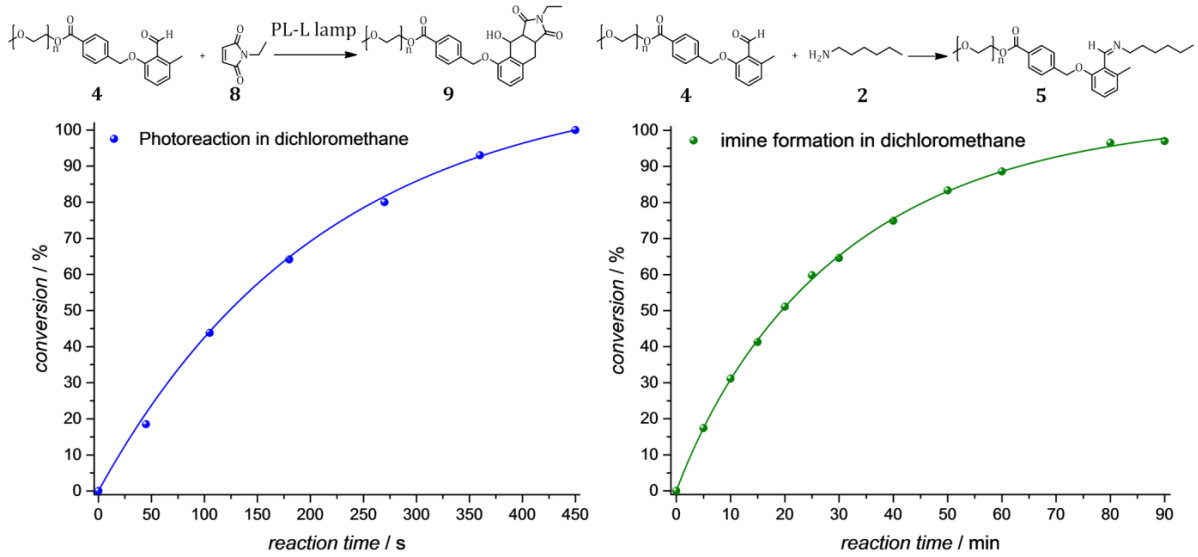

Figure 18: *The reaction kinetics of both the photoreaction and the imine formation were determined via Orbitrap ESI-MS. A diluted solution of* ***4*** *and* ***8*** *was irradiated with the PL-L lamp in DCM for 45 s, 105 s, 180 s, 270 s, 360 s, and 450 s (left). A diluted solution of* ***4*** *and* ***2*** *was stirred at ambient temperature for 5 min, 10 min, 15 min, 20 min, 25 min, 30 min, 40 min, 50 min, 60 min, 80 min, and 90 min (right). The image was modified from ref.*[297] *with permission from the American Chemical Society (ACS), 2016.*

Although the photoreaction is faster than the imine formation, a significant imine yield of approximately 25 % is obtained after 7.5 min (refer to Figure 18). The kinetic

investigation elucidated that both reaction paths proceed in a similar time range. Nevertheless, both reactions require a different trigger. The reaction between the *o*-methyl benzaldehyde and the maleimide species is light induced while the imine formation is immediately initiated after *o*-methyl benzaldehyde and hexylamine are combined regardless if a light source is switched on or off. For this reason, the reaction manifold shows orthogonality in the darktime. In contrast, the photo induced reaction path as well as the imine formation compete against each other within the reaction manifold during irradiation, with a strong preference for the light driven process as will be described below.

3.3.1. Semi-qualitative Kinetic Simulation of the Reaction Manifold

A theoretical reaction manifold consisting of *o*-methyl benzaldehyde terminated PEG **4** (M = 2000 g·mol^{-1}), ethyl maleimide **8** (M = 125.13 g·mol^{-1}), and hexylamine **2** (M = 101.19 g·mol^{-1}) was investigated via a semi-qualitative kinetic simulation by applying the PREDICI® program package. Hereby, the evolution of the photo induced Diels-Alder product **9** as well as the formed benzylic imine **5** were calculated in the presence of varying maleimide concentrations (refer to Figure 19).

The mechanism of the reaction manifold consists of four elementary reactions that compete with each other as depicted in Figure 19 a. It is established that the photochemical irradiation of the *o*-methyl benzaldehyde compound results in the formation of an E/Z mixture of the activated diene (photoenol) (refer to chapter 2.4.1). In this case, the E-form of the photoenol is exclusively able to undergo the Diels-Alder reaction with the ethyl maleimide **8**, while the Z-form of the photoenol is immediately reverted to the molecular ground state carrying the aldehyde functionality (*o*-methyl benzaldehyde). For that reason, the light induced process can be described as an equilibrium between the *o*-methyl benzaldehyde and the photoenol species. The rate coefficient of the photoenol deactivation (k_{deact} = 5·10^{-1} s^{-1}) was estimated based on the average lifetime of the deactivation process (τ = 2 s).[304] Moreover, the rate coefficient for the activation step of *o*-methyl benzaldehyde was adjusted according to

experimental data (refer to Figure 18), resulting in $k_{act} = 1.25 \cdot 10^{-1}\ s^{-1}$. The rate coefficient k_{photo} of the Diels-Alder reaction was assigned 50 $L \cdot mol^{-1} \cdot s^{-1}$ whereas the rate coefficient for the imine formation k_{imine} was set to 0.2 $L \cdot mol^{-1} \cdot s^{-1}$. Both rate coefficients were determined by a linear fitting of the second-order reactions. The values for both rate coefficients are in good agreement with the previously presented experimental kinetic data. Since light triggers the transformation of the *o*-methyl benzaldehyde into photoenol and the Z isomer of the photoenol reverts to the aldehyde form, the simulation of an irradiative process requires both k_{act} and k_{deact}. The simulation of an ideal darktime reaction does not include the activation of the *o*-methyl benzaldehyde by light which means k_{act} is set to 0. The simulation illustrates – not surprisingly – that the Diels-Alder reaction does not take place under non-irradiative conditions regardless of the maleimide concentration.

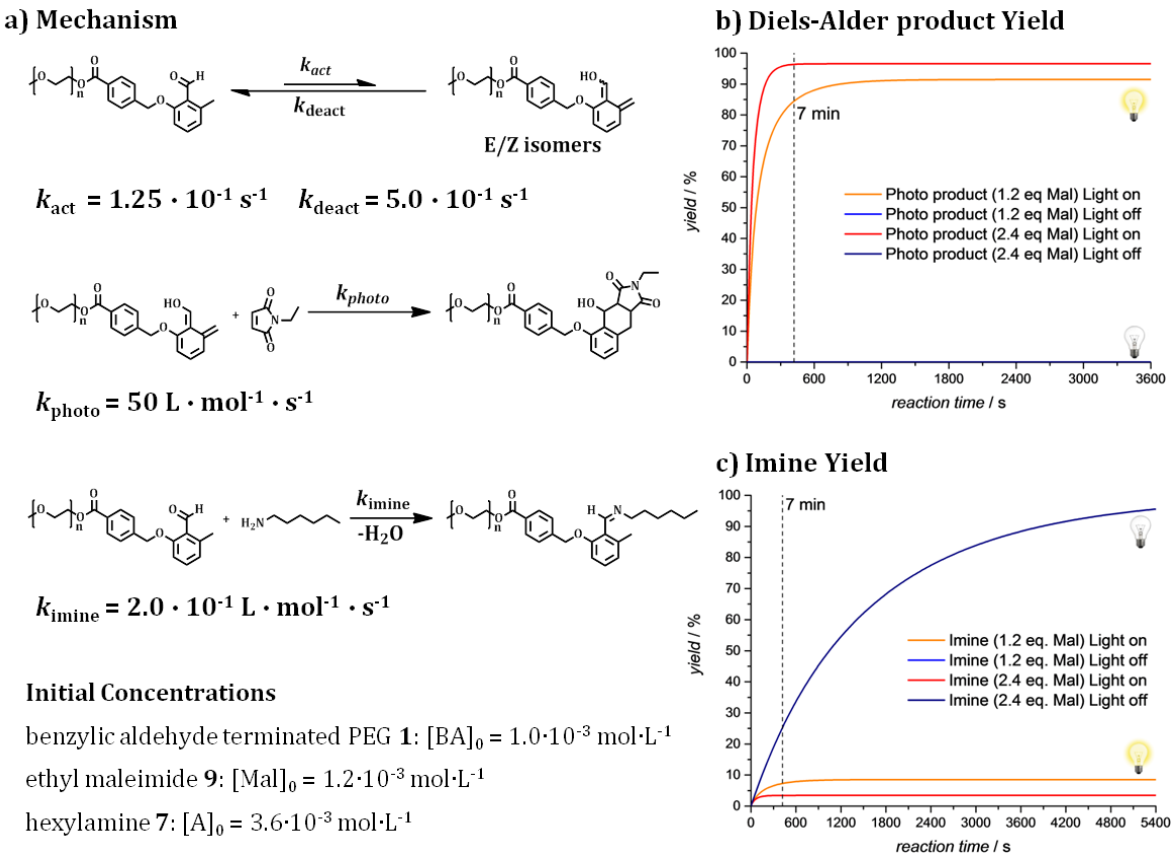

Figure 19: *The mechanism of the proposed light triggered reaction manifold is depicted including the assessed rate coefficients. The yield vs. time evolutions are simulated using the PREDICI® software package. The reactions entail an equilibrium between the o-methyl benzaldehyde PEG **4** and an in situ formed photoenol species, the [4+2]-cycloaddition of the photoenol (the diene or o-quinodimethane) with ethyl maleimide **8**, and the imine formation based on the reaction of **4** with hexylamine **2**. An increasing maleimide concentration leads to a higher Dies-Alder yield with a simultaneous decrease of the imine yield during irradiation. Non-irradiative conditions trigger only the imine reaction because no diene (o-quinodimethane) is present. The image was modified from ref.*[297] *with permission from the American Chemical Society (ACS), 2016.*

Instead, the imine formation proceeds in agreement with the kinetic data (refer to Figure 18) and yields 25 % after 7 min. Furthermore, a Diels-Alder product yield of 85 % is achieved in a manifold system containing 1.2 eq. maleimide and a yield of 97 % with 2.4 eq. maleimide after 7 min during irradiation. The respective imine yields are 7 % (1.2 eq. maleimide) and 3 % (2.4 eq.) under irradiative conditions after the same time. The simulated data evidence the clear influence of the maleimide concentration on the photoreaction path in the reaction manifold. The higher the concentration of **8** in the system, the more favoured becomes the light induced Diels-Alder product and the more suppressed is the imine formation.

The time-dependent progression of the concentrations featuring all inherent species that occur in the reaction manifold (1.2 eq. maleimide) (refer to Figure 19) during irradiation is depicted in Figure 20. The consumption of the *o*-methyl benzaldehyde is related to an intense increase of the Diels-Alder product concentration in combination with a slight increase of the imine concentration. Hereof, the photoenol concentration is initially increased followed by a subsequent consistent decrease, proving the existence of an equilibrium between the *o*-methyl benzaldehyde and the photoenol species. In addition, the evolution of all compounds underpins that the equilibrium is shifted to the photoenol moiety due to the fact that photoenol undergoes a reaction with maleimides, yet does not react with hexylamine.

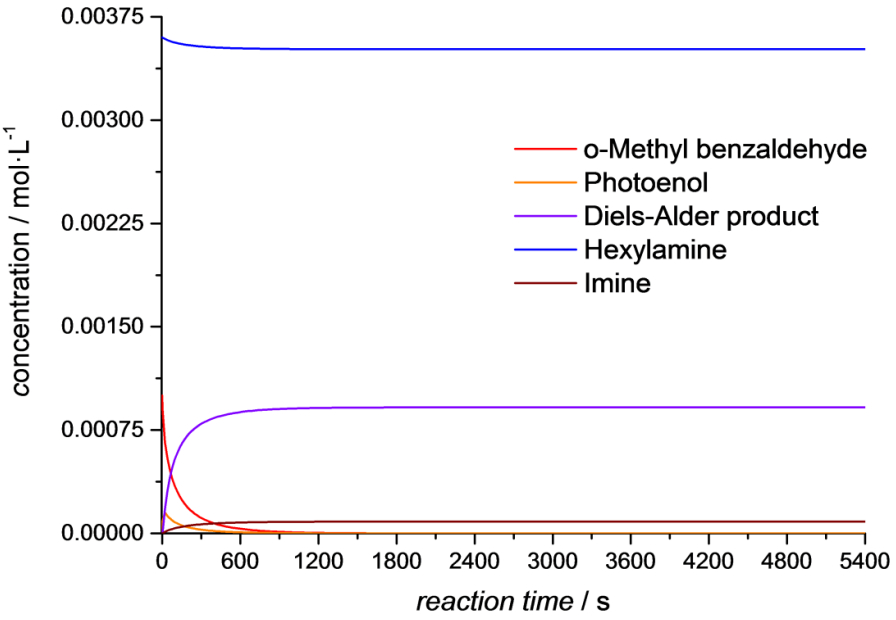

Figure 20: *Evolution of the concentrations of o-methyl benzaldehyde terminated PEG* ***4*** *(BA) (1.0 eq.), photoenol terminated PEG (PE), ethyl maleimide* ***8*** *(Mal) (1.2 eq.), hexylamine* ***2*** *(A) (3.6 eq.), benzylic imine terminated PEG* ***5****, and the photo product* ***9*** *as a function of time. The image was modified from ref.*[297] *with permission from the American Chemical Society (ACS), 2016.*

The assessed equilibrium coefficient was determined by the ratio of k_{act}/k_{deact} resulting in a value of 0.25. The time-dependent evolution of the ratio between the photoenol concentration [PE] and the *o*-methyl benzaldehyde concentration [BE] provides an explicit indication if the activation/deactivation process adjusts to the theoretically determined equilibrium constant. The manifold system with 1.2 eq. of maleimide and the one with 2.4. eq. of maleimide approach instantly a value of 0.24 and 0.22, respectively (refer to Figure 21).

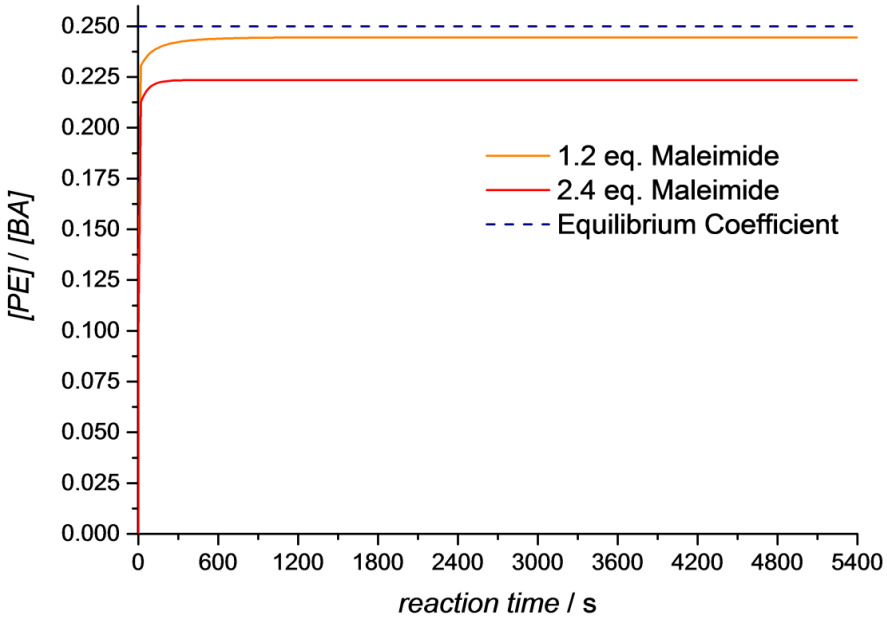

Figure 21: *Ratio of the concentration of the photoenol terminated PEG (PE) and the o-methyl benzaldehyde terminated PEG (BA) from Figure 20. The image was modified from ref.*[297] *with permission from the American Chemical Society (ACS), 2016.*

The previously obtained results can be summarised into three aspects. First, the *o*-methyl benzaldehyde reacts solely with hexylamine under non-irradiative conditions whereas the photoenol intermediate undergoes an exclusive light triggered [4+2]-cycloaddition with maleimides. In this context, a converse reactivity is inhibited, because the amine functionality can only attack the electrophilic aldehyde functionality of the ground state and the maleimide requires an electron-rich diene, such as photoenol, for the Diels-Alder reaction. Secondly, the *o*-methyl benzaldehyde and its photoenol state are in an equilibrium during irradiation. Even though one species is consumed in a reaction, the remaining compounds revert back to the equilibrium. Thirdly, the equilibrium is strongly influenced by a change in the maleimide concentration.

The three mentioned aspects are predictions of Le Chatelier's principle. Therefore, it can be assumed that ethyl maleimide **8** acts as a photoenol trap in the light induced reaction

manifold since the Diels-Alder reaction is irreversible in this case. The fast and consistent consumption of photoenol by the Diels-Alder reaction catalyses the transformation *o*-methyl benzaldehyde into photoenol during irradiation. The decreasing amount of accessible *o*-methyl benzaldehyde drastically reduces the imine formation. A schematic overview of the principle is depicted in Scheme 31.

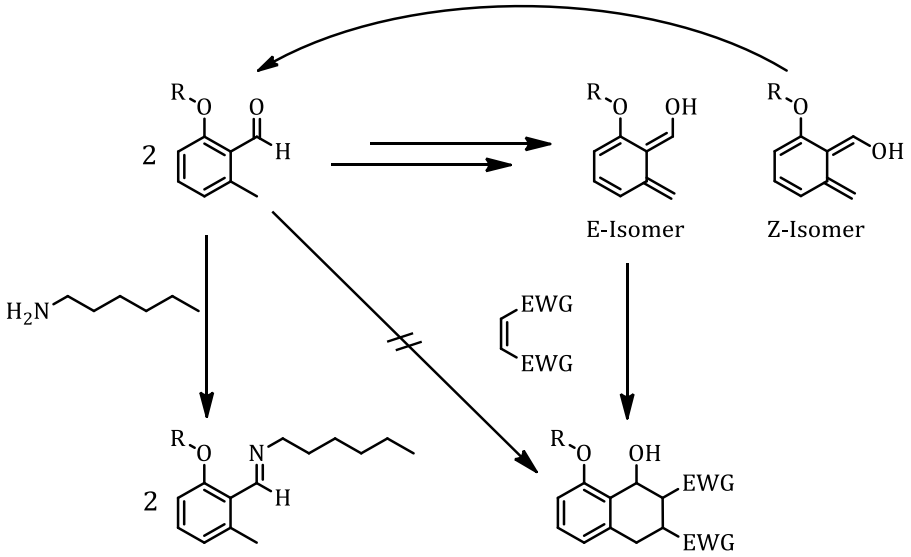

Scheme 31: *The light induced equilibrium between the o-methyl benzaldehyde and the photoenol (diene) form can be shifted towards the latter due to the presence maleimides during irradiation. The electron-poor ene acts as a diene trap for the E isomer of the o-quinodimethane, while the Z isomer is rapidly reverted to the aldehyde form leading to the fast and continuous light induced reformation of both diene forms. Therefore, the imine formation based on the o-methyl benzaldehyde is strongly suppressed. The image was modified from ref.*[297] *with permission from the American Chemical Society (ACS), 2016.*

3.3.2. Basic Kinetic Analysis of the Operational Principle of the Reaction Manifold

The light induced reaction manifold combines two independent reaction paths: a photochemically triggered Diels-Alder reaction as well as an imine formation.

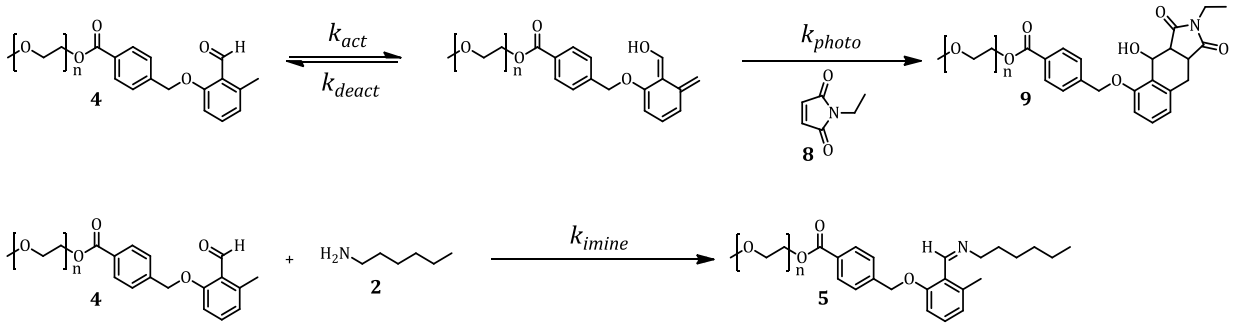

Scheme 32: *Overview of the photoreaction (top) as well as the imine formation (down) including kinetic rate coefficients. The image was modified from ref.*[297] *with permission from the American Chemical Society (ACS), 2016.*

The concentrations of the *o*-methyl benzaldehyde terminated PEG **4**, the photoenol terminated PEG, the ethyl maleimide **8**, the hexylamine **2**, the Diels-Alder product **9**, and the imine product **5** are defined as [BA], [PE], [Mal], [A], [PEMal] and [I], respectively.
The reaction manifold is characterised by the following differential equations whereby any volume effects are neglected:

$$\frac{\mathrm{d[BA]}}{\mathrm{dt}} = -k_{\mathrm{act}}[\mathrm{BA}] + k_{\mathrm{deact}}[\mathrm{PE}] - k_{\mathrm{imine}}[\mathrm{A}][\mathrm{BA}] \quad \text{(I)}$$

$$\frac{\mathrm{d[PE]}}{\mathrm{dt}} = k_{\mathrm{act}}[\mathrm{BA}] - k_{\mathrm{deact}}[\mathrm{PE}] - k_{\mathrm{photo}}[\mathrm{PE}][\mathrm{Mal}] \quad \text{(II)}$$

$$\frac{\mathrm{d[Mal]}}{\mathrm{dt}} = -k_{\mathrm{photo}}[\mathrm{PE}][\mathrm{Mal}] \quad \text{(III)}$$

$$\frac{\mathrm{d[PEMal]}}{\mathrm{dt}} = k_{\mathrm{photo}}[\mathrm{PE}][\mathrm{Mal}] \quad \text{(IV)}$$

$$\frac{\mathrm{d[A]}}{\mathrm{dt}} = -k_{\mathrm{imine}}[\mathrm{A}][\mathrm{BA}] \quad \text{(V)}$$

$$\frac{\mathrm{d[I]}}{\mathrm{dt}} = k_{\mathrm{imine}}[\mathrm{A}][\mathrm{BA}] \quad \text{(VI)}$$

Assumption of the quasi-steady state approximation for the photoenol species leads to the following equation:

$$0 = k_{\mathrm{act}}[\mathrm{BA}] - k_{\mathrm{deact}}[\mathrm{PE}] - k_{\mathrm{photo}}[\mathrm{PE}][\mathrm{Mal}] \quad \text{(VII)}$$

or

$$[\mathrm{PE}] = \frac{k_{\mathrm{act}}[\mathrm{BA}]}{k_{\mathrm{deact}} + k_{\mathrm{photo}}[\mathrm{Mal}]} \quad \text{(VII)}$$

The parameter optimisation, according to Chapter 3.3.1, is based on the experimental product yield stating that $k_{\mathrm{deact}} = 0.5\ \mathrm{s^{-1}}$ and $k_{\mathrm{photo}} = 50\ \mathrm{L{\cdot}mol^{-1}{\cdot}s^{-1}}$ leading to:

$k_{deact} >> k_{photo}$ [Mal]. For instance, assuming $[Mal]_0 = 1 \cdot 10^{-3}$ mol·L^{-1}, it follows that $k_{deact} = 0.5$ s^{-1} >> $k_{photo} \cdot [Mal]_0 = 0.06$ s^{-1} and thus a first approximation for the equation IX:

$$[PE] = \frac{k_{act}}{k_{deact}}[BA] \quad (IX)$$

Therefore, the kinetic rate law expression for the photoproduct **9** is:

$$\frac{d[PEMal]}{dt} = k_{photo}[PE][Mal] = \frac{k_{act}}{k_{deact}} k_{photo}[BA][Mal] \quad (X)$$

The kinetic rate law expression of the imine product **5** reads:

$$\frac{d[I]}{dt} = k_{imine}[BA][A] \quad (XI)$$

The instantaneous ratio between the imine **5** and photoproduct **9** is described by the ratio of the equations X and XI:

$$\frac{d[I]}{d[PEA]} = \frac{k_{imine}[BA][A]}{k_{photo}[PE][Mal]} = k_{imine}[BA][A]\frac{k_{act}}{k_{deact}} k_{photo}[BA][Mal] \quad (XII)$$

$$\frac{d[I]}{d[PEA]} = \frac{k_{deact}}{k_{act}}\frac{k_{imine}}{k_{photo}}\frac{[A]}{[Mal]} \quad (XIII)$$

The above equation states that an increase of the maleimide concentration [Mal] suppresses the imine formation for a given amine concentration [A]. In summary, the results of the above kinetic analysis are in perfect agreement with the PREDICI® simulation.

3.3.3. Experimental Investigation of a Switchable System

The computer-based simulation of the light induced reaction manifold containing the *o*-methyl benzaldehyde terminated PEG **4**, hexylamine **2**, and ethyl maleimide **8** in various concentrations has been initially performed. The obtained data for the hypothesis that the equilibrium between the *o*-methyl benzaldehyde and the photoenol species can be shifted by an increase in the maleimide amount according to Le Chatelier. Nevertheless, the results rely on several assumptions and mechanistic simplifications. Thus, the theoretically assessed concept of the light induced reaction manifold requires an

experimental validation. A switching experiment was performed using a mixture of *o*-methyl benzaldehyde terminated PEG **4** (1.0 eq.), hexylamine **2** (3.6 eq.), and ethyl maleimide **8** (1.2 eq.) in dry dichloromethane. The solution was initially irradiated for 1 min with the PL-L lamp (λ = 310-440 nm; λ_{max} = 365 nm) and was subsequently left for 5 min in the dark. All in all, the switching on and off procedure of the system was repeated three times. The solution containing the manifold system was analysed immediately via high resolution mass spectrometry after every switching on or off cycle in order to characterise the products in time. Besides, the yields of the Diels-Alder product **9** as well as the imine product **5** and the overall *o*-methyl benzaldehyde conversion were measured via high resolution mass spectrometry (refer to Figure 22).

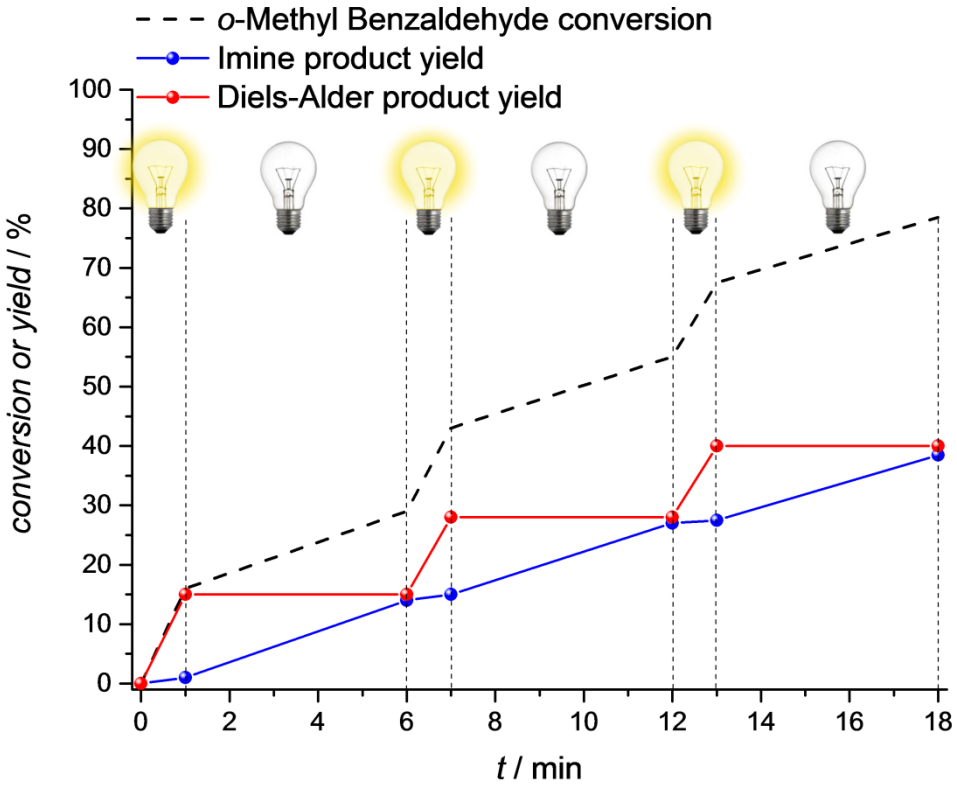

Figure 22: *A switchable system containing o-methyl benzaldehyde terminated PEG **4** (1.0 eq.), ethyl maleimide **8** (1.2 eq.), and hexylamine **2** (3.6 eq.), which was irradiated for 1 min and left non-irradiated for 5 min in an alternating fashion (three on-off cycles). The yield of the Diels-Alder product **9**, the yield of the benzylic imine **5**, and the o-methyl benzaldehyde conversion were determined via high resolution mass spectrometry: a linear interpolation was performed for simplicity. The image was modified from ref.*[297] *with permission from the American Chemical Society (ACS), 2016.*

The Diels-Alder product yield was increased during irradiation whereas no Diels-Alder product was detectable in the darktime due to the light dependent presence of photoenol. Instead, the imine was formed during the entire cycle, yet the yield was clearly suppressed during irradiation whereas the imine formation remained unaffected

without irradiation. The imine suppression during light exposure is a clear indication of a reduced *o*-methyl benzaldehyde concentration, based on a shift in the photochemical equilibrium towards the photoenol species. In this regard, the photoenol undergoes a fast [4+2]-cycloaddition with ethyl maleimide. In other words, the photoenol function is photochemically trapped by the maleimide compound and removed continuously from the equilibrium, which is the driving force for the steady reformation of photoenol under irradiative conditions. The experimental data required a comparison with the simulated data. Therefore, the same system was irradiated continuously for 7 min in dichloromethane featuring an ethyl maleimide amount of 1.2 eq. and 2.4. eq., respectively. The imine yield after irradiation was determined via ^{1}H NMR spectroscopy as well as high resolution mass spectrometry.

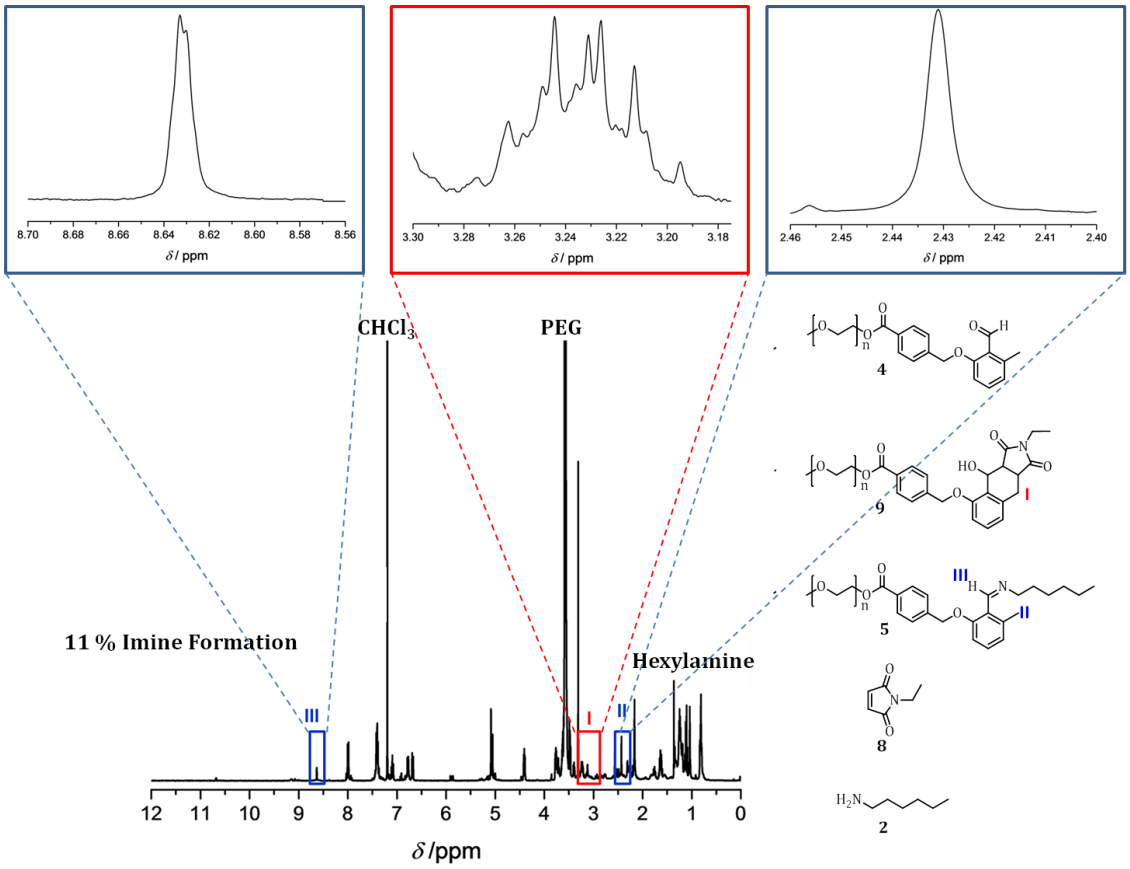

Figure 23: *^{1}H NMR data of the irradiation experiment of a system containing o-methyl benzaldehyde terminated PEG **4** (1.0 eq.), ethyl maleimide **8** (1.2 eq.), and hexylamine **2** (3.6 eq.) in dichloromethane. The imine yield is 11±2 % by assessing the imine resonance at 8.63 ppm and 2.43 ppm in relation to the aromatic signals at 8 ppm. The image was modified from ref.*[297] *with permission from the American Chemical Society (ACS), 2016.*

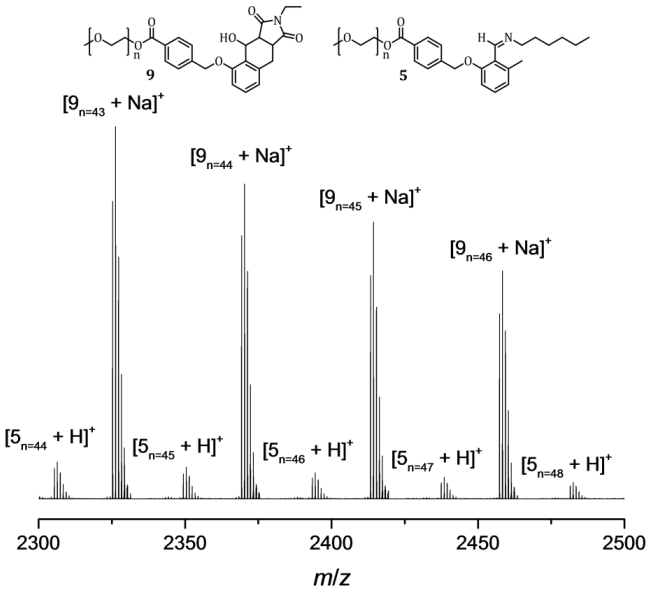

Figure 24: *A system containing o-methyl benzaldehyde terminated PEG* ***4*** *(1.0 eq.), ethyl maleimide* ***8*** *(1.2 eq.), and hexylamine* ***2*** *(3.6 eq.) in dichloromethane was irradiated for 7 min with a fluorescent PL-L lamp. The photo-cycloadduct* ***9*** *and the formed imine* ***5*** *were detected via Orbitrap ESI-MS. The yield of the imine species is 8±2 %. The image was modified from ref.*[297] *with permission from the American Chemical Society (ACS), 2016.*

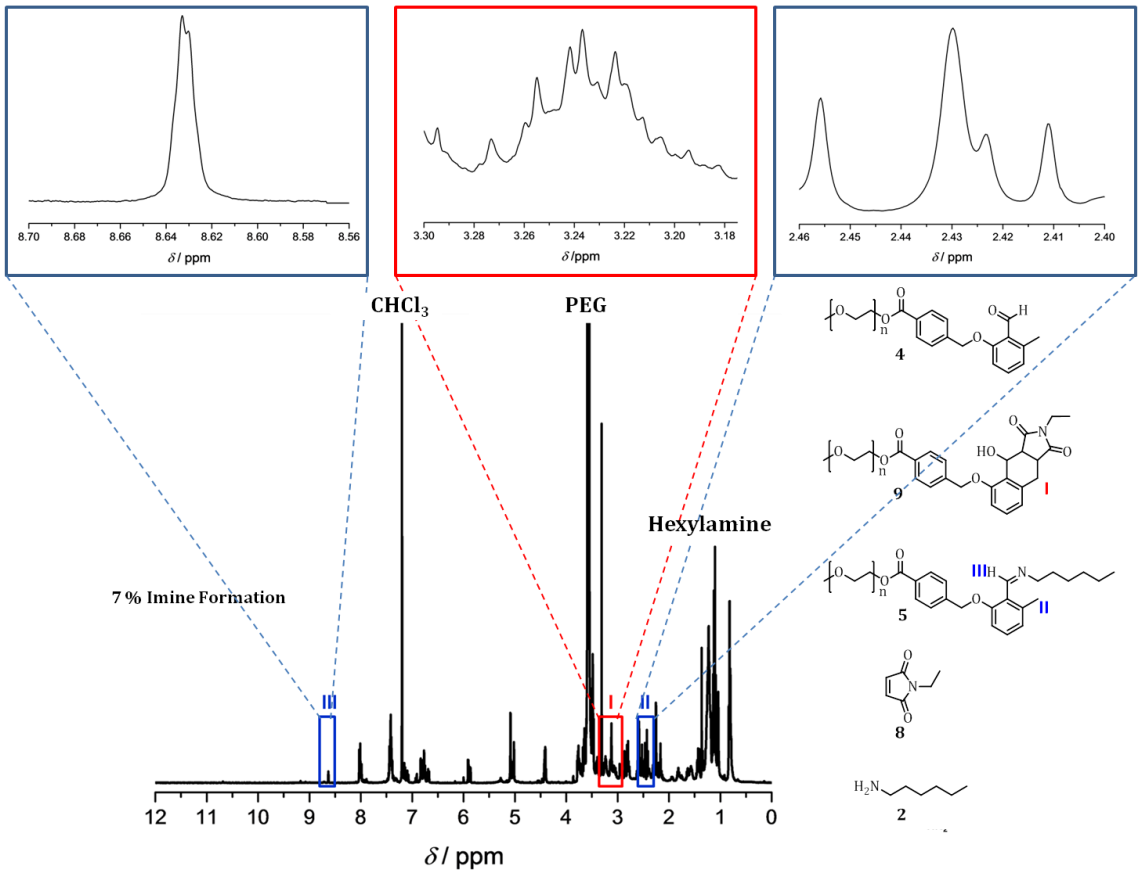

Figure 25: *^{1}H NMR data of the irradiation experiment of a system containing o-methyl benzaldehyde terminated PEG* ***4*** *(1.0 eq.), ethyl maleimide* ***8*** *(2.4 eq.), and hexylamine* ***2*** *(3.6 eq.) in dichloromethane. The imine yield is 7±2 % via assessment of the imine resonance at 8.63 ppm and 2.43 ppm in relation to the aromatic signals at 8 ppm. The image was modified from ref.*[297] *with permission from the American Chemical Society (ACS), 2016.*

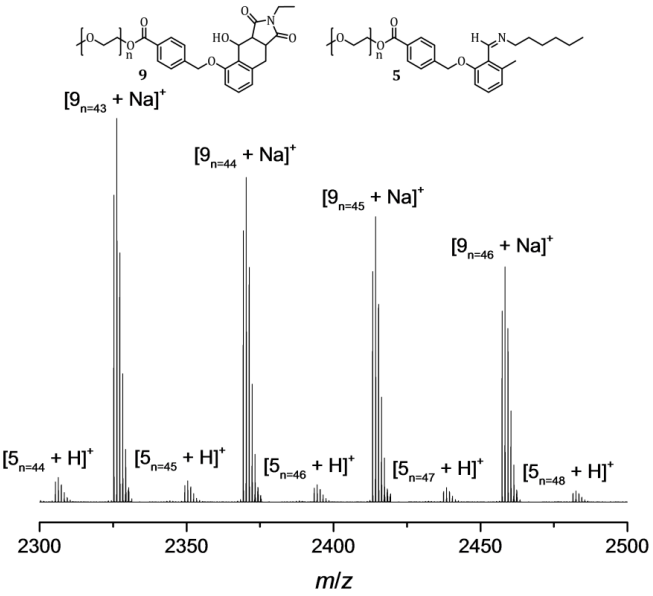

Figure 26: *A system containing o-methyl benzaldehyde terminated PEG* ***4*** *(1.0 eq.), ethyl maleimide* ***8*** *(2.4 eq.), and hexylamine* ***2*** *(3.6 eq.) in dichloromethane was irradiated for 7 min with a fluorescent PL-L lamp. The photo-cycloadduct* ***9*** *and the formed imine* ***5*** *were detected via Orbitrap ESI-MS. The yield of the imine species is 5±2 %. Reproduced with permission from the American Chemical Society.*

The reaction manifold system with an amount of 1.2 eq. maleimide resulted in an imine yield of 11±2 % according to ^{1}H NMR spectroscopy (refer to Figure 23) and 8±2 % according to mass spectrometric analysis (refer to Figure 24) after an irradiation time of 7 min. The imine formation in a system featuring 2.4 eq. ethyl maleimide **8** yields 7±2 % (determined via ^{1}H NMR spectroscopy) and 5±2 % (determined via Orbitrap ESI-MS) under the same conditions. The comparison of the experimental data with the simulated data of Chapter 3.3.1 is depicted in Table 1. It becomes apparent that the experimental data corroborate the theoretically simulated data.

PREDICI® simulation					Experiment	
Maleimide amount	*o*-Methyl benzaldehyde	Photoenol (diene)	Diels-Alder product	Imine	Diels-Alder product	Imine
0.0 eq.	75 %	0 %	0 %	25 %	0 %	23±2 %
1.2 eq.	7 %	1 %	85 %	7 %	92±2 %	8±2 %
2.4 eq.	0 %	0 %	97 %	3 %	95±2 %	5±2 %

Table 1: *Comparison of the Diels-Alder product yield and the imine yield determined by semi-qualitative PREDICI® simulations as well as experiments (mass spectrometric derived yields are shown) after a reaction of 7 min. In addition, the simulated non-converted fraction of the o-methyl benzaldehyde and the photoenol (diene) are added. The image was modified from ref.*[297] *with permission from the American Chemical Society (ACS), 2016.*

All in all, it can be stated that a reaction manifold in non-polar solvents such as dichloromethane, achieves orthogonality due to the suppression of the imine formation path by the light induced Diels-Alder reaction path in combination with a slight kinetic preference of the photoreaction. As a result, the inherent equilibrium between *o*-methyl benzaldehyde and photoenol can be shifted towards the photoenol species by an increase of the maleimide concentration during irradiation.

3.4. Block copolymer Synthesis via the Kinetic Preference of the Photoreaction

In polar solvents such as acetonitrile, the photoreaction kinetics are preferred in comparison to the imine formation in the dark. Further, the imine formation rate is not solvent dependent and is merely influenced by the amount of water in the solvents. The photo-activated Diels-Alder reaction between *o*-methyl benzaldehyde and a maleimide is much faster than the reaction between *o*-methyl benzaldehyde and thus – under these conditions – the achieved manifold selectivity is merely kinetic in nature. A mixture of *o*-methyl benzaldehyde terminated PEG **4** and ethyl maleimide **8** in acetonitrile was irradiated with the PL-L lamp ($\boldsymbol{\lambda}$ = 310-440 nm; $\boldsymbol{\lambda}_{max}$ = 365 nm; 36 W) for several time intervals to determine the photoreaction kinetics. The experimental data of the kinetics are presented in chapter 7. Furthermore, a mixture of **4** and **2** in acetonitrile was stirred at several times in order to determine the imine formation kinetics. The evolution of both particular products was analysed via high resolution mass spectrometry. The Diels-Alder product was obtained after 3 min whereas the imine formation took again 90 min, as already reported in section 3.3.

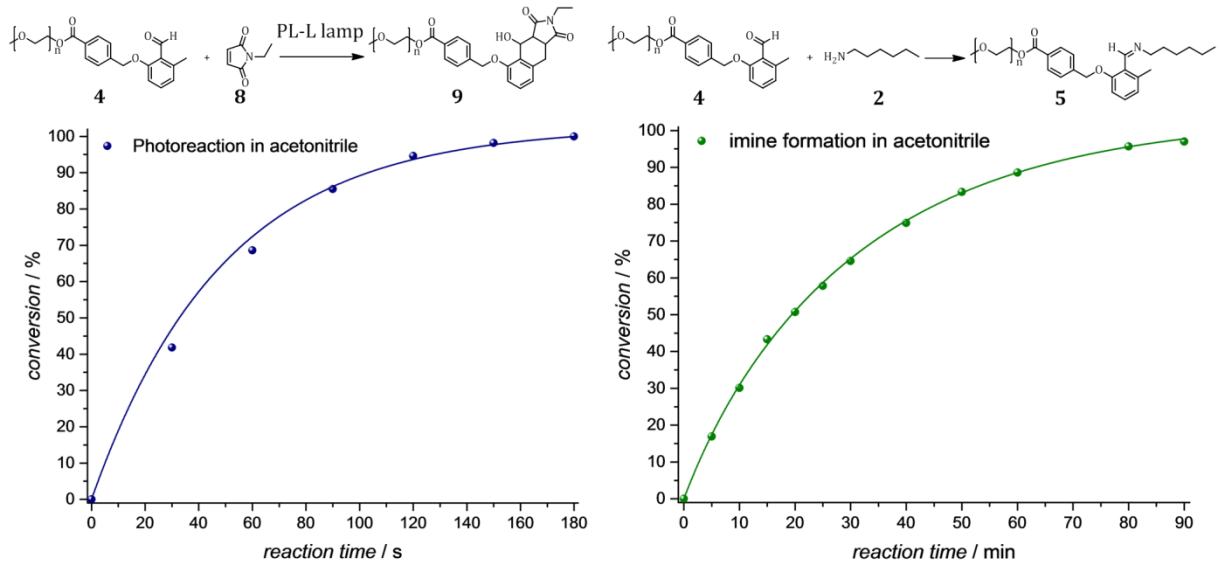

Figure 27: *The reaction kinetics of both the photoreaction and the imine formation were determined via Orbitrap ESI-MS. A diluted solution of* ***4*** *(1.0 eq.) and* ***8*** *(1.2 eq.) was irradiated with the PL-L lamp in acetonitrile for 30 s, 60 s, 90 s, 120 s, 150 s, and 180 s (left). A diluted solution of* ***4*** *(1.0 eq.) and* ***2*** *(3.6 eq.) was stirred at ambient temperature for 5 min, 10 min, 15 min, 20 min, 25 min, 30 min, 40 min, 50 min, 60 min, 80 min, and 90 min (right). The image was modified from ref.*[297] *with permission from the American Chemical Society (ACS), 2016.*

The imine formation yields less than 8 % after 3 min (refer to Figure 27). In addition, the fast reaction kinetics of the photoreaction lead to a rapid photoenol consumption and thus a drastic decrease of the *o*-methyl benzaldehyde concentration according to Le Chatelier. As a result, the imine formation is expected to be negligible in a manifold system which is established in acetonitrile. Therefore, the reaction manifold shows perfect orthogonality for both reaction paths and can be employed as a versatile tool for the synthesis of block copolymers. In the following, all irradiations were performed with three connected high power LEDs which improve the efficiency of the irradiation.

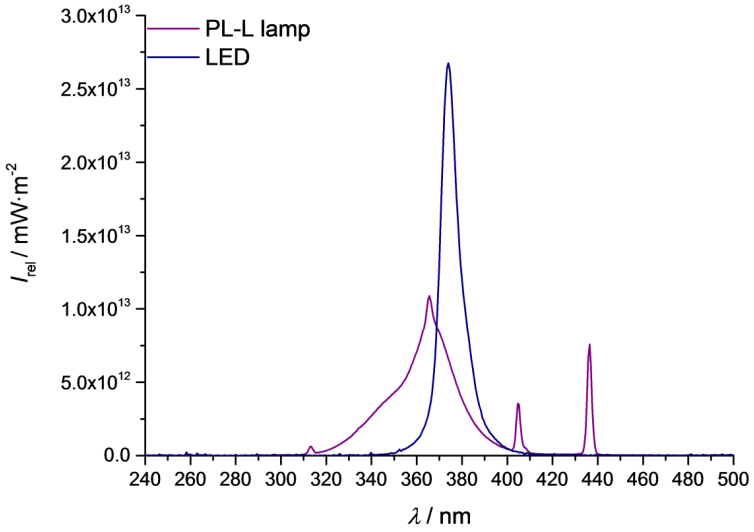

Figure 28: *Emission spectra of the previously employed compact low-pressure fluorescent lamp PL-L (36 W, λ_{max} = 365 nm) and the high power LEDs (3 W, λ_{max} = 375 nm). The emission spectra were recorded with a UV sensor (Opsytec Dr. Gröbel GmbH; Ettlingen, Germany). The image was modified from ref.*[297] *with permission from the American Chemical Society (ACS), 2016.*

3.4.1. Photoselective Block Copolymer Formation via a Two Polymer One-Pot Approach

A one-pot system containing two polymers and hexylamine was established to selectively synthesise a block copolymer via irradiation and an end group transformation without irradiation. The utilisation of hexylamine instead of a macromolecular amine was realised in order to simplify the analysis of the obtained block copolymer. An overview of the orthogonal reaction paths are depicted in Scheme 27. The synthesis of the block copolymer **11** was performed in acetonitrile by

irradiating the system with three LEDs (λ = 340-410 nm; λ_{max} = 375 nm, 3 W) for 1 h. The block copolymer was analysed via ^{1}H NMR spectroscopy and GPC.

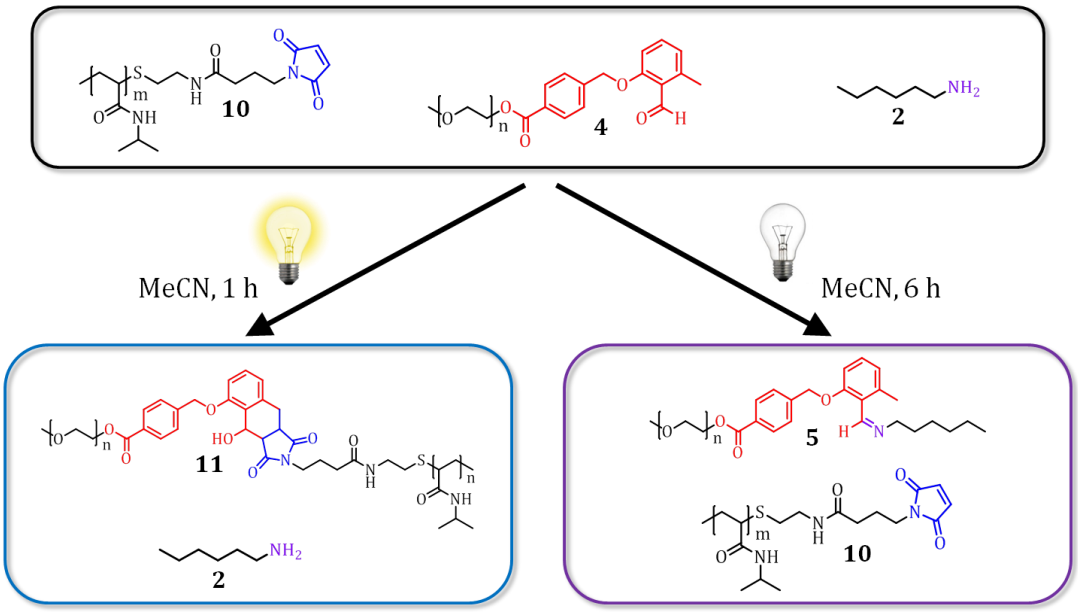

Scheme 33: *Orthogonal block copolymer formation of a one pot system containing o-methyl benzaldehyde terminated PEG* ***4****, poly(N-isopropylacrylamide) maleimide* ***10****, and hexylamine* ***2*** *in acetonitrile. The photo triggered reaction leads to the formation of PEG-block-pNIPAAm* ***11*** *while hexylamine* ***2*** *remains unreacted. The non-irradiative imine formation selectively leads to the formation of* ***5****, while poly(N-isopropylacrylamide) maleimide* ***10*** *remains unreacted. The image was modified from ref.*[297] *with permission from the American Chemical Society (ACS), 2016.*

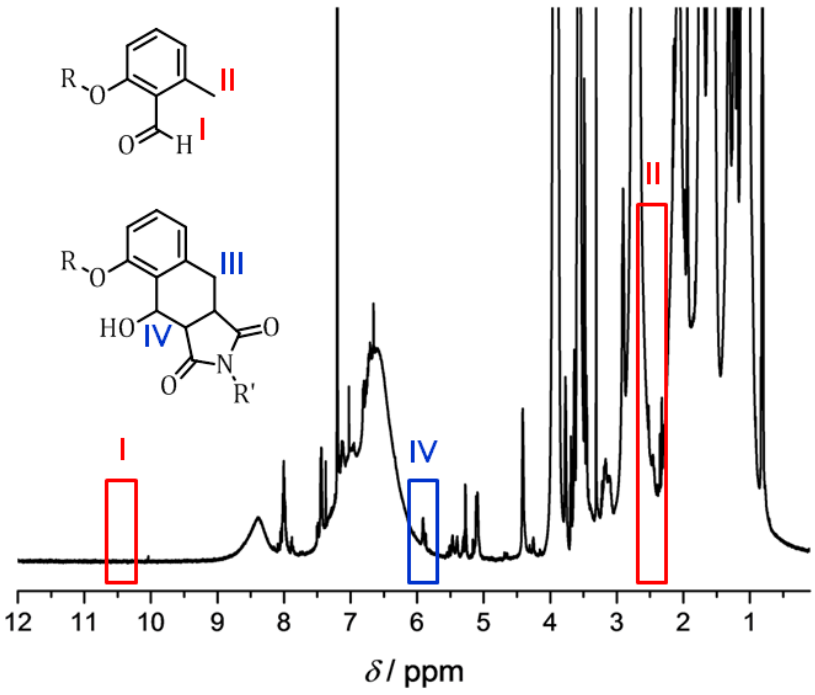

Figure 29: *^{1}H NMR data of the PEG-block-pNIPAAm* ***11*** *and hexylamine* ***2*** *in $CDCl_3$ synthesised by the orthogonal photo reaction pathway. The complete conversion of o-methyl benzaldehyde into the Diels-Alder product is detectable, whereas no imine formation can be observed. The image was modified from ref.*[297] *with permission from the American Chemical Society (ACS), 2016.*

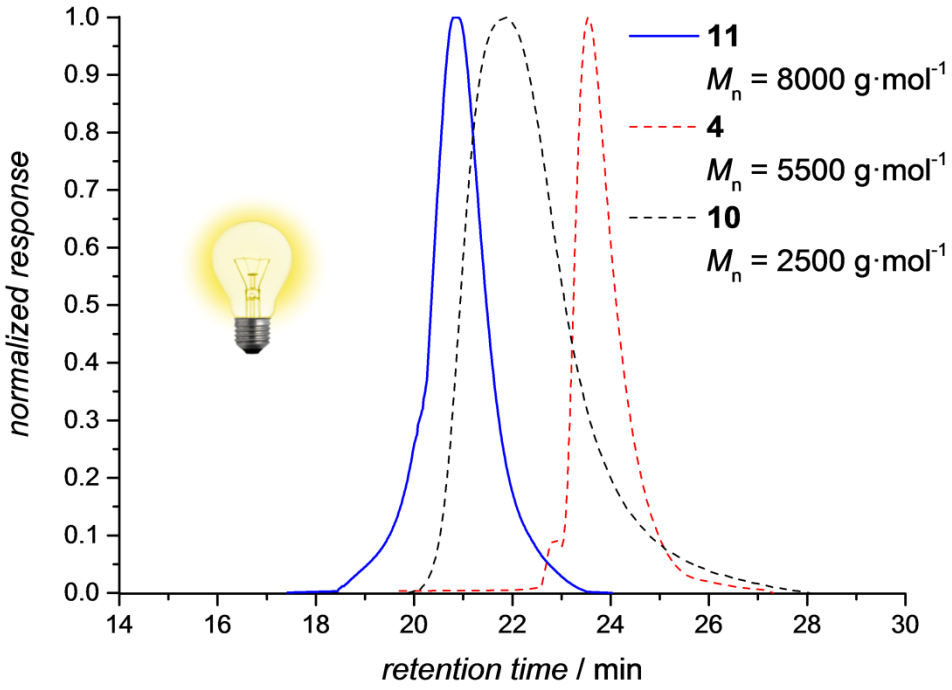

Figure 30: *GPC traces of the photoreaction path. The photo triggered reaction of o-methyl benzaldehyde terminated PEG* ***4****, pNIPAAm-maleimide* ***10****, and hexylamine* ***2*** *leads to the selective formation of PEG-block-pNIPAAm* ***11****. The starting materials* ***10*** *as well as* ***4*** *are additionally added in dashed lines. The image was modified from ref.*[297] *with permission from the American Chemical Society (ACS), 2016.*

The absence of significant *o*-methyl benzaldehyde resonances (the aldehyde signal I: δ = 10.69 ppm as well as the aryl methyl signal II: δ = 2.53 ppm) indicate the complete conversion of **4** (refer to Figure 29). The significant Diels-Alder product resonances of **11** (ring signal III: δ = 2.91-3.24 ppm) are not detectable due to overlapping polymer backbone signals, yet another Diels-Alder product resonance (the α-hydroxy signal IV: δ = 5.89 ppm) is visible. Furthermore the absence of any imine resonances indicates that **4** had reacted with the **10** during irradiation.

The GPC trace clearly evidence the successful block copolymer formation of **11** between **4** and **10** during irradiation. The remaining hexylamine **2** remains under the lower separation limit of the columns and thus it was not detectable. The GPC traces of the starting materials **4** (M_n = 2500) and **10** (M_n = 5500) disappeared completely, while the photoconjugated block copolymer **11** (M_n = 8000) was formed exclusively (refer to Figure 30).

The end group transformation of **4**, yielding the imine **5**, was performed by stirring the system in dry acetonitrile for 6 h at ambient temperature. The products were analysed via ^{1}H NMR spectroscopy and GPC.

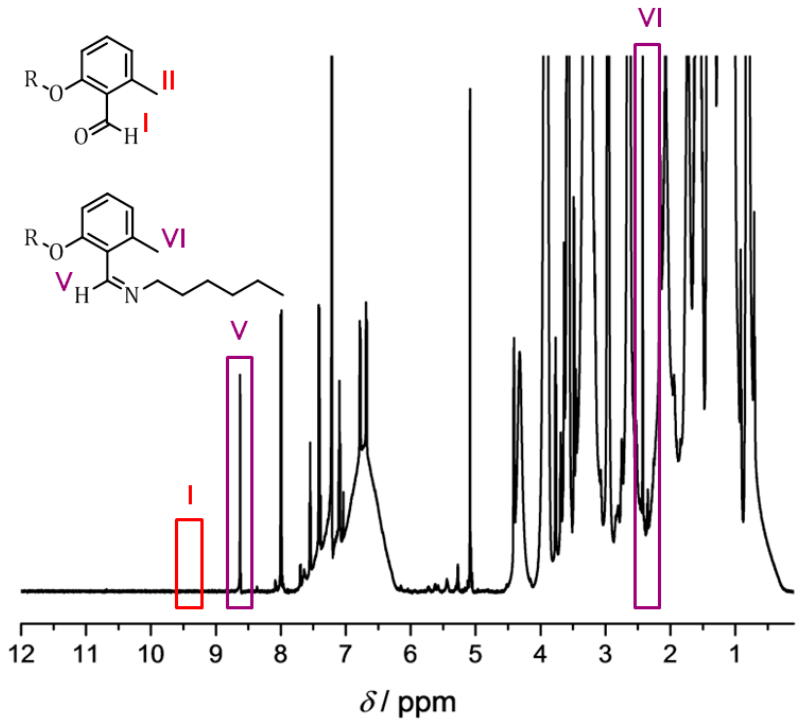

Figure 31: *^{1}H NMR data of PEG imine **5** and pNIPAAm-maleimide **10** in $CDCl_3$ synthesised by the non-irradiative imine formation pathway. The complete conversion of o-methyl benzaldehyde into the imine is detectable whereas no formation of the Diels-Alder product can be observed. The image was modified from ref.*[297] *with permission from the American Chemical Society (ACS), 2016.*

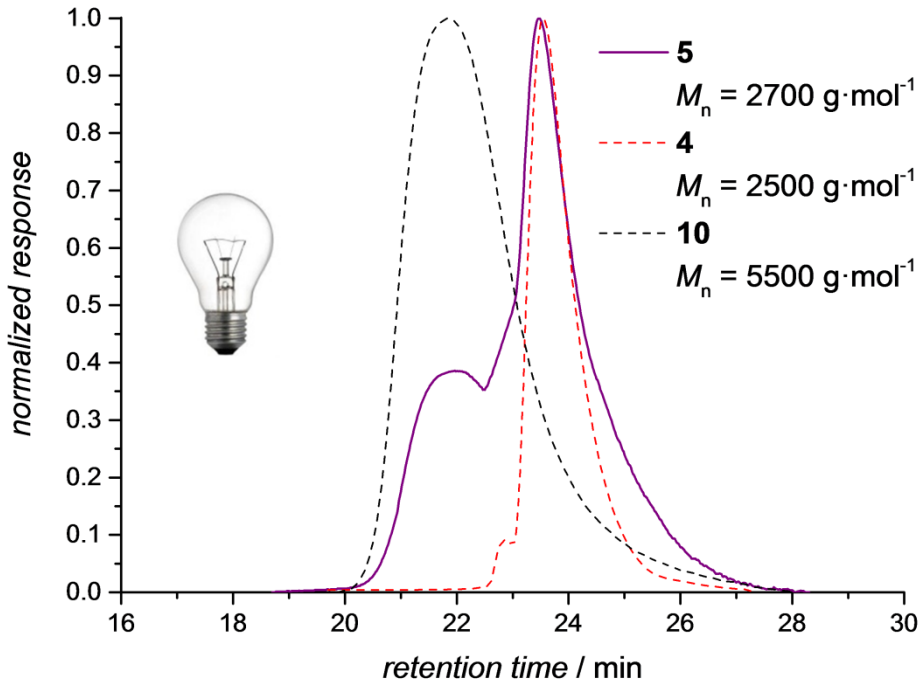

Figure 32: *GPC traces of the imine formation path. The darktime reaction of o-methyl benzaldehyde terminated PEG **4**, pNIPAAm-maleimide **10**, and hexylamine **2** leads to the selective formation of PEG imine **5**. The starting materials **10** as well as **4** are additionally added in dashed lines. The image was modified from ref.*[297] *with permission from the American Chemical Society (ACS), 2016.*

The absence of both significant *o*-methyl benzaldehyde resonances (the aldehyde signal I: δ = 10.69 ppm as well as the aryl methyl signal II: δ = 2.53 ppm) indicates the complete conversion of **4** (refer to Figure 31). The appearance of the distinct imine resonances of **5** (the imine signal V: δ = 8.63 ppm as well as the shifted aryl methyl signal VI: δ = 2.43 ppm) clearly indicate that the aldehyde functionality of **4** was turned into an imine functionality. The maleimide resonances of the unreacted compound **10** (δ = 6.63 ppm) overlap with signals of the polymer backbone. In addition, the absence of any Diels-Alder product resonances (the α-hydroxy signal IV: δ = 5.91 ppm) evidence that **2** have exclusively reacted with **10** under non-irradiative conditions.

The GPC trace clearly evidences that the end group formation of **4** into the imine **5** was successful in the presence of unreacted **10** without irradiation. The resulting GPC trace is a bimodal distribution. The first distribution maximum is at a retention time of 21 min and belongs to the remaining maleimide terminated polymer **10** (M_n = 5500). The second distribution has its maximum at a retention time of 23.8 min and is more intense than the first distribution. Further, the second distribution is slightly shifted to higher molar masses compared to the starting material **4** (M_n = 2500) implying the presence of **5** (refer to Figure 32).

All in all, the block copolymer formation was performed by the photoreaction path, whereas the polymer end group transformation was implemented by the non-irradiative imine formation path. The experiments underpin the orthogonal character of both reaction paths in acetonitrile.

3.4.2. Photoselective Block Copolymer Formation via a Three Polymer One-Pot Approach

The previously presented system was extended to a one-pot system in which the small molecular amine functionality is substituted by an amine terminated polymer. Thus, a system containing a set of three polymers was employed in order to synthesise block copolymers via the kinetic version of the reaction manifold either via irradiation or without irradiation. This strategy involved only polymers as reactants results in complex

products containing a block copolymer species and a remaining homopolymer. An overview of the orthogonal reaction paths are depicted in Scheme 28.

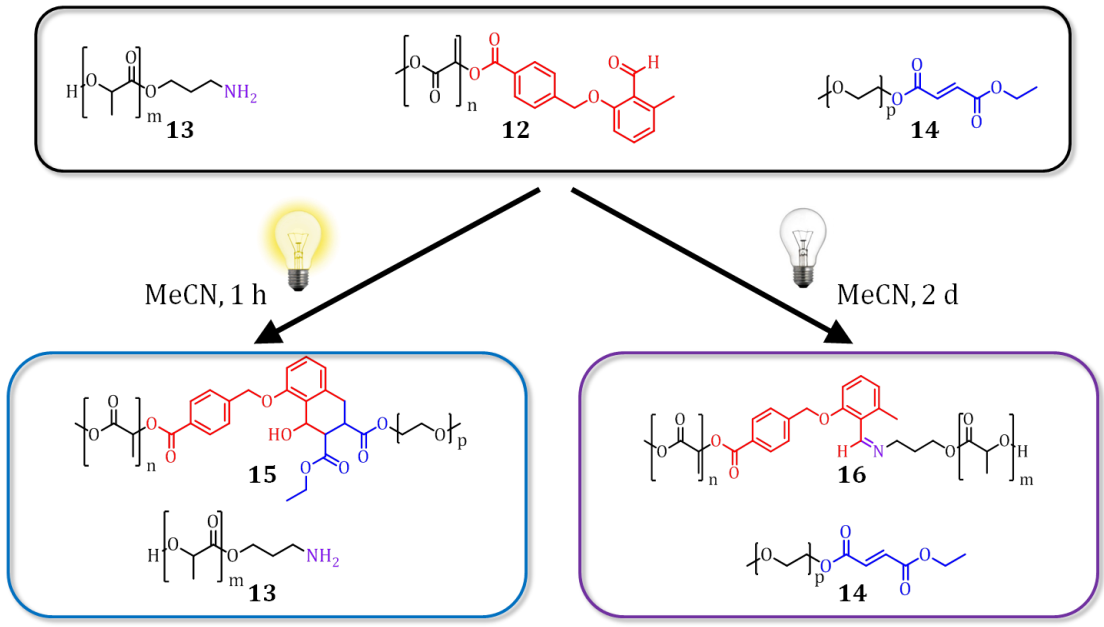

Scheme 34: *Orthogonal block copolymer formation of a one pot system containing o-methyl benzaldehyde terminated polylactide* ***12****, amine terminated polylactide* ***13*** *(pL-amine), and PEG-fumarate* ***14*** *in acetonitrile. The photo triggered reaction leads to the formation of pL-block-PEG* ***15*** *while pL-amine* ***13*** *remains unreacted. The non-irradiative path yields pL-block-pL* ***16****, while PEG-fumarate* ***14*** *remains unreacted. The image was modified from ref.*[297] *with permission from the American Chemical Society (ACS), 2016.*

The synthesis of the Diels-Alder conjugated block copolymer **15** was performed in acetonitrile by irradiating the system with three LEDs (λ = 340-410 nm; λ_{max} = 375 nm, 3 W) for 1 h. The block copolymer was analysed via ^{1}H NMR spectroscopy and GPC.

The disappearance of two distinct *o*-methyl benzaldehyde resonances (the aldehyde signal I: δ = 10.69 ppm as well as the aryl methyl signal II: δ = 2.53 ppm) indicates the complete conversion of **12**. The presence of both significant Diels-Alder product resonances of **11** (the ring signal III: δ = 2.91-3.24 ppm as well as the α-hydroxy signal IV: δ = 6.12 ppm) in combination with the absence of any imine resonances (the imine signal V: δ = 8.63 ppm as well as the shifted aryl methyl signal VI: δ = 2.43 ppm) indicates the formation of the Diels-Alder conjugated block copolymer **15** (refer to Figure 33). The absence of the fumarate signals (δ = 6.81 ppm) of **13** cannot be definitely proven due to an overlapping of the signals with inherent polymer resonances.

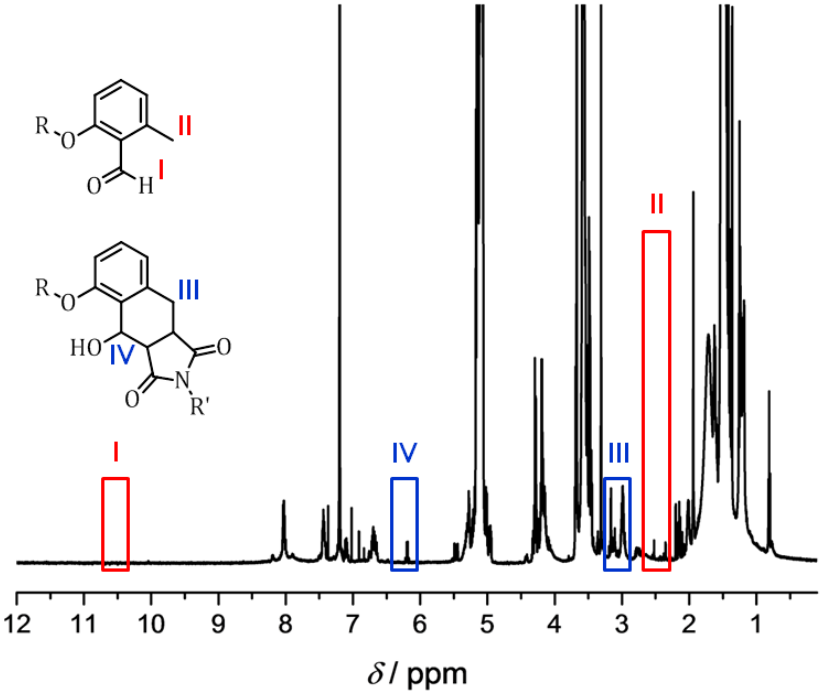

Figure 33: *^{1}H NMR data of the pL-block-PEG **15** and the pL-amine **13** in $CDCl_3$ synthesised by the photo reaction pathway. The complete conversion of o-methyl benzaldehyde into the Diels-Alder product is detectable whereas no imine formation can be observed. The image was modified from ref.*[297] *with permission from the American Chemical Society (ACS), 2016.*

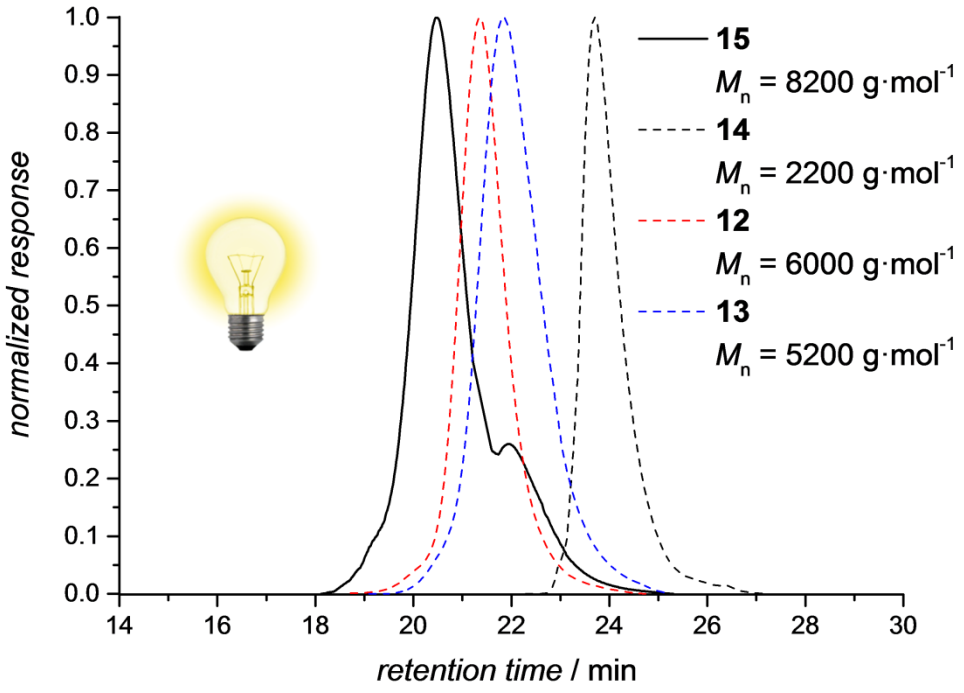

Figure 34: *GPC traces of the photoreaction path. The photo triggered reaction of o-methyl benzaldehyde terminated pL **12**, pL-amine **13**, and PEG-fumarate **14** leads to the selective formation of the pL-block-PEG **15** whereas **13** remains unreacted. The starting materials **12**, **13** and **14** are additionally added in dashed lines. The image was modified from ref.*[297] *with permission from the American Chemical Society (ACS), 2016.*

The GPC trace indicates the formation of the block copolymer **15** during irradiation as the starting materials **12** (M_n = 6000) and **14** (M_n = 2200) disappeared and the resulting product was shifted to a lower retention time. The obtained GPC trace indicates a shoulder in the retention time range of 21.9 - 25.0 min, which is associated with the unreacted pL-amine **13** (refer to Figure 34). In addition, the GPC traces were deconvoluted using the PeakFitv4.12 program in order to evidence the successful photoreaction yielding **15** by excluding the possible formation of the imine **16** (refer to Figure 35). Hence, the RI response of pL-amine **13** after the photoreaction was assigned to its initial sample weight before the irradiation. The RI signal of **13** (m = 3.94 mg) was determined as 3.47789 mV resulting in a relative response of $R_{relative}$ = 1.3287 mg/mV. The GPC sample weight of the photoreaction was 4.07 mg whereby the mass ratio of **13** was 38.3 % leading to a theoretical amount of $m_{theoretical}$ = 1.56 mg for **13**. The deconvoluted GPC trace of **13** yielded an absolute RI response of $I_{deconvoluted}$ = 1.35028 mV. Thus, the actual amount of **13** was calculated as $m_{theoretical} = R_{relative} \cdot I_{deconvoluted}$ = 1.53 mg. The calculated and the theoretical amount of **13** fit well together with a deviation of 2 %. Thus, it was demonstrated that the pL-amine **13** remained unreacted during irradiation confirming that the Diels-Alder conjugated block copolymer **15** was exclusively formed via the photoreaction.

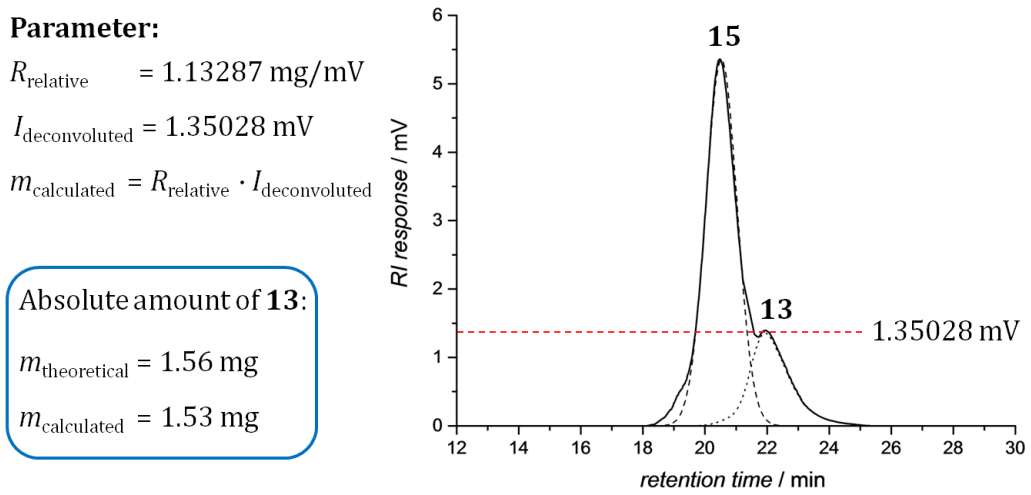

Figure 35: *Deconvoluted GPC traces (via PeakFitv4.12 program package) of the photo triggered path containing pL block PEG **15** and pL-amine **13**. The isolated pL-amine signal **13** corresponds to a mass of 1.53 mg in the GPC sample of the photoreaction (overall mass of **15** and **13** in the GPC sample: 4.07 mg). This value fits well to a theoretical amount of 1.56 mg. The image was modified from ref.*[297] *with permission from the American Chemical Society (ACS), 2016.*

The synthesis of the imine conjugated block copolymer **16** was performed by stirring the system in dry acetonitrile for 2 d at ambient temperature. The products were analysed via ^{1}H NMR spectroscopy and GPC.

According to the ^{1}H NMR study, the *o*-methyl benzaldehyde terminated polylactide **12** (the aldehyde signal I: δ = 10.69 ppm as well as the aryl methyl signal II: δ = 2.53 ppm) was converted to 98 %. The appearance of both significant imine resonances (the imine signal V: δ = 8.63 ppm as well as the shifted aryl methyl signal VI: δ = 2.43 ppm) in combination with the presence of the fumarate signal (δ = 6.81 ppm) of **13** indicate the formation of the imine conjugated block copolymer **16** (refer to Figure 36). The absence of any Diels-Alder product signals (the aldehyde signal I: δ = 10.69 ppm as well as the aryl methyl signal II: δ = 2.53 ppm) of **15** suggests that the imine formation was exclusive and quantitative.

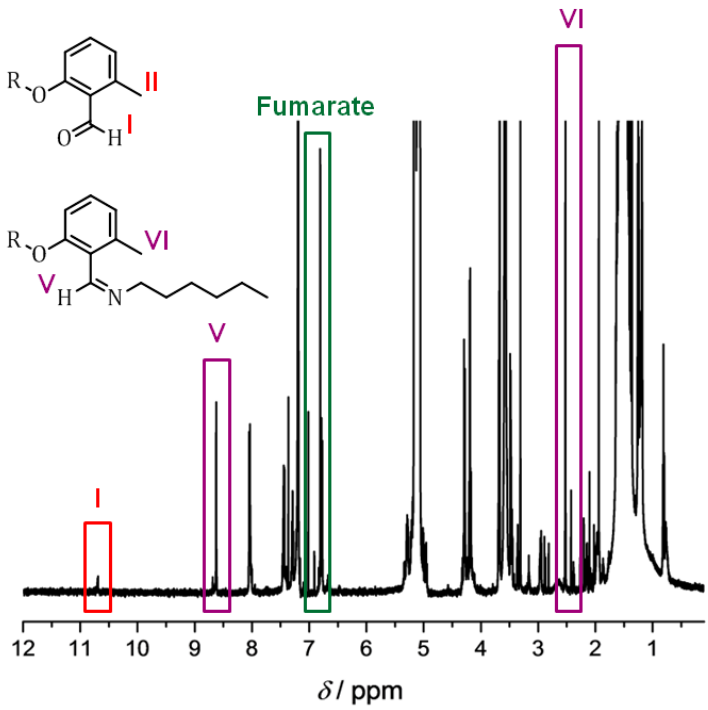

Figure 36: *^{1}H NMR data of the pL-block-pL **16** and the PEG-fumarate **14** in $CDCl_3$ synthesised by the orthogonal imine formation pathway. A conversion of 98 % of **12** into the imine **16** is detectable whereas the Diels-Alder reaction of **12** and **14** cannot be observed. The image was modified from ref.*[297] *with permission from the American Chemical Society (ACS), 2016.*

The GPC trace indicates the formation of the block copolymer **16** in the darktime as the starting materials **12** (M_n = 6000) and **13** (M_n = 5200) disappeared and the resulting product was shifted to a lower retention time. The obtained GPC trace feature a shoulder in the retention time range of 21.9-25.0 min, fitting to the unreacted PEG-fumarate **14** (refer to Figure 37).

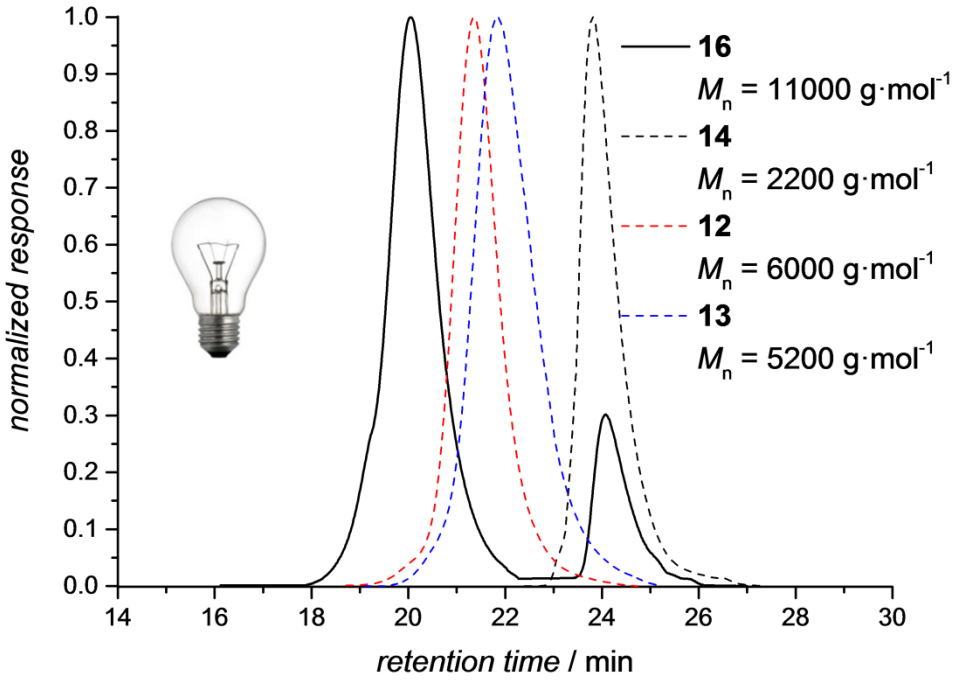

Figure 37: *GPC traces of the imine formation path. The darktime reaction of o-methyl benzaldehyde terminated pL* ***12****, pL-amine* ***13****, and PEG-fumarate* ***14*** *leads to the selective formation of pL-block-pL* ***16*** *whereas* ***14*** *remains unreacted. The starting materials* ***12****,* ***13*** *and* ***14*** *are additionally added in dashed lines. The image was modified from ref.*[297] *with permission from the American Chemical Society (ACS), 2016.*

Parameter:

$R_{relative}$ = 11.86894 mg/mV

$I_{deconvoluted}$ = 0.34628 mV

$m_{calculated}$ = $R_{relative} \cdot I_{deconvoluted}$

Absolute amount of **14**:

$m_{theoretical}$ = 0.68 mg

$m_{calculated}$ = 0.66 mg

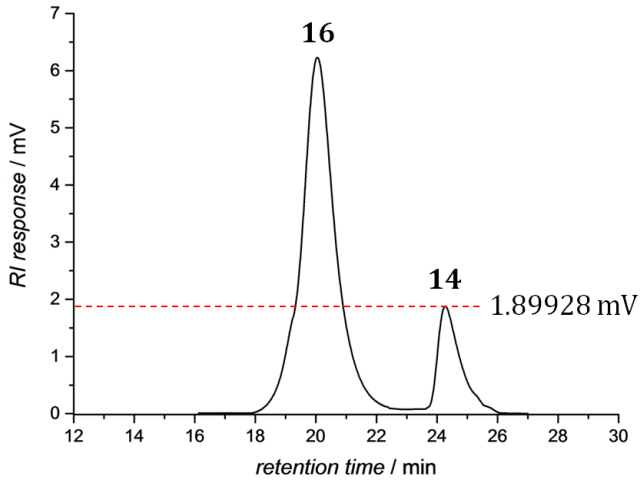

Figure 38: *Deconvoluted GPC traces (via PeakFitv4.12 program package) of the non-irradiative path containing the pL block pL* ***16*** *and the PEG-fumarate* ***14****. The isolated PEG-fumarate* ***14*** *corresponds to a mass of 0.66 mg in the GPC sample of the photoreaction (overall mass of* ***16*** *and* ***14*** *in the GPC sample: 4.05 mg). This value fits well to a theoretical amount of 0.68 mg. The image was modified from ref.*[297] *with permission from the American Chemical Society (ACS), 2016.*

The deconvolution of the GPC signals was performed by using the PeakFitv4.12 program in order to evidence the successful imine formation yielding **16** by excluding the possible formation of the Diels-Alder product **15** (refer to Figure 38). Therefore, the RI response of the PEG-fumarate **14** after the reaction was assigned to its initial sample

weight before the imine formation. The RI signal of **14** (m = 4.11 mg) was determined as 11.86894 mV resulting in a relative response of $R_{relative}$ = 0.34628 mg/mV. The GPC sample weight of the imine transformation was 4.05 mg whereby the mass ratio of **14** was 16.8 %, leading to a theoretical amount of $m_{theoretical}$ = 0.68 mg for **14**. The deconvoluted GPC trace of **14** yielded an absolute RI response of $I_{deconvoluted}$ = 1.89928 mV. Thus, the actual amount of **14** was calculated as $m_{theoretical} = R_{relative} \cdot I_{deconvoluted}$ = 0.66 mg. The calculated and the theoretical amount of **14** fit well together with a deviation of 3 %. Thus, it is demonstrated that PEG-fumarate **14** remained unreacted without irradiation which confirms the exclusive formation of the imine conjugated block copolymer **15**.

3.5. Conclusions

A light induced reaction manifold including two selective reaction paths of *o*-methyl benzaldehyde in a one-pot system was developed. The reaction paths were initiated by opposing triggers. The first reaction path demanded light in order to perform a Diels-Alder reaction with maleimides whereas the imine formation as second reaction path was performed without irradiation. Hence, the imine formation in the dark time was able to proceed unaffected from the other reaction path. The defining aspect of the reaction manifold is the preferential use of the photoreaction in a one-pot system based on the suppression of the imine formation. Since the photoreaction kinetics were dependent of the solvent polarity, the photoreaction was slightly faster than the imine formation in dichloromethane and exceeded the imine formation in acetonitrile.

Thus, the reaction manifold in dichloromethane was applied for the highly selective polymer end group modification of *o*-methyl benzaldehyde terminated PEG with ethyl maleimide or hexylamine. The reaction manifold in acetonitrile featuring functionalised polymers such as PEG, polylactide or pNIPAAm was applied in order to synthesise a set of different block copolymers in an orthogonal fashion. In addition, the manifold system was investigated with semi-qualitative kinetic simulations. The data clearly demonstrated that *o*-methyl benzaldehyde and the light induced photoenol species form an equilibrium in the manifold system during irradiation. In this regard, the photoenol species is rapidly converted by the maleimide moiety and thus the photoenol has the role of a maleimide trap. Therefore, the decreasing photoenol concentration is counteracted by the photo triggered transformation of the *o*-methyl benzaldehyde into the photoenol species according to Le Chatelier. As a result, the *o*-methyl benzaldehyde concentration and thus the availability of aldehyde functionalities is steadily ceased which leads to an inhibition of the imine formation. Experimental data have evidenced that the imine suppression can be enhanced by an increase of the maleimide concentration in good agreement to the simulation.

4

4. λ-Orthogonal Photoligation

Parts of the present chapter were reproduced with permission from K. Hiltebrandt, T. Pauloehrl, J. P. Blinco, K. Linkert, H. G. Börner, C. Barner-Kowollik, *Angew. Chem. Int. Ed.*, **2015**, 54, 2838-2843 (DOI: 10.1002/anie.201410789) as well as with permission from K. Hiltebrandt, M. Kaupp, .E. Molle, J. P. Menzel, J. P. Blinco, C. Barner-Kowollik, *Chem. Comm.*, **2016**, 52, 9426-9429 (DOI: 10.1039/C6CC03848D). Copyright Wiley 2015 and Royal Society of Chemistry (RSC) 2016.

4.1. Introduction

The reaction system which has been presented in Chapter 3 exploits the orthogonality of an *o*-methyl benzaldehyde species via a light induced reaction manifold. In this case, the *o*-methyl benzaldehyde enables either a photoreaction or a non-irradiative thermally induced reaction path. Although the system has been established as a versatile reaction protocol for the selective synthesis of block copolymers, it is evident that the non-irradiative imine formation lacks spatial and temporal control. Moreover, a set of two photoreactions in which each reaction path can be activated exclusively by light of a distinct wavelength enables ***λ***-orthogonality. Accordingly, a ***λ***-orthogonal system offers highly sophisticated possibilities for polymer chemistry and materials science. For example, such a one-pot system allows the specific wavelength dependent design of material properties by introducing a specific functionality within one wavelength regime and inserting alternative functionalities within another one.

The utilisation of photoreactions in different wavelength ranges has been described before. For instance, it was demonstrated that several photolabile protecting groups on surfaces are able to release small molecules after irradiation with an appropriate wavelength.[305] In addition, the generation of a photoacid at the polymer backbone is reported at 365 nm, followed by a subsequent photoimmobilisation step at 254 nm.[306] Furthermore, the wavelength dependent grafting of alkenes onto single-crystal TiO_2 surfaces[307] as well as the selective photodecomposition of a distinct azo-functionality in a bis(diazo) ketone[308] via different wavelengths are further examples for wavelength dependent reactions.

Although the reported photoreactions demonstrate the efficiency of wavelength selective reactions, they cannot be employed for ***λ***-orthogonal ligation procedures in a one-pot system. To address this gap, the present chapter introduces the development of a ***λ***-orthogonal system on the basis of an *o*-methyl benzaldehyde, a diphenyl tetrazole, and a maleimide moiety. The different absorptivities of *o*-methyl benzaldehyde and diphenyl tetrazole allow the exclusive *o*-methyl benzaldehyde activation in the presence of diphenyl tetrazole. The converse reaction path, allowing the exclusive diphenyl tetrazole activation in the presence of *o*-methyl benzaldehyde, requires the photochemical deactivation of the *o*-methyl benzaldehyde species via the reversible

transformation of *o*-methyl benzaldehyde into a photochemically inactive imine (refer to Figure 39).

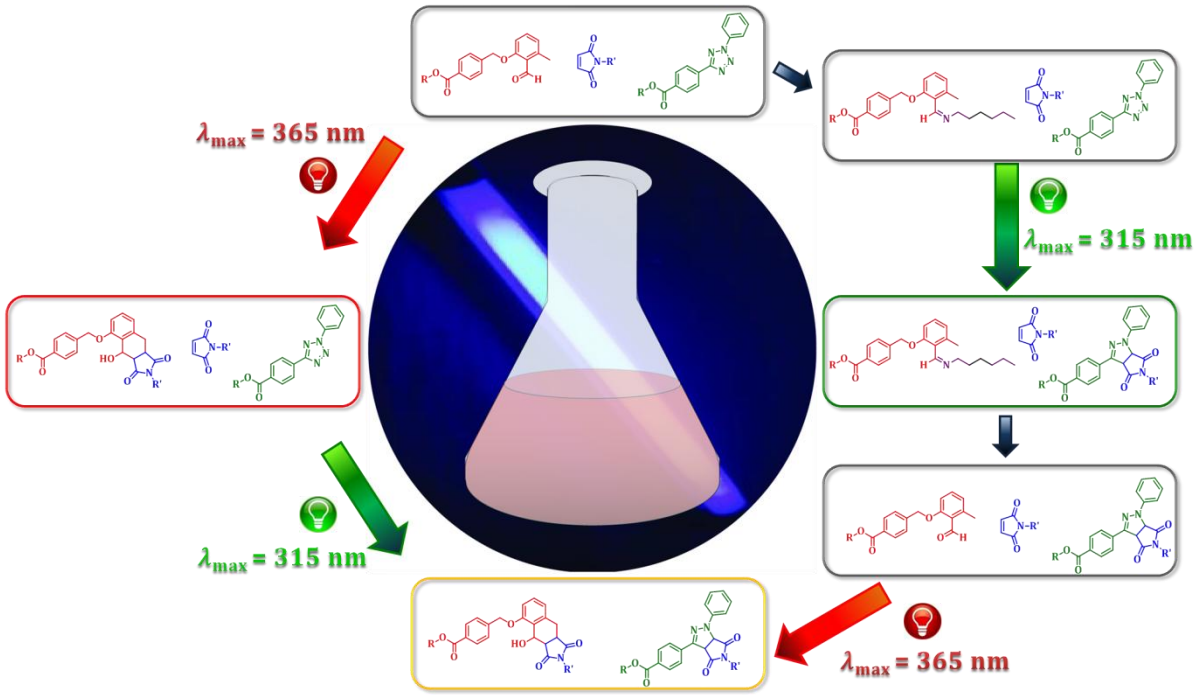

Figure 39: *The λ-orthogonal principle in one direction relies on the initial o-methyl benzaldehyde activation in the presence of diphenyl tetrazole (left). The converse photoreaction path, allowing the initial diphenyl tetrazole activation in the presence of o-methyl benzaldehyde, requires the transformation of the photoactive o-methyl benzaldehyde species into the photochemically inactive imine. After the NITEC reaction, the o-methyl benzaldehyde species is reactivated by the hydrolysis of the imine. Subsequently, the light induced Diels-Alder reaction between o-methyl benzaldehyde and maleimide (right).*

4.2. Polymer End Group Modifications and Block Copolymer Formations via λ-Orthogonality in One Direction

The present section introduces a photochemical strategy for achieving λ-orthogonality in one direction using *o*-methyl benzaldehyde, diphenyl tetrazole as well as electron-poor enes in a one-pot system. The emission spectra of both photoactive compounds illustrate that the absorption area of *o*-methyl benzaldehyde and tetrazole overlap below 310 nm. The intrinsic orthogonal absorption area is located in the wavelength range between 310-350 nm, where *o*-methyl benzaldehyde absorbs exclusively. The compact fluorescent lamp PL-L (λ_{max} = 365 nm) overlaps with the absorption spectrum of the *o*-methyl benzaldehyde, however, the overlap with the absorption of the diphenyl tetrazole is negligible between 310-350 nm orthogonal range (refer to Figure 40).

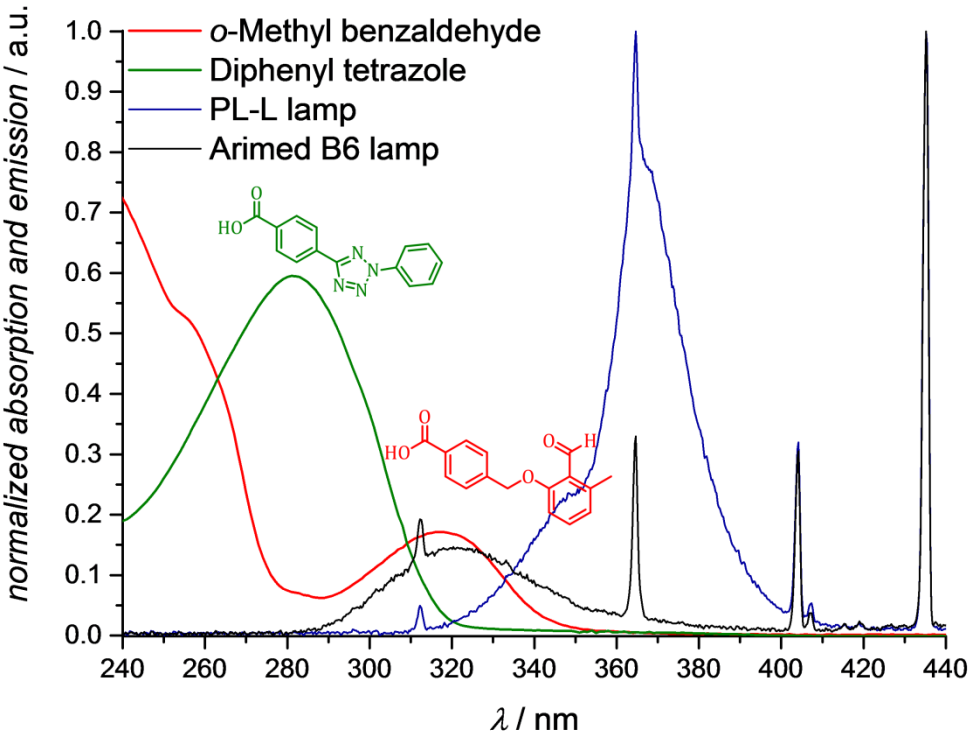

Figure 40: *UV/vis absorption spectrum of o-methyl benzaldehyde and diphenyl tetrazole superimposed with the emission spectra of the PL-L lamp (λ = 310-440 nm; λ_{max} = 365 nm; 36 W) and the Arimed B6 lamp (λ = 280-440 nm; λ_{max} = 315 nm; 36 W). The absorption area of the diphenyl tetrazole shows a negligible overlapping with the PL-L emission area whereas the o-methyl benzaldehyde can be activated exclusively in the wavelength range between 310-350 nm by the PL-L lamp. The image was modified from ref.*[18] *with permission from Wiley-VCH, 2016.*

Therefore, a system containing an *o*-methyl benzaldehyde species, a diphenyl tetrazole compound, and an electron-poor dienophile such as maleimide allows for light induced orthogonality in one direction (refer to Scheme 35). Thus, the specific absorptions of both photoactive species allow a photochemical selectivity provided that the photoenol reaction involving the *o*-methyl benzaldehyde and maleimide is initially activated by the PL-L lamp. In the meantime, diphenyl tetrazole remains unreacted, however, the reaction between the diphenyl tetrazole and the maleimide can be activated subsequently via irradiation with the Arimed B6 lamp.

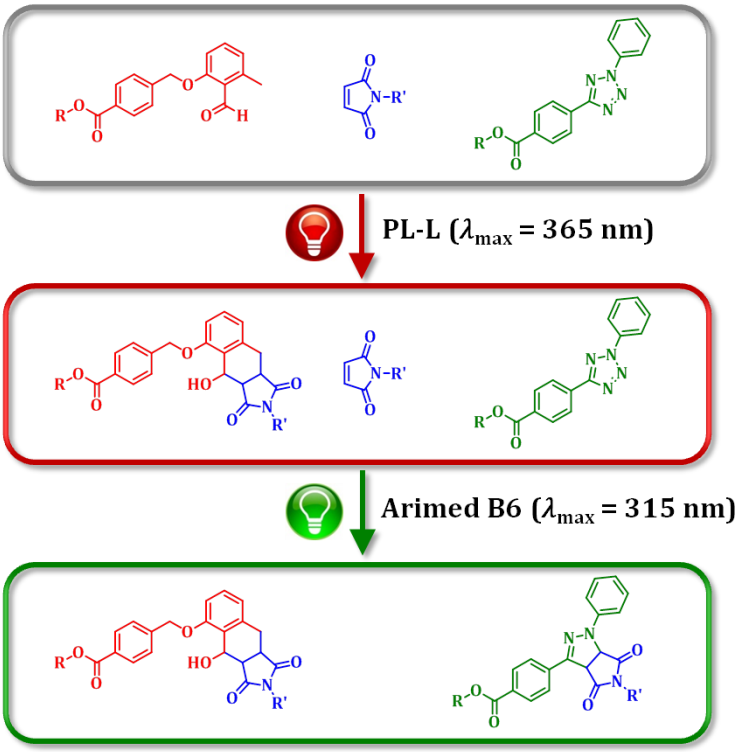

Scheme 35: *Evidencing the λ-orthogonal principle in one direction. The system consists of an o-methyl benzaldehyde derivative, a diphenyl tetrazole derivative and a dienophile such as maleimide in a true one-pot system. Irradiating the system with the PL-L lamp selectively affords the photoenol cycloadduct. Subsequently, the diphenyl tetrazole moiety can be transformed into the 4,5-dihydro pyrazole derivative via irradiation with the Arimed B6 lamp.*

The converse reaction sequence, i.e. the selective tetrazole activation in the presence of *o*-methyl benzaldehyde cannot be performed by irradiating the system with a distinct wavelength due to the concomitant absorption of light below 310 nm of both compounds. Indeed, irradiation in the noted wavelength range leads to a joint activation of both compounds.

4.2.1. Kinetic Investigation of the λ-Orthogonality via End Group Modifications in a Two Polymer One-Pot System

The kinetic parameters of the λ-orthogonal principle in one direction were investigated via selective end group modifications of a system containing *o*-methyl benzaldehyde terminated PEG **4**, diphenyl tetrazole terminated PEG **17**, and maleimide **6** in varying ratios. The photoreactions of **4** with **6** as well as **17** with **6** are depicted in Scheme 36.

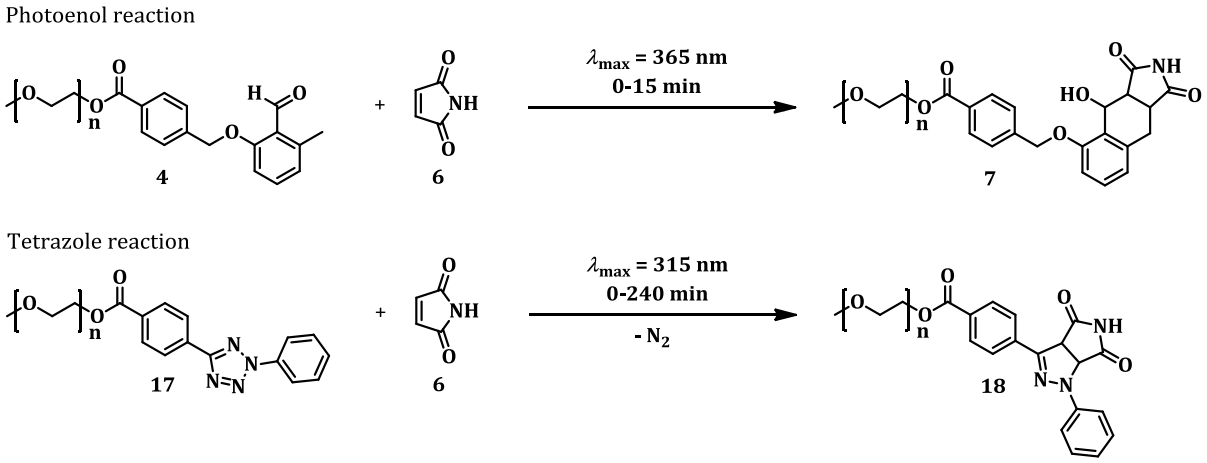

Scheme 36: *The photoenol reaction converts the terminal o-methyl benzaldehyde functionality into the respective Diels-Alder product* ***7****. The diphenyl tetrazole reaction transforms the tetrazole moiety into the 4,5-dihydro pyrazole* ***18****.*

Initially, the system featuring an equimolar mixture of **4** and **17** as well as a 10.7 eq. excess of **6** in DCM was irradiated for pre-set time intervals starting from 0 to 15 min using the PL-L lamp (λ = 310-440 nm; λ_{max} = 365 nm; 36 W) in order to determine the photoenol reaction kinetics. Here, the evolution of the species **4**, **7**, **17**, and **18** were traced during the irradiation procedure via mass spectrometry (refer to Figure 41a). The end group conversion of **4** into **7** is displayed by the decay of **4**, while **7** increases. The end group conversion of **4** is quantitative after 15 min, which was also evidenced via ^{1}H NMR spectroscopy (refer to Figure 42). The disappearance of resonances associated with **4** (I: δ = 10.69 ppm; III: δ = 2.53 ppm) in combination with the appearance of resonances belonging to **7** (II: δ = 10.69 ppm) evidences the quantitative end group transformation of the *o*-methyl benzaldehyde moiety into the Diels-Alder product. Furthermore, the parallel conversion of **17** into **18** after an irradiation time of 15 min with the PL-L lamp is negligible and affords a yield of less than 3 % (refer to Figure 41a).

Hence, the irradiation in the wavelength range between 310-350 nm allows the orthogonal activation of *o*-methyl benzaldehyde in the presence of diphenyl tetrazole.

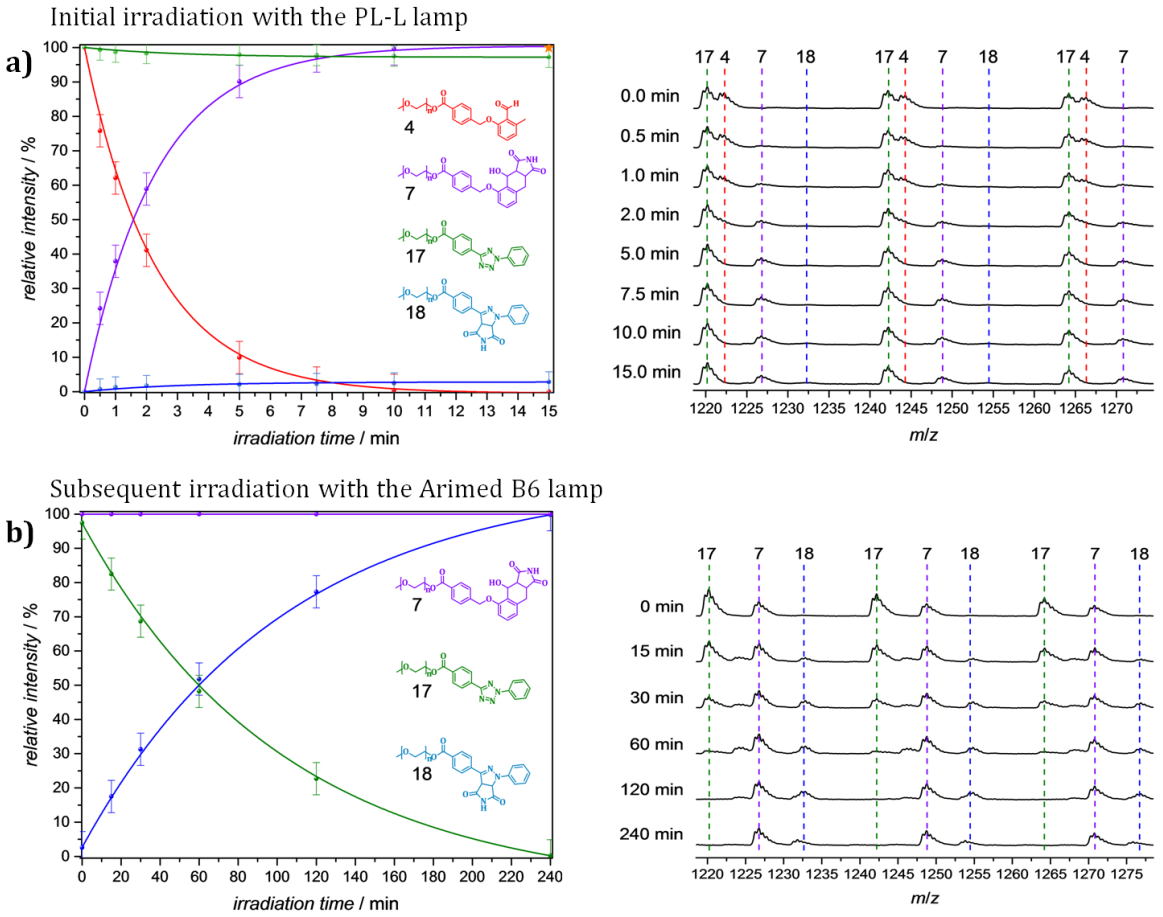

Figure 41: *Kinetic data plot showing the evolution of the relative intensities of* ***4*** *(1 eq.),* ***17*** *(1 eq.) and* ***6*** *(10.7 eq.) when irradiated following the sequence depicted in Scheme 35. A zoom of the mass spectra in the double charged region is included for each data point in the kinetic plot: a) eight samples were irradiated with the PL-L lamp at* λ_{max} *= 365 nm up to 15 min. The intensity of the mass spectrum signal of* ***4*** *decreases as a function of time, in combination with a signal intensity increase of* ***7****. The signal intensity of* ***17*** *decreases negligibly. The quantitative conversion of* ***4*** *into* ***7*** *was also determined via* ^{1}*H NMR and is marked in the kinetic plot by the orange star. b) All six of the samples were initially irradiated with the PL-L lamp for 15 min. The kinetic data plot was determined by irradiating the six samples with the Arimed B6 lamp at* λ_{max} *= 315 nm up to 240 min. A decrease in the relative abundance of* ***17*** *and an increase of cycloadduct* ***18*** *is observed. Compound* ***4*** *was completely converted into compound* ***7*** *prior to irradiation at* λ_{max} *= 365 nm. The image was modified from ref.*[18] *with permission from Wiley-VCH, 2016.*

Next, the diphenyl tetrazole reaction kinetics were investigated. The same system (an equimolar amount of **4** and **17** as well as a 10.7 eq. excess of **6** in DCM) was initially irradiated with the PL-L lamp for 15 min in order to remove all *o*-methyl benzaldehyde functionalities from the system. The remaining diphenyl tetrazole species **17** was subsequently irradiated for pre-set time intervals starting from 0 to 240 min using the Arimed B6 lamp (λ = 280-440 nm; λ_{max} = 315 nm; 36 W) whereby the evolution of the

species **17** as well as **18** were traced via mass spectrometry during the irradiation (refer to Figure 41b). The kinetic data elucidate the decay of **17** and the simultaneous increase of **18** including a quantitative yield of the end group transformation after 240 min.

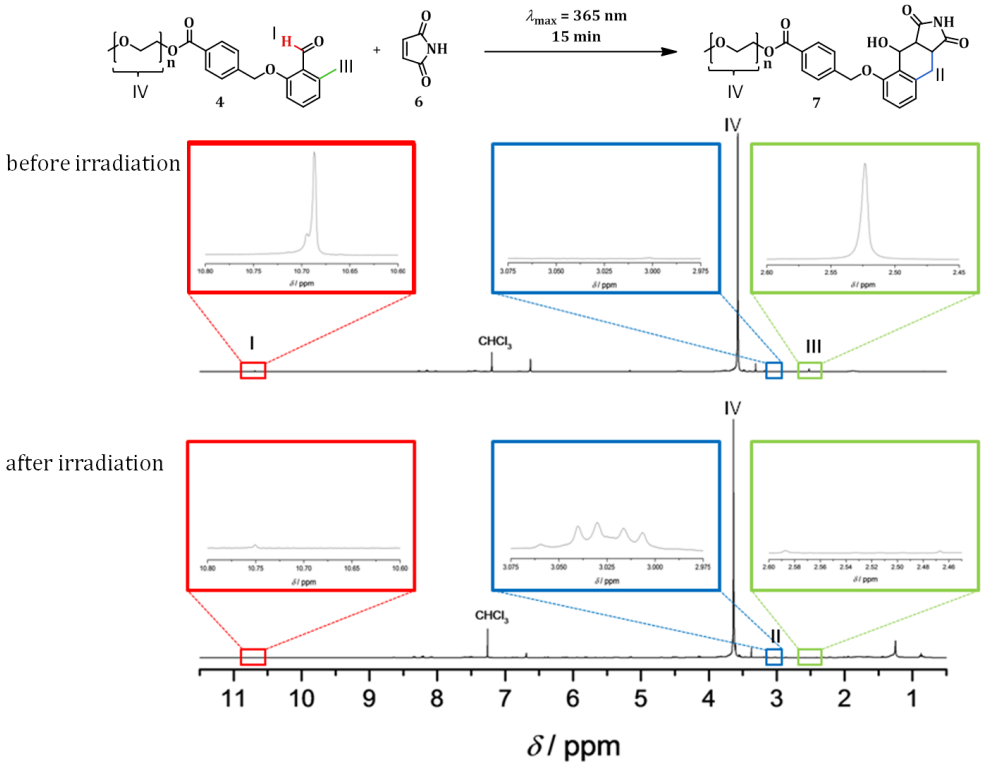

Figure 42: *The selective orthogonal transformation of **4** into the [4+2]-cycloadduct **7** was followed via resonance shifts detected by ^{1}H NMR spectroscopy. An equimolar mixture of **4** and **17** was initially dissolved in $CDCl_3$ and analysed via ^{1}H NMR spectroscopy. A mixture of **4** (1 eq.), **17** (1 eq.), and **6** (10.7 eq.) was subsequently irradiated in dichloromethane for 15 min with the PL-L lamp and analysed via ^{1}H NMR spectroscopy in $CDCl_3$. The image was modified from ref.*[18] *with permission from Wiley-VCH, 2016.*

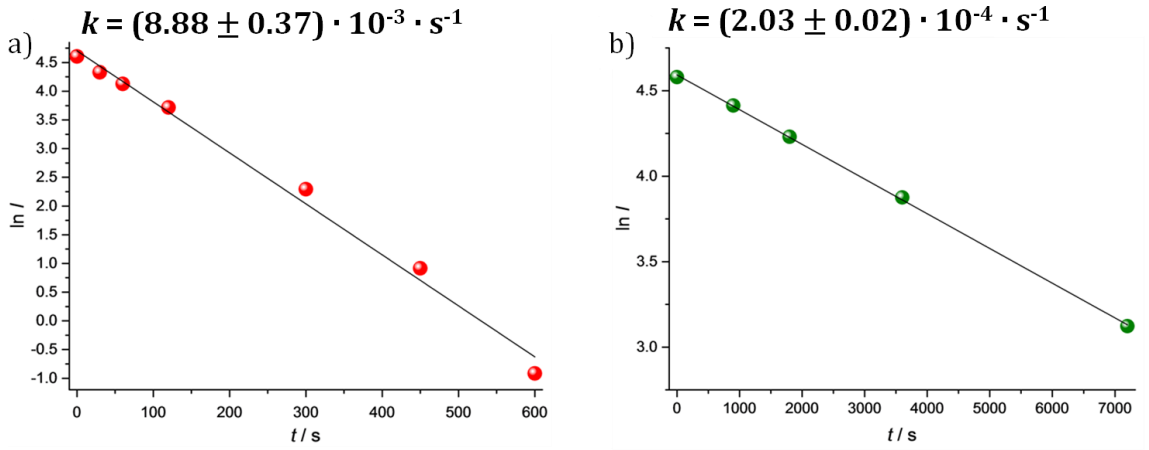

Figure 43: *a) First order plot of the relative intensities of the o-methyl benzaldehyde capped PEG **4** (1 eq.) irradiated in the presence of **17** (1 eq.) and **6** (10.7 eq) in a one-pot reaction. b) First order plot of the diphenyl tetrazole capped PEG **17** depletion (1 eq.) that was irradiated after **4** had been converted into **7**. The image was modified from ref.*[18] *with permission from Wiley-VCH, 2016.*

The decay of both **4** and **17** in the λ-orthogonal system follows pseudo first order kinetics. The rate coefficient for the photoenol reaction is $k = (8.88 \pm 0.37) \cdot 10^{-3}$ $s^{-1}$and $k = (2.03 \pm 0.02) \cdot 10^{-4}$ s^{-1} for the NITEC reaction under the chosen conditions (refer to Figure 43). The differing rate coefficients as well as the different reaction times for both photoactive compounds suggest the orthogonality in one direction between *o*-methyl benzaldehyde and tetrazole is underpinned by a kinetic rate effect. Thus, the diphenyl tetrazole terminated PEG **17** and **6** were irradiated for 15 min with the PL-L and Arimed B6 lamp, respectively.

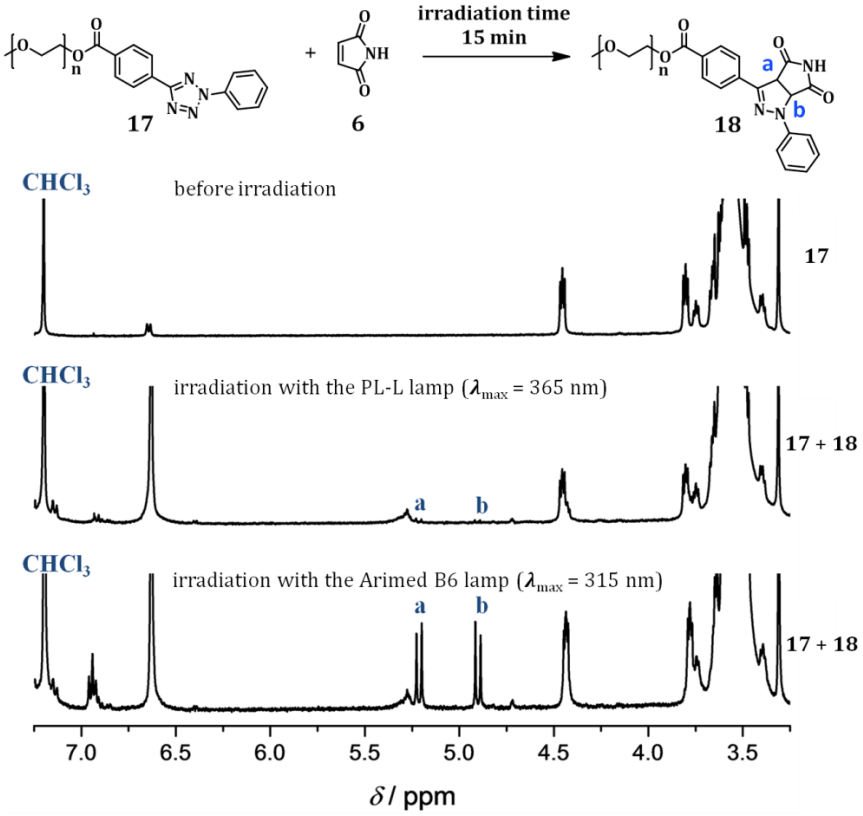

Figure 44: *Following the transformation of **17** into **18** after an irradiation time of 15 min with two lamps: Irradiation with the PL-L lamp (λ_{max} = 365 nm) leads to a conversion of 4%. The irradiation with the Arimed B6 lamp (λ_{max} = 315 nm) leads to a conversion of 13%. The conditions were selected identical to those used for the experiments reported in Figure 41 with the only difference that **4** was not present. The conversion was determined by rationing a specific set of aromatic protons of the diphenyl tetrazole (**δ** = 8.27 ppm, 2H) with the generated resonances a (**δ** = 5.19 ppm) and b (**δ** = 4.93 ppm) of the cycloadduct. The image was modified from ref.*[18] *with permission from Wiley-VCH, 2016.*

The emission of the Arimed B6 lamp shows a better overlap with the absorption of the diphenyl tetrazole compared to the PL-L lamp. Thus, the investigation of the wavelength dependent diphenyl tetrazole conversion, which is the key aspect of λ-orthogonality, was traced via ^{1}H NMR spectroscopy by the appearance of inherent 4,5-dihydro pyrazole resonances (a: δ = 5.19 ppm; b: δ = 4.93 ppm) (refer to Figure 44). As a result, the

irradiation with the PL-L lamp leads to a diphenyl tetrazole conversion of 4 %, whereas the diphenyl tetrazole conversion is 13 % featuring the Arimed B6 lamp under identical conditions. The experimental data demonstrates that ***λ***-orthogonality of the present system was not necessarily achieved by kinetic effects. Moreover, the wavelength dependent selectivity was generated by the choice of an appropriate light source. In general, *click* chemistry requires equimolarity.[230] Therefore, a second kinetic study was performed with the same system containing **4**, **17**, and **6.** The maleimide concentration was reduced from 10.7 eq. close to 2 eq. whereby one equivalent of **6** was provided for **4** and **17**, respectively.

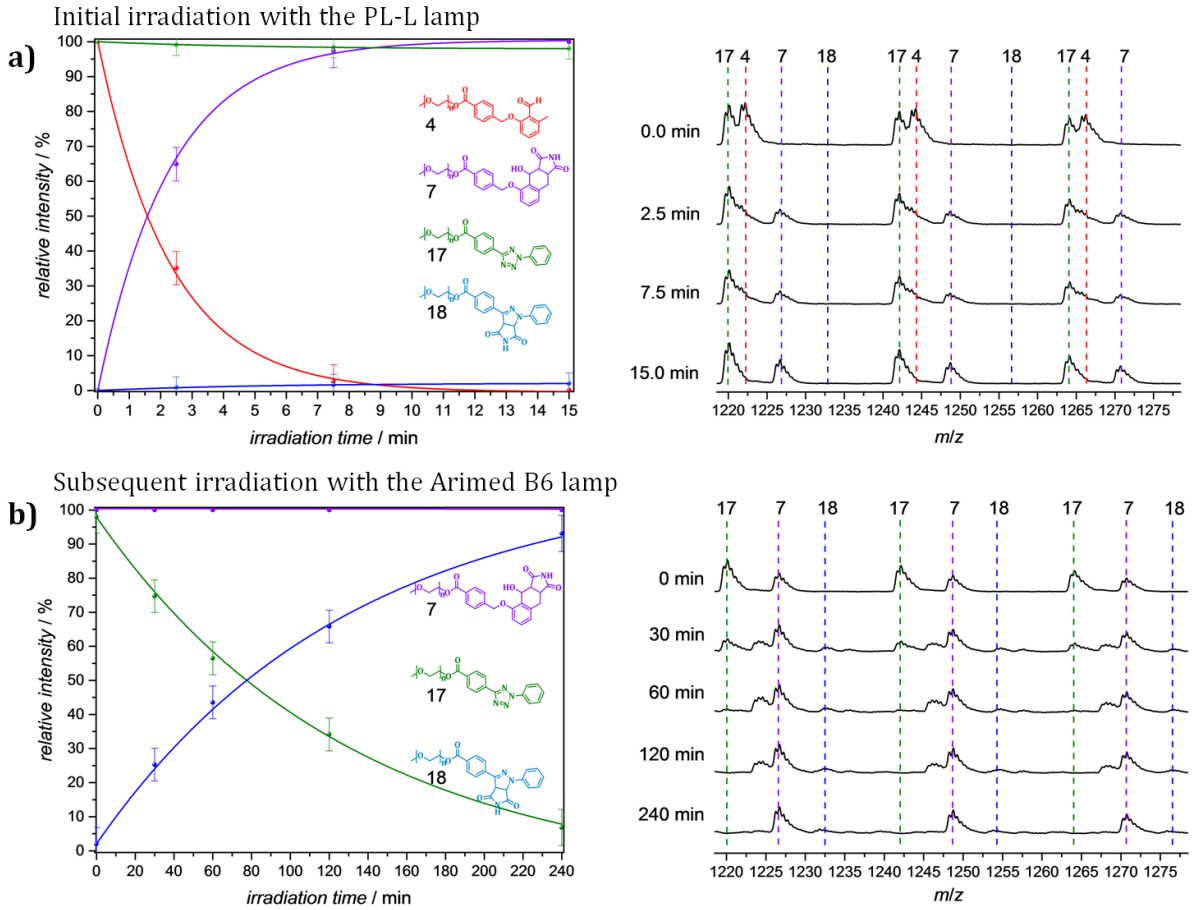

Figure 45: *Kinetic data plot showing the evolution of the relative intensities of* ***4*** *(1 eq.),* ***17*** *(1 eq.) and* ***6*** *(2.4 eq.). A zoom (m/z = 1218.50 - 1278.50) of the mass spectra into the double charged region is included for each data point in the kinetic plot: a) four samples were irradiated with the PL-L lamp (λ_{max} = 365 nm) for up to 15 min. The intensity of the mass spectrum signal of* ***4*** *decreased concomitantly with a signal intensity increase of* ***7****. The signal intensity of* ***17*** *decreased negligibly. b) All of the five samples were initially irradiated with the PL-L lamp (λ_{max} = 365 nm) for 15 min. Next, the kinetic data plot for the reaction with the diphenyl tetrazole species was determined by irradiating the five samples with the Arimed B12 lamp (λ_{max} = 315 nm) up to 240 min. The intensity of the signals associated with* ***17*** *decreased subsequently in combination with a signal intensity increase of the signals associated with species* ***18****. The image was adapted from ref.*[18] *with permission from Wiley-VCH, 2016.*

The **λ**-orthogonal principle in one direction was employed according to the sequential irradiation strategy: initial photoreaction of **4** with the PL-L lamp, followed by the subsequent photoreaction of **17** with the Arimed B6 lamp. The kinetic study featuring 2.4 eq. of **6** was performed via mass spectrometric analysis in a similar fashion as the previous kinetic study featuring 10.7 eq. of **6**.The end group conversion of **4** into **7** after the irradiation up to 15 min with the PL-L lamp is displayed in the kinetic data by the decay of **4**, while **7** increased simultaneously. The end group conversion of **4** is quantitative after 15 min, whereas the conversion of **17** into **18** after irradiation with the PL-L lamp in the same time range shows a negligible yield of less than 3 % (refer to Figure 45a). The investigation of the diphenyl tetrazole reaction kinetics was carried out after the initial irradiation of the *o*-methyl benzaldehyde species. The remaining tetrazole species **17** was subsequently irradiated for pre-set time intervals between 0 to 240 min using the Arimed B6 lamp, whereby the relative amount of **17** decreases and **18** shows a concomitant increase (refer to Figure 41b).

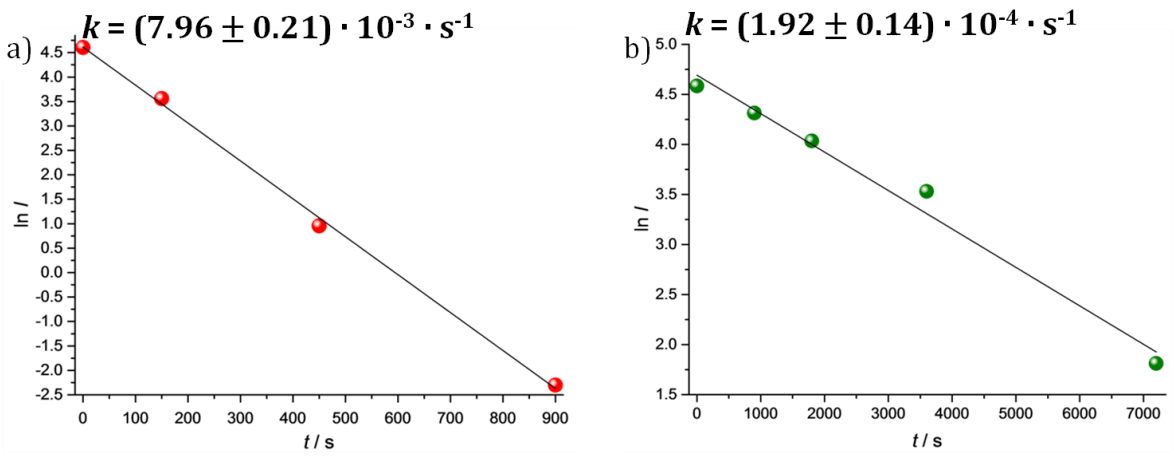

Figure 46: *a) First order plot of the relative intensities of the o-methyl benzaldehyde capped PEG* ***4*** *(1 eq.) irradiated in the presence of* ***17*** *(1 eq.) and* ***6*** *(10.7 eq) in a one-pot reaction. b) First order plot of the diphenyl tetrazole capped PEG* ***17*** *depletion (1 eq.), irradiated after* ***4*** *had been converted into* ***7****. The image was adapted from ref.*[18] *with permission from Wiley-VCH, 2016.*

The decay of both **4** and **17**, respectively, follows again pseudo first order kinetics. The first order plot of the system featuring 2.4 eq. of **6** results in a rate coefficient for **4** of $k = (7.96 \pm 0.21) \cdot 10^{-3}$ $s^{-1}$and for **17** of $k = (1.92 \pm 0.14) \cdot 10^{-4}$ s^{-1} (refer to Figure 46). The kinetic rate coefficients of both photoactive compounds are slightly decreased compared to the system containing 10.7 eq. of **6** (refer to Figure 43). Nevertheless, the kinetic investigation clearly states that the inherent maleimide concentration of the **λ**-

orthogonal system only has a small influence on the reaction time and the light induced selectivity of the *o*-methyl benzaldehyde as well as the diphenyl tetrazole.

In summary, the presented **λ**-orthogonal polymer end group transformations, featuring a varying amount of the maleimide species **6**, demonstrated that *o*-methyl benzaldehyde can be exclusively activated in the presence of diphenyl tetrazole. Although, the *o*-methyl benzaldehyde reaction kinetics exceed the diphenyl tetrazole reaction kinetics, **λ**-orthogonality of the system is not solely achieved by a kinetic effect. In this regard, the wavelength dependent irradiation of diphenyl tetrazole indicates that the overlapping between absorption of the diphenyl tetrazole compound and the emission of the light source has an even more significant influence on the conversion than kinetic effects of the photoreaction.

4.2.2. End Group Modifications in a One Polymer One-Pot System

The fusing of the **λ**-orthogonal photosystem into one molecule based on an oligomer PEG chain generates the α,ω-functional bilinker **19**, which carries *o*-methyl benzaldehyde and diphenyl tetrazole at each chain end. The oligomer bilinker **19** is a monodisperse macromolecule containing precisely 19 ethylene oxide repeating units and has a molar mass of M = 1480.65 g·mol^{-1} (refer to Scheme 37).

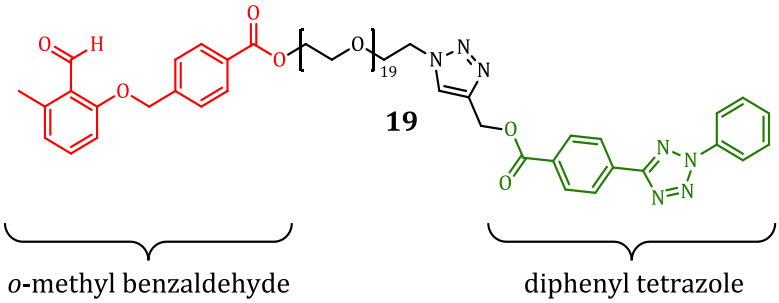

Scheme 37: *The oligomer α,ω-functional bilinker **19** carrying an o-methyl benzaldehyde as well as a diphenyl tetrazole moiety at each PEG chain end. The macromolecule is monodisperse and has a molar mass of 1480.65 g·mol^{-1}.*

Compound **19** absorbs light below 400 nm according to UV/vis spectroscopy and the absorption could be deconvulated into the respective absorptions of *o*-methyl benzaldehyde and diphenyl tetrazole (refer to Figure 47).

The utilisation of **19** significantly extends the application scope of **λ**-orthogonality, as it allows two consecutive polymer end group transformations on one macromolecule in a site-specific fashion.

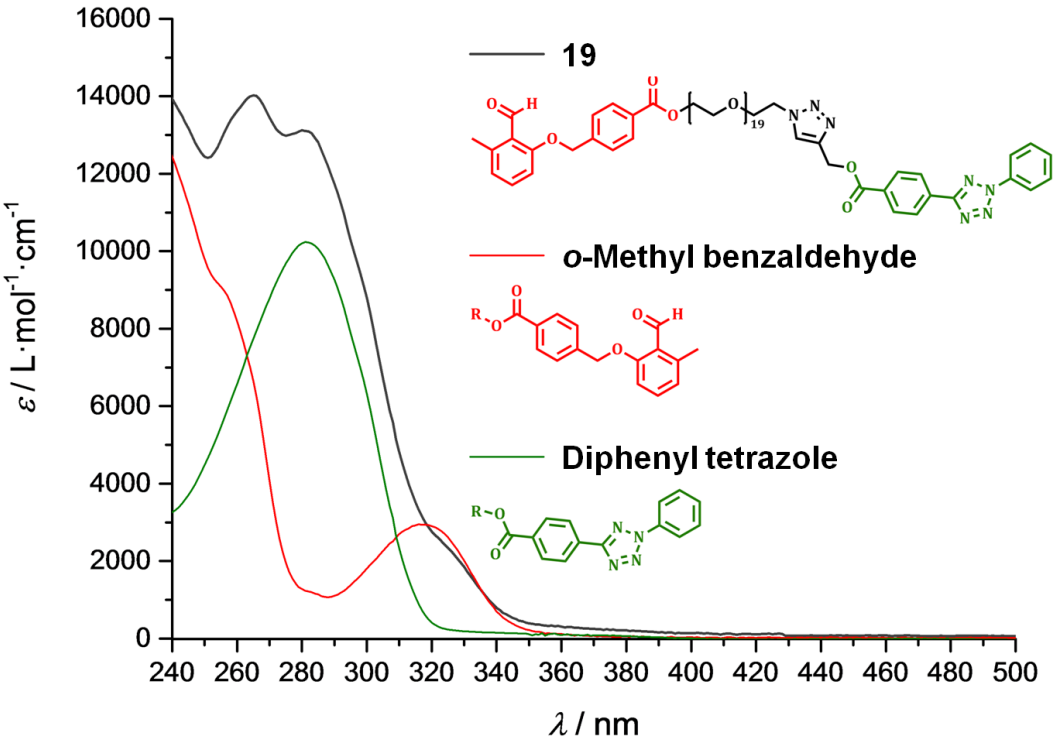

Figure 47: *UV/vis spectrum of* ***19****. The absorption of* ***19*** *can be deconvulated into the UV/vis absorption of o-methyl benzaldehyde and diphenyl tetrazole. The image was adapted from ref.*[303] *with permission from the Royal Society of Chemistry (RSC), 2016.*

The **λ**-orthogonal principle in one direction was established by the wavelength dependent addition of maleimide **6** onto **19** in DCM. The mixture was initially irradiated for 15 min with the PL-L lamp followed by an irradiation period of 4 h using the Arimed B6 lamp. The obtained product of the photoenol reaction **20** and the product of the subsequent NITEC reaction **21** were analysed via mass spectrometry (refer to Figure 48).

The mass spectrometry data reveals the complete *o*-methyl benzaldehyde end group transformation of **19** yielding **20** in combination with an additional diphenyl tetrazole conversion of 3 % resulting in the formation of **21** during irradiation with the PL-L lamp proving that the **λ**-orthogonal principle can be incorporated into a unimolecular system.

The following irradiation step with the Arimed B6 led to a complete end group modification of **19** resulting in **21**. A zoom into the mass spectrometric signal of **21** unveils the presence of two overlapping products. The first product is the expected 4,5-dihydro pyrazole conjugated bilinker **21**. The other product **21-2H** is obtained by the aromatisation of **21** via removal of two hydrogen atoms in the 4,5-dihydro pyrazole ring (refer to Figure 49).

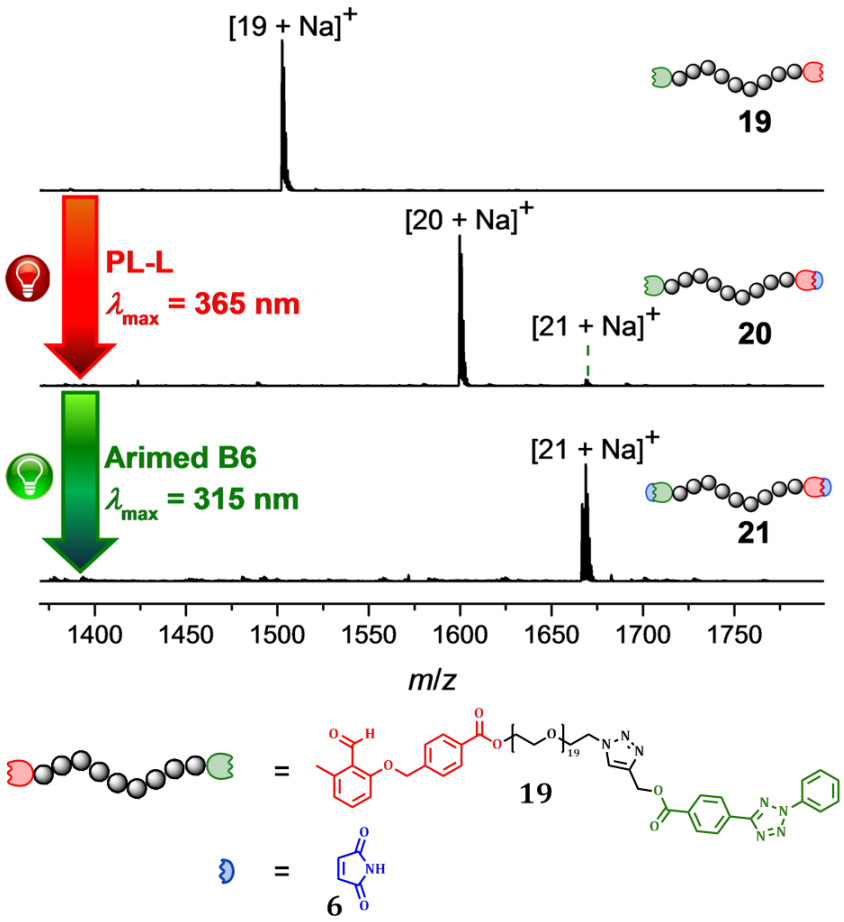

Figure 48: *A system consisting of the bilinker **19** and maleimide **6** was irradiated for 15 min with the PL-L lamp leading to the formation of **20** via the regioselective addition of **6** towards the o-methyl benzaldehyde end group of **19**. The system was subsequently irradiated for 4 h with the Arimed B6 lamp forming the product **21** in which both end groups were quantitatively converted. The image was modified from ref.*[18] *with permission from Wiley-VCH, 2016.*

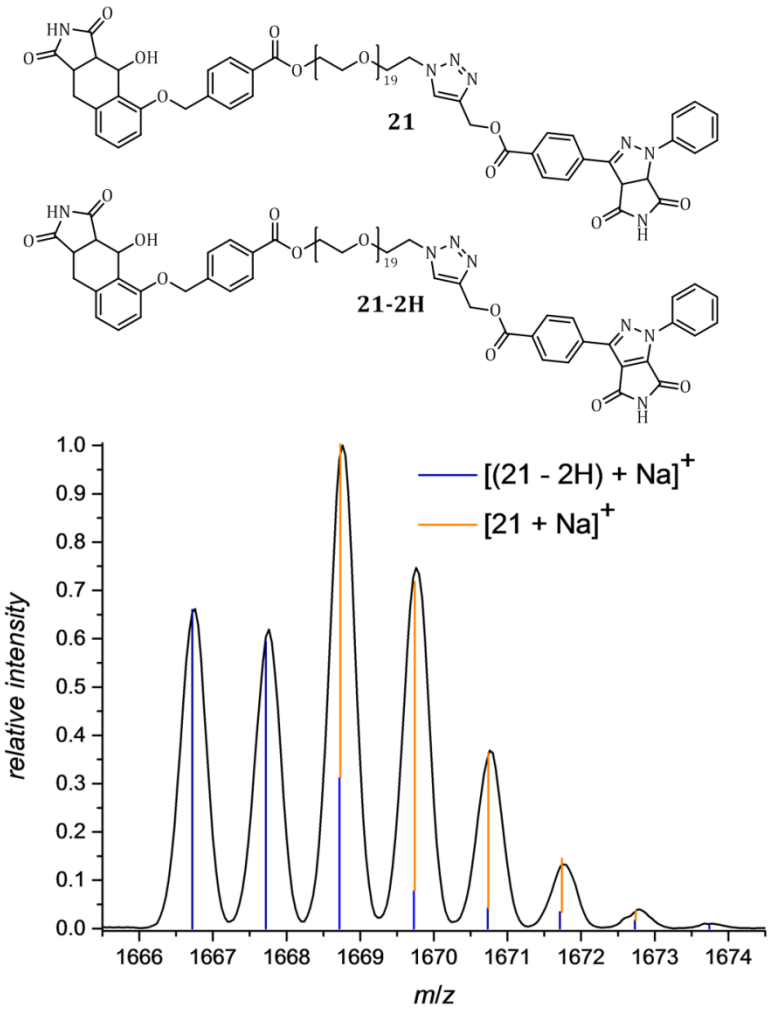

Figure 49: *A zoom into m/z range of 1665.5-1674.5 of the isotopic pattern reveals the NITEC reaction yielded two products: the previously detected 4,5-dihydro pyrazole* ***21*** *as well as the pyrazole* ***21-2H*** *which was obtained via aromatisation of* ***21****. The image was modified from ref.*[18] *with permission from Wiley-VCH, 2016.*

Another ***λ***-orthogonal site-specific addition was carried out with application-oriented functionalities such as fluorescein which shows wide applicability in areas such as antibody tests[309] and biochemistry.[310] The end group transformation was implemented for a system containing an equimolar amount of **19** and fluorescein 5-maleimide **22** in DCM. The mixture was initially irradiated for 20 min with the PL-L lamp. Subsequently, the system was mixed with acrylic acid and irradiated for 4 h with the Arimed B6 lamp. The obtained product of the photoenol reaction **23** and the product of the subsequent diphenyl tetrazole reaction **24** were analysed via mass spectrometry (refer to Figure 50).

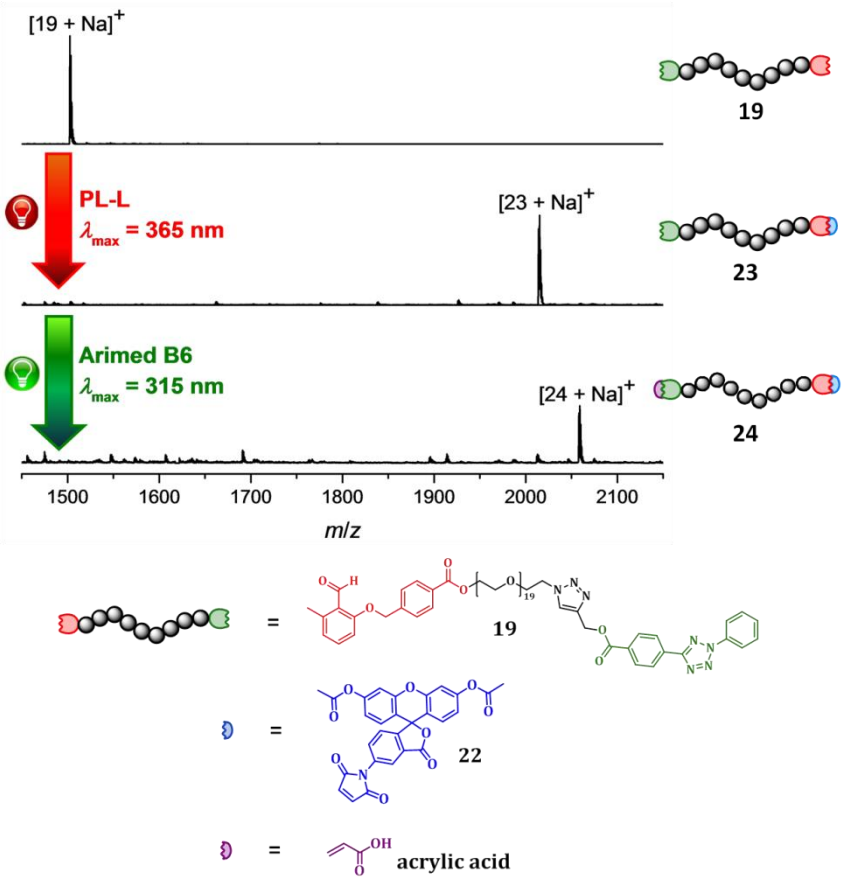

Figure 50: *A system consisting of the bilinker* ***19*** *and fluorescein 5-maleimide* ***22*** *was irradiated for 20 min with the PL-L lamp leading to the formation of* ***23*** *via the regioselective addition of* ***22*** *towards the o-methyl benzaldehyde end group of* ***19****. The system was subsequently irradiated with acrylic acid for 4 h with the Arimed B6 lamp forming the product* ***24*** *in which both end groups were quantitatively converted. The image was modified from ref.*[18] *with permission from Wiley-VCH, 2016.*

The mass spectrometry data demonstrate the complete *o*-methyl benzaldehyde end group transformation of **19** yielding **23** during irradiation with the PL-L lamp. Thus, the **λ**-orthogonal principle in one direction is also verified for a maleimide carrying further functionalities. The subsequent irradiation step with the Arimed B6 leads to a complete end group modification of **19** resulting in **24**.

4.2.3. Triblock Copolymer Formation via an Oligomeric Bilinker Intermediate

The previous section demonstrated the wavelength dependent attachment of small molecules onto the oligomer bilinker **19** leading to selective end group transformations. The substitution of small enes by maleimide terminated macromolecules in the process allows the site-specific formation of triblock copolymers. Thus, the maleimide terminated polylactide **25** (maleimide terminated pL) (M_n = 4600) was synthesised for its selective attachment onto **19**. The structure of **25** is depicted in Scheme 38.

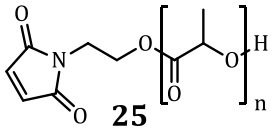

Scheme 38: *The maleimide terminated pL **25** (M_n = 4600).*

The stepwise triblock copolymer formation was carried out in a mixture of **19** (1.0 eq.) and an excess of **25** (2.3 eq.) in DCM. The system was initially irradiated for 15 min with the PL-L lamp leading to the formation of the diblock copolymer **26** followed by an irradiation period of 6 h with the Arimed B6 lamp, affording the triblock copolymer **27**. The obtained structures **26** and **27** are depicted in Scheme 39.

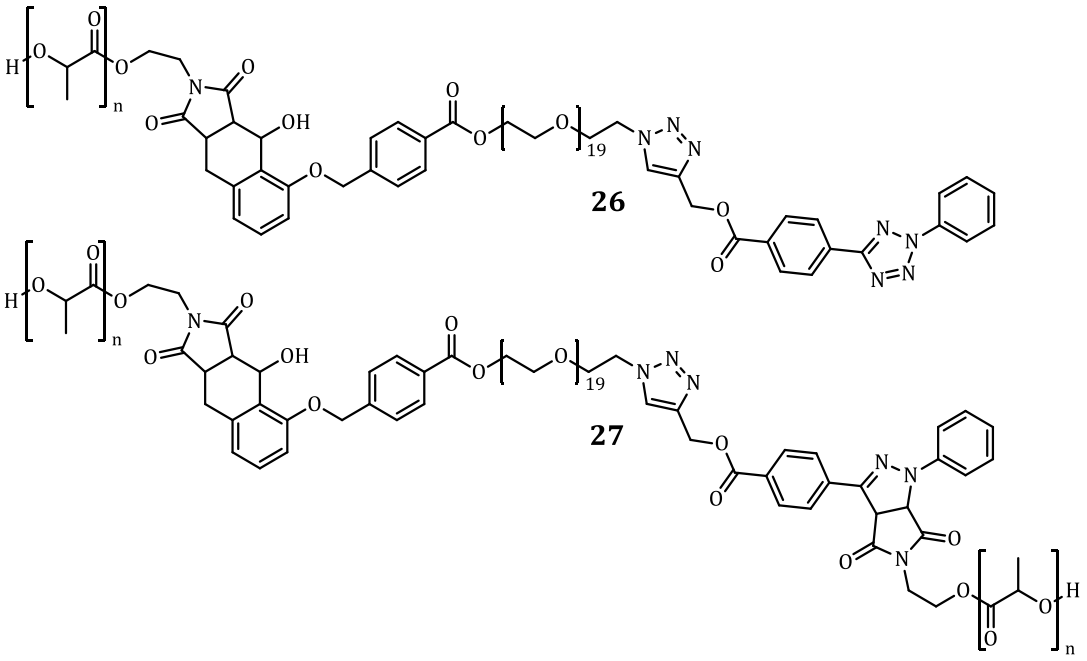

Scheme 39: *The diblock **26** is formed after the first irradiation with the PL-L lamp and the triblock copolymer **27** is formed after the subsequent irradiation with the Arimed B6 lamp.*

The efficiency of the **λ**-orthogonal block copolymer formation was evidenced via GPC. The GPC data indicate the clear peak shift of **19** (M_n = 1500) to the diblock **26** (M_n = 6000) due to the selective attachment of **25** after the irradiation with the PL-L lamp. The subsequent shift of **26** to **27** (M_n = 6000) indicates the complete triblock copolymer formation due to the addition of **25** to the diphenyl tetrazole moiety (refer to Figure 51).

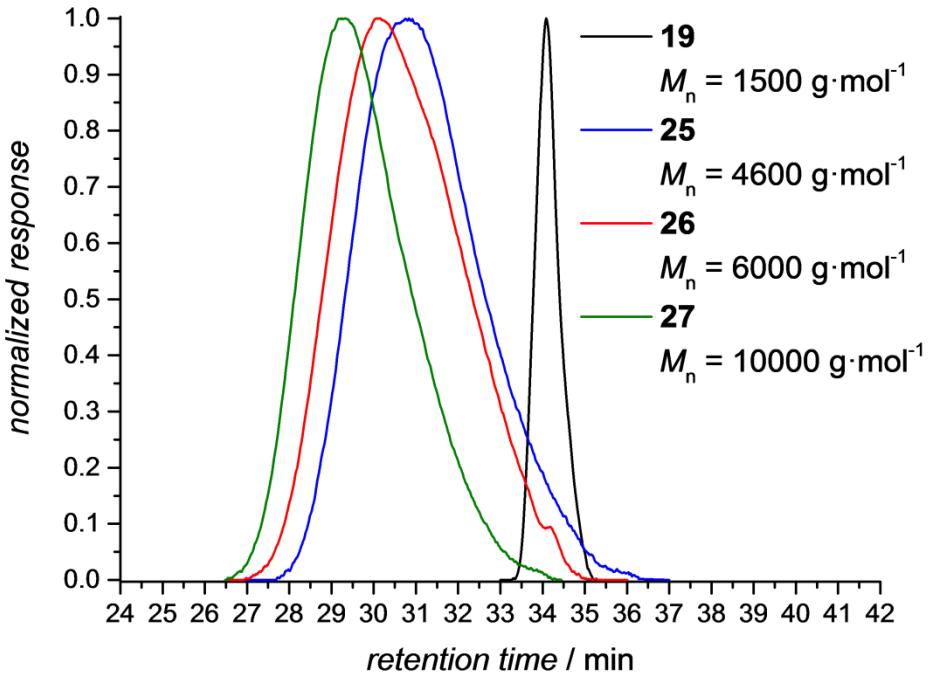

Figure 51: *A system consisting of the bilinker **19** and the maleimide capped terminated pL **25** (M_n = 4600) was irradiated for 15 min with the PL-L lamp forming selectively the diblock polymer **26**. The system was subsequently irradiated for 6 h with the Arimed B6 forming the triblock **27**. GPC reported relative to a PMMA calibration. The image was adapted from ref.*[18] *with permission from Wiley-VCH, 2016.*

The ^{1}H NMR analysis of the block copolymer formation allows for a closer examination. Hereby, the quantitative formation of the diblock copolymer **26** after the first irradiation procedure is revealed by the disappearance of the significant *o*-methyl benzaldehyde resonances (the aldehyde signal I: δ = 10.69 ppm as well as the aryl methyl signal II: δ = 2.53 ppm) whereas the resonances associated with the Diels-Alder conjugated ring (III: δ = 2.91-3.24 ppm) appear. In addition, the tetrazole conversion (IV: δ = 5.47 ppm) after the first irradiation is 3 %. The resonances of the remaining maleimide terminated pL **25** (V: δ = 6.73 ppm) are still detectable, despite an overlap of the signal with aromatic resonances of **19**, indicating that one equivalent reacted with **19** (refer to Figure 52). The complete NITEC reaction after the subsequent irradiation step with the

Arimed B6 lamp is evidenced by the quantitative increase of signal IV in combination with the absence of the maleimide resonance V.

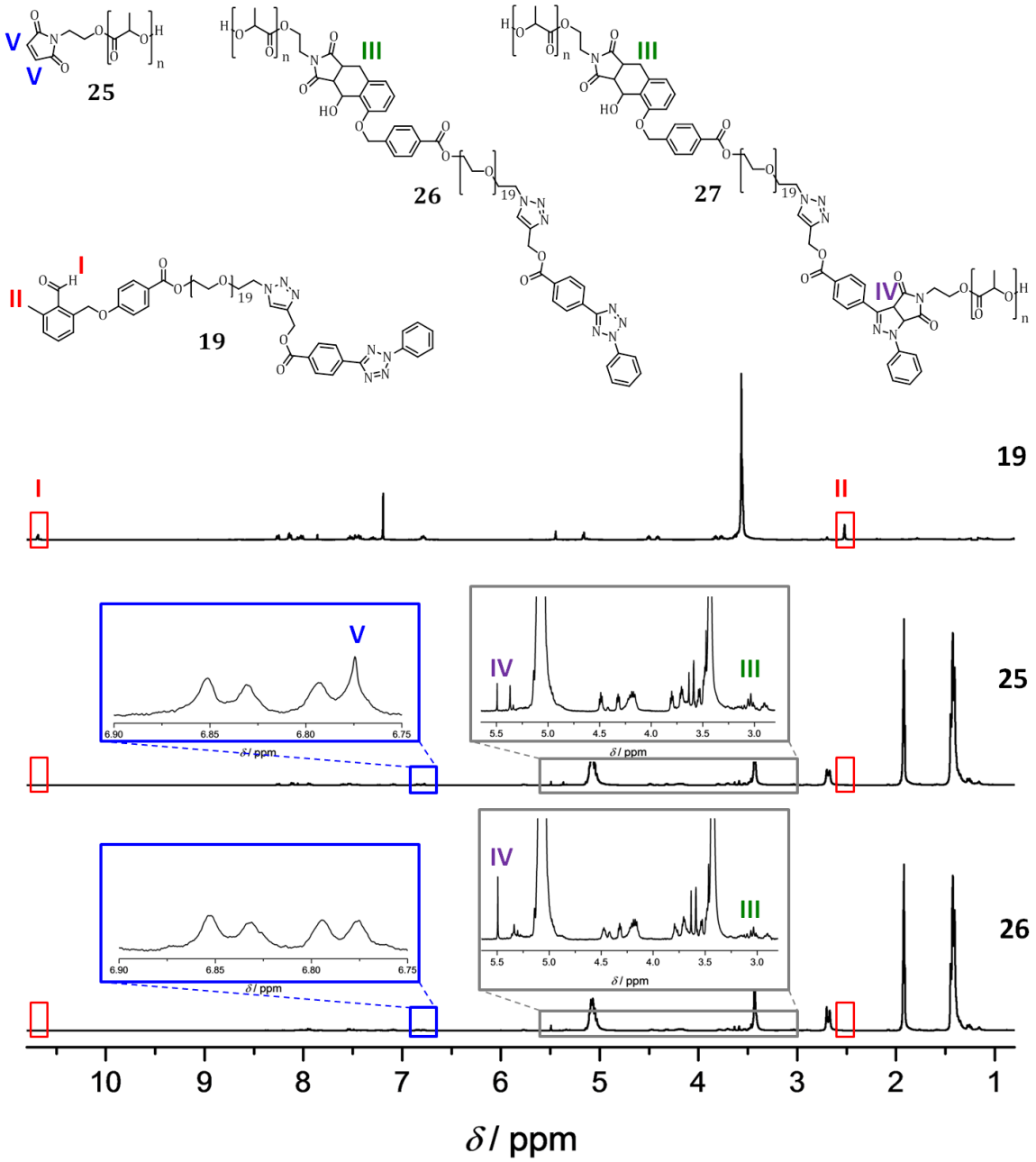

Figure 52: *^{1}H NMR analysis of the stepwise λ-orthogonal triblock synthesis. The photo triggered conversion of* ***19*** *with an excess of* ***25*** *is visible in the central spectrum. While the signals of 9 disappears, fundamental signals of 14 and left over 11 are detectable after the first irradiation. The lower spectrum demonstrates the final triblock conversion after the last irradiation step. The image was modified from ref.*[18] *with permission from Wiley-VCH, 2016.*

In addition, the ***λ***-orthogonality concept was applied for the selective attachment of the antimicrobial peptide magainin[311] towards the bilinker **19** in order to form a novel block copolymer hybrid structure combining the properties of artificial polymers and bioactive macromolecules. A system containing **19** and maleimide capped magainin **28**

in dimethylformamide (DMF) was irradiated for 30 min with the PL-L lamp. Subsequently, the obtained diblock **29** and maleimide terminated pL **30** (M_n = 8000) were irradiated for 6 h with the Arimed B6 lamp (refer to Scheme 40) yielding the hybrid triblock **31**. The complete formation of the hybrid diblock **29** was verified via mass spectrometry (refer to Figure 53) by a clear signal shift regarding the mass of the starting material **19**.

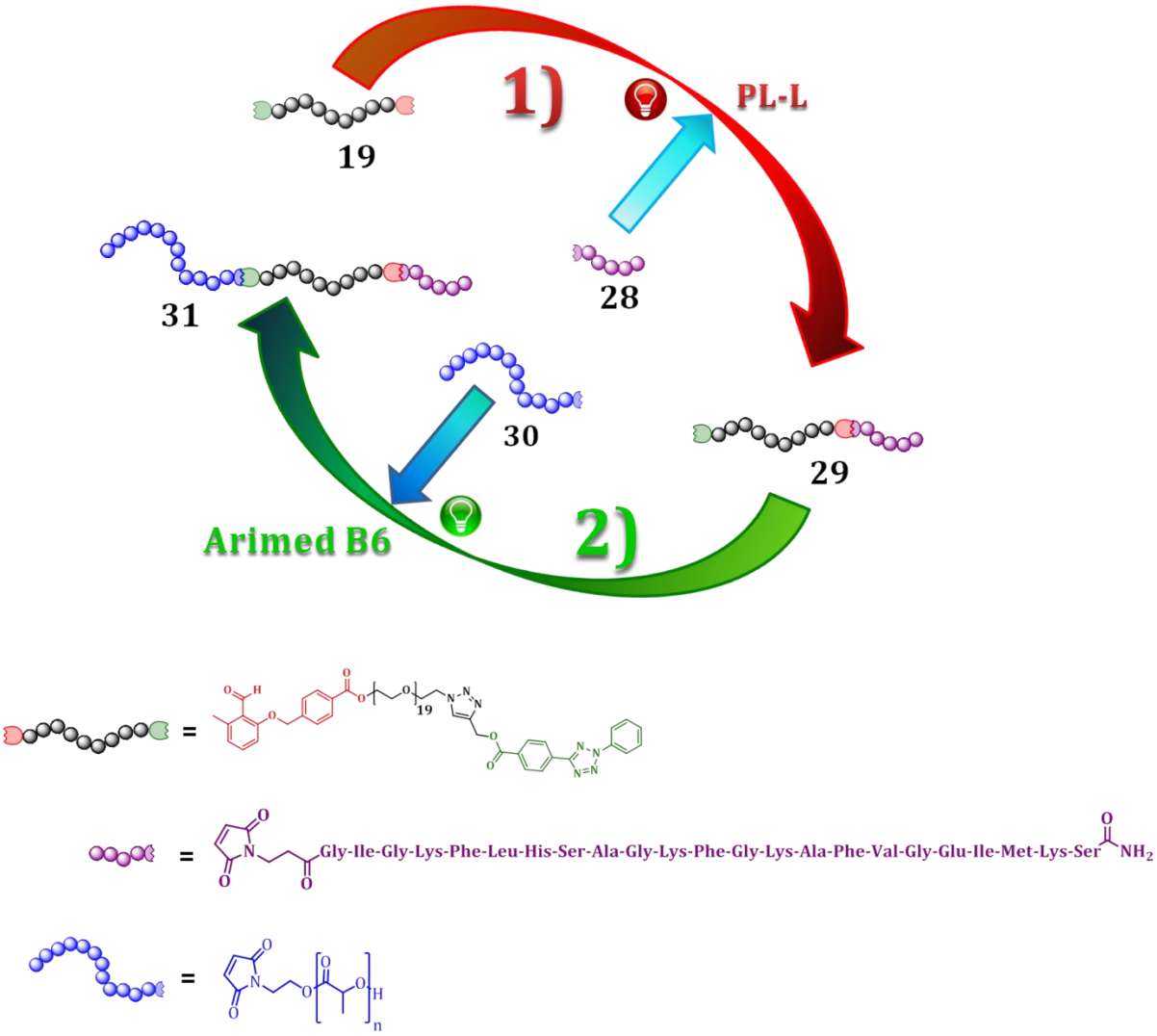

***Scheme 40*:** *Stepwise construction of the triblock polymer/peptide hybrid **30** starting from the bilinker **19**. The irradiation with the PL-L lamp of **19** and an equimolar amount of the maleimide capped magainin **28** leads to the site-specific formation of the magainin-PEG diblock **29**. The subsequent irradiation of **29** with an equimolar amount of **25** with the Arimed B6 lamp forms the hybrid triblock macromolecule **30**. The image was adapted from ref.*[18] *with permission from Wiley-VCH, 2016.*

The triblock formation was traced via GPC. The data indicates a distinct shift of the bilinker **19** (M_n = 1500) to the diblock **29** (M_n = 4000) due to the selective attachment of **28** after the initial irradiation with the PL-L lamp. The magainin moiety **28** (M_n = 4000)

is not included in the GPC analysis due to its insolubility in THF. The subsequent shift of **29** to **31** (M_n = 12000) reveals the complete hybrid triblock copolymer formation due to the addition of **30** (M_n = 12000) to the tetrazole moiety (refer to Figure 54).

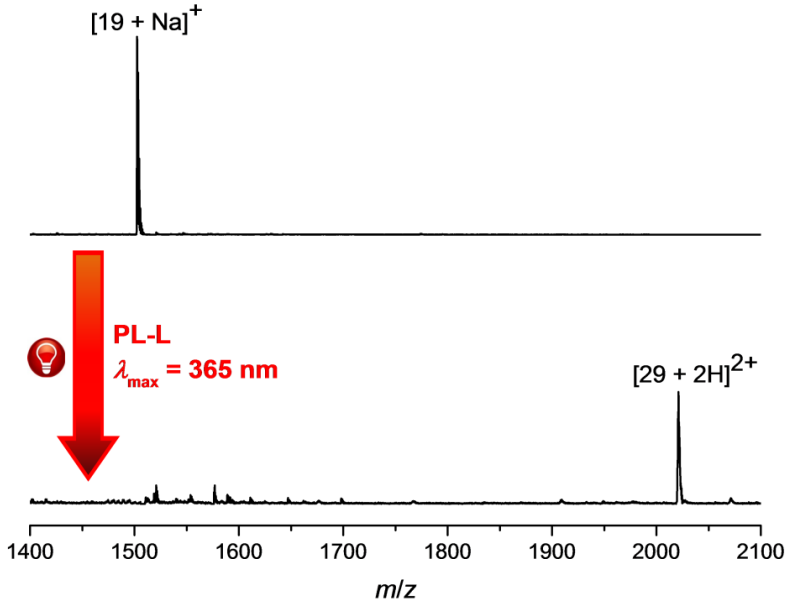

Figure 53: *A system consisting of the bilinker **19** and an equimolar amount of magainin maleimide **28** was irradiated for 30 min with the PL-L lamp leading to the site-specific addition of magainin at the o-methyl benzaldehyde terminus of the bilinker **19**, affording **29**. The image was modified from ref.*[18] *with permission from Wiley-VCH, 2016.*

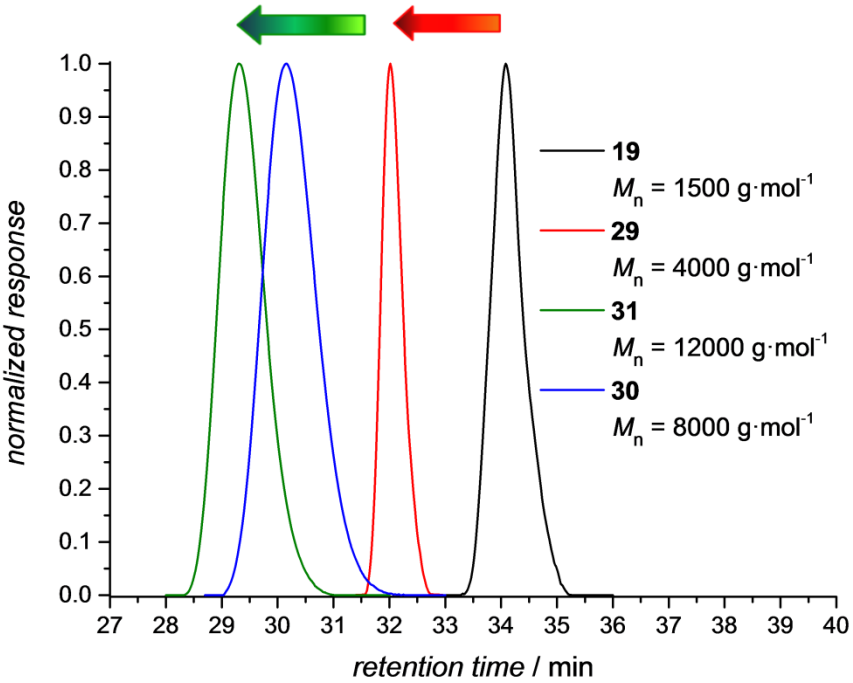

Figure 54: *A system consisting of the bilinker **19** and an equimolar amount of the magainin maleimide **28** was irradiated for 30 min with the PL-L lamp selectively forming the peptide-PEG diblock **29**. The system was subsequently mixed with the maleimide capped polylactide **30** and irradiated for 6 h with the Arimed B6 lamp forming the hybrid triblock **31**. GPC reported relative to a PMMA calibration. The image was adapted from ref.*[18] *with permission from Wiley-VCH, 2016.*

In summary, the λ-orthogonal principle was successfully implemented on the single oligomeric bilinker **19** carrying *o*-methyl benzaldehyde and diphenyl tetrazole at each chain end. In addition, the bilinker was employed for the wavelength dependent, site-specific attachment of various enes carrying distinct functionalities. Moreover, several triblock copolymer formations were applied in the basis of the bilinker **19**. In this respect, a maleimide terminated polymer was initially attached to the *o*-methyl benzaldehyde chain end at λ_{max} = 365 nm, followed by site-specific attachment of another maleimide terminated polymer to diphenyl tetrazole terminus at λ_{max} = 315 nm.

4.3. Star Polymer Formation via λ-Orthogonality in Both Directions

The previously presented ***λ***-orthogonal principle in one direction relies on the preference of the light induced reactivity of *o*-methyl benzaldehyde with maleimides over diphenyl tetrazole in the wavelength regime between 310-350 nm. However, the converse photoreaction path, i.e. the selective light triggered diphenyl tetrazole reaction in the presence of *o*-methyl benzaldehyde is not possible. An initial diphenyl tetrazole activation is not possible, as the absorptivities of both photoactive compounds below 310 nm (refer to Figure 40, Chapter 4.2) overlap. Therefore, a complete orthogonal photoreaction system requires two photoactive compounds that can be exclusively activated in both directions.

However, the reversible photochemical deactivation of *o*-methyl benzaldehyde allows the exclusive photoreaction of the diphenyl tetrazole within a fully ***λ***-orthogonal system. The imine transformation of *o*-methyl benzaldehyde with hexylamine (refer to Chapter 3.2) represents an ideal reaction method for its photochemical deactivation, since the obtained imine is stable in solution, does not undergo a photochemical reaction with maleimides, and can be readily converted into the photoactive *o*-methyl benzaldehyde via hydrolysis (refer to Scheme 41).

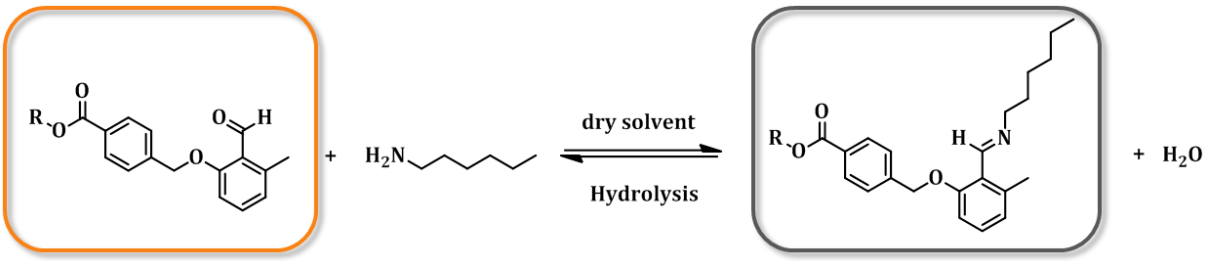

Scheme 41: *The photoactive o-methyl benzaldehyde species can be readily transformed into the respective photochemically inactive imine species via the addition of hexylamine. In this case, the imine is utilised as a protecting group which inhibits the light induced Diels-Alder reaction of the o-methyl benzaldehyde in dry solvents. Hydrolysis of the imine induces the re-formation o-methyl benzaldehyde and thus the photochemical reactivation of the system.*

The novel photoreaction sequence (initial tetrazole reaction in the presence of *o*-methyl benzaldehyde) featuring the deactivation of *o*-methyl benzaldehyde in combination with the classic ***λ***-orthogonal principle (initial *o*-methyl benzaldehyde activation in the

presence of diphenyl tetrazole) were implemented for the wavelength dependent synthesis of star polymers. The strategies for both photoreaction paths are depicted in Scheme 42.

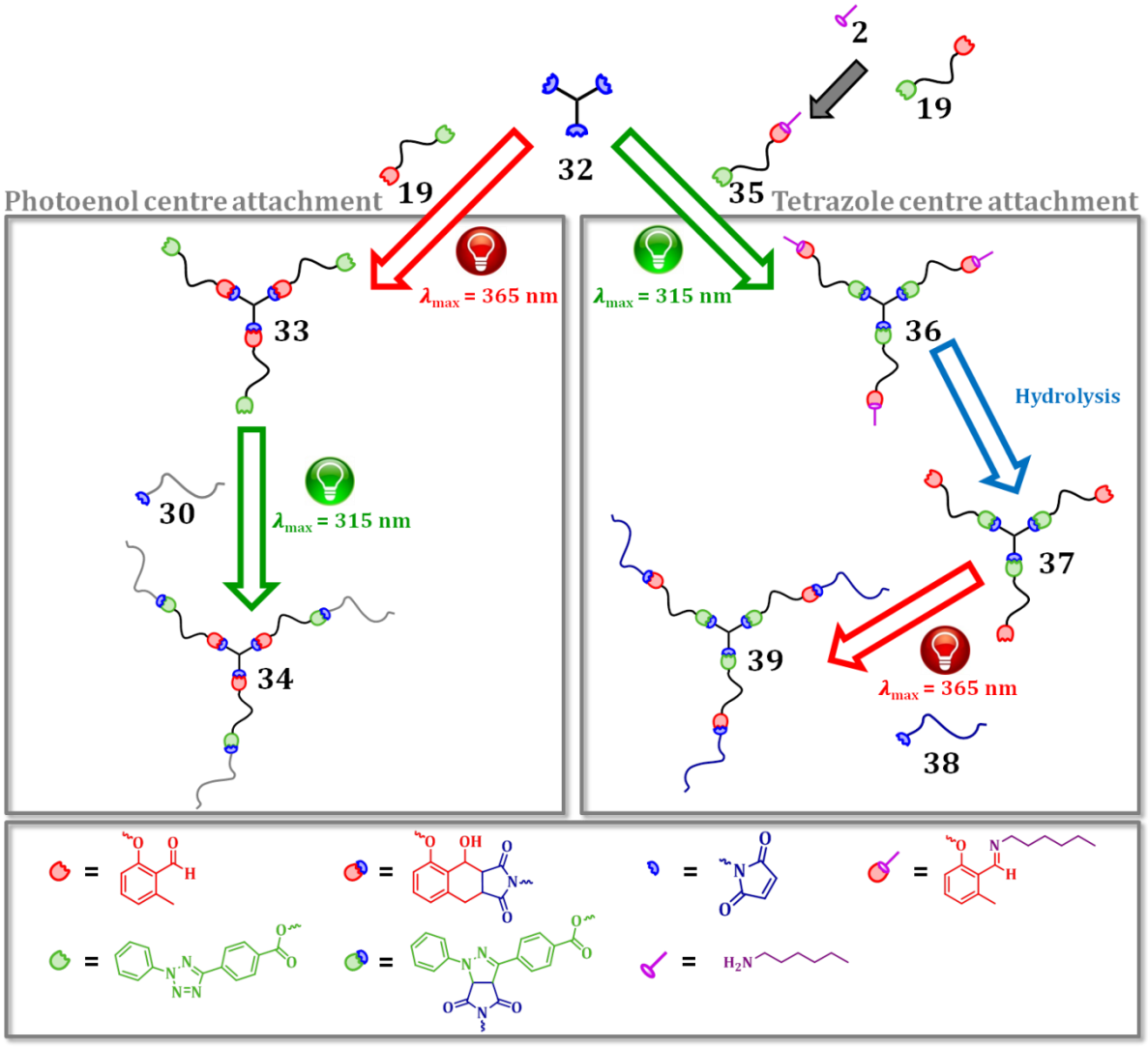

Scheme 42: *Light induced orthogonal star polymer synthesis via the selective addition of the α,ω-functional bilinker* ***19*** *carrying a benzaldehyde (red) and a tetrazole (green) functionality to the trifunctional maleimide centre* ***32****. The reaction strategy – selective benzaldehyde activation before tetrazole activation – was performed by the photochemical ligation of* ***19*** *towards* ***32*** *with the PL-L lamp (*λ_{max} *= 365 nm) resulting in the photoenol centre attached precursor* ***33****. The subsequent irradiation of* ***19*** *with pL-maleimide* ***30*** *with the Arimed B6 lamp (*λ_{max} *= 315 nm) leads to the star polymer* ***34*** *(left part). The irradiation of* ***32****(1 eq.) and the imine protected telechelic* ***35*** *(3 eq.) with the Arimed B6 lamp (*λ_{max} *= 315 nm) leads to the selective tetrazole attachment to* ***32****. The resulting star shaped structure* ***36*** *is terminated with an aryl imine. Subsequent imine hydrolysis results in the reactivation of the aldehyde end groups* ***37****. The star shaped structure containing benzaldehyde end groups* ***37*** *(1 eq.) and PEG-maleimide* ***38*** *(3 eq.) are irradiated with the PL-L lamp (*λ_{max} *= 365 nm) yielding the star polymer* ***39*** *(right part). The image was modified from ref.*[303] *with permission from the Royal Society of Chemistry (RSC), 2016.*

4.3.1. Triblock Copolymers Synthesis via the General λ-Orthogonal Ligation Principle

The λ-orthogonal principle employing the initial attachment of *o*-methyl benzaldehyde and the subsequent addition of diphenyl tetrazole towards a maleimide centre was implemented for the synthesis of a star block copolymer. Therefore, a system containing the trifunctional maleimide core **32** (1 eq.) as well as the oligomer bilinker **19** (3 eq.) was irradiated for 3 h with the PL-L lamp (λ_{max} = 365 nm) resulting in the formation of the diphenyl tetrazole terminated star shaped precursor **33**. The reaction including all structures is depicted in Scheme 43.

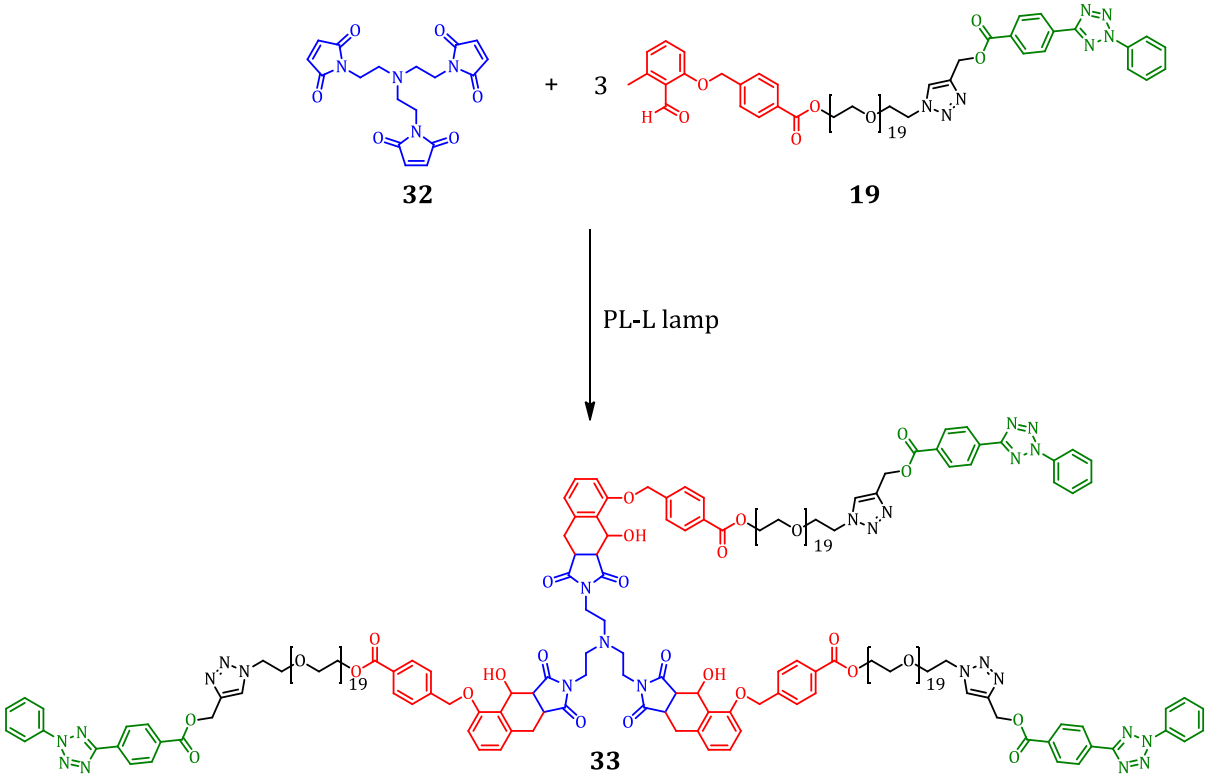

Scheme 43: *Overview of the selective photoreaction with the PL-L lamp between the o-methyl benzaldehyde end group of the α,ω-functional bilinker* ***19*** *(3 eq.) and the trifunctional maleimide centre* ***32*** *(1 eq.) yielding* ***33****.*

The star shaped oligomer **33**, which is the photoproduct of the initial photoreaction sequence between **19** and **32**, was investigated via ^{1}H NMR spectroscopy (refer to Figure 55). The data clearly demonstrates the absence of any resonances referring to the *o*-methyl benzaldehyde terminus of **19** (the aldehyde signal: δ = 10.69 ppm as well as the aryl methyl signal: δ = 2.53 ppm). Moreover, the presence of Diels-Alder product resonances (a: δ = 5.89 ppm and b: δ = 2.91-3.24 ppm) as well as the absence of

maleimide resonances (δ = 6.78 ppm) indicates that the *o*-methyl benzaldehyde end groups and the maleimide functionalities of the starting material **32** were conjugated via a Diels-Alder reaction. Moreover, the covalent linking between the maleimide moieties of **32** and the *o*-methyl benzaldehyde end groups of **19** can be traced by one distinct signal (x: δ = 2.57 ppm). The other resonance (y: δ = 2.74 ppm) referring to the covalent linkage between maleimide and *o*-methyl benzaldehyde overlaps with the spacer group resonance u of **32** (refer to Figure 55). Furthermore, all remaining signals could be assigned to the structure **33**. In addition, the diphenyl tetrazole end group conversion after the irradiation with the PL-L lamp is less than 4 % (δ = 5.24 ppm). As a result, the site-specific attachment of *o*-methyl benzaldehyde to the maleimide centre could be verified.

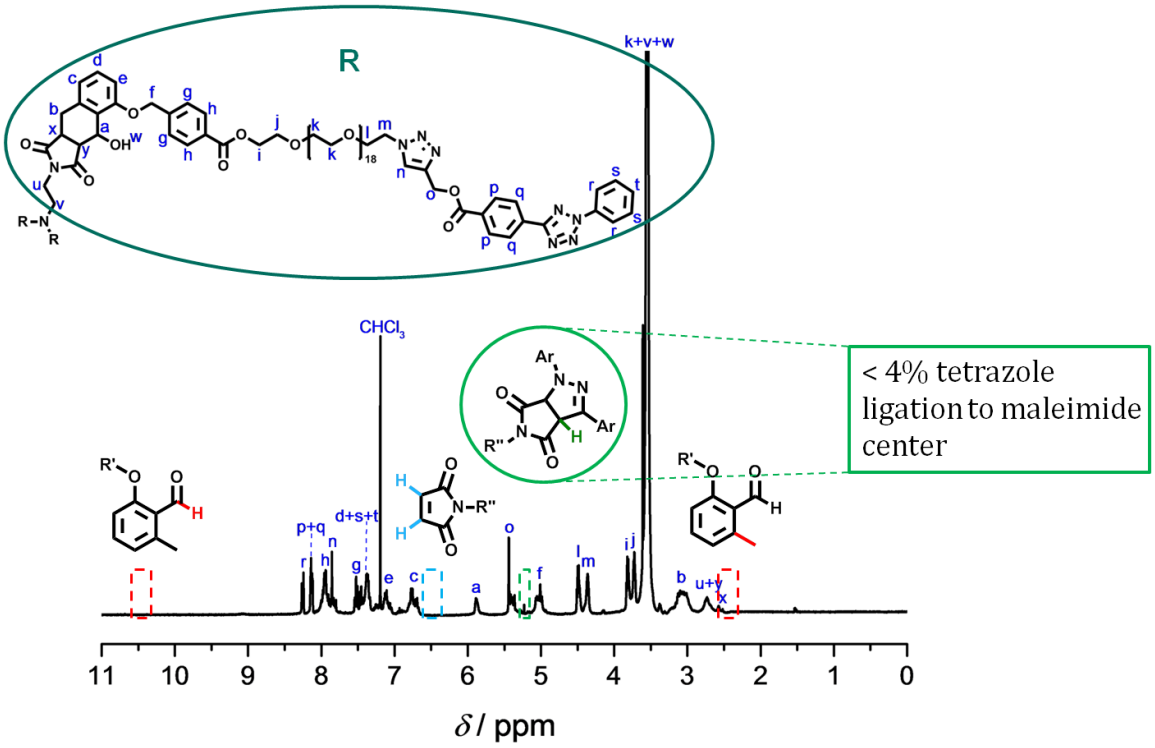

Figure 55: *The ^{1}H NMR analysis of the tetrazole terminated star shaped polymer **33** verifies the selective addition of the o-methyl benzaldehyde end group regarding **19** (3 eq.) to the maleimide centre **32** (1 eq.). Less than 4 % of the tetrazole chain end regarding **19** have reacted with **32**. The image was adapted from ref.*[303] *with permission from the Royal Society of Chemistry (RSC), 2016.*

The trifunctional structure **33** (M_n = 4800) carries diphenyl tetrazole end groups which are the basis for the subsequent photo triggered conjugation step leading to the formation of the star polymer **34**. In this regard, the consecutive irradiation of a mixture containing the precursor **33** (1 eq.) and the maleimide terminated pL **30** (3 eq.) in DCM

was performed for 13 h using the Arimed B6 lamp (λ_{max} = 315 nm). The photoreaction including all inherent structures is depicted in Scheme 44.

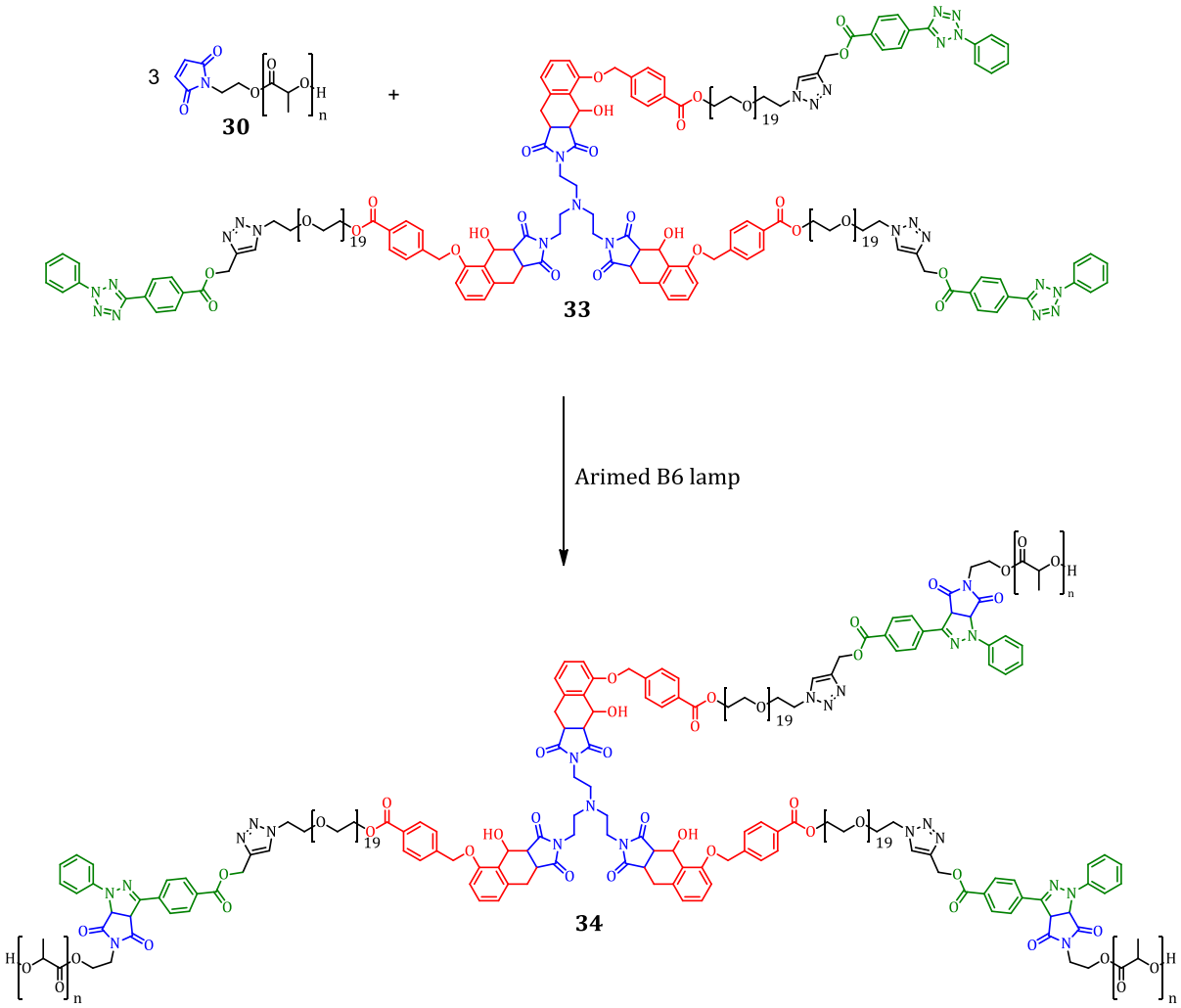

Scheme 44: *Overview of the subsequent photoreaction with the Arimed B6 lamp between the maleimide terminated pL* ***30*** *(3 eq.) and tetrazole end groups of the trifunctional precursor* ***33*** *(1 eq.) yielding the star polymer* ***34****.*

The obtained star polymer **34** carrying three polylactide termini was investigated via ^{1}H NMR spectroscopy (refer to Figure 56). The data show the quantitative attachment of the maleimide terminated pL **30** towards the diphenyl tetrazole end groups of **33** via a 4,5-dihydro pyrazole conjugation (T1: δ = 5.24 ppm and T2: δ = 4.91 ppm). Moreover, all remaining signals including the resonances of the polylactide backbone could be assigned to the star polymer **34**. All in all, the site-specific star polymer formation was verified.

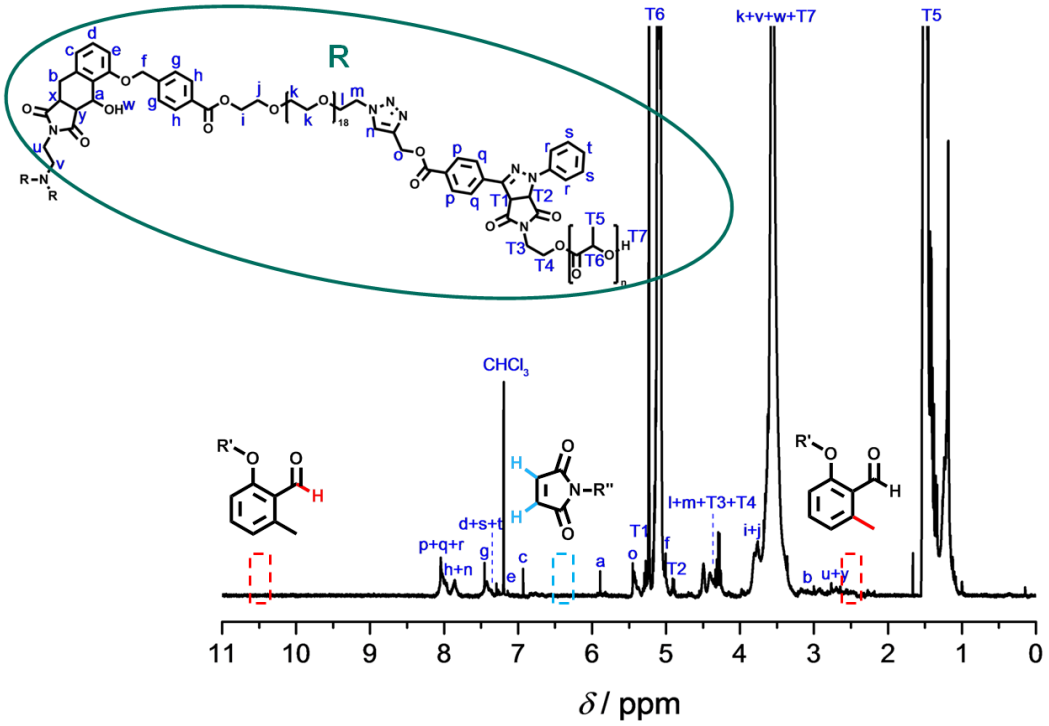

Figure 56: *The ^{1}H NMR analysis of the star shaped polymer **34** verifying the complete addition of the maleimide terminated pL **30** (3 eq.) to the diphenyl tetrazole terminated precursor **33** (1 eq.). The image was adapted from ref.*[303] *with permission from the Royal Society of Chemistry (RSC), 2016.*

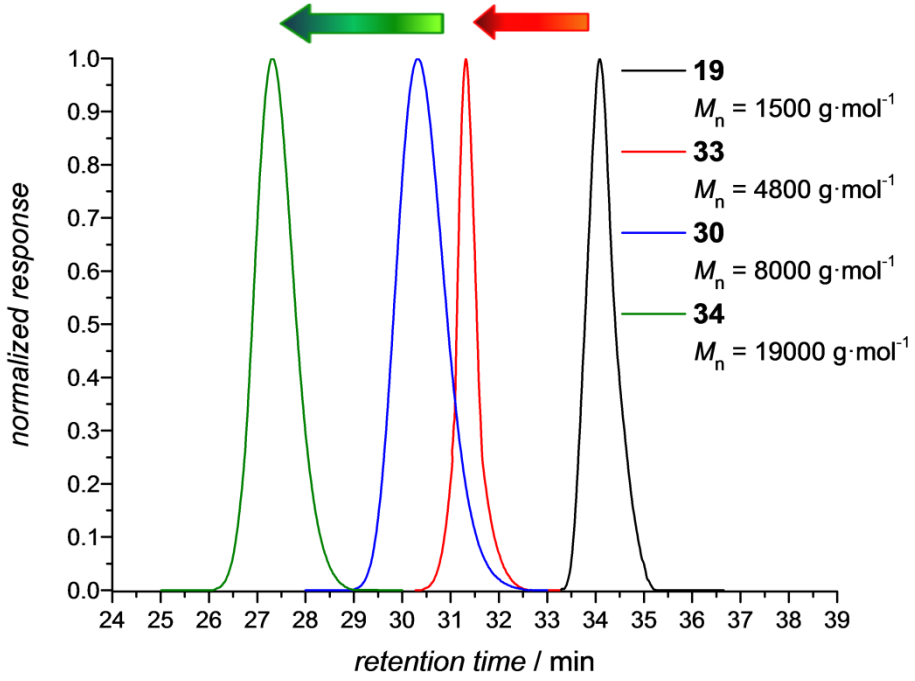

Figure 57: *A system consisting of the trifunctional maleimide **32** and the α,ω-functional bilinker **19**, carrying the o-methyl benzaldehyde and diphenyl tetrazole end group functionalities, was irradiated for 3 h with the PL-L lamp leading to the selective formation of **33**. The star shaped oligomer **33** was subsequently mixed with the maleimide terminated polylactide **30** and irradiated for 13 h with the Arimed B6 lamp forming the star polymer **34**. GPC reported to a PS calibration. The image was adapted from ref.*[303] *with permission from the Royal Society of Chemistry (RSC), 2016.*

The consecutive **λ**-orthogonal photoreaction paths leading to the formation of the star polymer **34** were additionally traced via GPC (refer to Figure 57). The data indicates a distinct shift of the bilinker **19** (M_n = 1500) to the trifunctional diphenyl tetrazole terminated structure **33** (M_n = 4800) via the selective conjugation of **19** (3 eq.) and **32** (1 eq.) after the initial irradiation with the PL-L lamp. The subsequent shift of **33** towards the star polymer **34** (M_n = 19000) after the irradiation with the Arimed B6 lamp reveals the complete conjugation of the maleimide terminated pL **30** (M_n = 4800) (3 eq.) towards **33** (1 eq.).

4.3.2. Triblock Copolymers via the Novel Tetrazole-Photoenol Ligation

The application of the tetrazole reaction in the presence of *o*-methyl benzaldehyde requires the reversible photochemical deactivation of *o*-methyl benzaldehyde. Therefore, a system containing hexylamine **2** as well as the α,ω-functional bilinker **19** in dry THF was stirred for 3 h resulting in the formation of the structure **35** carrying a diphenyl tetrazole and an imine group at each chain end. The imine insertion including all structures is depicted in Scheme 45.

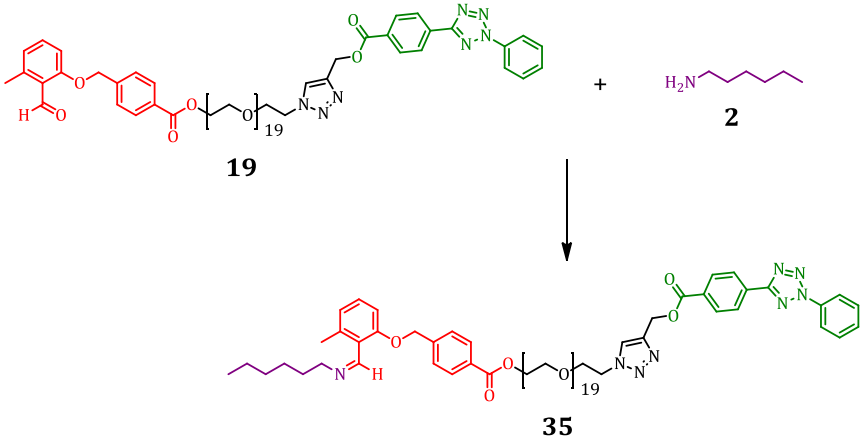

Scheme 45: *Overview of the o-methyl benzaldehyde deactivation of the α,ω-functional bilinker **35** with hexylamine **2** yielding the imine **35**.*

The obtained imine **35** was analysed via ^{1}H NMR spectroscopy, whereby all resonances could be assigned (refer to Figure 58). The data demonstrate an imine yield of 99 %

based on the presence of significant imine resonances (a: δ = 8.63 ppm; b: δ = 2.43 ppm). The residual *o*-methyl benzaldehyde signals (the aldehyde signal: δ = 10.69 ppm as well as the aryl methyl signal b': δ = 2.53 ppm) indicate that only 1 % of the starting material **19** was not converted.

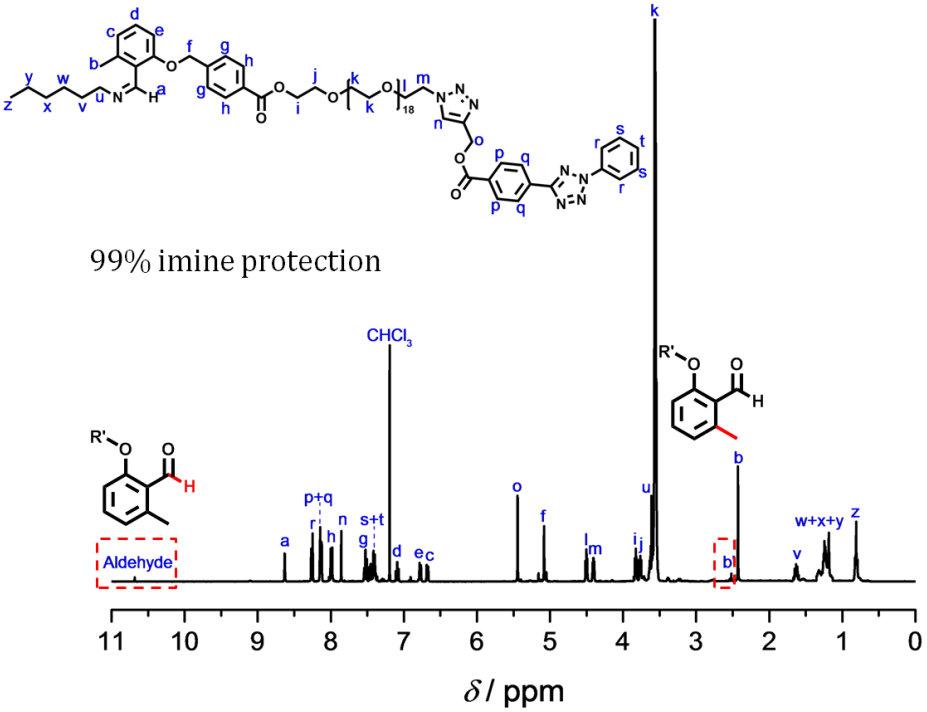

Figure 58: *The ^{1}H NMR analysis of the imine protected bilinker **35** in $CDCl_3$. The image was adapted from ref.*[303] *with permission from the Royal Society of Chemistry (RSC), 2016.*

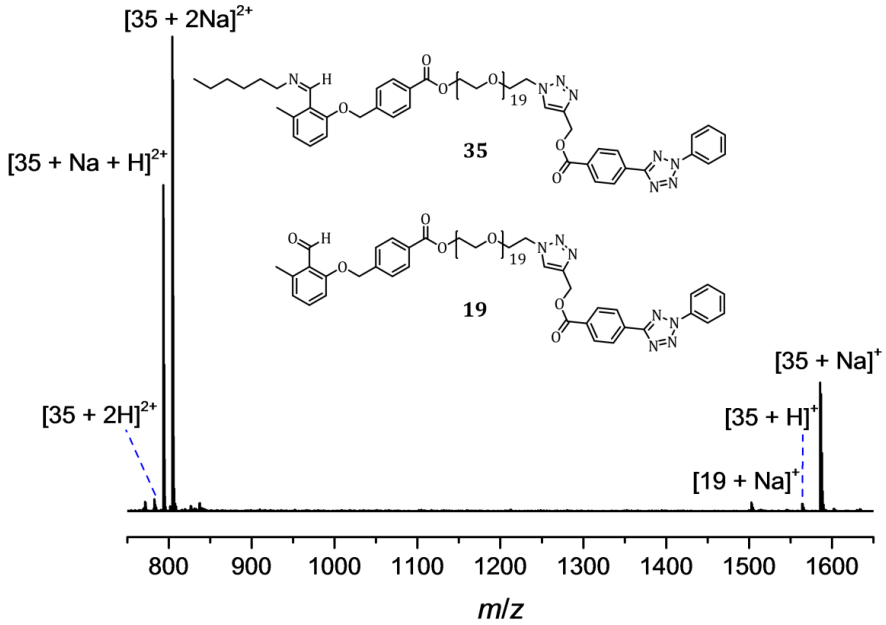

Figure 59: *Orbitrap ESI-MS analysis of **35**. A residual amount (1 %) of the bilinker **19** is still detectable. The image was adapted from ref.*[303] *with permission from the Royal Society of Chemistry (RSC), 2016.*

Furthermore, the structure **35** was analysed via high resolution mass spectrometry (refer to Figure 59). The signals in the single and double charged m/z range fit very well to the expected values (refer to Table 2).

m/z_{exp}	ion assignment	formula	m/z_{theor}	$\Delta m/z_{exp}$
782.3926	[**35** + 2H]$^{2+}$	$[C_{79}H_{120}N_8O_{24}]^{2+}$	782.4202	0.0276
793.4151	[**35** + Na + H]$^{2+}$	$[C_{79}H_{119}N_8NaO_{24}]^{2+}$	793.4112	0.0039
804.4060	[**35** + 2Na]$^{2+}$	$[C_{79}H_{118}N_8Na_2O_{24}]^{2+}$	804.4022	0.0038
1563.8417	[**35** + H]$^{+}$	$[C_{79}H_{119}N_8O_{24}]^{+}$	1563.8332	0.0085
1585.8239	[**35** + Na]$^{+}$	$[C_{79}H_{118}N_8NaO_{24}]^{+}$	1585.8152	0.0087

Table 2: *Overview of the m/z values of **35**.*

A signal with small intensity of the starting material **19** is detectable. The ^{1}H NMR analysis as well as the mass spectrum evidence the successful transformation of **19** into **35**. The deactivation of the *o*-methyl benzaldehyde end group in **35** allows the selective phototriggered activation of the diphenyl tetrazole end group. A system containing the trifunctional maleimide core **32** (1 eq.) as well as the imine protected bilinker **35** (3 eq.) was irradiated for 13 h with the Arimed B6 lamp (λ_{max} = 315 nm) resulting in the formation of the imine terminated star shaped precursor **36** (refer to Scheme 46).

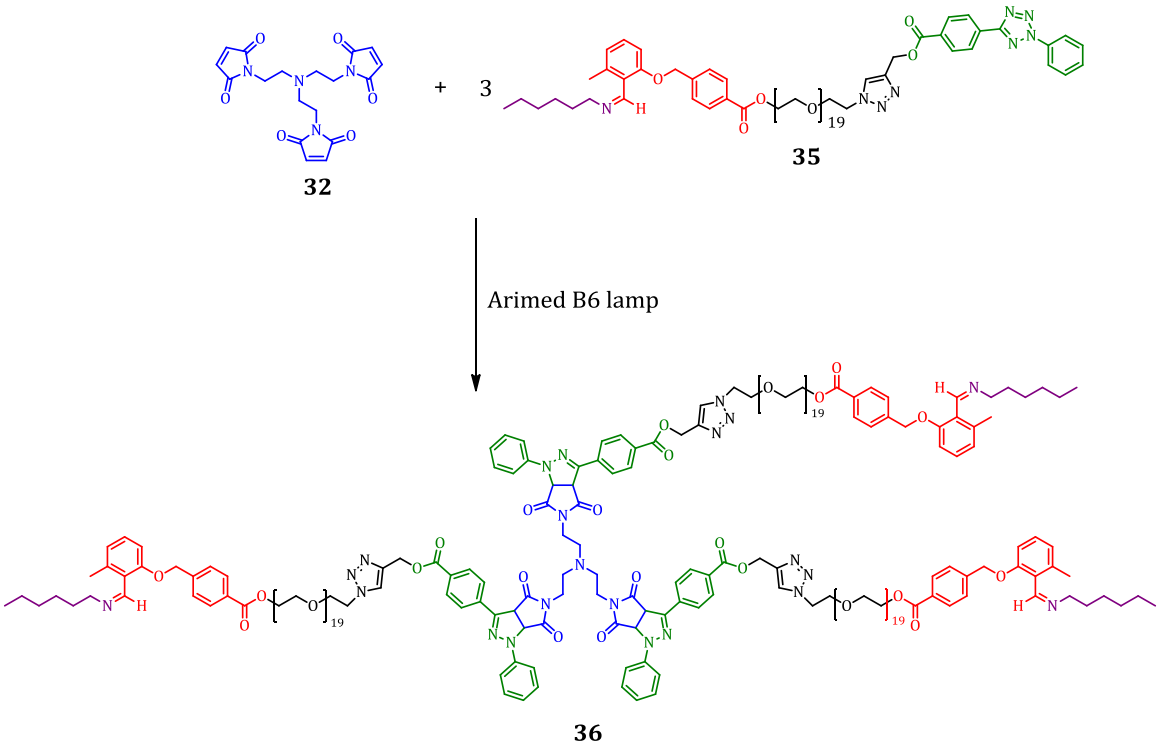

Scheme 46: *Overview of the selective photoreaction with the Arimed B6 lamp between the diphenyl tetrazole end group of the imine protected oligomer* ***35*** *(3 eq.) and the trifunctional maleimide centre* ***32*** *(1 eq.) yielding* ***36****.*

The obtained star structure **36** carrying three imine termini was analysed via ^{1}H NMR spectroscopy whereby all signals could be assigned (refer to Figure 60). The data demonstrate the quantitative attachment of the three diphenyl tetrazole end groups of the imine protected bilinker **35** to the trifunctional maleimide centre **32** by the appearance of 4,5-dihydro pyrazole conjugation signals (x: δ = 2.53 ppm and w: δ = 4.91 ppm) as well as the complete disappearance of the maleimide resonances of **32** (δ = 6.78 ppm). The presence of imine resonances (a: δ = 8.63 ppm; b: δ = 2.43 ppm) as well as the absence of any signals related to the respective Diels-Alder product (the ring formation signal: δ = 2.91-3.24 ppm as well as the α-hydroxy signal: δ = 5.89 ppm) indicate that *o*-methyl benzaldehyde remained unreacted during the irradiation. Nevertheless, a small amount (< 3 %) of the imine end group regarding **35** was transformed into the respective *o*-methyl benzaldehyde. In summary, the site-specific diphenyl tetrazole attachment to the maleimide centre could be verified.

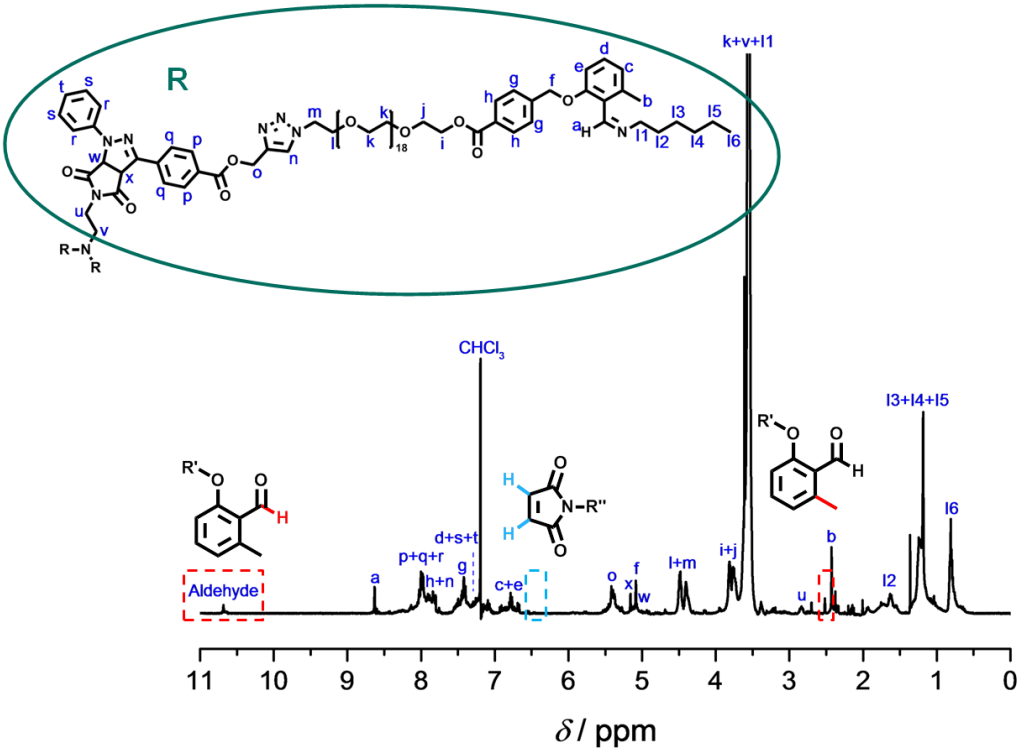

Figure 60: *The ^{1}H NMR analysis of the star shaped polymer* ***36*** *verifies the selective addition the tetrazole end group of* ***35*** *(3 eq.) to the maleimide centre* ***32*** *(1 eq.). The image was adapted from ref.*[303] *with permission from the Royal Society of Chemistry (RSC), 2016.*

The reactivation of **36** for the subsequent irradiation procedure was performed by the hydrolytic removal of the imine moiety leading to the *o*-methyl benzaldehyde terminated precursor **37**. The hydrolysis including all structures is depicted in Scheme 47.

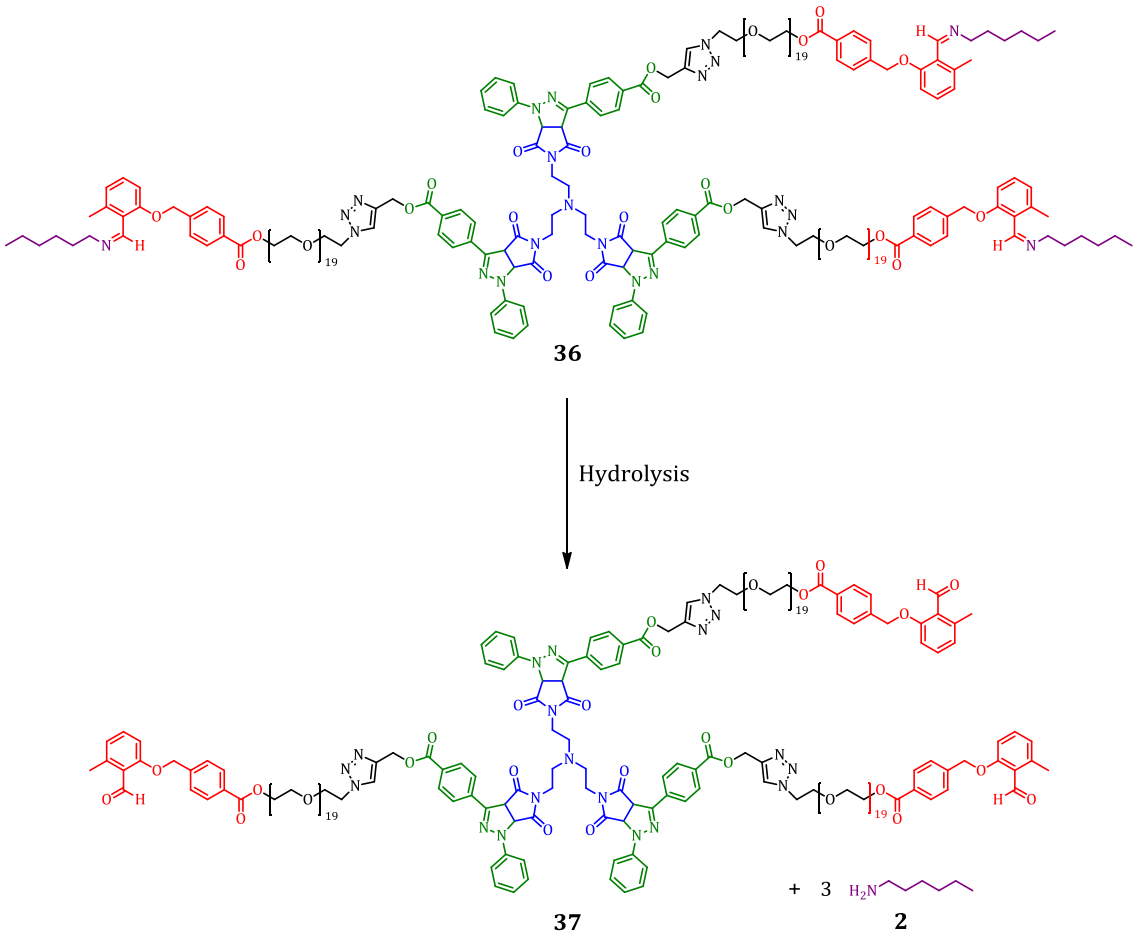

Scheme 47: *Overview of the hydrolysis of the imine terminated star shaped oligomer* ***36*** *yielding the o-methyl benzaldehyde terminated precursor* ***37****.*

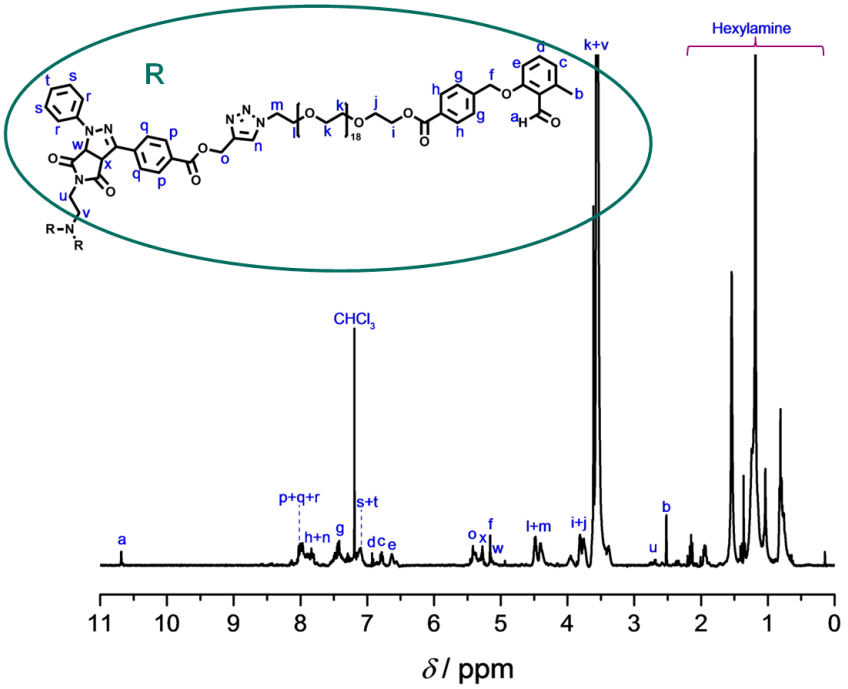

Figure 61: *The* ^{1}H *NMR analysis verifies the quantitative hydrolysis of* ***36*** *yielding the o-methyl benzaldehyde terminated structure* ***37****. The picture was modified from ref.*[303] *with permission from RSC, 2016.*

The imine removal of **36** via hydrolysis was analysed via ^{1}H NMR spectroscopy (refer to Figure 61). The data evidence the complete transformation of the terminal imine functionalities into the respective *o*-methyl benzaldehydes end groups by the disappearance of distinct imine associated resonances (the imine signal: δ = 8.63 ppm and the aryl methyl signal: δ = 2.43 ppm) as well as the reappearance of significant *o*-methyl benzaldehyde signals (a: δ = 10.69 ppm; b: δ = 2.53 ppm).

The restoration of the *o*-methyl benzaldehyde end groups allows for the subsequent light induced photoenol reaction of the star shaped oligomer **37**. In this context, the irradiation of a mixture containing the precursor **37** (1 eq.) and the maleimide terminated PEG **38** (3 eq.) in DCM was performed for 3 h using the PL-L lamp (λ_{max} = 365 nm), yielding the star polymer **39**. The photoreaction including all relevant structures is depicted in Scheme 48.

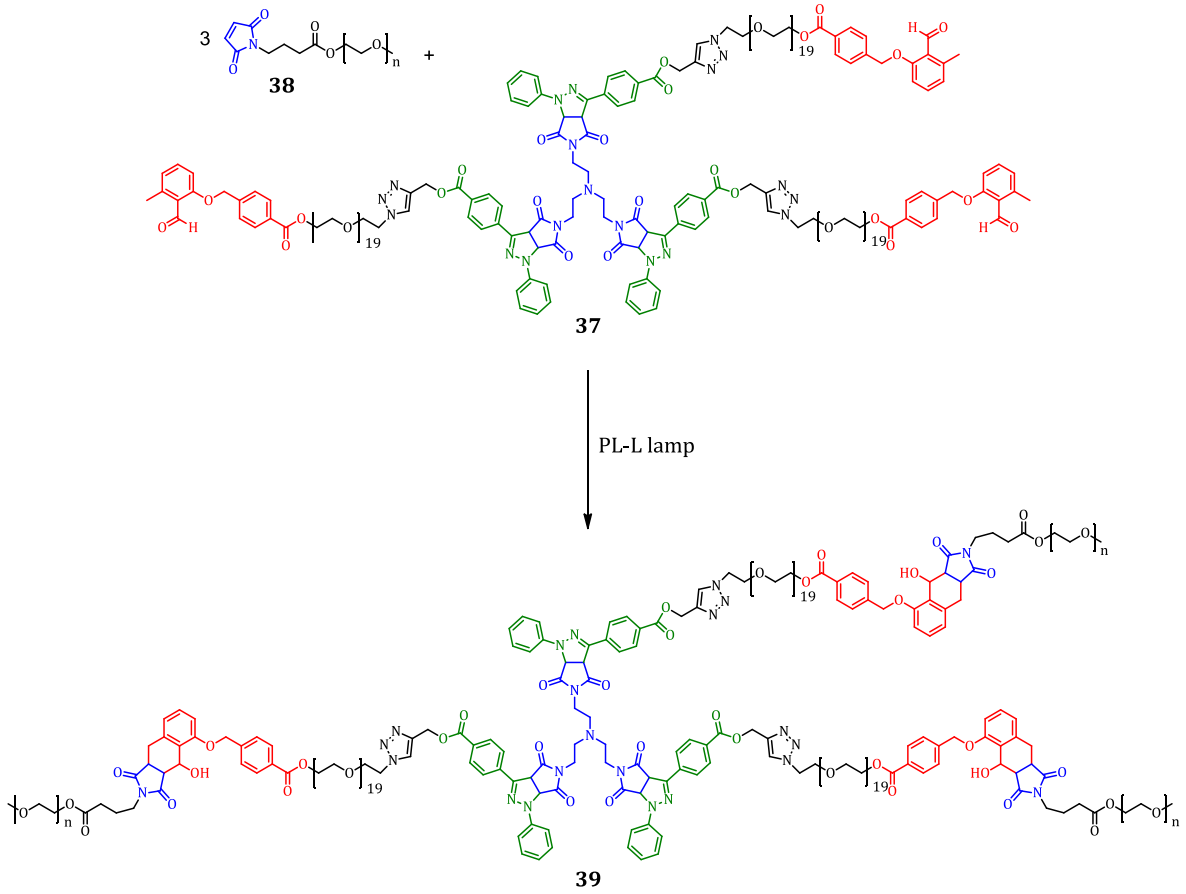

Scheme 48: *Overview of the subsequent photoreaction with the PL-L lamp between the maleimide terminated PEG* ***38*** *(3 eq.) and the o-methyl benzaldehyde end groups of the trifunctional precursor* ***37*** *(1 eq.) yielding the star polymer* ***39****.*

The star polymer **39** was investigated via ^{1}H NMR spectroscopy (refer to Figure 62). The data clearly demonstrate the absence of any signal referring to the *o*-methyl

benzaldehyde terminus of **37** (the aldehyde signal: δ = 10.69 ppm as well as the aryl methyl signal: δ = 2.53 ppm). Moreover, the presence of the Diels-Alder product resonances (a: δ = 5.92 ppm and b: δ = 2.91-3.24 ppm) as well as the absence of maleimide resonances (δ = 6.78 ppm) reveal that the *o*-methyl benzaldehyde end groups and the maleimide functionalities of the starting material **32** were conjugated via a [4+2]-cycloaddition. The signals referring to the covalent linkage between the maleimide end group of **38** and the *o*-methyl benzaldehyde termini of **37** (P2: δ = 2.17 ppm; P1: δ = 2.34 ppm) overlap with spacer units.

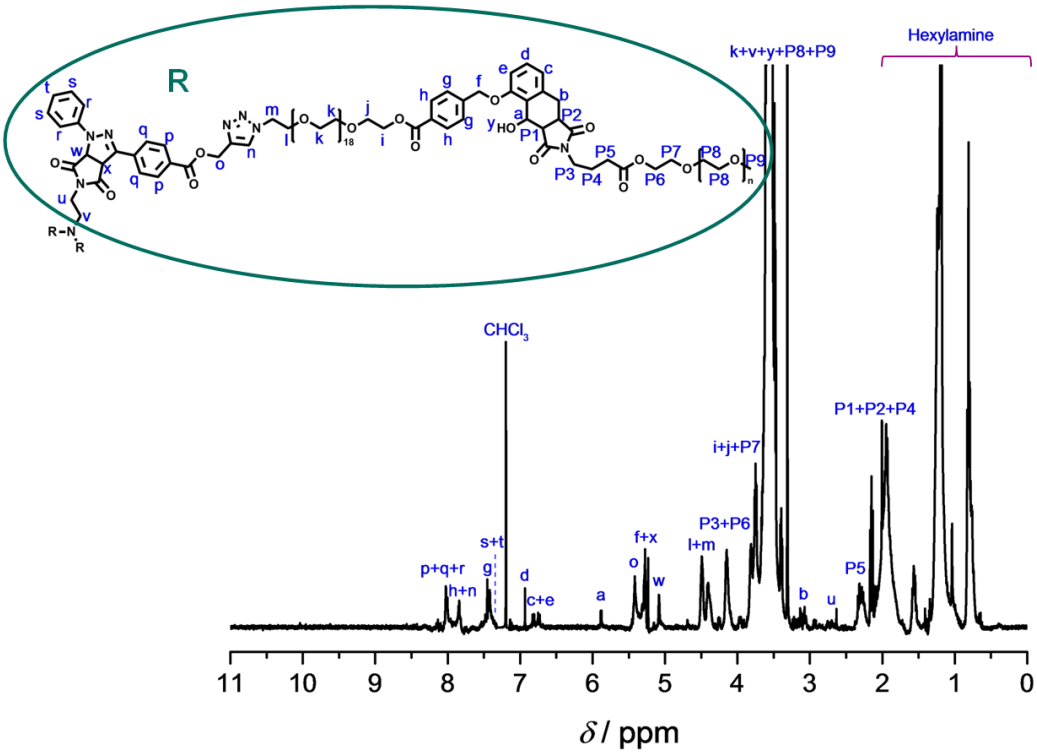

Figure 62: *The [1]H NMR analysis of the star shaped polymer **39** verifies the complete addition of the maleimide terminated PEG **30** (3 eq.) to the o-methyl benzaldehyde terminated precursor **37** (1 eq.). The image was adapted from ref.*[303] *with permission from the Royal Society of Chemistry (RSC), 2016.*

In addition, the novel photoreaction path, which includes the initial tetrazole ligation step and the subsequent *o*-methyl benzaldehyde reaction for the synthesis of the star polymer **39**, was traced via GPC (refer to Figure 62). The data indicate the transformation of **19** (M_n = 1500) into the imine **35** (M_n = 1600) by a small signal shift before the irradiation. A distinct shift of the imine terminated bilinker **35** to the trifunctional imine terminated structure **36** (M_n = 5000) after the initial irradiation with the Arimed B6 lamp evidences the selective diphenyl tetrazole conjugation of **35** (3 eq.) and **32** (1 eq.). The hydrolysis of the imine end groups of **36** is evident by a small shift

towards **37** (M_n = 4800). The subsequent shift of **37** towards the star polymer **39** (M_n = 11000) after the irradiation with the PL-L lamp reveals the complete conjugation of the maleimide terminated PEG **30** (M_n = 2100) (3 eq.) towards **37** (1 eq.).

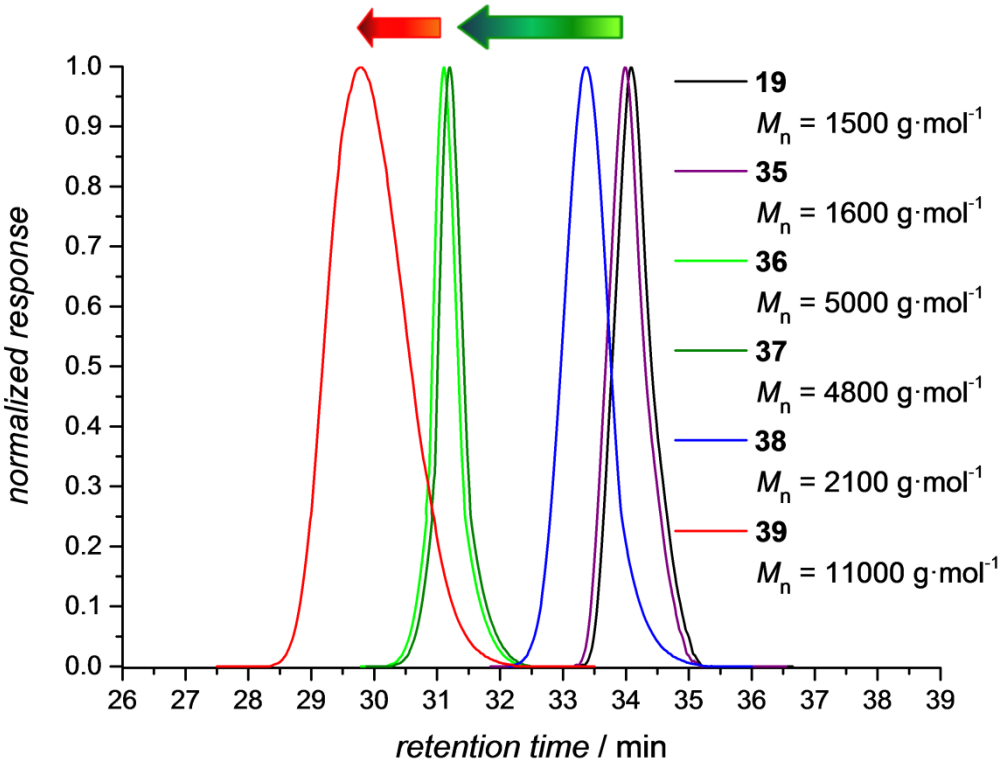

Figure 63: *The initial diphenyl tetrazole activation in the presence of o-methyl benzaldehyde requires the transformation of the photoactive aldehyde **19** into the photoinactive imine **35**. A system consisting of the trifunctional maleimide **32** and the protected bilinker **35**, carrying an imine and a diphenyl tetrazole end group functionality, was irradiated for 13 h with the Arimed B6 lamp leading to the selective formation of **36** carrying photoinactive imine end groups. The photochemical reactivation of the end groups regarding **36** were performed via hydrolysis generating the o-methyl benzaldehyde terminated structure **37**. The star shaped oligomer **37** was subsequently mixed with the maleimide terminated PEG **38** and irradiated for 3 h with the PL-L lamp forming the star polymer **39**. GPC reported to a PS calibration. The image was adapted from ref.*[303] *with permission from the Royal Society of Chemistry (RSC), 2016.*

4.4. Conclusions

The **λ**-orthogonal pericyclic reaction principle featuring *o*-methyl benzaldehyde, tetrazole, and a maleimide moiety is introduced. The principle rests on the exclusive photo triggered reaction of *o*-methyl benzaldehyde with maleimides at **λ** = 310-350 nm in the presence of diphenyl tetrazole based on their absorption spectra leading to a wavelength dependent selectivity in one direction.

The **λ**-orthogonal principle in one direction is initially implemented by the selective photochemical end group modification of *o*-methyl benzaldehyde terminated PEG and diphenyl tetrazole terminated PEG with varying maleimide concentrations in a one-pot system. In addition, these end group modifications are the basis of a kinetic investigation demonstrating the preference of the *o*-methyl benzaldehyde conversion in comparison to the diphenyl tetrazole conversion. It could be proven that the choice of an appropriate wavelength for the activation of both photoactive compounds has also a strong influence on the selectivity.

Furthermore, an oligomer α,ω-functional bilinker carrying both an *o*-methyl benzaldehyde and a diphenyl tetrazole end group is employed according to the previously mentioned **λ**-orthogonal principle in one direction. Here, the bilinker is employed as a pivotal system for selective end group modifications via enes carrying various functionalities as well as the synthesis of complex triblock copolymers in a light induced site-specific fashion.

The last section introduces the reverse photoreaction path enabling the initial diphenyl tetrazole reaction and the subsequent *o*-methyl benzaldehyde reaction and thus generates complete **λ**-orthogonality. The novel reaction path requires the temporary deactivation of *o*-methyl benzaldehyde which is realised by its reversible transformation into a photoinactive imine. Herein, both orthogonal photoreaction paths are applied for the photochemical synthesis of star block copolymers by the selective addition of the α,ω-functional bilinker to a trifunctional maleimide centre.

5

5. Selective Design of Networks and Three-Dimensional Structures via λ-Orthogonal Photochemistry

---

The synthesis of the RAFT star polymers as well as the phototriggered network formations in Chapter 5.2 were performed by M. Kaupp (Institute for Chemical Technology and Polymer Chemistry, KIT). The DLW experiments in Chapter 5.4 were carried out by P. Müller (Institute of Applied Physics, KIT). XPS measurements were performed by V. Trouillet (Institute for Applied Materials and Energy Storage Systems, KIT) Parts of the present chapter were reproduced with permission from M. Kaupp, K. Hiltebrandt, V. Trouillet, P. Mueller, A. S. Quick, M. Wegener, C. Barner-Kowollik, *Chem. Comm.*, **2016**, 52, 1975-1978. (DOI: 10.1039/C5CC09444E). Copyright RSC 2016.

5.1. Motivation

Polymer networks are widely employed, for example, in hydrogels[312] or find further applications in areas such as gas storage[313] and drug delivery.[314] Networks made of a tailored nanostructured building blocks are known as metamaterials.[315] For instance, metamaterials can be photonic crystals for telecommunications[256] or photonic gold helices used as circular polariser for light.[316]

In general, networks are synthesised by the cross-linking of multifunctional polymer chains[317] or the polymerisation of multifunctional monomers[318]. Importantly, the network properties can be adapted by the cross-linking density,[319] and the type of multifunctional monomer.[320] Specifically, the light triggered conjugation of multifunctional photoactive compounds allows for a straightforward cross-linking procedure for the design of networks. For instance, photo induced cross-linking can be achieved via photosensitisers enabling the formation of radicals by light induced hydrogen abstraction reactions. In this respect, thiol-ene cross-linking reactions[321] and the recombination of macroradicals[322],[323] were employed for the light induced synthesis of networks. Moreover, cross-linking can also be achieved via light induced ligation reactions. For instance, the photoinduced cross-linking of polymers via bisbenzodioxinones at $\lambda > 300$ nm.[324], the photoinduced cross-linking of polymers via the formation of polymer radicals at $\lambda = 254$ nm for the synthesis of hydrogels[325], and the dimerisation of anthracene units in the backbone of polymer chains at $\lambda = 254$ nm[326] were reported.

The phototriggered network formation using two competing photoreactions has never been employed before. In theory, the λ-orthogonal principle, established in the current thesis, based on the initial activation of *o*-methyl benzaldehyde and the subsequent diphenyl tetrazole activation (refer to chapter 4), allows the wavelength dependent design of networks with distinct properties via low energetic lamps. For instance, diphenyl tetrazole yields a fluorescent conjugate whereas *o*-methyl benzaldehyde forms a non-fluorescent structure. In addition, the insertion of *o*-methyl benzaldehyde into stiff polymers such as poly(methyl methacrylate) (pMMA) as well as the modification of flexible polymers such as poly(methyl acrylate) (pMA) with diphenyl tetrazole moieties generates a versatile system in which the physical material properties of the obtained network are determined by the applied wavelength (refer to Figure 64).

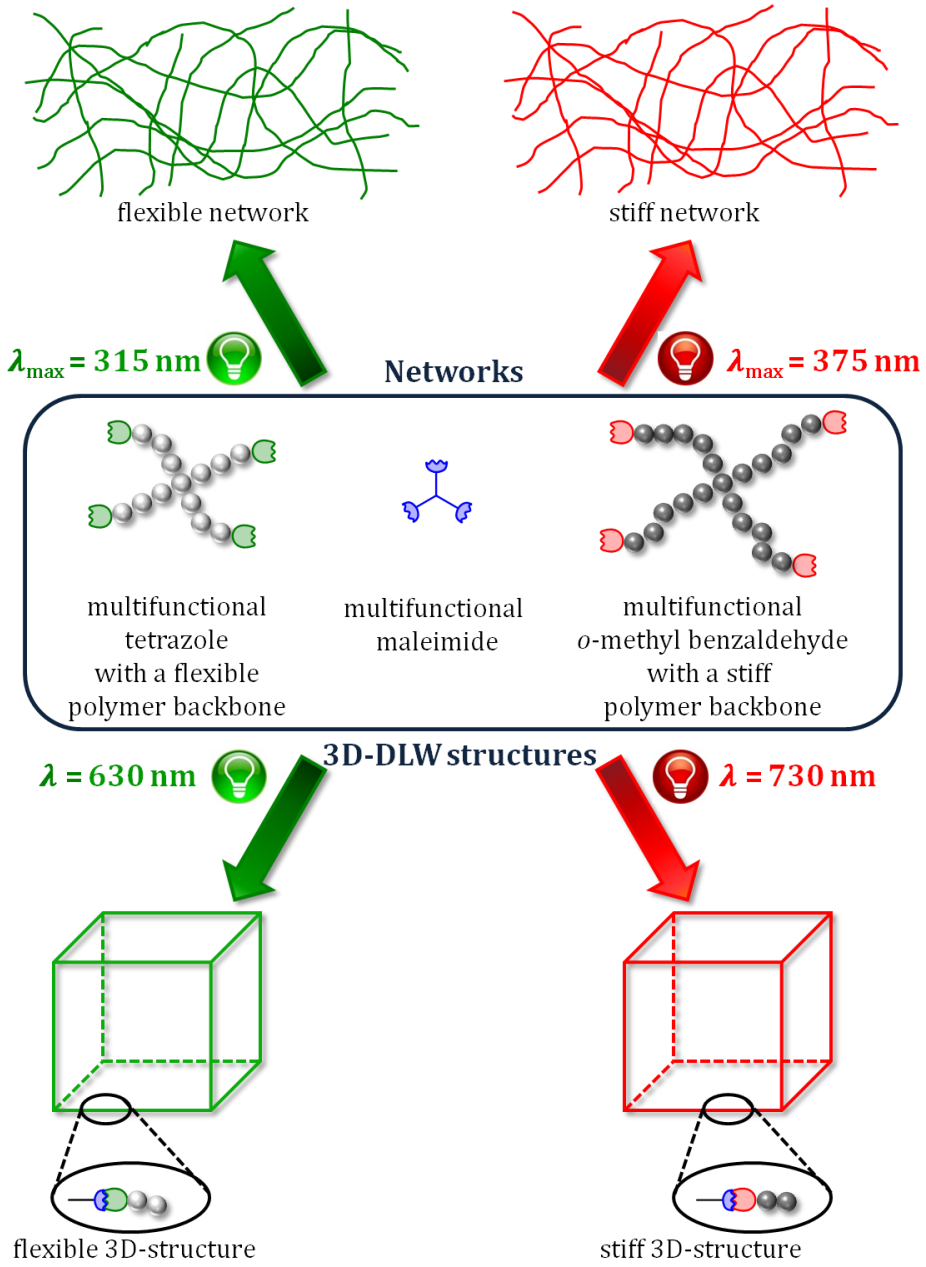

Figure 64: *The λ-orthogonal principle in one direction allowing the initial o-methyl benzaldehyde activation in the presence of diphenyl tetrazole is employed on a photoresist containing a multifunctional stiff polymer carrying o-methyl benzaldehyde moieties, a multifunctional flexible polymer carrying tetrazole moieties, and a multifunctional maleimide. The photoresist generates networks whose properties depend on the applied wavelength (top). In addition, the photoresist can generate three-dimensional microstructures differing in their properties when a DLW process is employed, allowing for two-photon excitation at a distinct wavelength (bottom).*

DLW enables the design of three-dimensional structures in (almost) any shape due to a two-photon excitation (refer to chapter 2.6) in contrast to network formation induced by light sources leading to a one-photon absorption of the photoactive compounds. Therefore, a photoresist containing a stiff polymer carrying several *o*-methyl benzaldehyde species, a flexible polymer carrying several tetrazole species, and a multifunctional maleimide are investigated for the wavelength selective design of three-

dimensional structures with distinct, wavelength dependent property profiles. The obtained structures are targeted to yield stiff three-dimensional structures for low wavelengths whereas high wavelengths should result in stiff three-dimensional structures.

5.2. Wavelength Selective Polymer Network Formation via Low Energetic Light Sources

The present section explores the wavelength selective network formation of the previously introduced photoactive compounds *o*-methyl benzaldehyde and diphenyl tetrazole. For this purpose, both *o*-methyl benzaldehyde and diphenyl tetrazole are introduced as end groups into a four-arm star shaped polymer, respectively, resulting in photoactive star polymers. The four photoactive end groups of each star polymer are able to undergo light induced cross-linking with a multifunctional maleimide. In theory, the different absorptivities of *o*-methyl benzaldehyde and diphenyl tetrazole allow for the use of distinct wavelengths (refer to Chapter 4.2).

5.2.1. Networks on the Basis of *o*-Methyl Benzaldehyde at λ_{max} = 375 nm

A system containing the *o*-methyl benzaldehyde terminated star polymer **40** (3 eq.), synthesised via RAFT polymerisation, as well as the trifunctional maleimide centre **32** (4 eq.) allows for the phototriggered cross-linking of both compounds yielding a Diels-Alder based network (refer to Scheme 49).

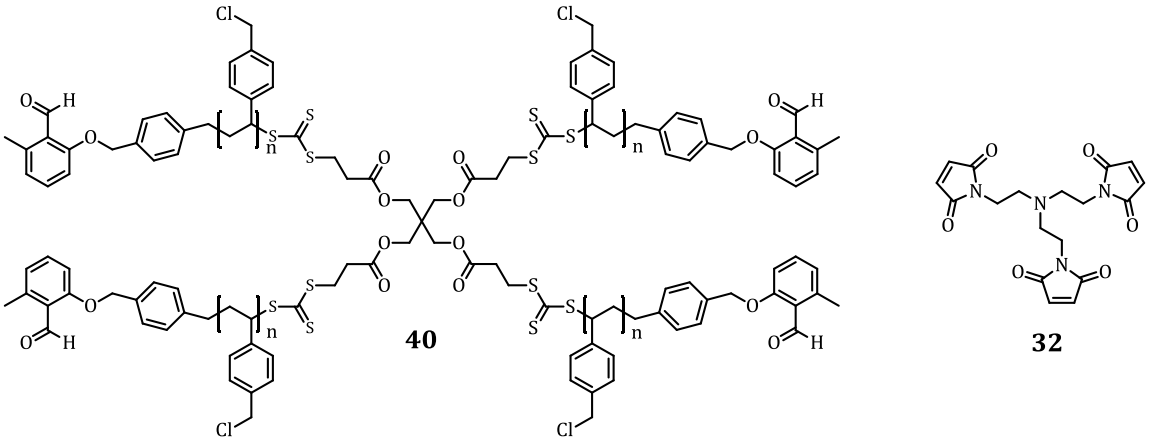

Scheme 49: *The o-methyl benzaldehyde terminated star polymer* ***40*** *(M_n = 4400) and the trifunctional maleimide* ***32*** *are used for a cross-linking based on a phototriggered Diels-Alder reaction.*

A high cross-linking yield of the employed reactions leads to an efficient network formation. Therefore, highly concentrated solutions of the starting materials are required. Thus, the concentration of the reaction mixture has a 37 times higher concentration than the previously presented photoreactions (refer to Chapter 3 and Chapter 4). The concentrated solution containing **40** and **32** in DCM was irradiated for 2.5 h with three LEDs (λ = 340-410 nm; λ_{max} = 375 nm, 3 W). The efficiency of the cross-linking between **40** and **32** was qualitatively determined by the transformation of the solution into an insoluble solid (refer to Figure 65).

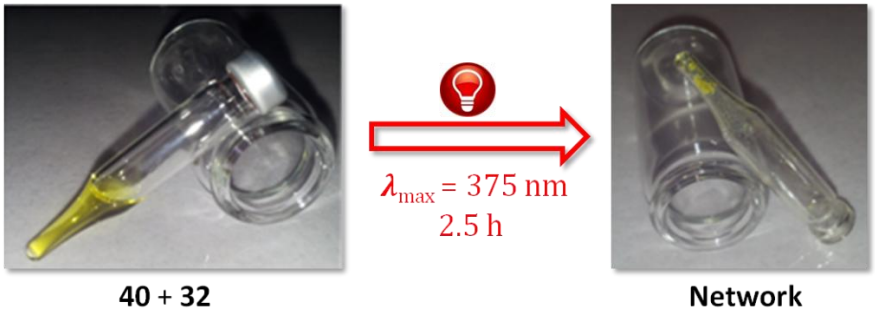

Figure 65: *The network formation of a concentrated mixture containing* ***40*** *and* ***32*** *in DCM is demonstrated by the solidification of the solution after irradiation at* λ_{max}*= 375 nm. The image was modified from ref.*[144] *with permission from the Royal Society of Chemistry (RSC), 2016.*

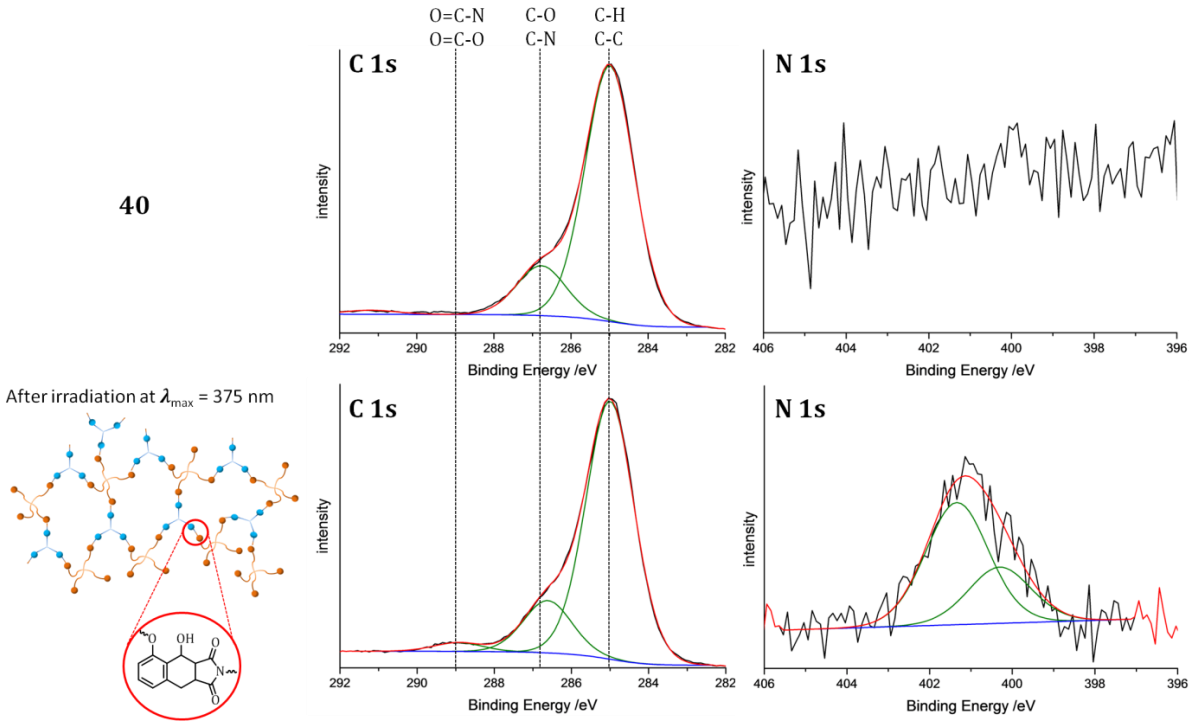

Figure 66: *The successful network formation generated by the phototriggered cross-linking of* ***40*** *and* ***32*** *via a Diels-Alder reaction is analysed via XPS. The cross-linking is verified by an intensity increase of the carbon signal O=C-O in the C 1s spectrum as well as the appearance of a nitrogen signal in the N 1s spectrum. The image was modified from ref.*[144] *with permission from the Royal Society of Chemistry (RSC), 2016.*

The obtained network was analysed via XPS. The N 1s spectra clearly demonstrate that nitrogen was incorporated into the network by the cross-linking of **40** and the nitrogen containing **32**. The C 1s spectra indicate an intensity increase of the carbon signal O=C-O deriving from the covalent attachment of the maleimide functionalities of **32** to the *o*-methyl benzaldehyde terminated star polymer **40** (refer to Figure 66).

5.2.2. Networks on the Basis of Diphenyl Tetrazole at λ_{max} = 320 nm

A system containing the diphenyl tetrazole terminated star polymer **41** (3 eq.), synthesised via RAFT polymerisation, as well as the trifunctional maleimide centre **32** (4 eq.) allows for the phototriggered cross-linking of both compounds yielding a NITEC reaction conjugated network (refer to Scheme 50).

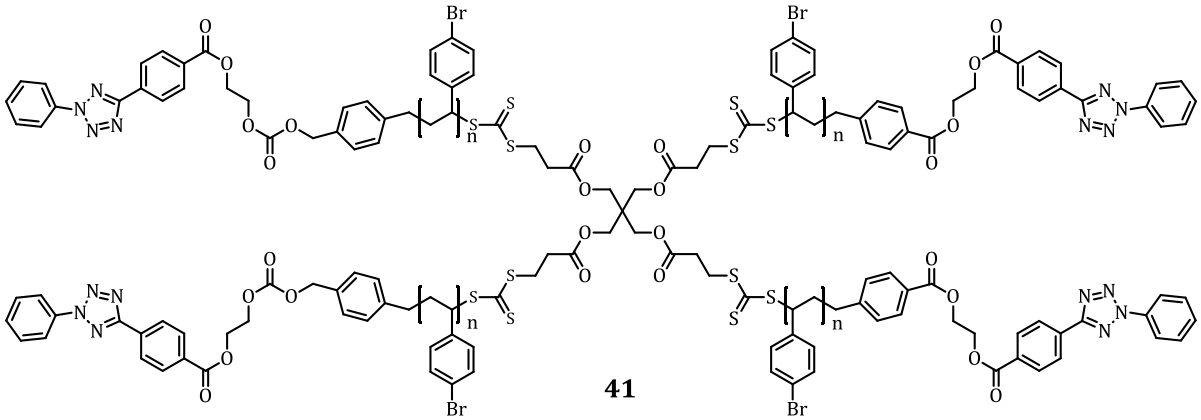

41

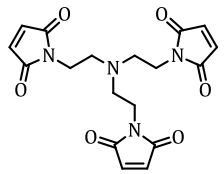

32

Scheme 50: *The diphenyl tetrazole terminated star polymer **41** (M_n = 3800) and the trifunctional maleimide **32** are used for cross-linking based on the phototriggered NITEC reaction.*

The mixture containing **41** and **32** in DCM was irradiated for 23.5 h with the Arimed B6 lamp (λ = 280-440 nm; λ_{max} = 315 nm, 36 W). The efficiency of the cross-linking

between **41** and **32** was qualitatively determined by the transformation of the solution into an insoluble solid(refer to Figure 67).

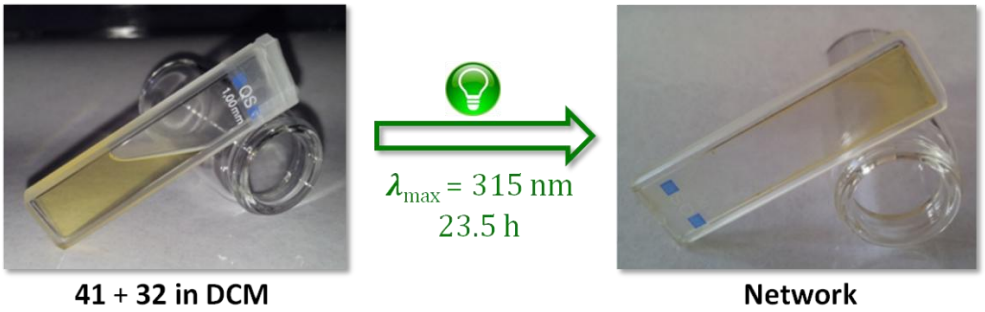

Figure 67: *The network formation of a concentrated mixture containing* ***41*** *and* ***32*** *in DCM is demonstrated by the solidification of the solution after irradiation at* λ_{max}*= 315 nm. The picture was modified from ref.*[144] *with permission from the Royal Society of Chemistry (RSC), 2016.*

Moreover, the network is fluorescent due to the 4,5-dihydro pyrazole cross-linking forming a 4,5-dihydro pyrazole. The fluorescence of the network can be excited with a handheld TLC lamp at λ_{ex} = 365 nm (refer to Figure 68).

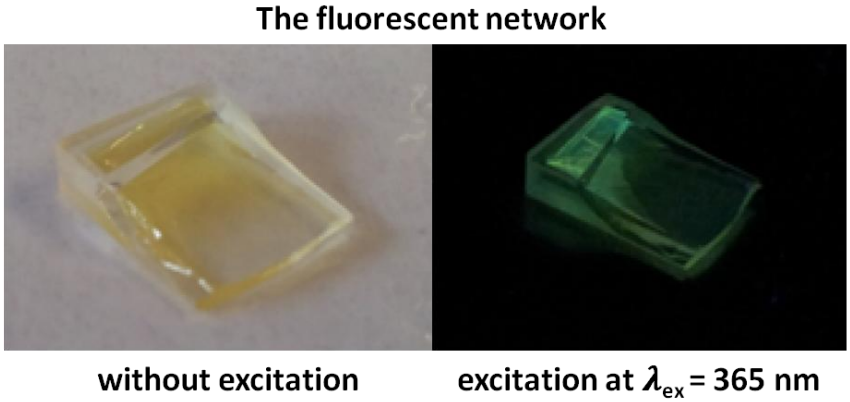

Figure 68: *Illustration of the fluorescent network without excitation and with excitation at* λ_{ex} *= 365 nm. The image was modified from ref.*[144] *with permission from the Royal Society of Chemistry (RSC), 2016.*

In addition, the obtained network was analysed via XPS. The C 1s spectra indicate an intensity increase of the carbon signal O=C-O associated with the covalent attachment of the maleimide functionalities of **32** to the tetrazole terminated star polymer **41.** Moreover, the data demonstrate an increase in the N 1s spectrum of the formed network at a binding energy of 403 eV in comparison to the signal of **41**. The nitrogen increase can be explained by the light induced NITEC reaction between **41** and **32**. In this context, **41** is initially transformed into a nitrile imine intermediate under the release of N_2. Subsequently, **32** containing 4 nitrogen atoms is added to the nitrile imine yielding a 4,5-dihydro pyrazole (refer to Figure 69).

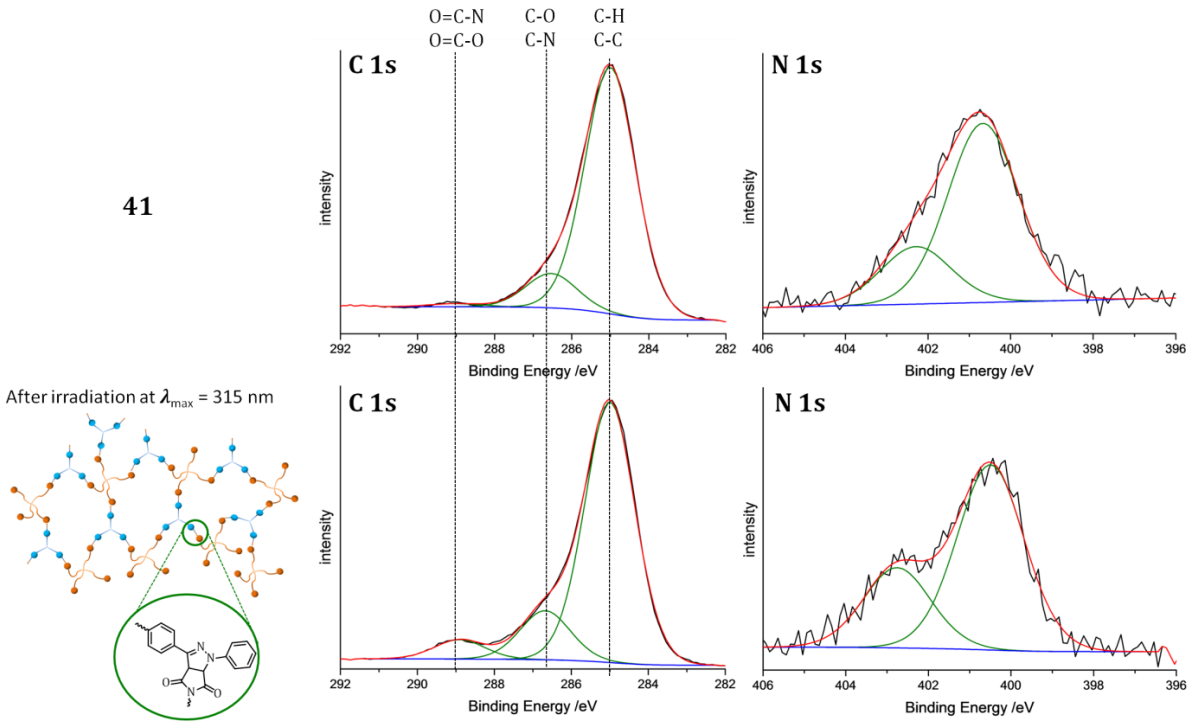

Figure 69: *The successful network formation caused by the phototriggered cross-linking of* ***41*** *and* ***32*** *via a NITEC reaction is analysed via XPS. The cross-linking is verified by an intensity increase of the carbon signal O=C-O in the C 1s spectrum as well as the change in the N 1s spectrum deriving from the of N_2 release and the insertion of the nitrogen atoms from* ***32*** *after the NITEC reaction. The image was modified from ref.*[144] *with permission from the Royal Society of Chemistry (RSC), 2016.*

Importantly, the irradiation of **41** and **32** at λ_{max} = 375 nm under *o*-methyl benzaldehyde activation conditions (refer to Chapter 5.2.1) does not result in a network formation. Thus, it can be stated that both *o*-methyl benzaldehyde and diphenyl tetrazole are able to undergo a wavelength selective network formation, respectively.

5.2.3. Investigation of the Combined Use of *o*-Methyl Benzaldehyde and Diphenyl Tetrazole for Selective Network Formation

In the present section, the wavelength selective network formation according to the λ-orthogonal principle allowing the exclusive activation of *o*-methyl benzaldehyde in the presence of diphenyl tetrazole (refer to Chapter 4.2) was investigated. Therefore, a system containing **40**, **41**, and **32** was irradiated with three LEDs at λ_{max} = 375 nm for

2.5 h in order to exclusively trigger the photoenol reaction. The efficiency of the orthogonal network formation can be determined via a XPS measurement, since the *o*-methyl benzaldehyde terminated star polymer **40** consists of 4-bromostyrene units (refer to Scheme 49) and the diphenyl tetrazole terminated star polymer **41** consists of 4-vinylbenzyl chloride units (refer to Scheme 50). The Cl 2p spectrum of the obtained network indicates the presence of two chlorine signals associated with the expected insertion of **40** in the network. Surprisingly, the appearance of a bromine signal in the Br 3d spectrum demonstrates that **41** was additionally introduced into the network (refer to Figure 70). Therefore, the network was received by the simultaneous cross-linking of *o*-methyl benzaldehyde and diphenyl tetrazole at λ_{max} = 375 nm.

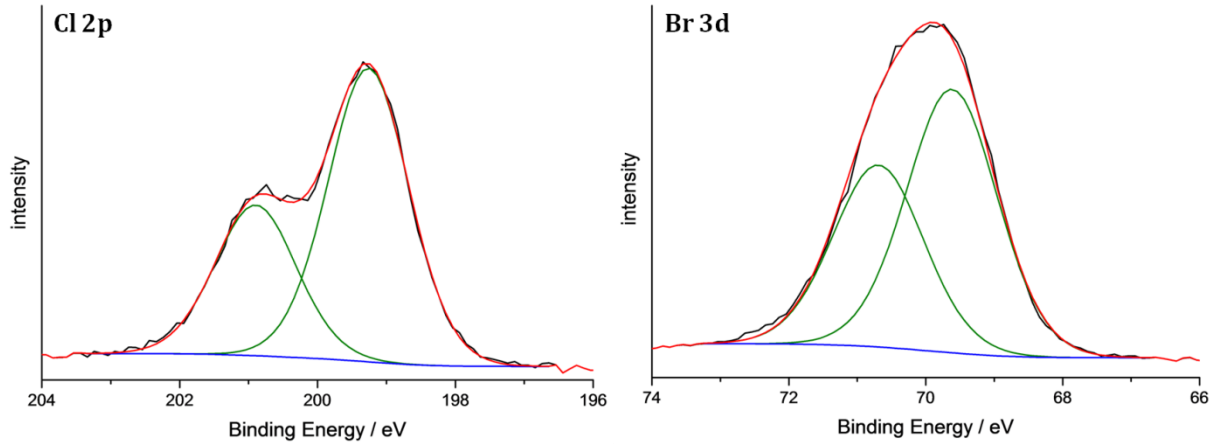

Figure 70: *The irradiation of a system containing the o-methyl benzaldehyde terminated* ***40*** *consisting of 4-bromo styrene units, the diphenyl tetrazole terminated* ***41*** *consisting of 4-vinylbenzyl chloride units, and the trifunctional maleimide* ***32*** *in DCM at* λ *= 375 nm leads to the cross-linking via both the o-methyl benzaldehyde and the diphenyl tetrazole. The simultaneous formation of both networks is evident by the presence of a chlorine signal in the Cl 2p spectrum as well as the presence of a bromine signal in the Br 3d spectrum. Thus, exclusive o-methyl benzaldehyde cross-linking is not possible in the presence of diphenyl tetrazole.*

In summary, the λ-orthogonal concept, featuring the independent photoreaction of *o*-methyl benzaldehyde in the presence of diphenyl tetrazole, cannot be employed for network formation. Instead, diphenyl tetrazole is also activated while *o*-methyl benzaldehyde undergoes a photoreaction. The simultaneous diphenyl activation during the photoenol photoreaction at λ > 350 nm is not observed in diluted solutions (refer to Chapter 4). Therefore, the highly concentrated solutions used for the network formation lead to a mutual interference of both photoactive compounds.

5.3. Overview of the Development of λ-Orthogonal Photoresists for the Application in DLW

The previously described phototriggered cross-linking of multifunctional compounds via low energetic light sources such as LEDs and lamps, generates networks without a distinct shape as the light penetrates all molecules within the system.
Although, the exclusive Diels-Alder conjugated network formation was not possible in the presence of diphenyl tetrazole via the irradiation with the three LEDs at λ = 375 nm (refer to Chapter 5.2.3) – in theory – the DLW setup allows for the activation of the photoactive compounds at a distinct wavelength via a tuneable femtosecond laser. The following sections describe the development of a DLW-photoresist which should enable the design of three-dimensional structures with different properties as a function of the applied laser wavelength. Thus, the photoresists always consist of an *o*-methyl benzaldehyde multifunctionalised pMMA, a tetrazole multifunctionalised pMA, and a multifunctional maleimide.

5.3.1. Investigation of a λ-orthogonal Photoresist on the Basis of End Group Functionalised Star Polymers

The first generation of photoresists for the λ-orthogonal DLW investigations was based on tetrafunctional photoactive star polymers, synthesised via ATRP, which are able to undergo a phototriggered cross-linking. The system consists of the *o*-methyl benzaldehyde terminated pMMA star polymer **42**, the diphenyl tetrazole terminated pMA star polymer **43**, and the trifunctional maleimide **32** (refer to Scheme 51).
Initially, the DLW writing parameters for **42** and **43** were determined, respectively, in order to find the cross-linking threshold in dependence of the applied laser power at a constant writing speed and a constant excitation wavelength for both photoactive structures.

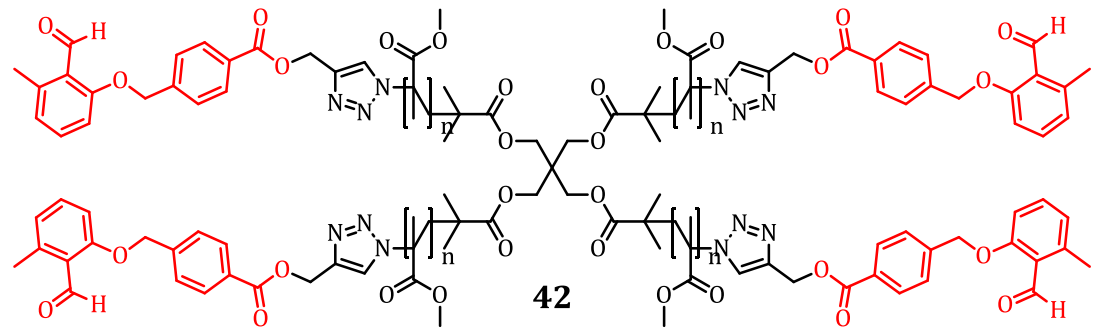

42

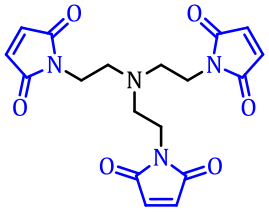

32

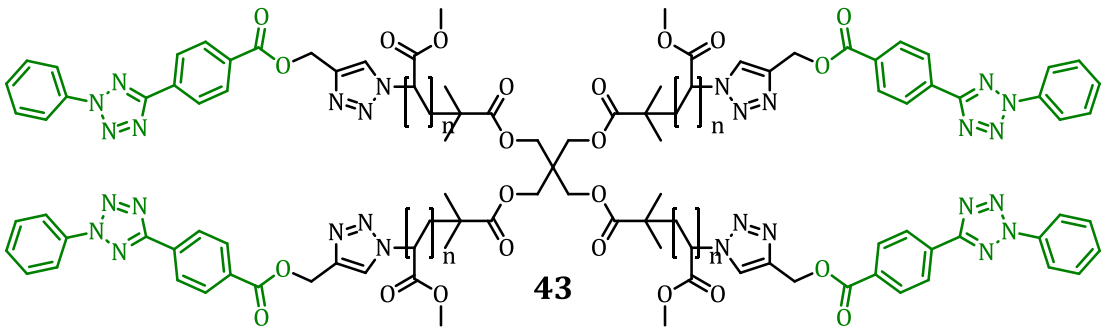

43

Scheme 51: *The first photoresist consists of the o-methyl benzaldehyde terminated pMMA star polymer* ***42****, the diphenyl tetrazole terminated pMA star polymer* ***43****, and the trifunctional maleimide* ***32****.*

Therefore, a photoresist containing **42** (3 eq.) and **32** (4 eq.) in acetophenon (mass fraction: w_i = 20 %) was employed to write lines under DLW conditions with an OPO laser at various positions referring to a distinct laser power. The writing speed was set to 10 μm·s^{-1} and the centre wavelength of the two-photon process was employed at λ = 680 nm corresponding to two individual photons with λ = 340 nm. Unfortunately, the two-photon absorption of the photoresist leads to many random microexplosions making it impossible to generate a controlled writing even for low laser energies (refer to Figure 71a). The same cross-linking threshold investigation was carried out for a photoresist containing **43** (3 eq.) and **32** (4 eq.) in acetophenon (mass fraction: w_i = 20 %). The writing speed was set to 10 μm·s^{-1} and the centre wavelength of the two-photon process was set to λ = 640 nm (corresponding to a one-photon process at λ = 320 nm) as well as λ = 520 nm (corresponding to a one-photon process at

λ = 260 nm). The two-photon absorption of the photoresist shows a wavelength independent behaviour, since the diphenyl tetrazole moiety **43** is activated at λ = 640 nm and λ = 520 nm. The cross-linking threshold for both wavelengths is 8 mW. In addition, the writing of the photoresist at 640 nm leads to microexplosions for higher laser powers (refer to Figure 71b).

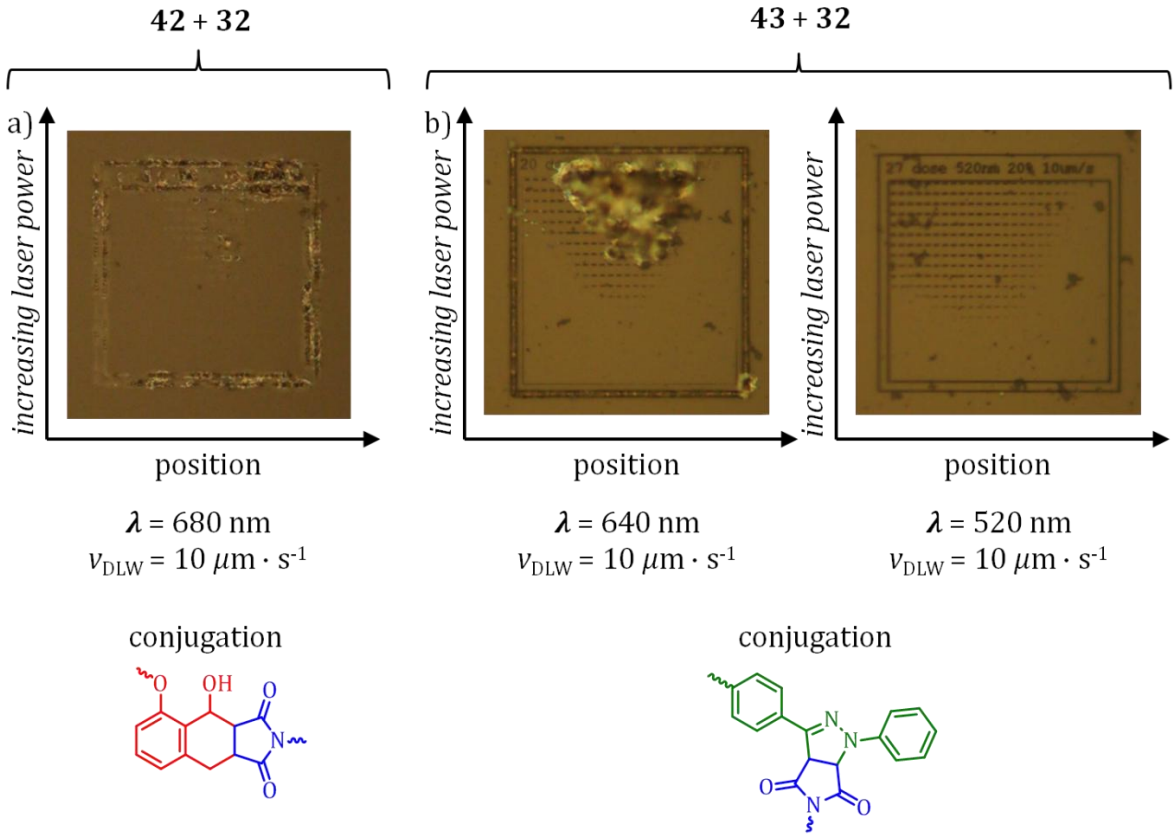

Figure 71: *The cross-linking threshold investigation was performed for a photoresist containing* ***42*** *and* ***32*** *as well as a photoresist containing* ***43*** *and* ***32****, respectively. The photoenol conjugated structures exploded at* λ *= 680 nm with a writing speed of 10* $\mu m \cdot s^{-1}$ *(a). The NITEC conjugated structures can be written in a controlled fashion for small laser powers at* λ *= 520 nm with a writing speed of 10* $\mu m \cdot s^{-1}$ *whereas the writing at* λ *= 640 nm results in microexplosions (b).*

In summary, the DLW-threshold investigation demonstrates that the photoresist containing **42** and **32** as well as the photoresist containing **43** and **32** can only be employed at a slow writing speed of 10 $\mu m \cdot s^{-1}$. Moreover, both *o*-methyl benzaldehyde containing photoresists cannot be used for the design of controlled three-dimensional structures, while the diphenyl containing photoresist can only be employed at relatively slow writing speeds. In both cases, the low density of photoactive functionalities in the star polymers as well as the small amount of maleimide groups in **32** prevent a good cross-linking rate for small conversions. Therefore, the photoactive species in the

photoresists store the high laser energy resulting in the observed microexplosions, instead of transferring the excitation energy into the phototriggered cross-linking.

5.3.2. Investigation of a λ-Orthogonal Photoresist on the Basis of Side Chain Functionalised Copolymers

The second generation of photoresists for the λ-orthogonal DLW investigations was based on side-chain functionalised photoactive copolymers, synthesised via ATRP, allowing a higher cross-linking rate even at low conversions due to an increasing amount of photoactive groups in contrast to the previously presented photoresists on the basis of star polymers (refer to Chapter 5.3.1). The system consists of the copolymer **44** with a pMMA backbone carrying 25 *o*-methyl benzaldehyde side groups on average (M_n = 12200; n = 25), the copolymer **45** with a pMA backbone carrying 14 diphenyl tetrazole side groups on average (M_n = 6500; n = 14), and the copolymer **46** with a pMMA backbone carrying 25 maleimide side groups on average (M_n = 7900; n = 25) (refer to Scheme 52).

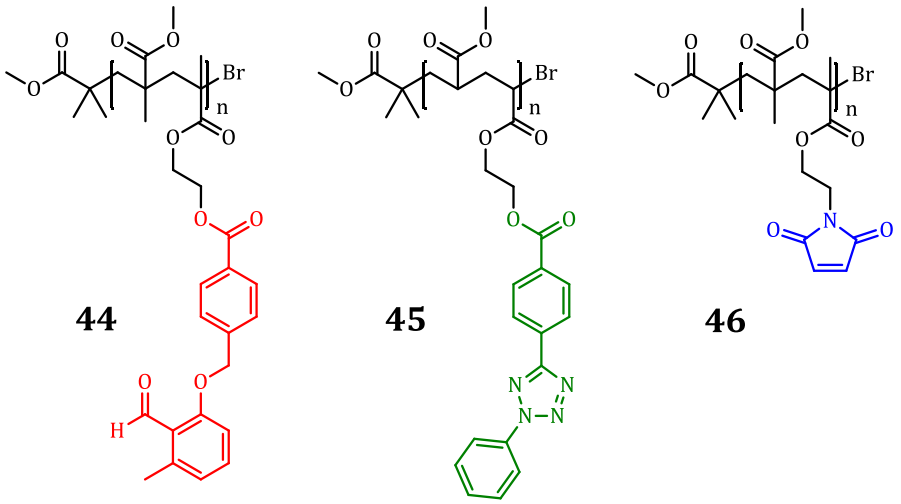

Scheme 52: *The second photoresist consists of the copolymer **44** carrying o-methyl benzaldehyde side groups, the copolymer **45** carrying diphenyl tetrazole side groups, and the copolymer **46** carrying maleimide side groups.*

The cross-linking threshold assessment was repeated for a photoresist containing **44** and **46** in a 1:1 mixture of acetophenon and γ-butyrolactone (GBL) (mass fraction: w_i = 18 %) as well as a photoresist containing **44** and **46** in 1:1 mixture of acetophenon

and GBL (mass fraction: w_i = 18 %), respectively. The writing speed for the photoresist containing **44** and **46** was set to 100 μm·s^{-1} and the centre wavelength of the two-photon process was set to λ = 780 nm (corresponding to a one-photon process at λ = 390 nm). The two-photon absorption of the *o*-methyl benzaldehyde containing photoresist generates controlled structures within a laser power range of 8-12 mW (refer to Figure 72a). The writing speed for the photoresist containing **45** and **46** was set to 100 μm·s^{-1} and the centre wavelength of the two-photon process was also set to λ = 780 nm (corresponding to a one-photon process at λ = 390 nm). According to the UV/vis absorption spectrum (refer to Figure 40, Chapter 4.2), diphenyl tetrazole should not be activated at λ = 390 nm. Surprisingly, the two-photon absorption of the diphenyl tetrazole containing photoresist generates controlled structures within a laser power range of 7-12 mW whereas microexplosions occur at high laser powers (refer to Figure 72b).

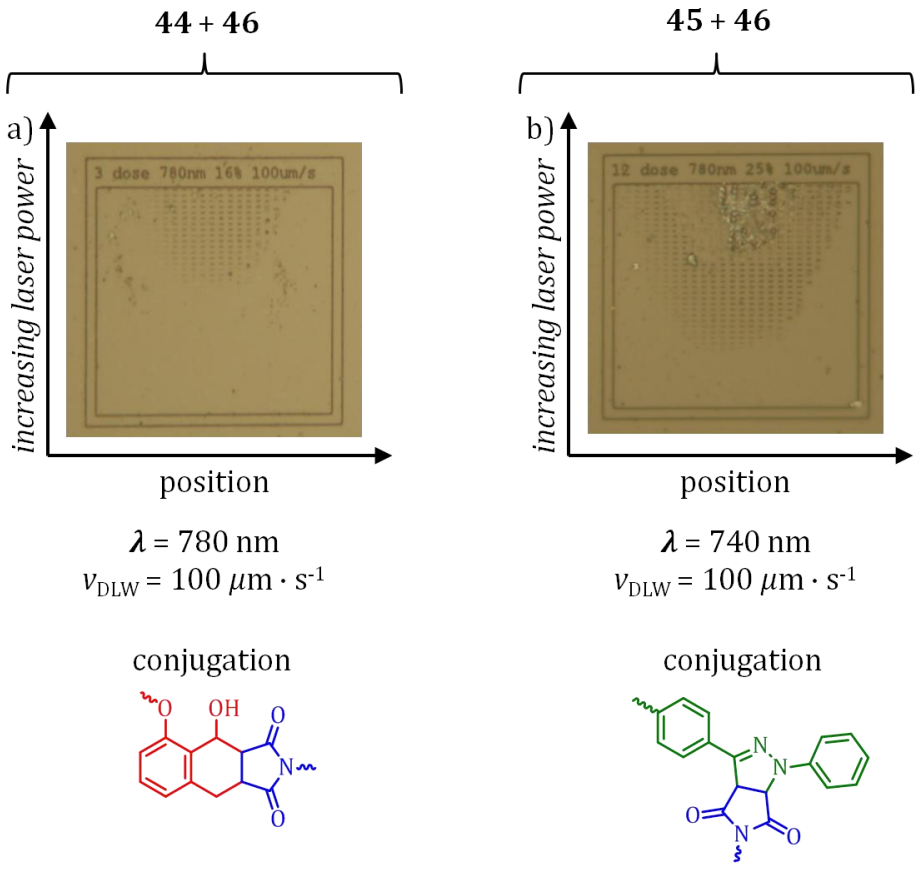

Figure 72: *The cross-linking threshold investigation was performed for a photoresist containing* ***44*** *and* ***46*** *as well as a photoresist containing* ***45*** *and* ***46****, respectively. The photoresist containing* ***44*** *and* ***46*** *yielded controlled structures at* λ *= 780 nm with a writing speed of 100* μm·s^{-1} *within the complete laser power range (a). The photoresist containing* ***44*** *and* ***46*** *afforded controlled structures at* λ *= 780 nm with a writing speed of 100* μm·s^{-1}*, whereas microexplosions occur at higher laser powers (b).*

The threshold investigations demonstrated that both photoresists of the second generation can be applied for the design of controlled three-dimensional structures in contrast to the photoresists of the first generation which generate microexplosions (refer to Figure 73).

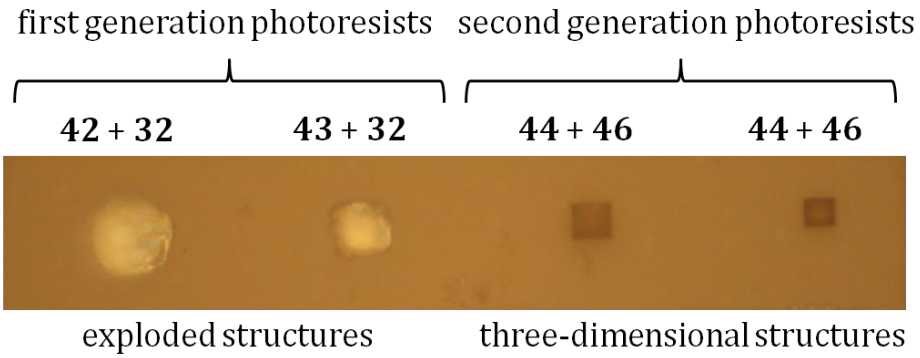

Figure 73: *The photoresists of the first generation on the basis of star polymers (refer to Chapter 5.3.1) lead to microexplosions in the DLW process at the conditions in Figure 71 (left). The photoresists of the second generation allow the controlled writing of three-dimensional structures in the DLW process under the conditions in Figure 72 (right).*

Although the writing parameters for the second photoresist generation have improved enormously, thus enabling the controlled design of three-dimensional structures, the photoresists still lack a wavelength dependent activation of the *o*-methyl benzaldehyde and the diphenyl tetrazole moiety. In fact, diphenyl tetrazole shows a wavelength independent activation in the presence of *o*-methyl benzaldehyde during a two-photon absorption process at $\lambda > 700$ nm (corresponding to a one-photon process at $\boldsymbol{\lambda} = 350$ nm), comparable to the results during the network formation (refer to Chapter 5.2.3). In addition, the threshold limit for diphenyl tetrazole is lower than the one for *o*-methyl benzaldehyde during a two-photon absorption at $\boldsymbol{\lambda} = 780$ nm making it impossible to activate the *o*-methyl benzaldehyde moiety in the presence of diphenyl tetrazole (refer to Figure 72).

Therefore, one photoactive compound needs to be temporarily deactivated in a system including both compounds allowing the exclusive activation of one distinct photoactive species while the other one remains unreacted. In this case, the photoenol depletion is a interesting opportunity to deactivate the phototriggered, highly reactive diene form of *o*-methyl benzaldehyde.[327] The photoenol depletion takes advantage of the light induced transformation of the photoactive E-isomer into the inactive Z- isomer at $\boldsymbol{\lambda} = 440$ nm.[328] Therefore, the [4+2]-cycloaddition between the E-isomer of photoenol and the

maleimide can be deactivated. Instead, the present Z-isomer species is directly transformed into the *o*-methyl benzaldehyde (refer to Scheme 14, Chapter 2.4.1).

A further experiment was necessary in order to investigate the photochemical behaviour of *o*-methyl benzaldehyde and diphenyl tetrazole during photo-depletion. Therefore, a cross-linking experiment was performed for a photoresist containing **44** and **46** as well as a photoresist containing **44** and **46**, respectively. The writing speed for both photoresists was set to 100 $\mu m \cdot s^{-1}$ and the centre wavelength of the two-photon process was employed at λ = 700 nm (corresponding to a one-photon process at λ = 350 nm). In addition, a confined area, within the activated DLW-threshold area, was stimulated with a diode-laser emitting at λ = 440 nm causing depletion (refer to Figure 74a).

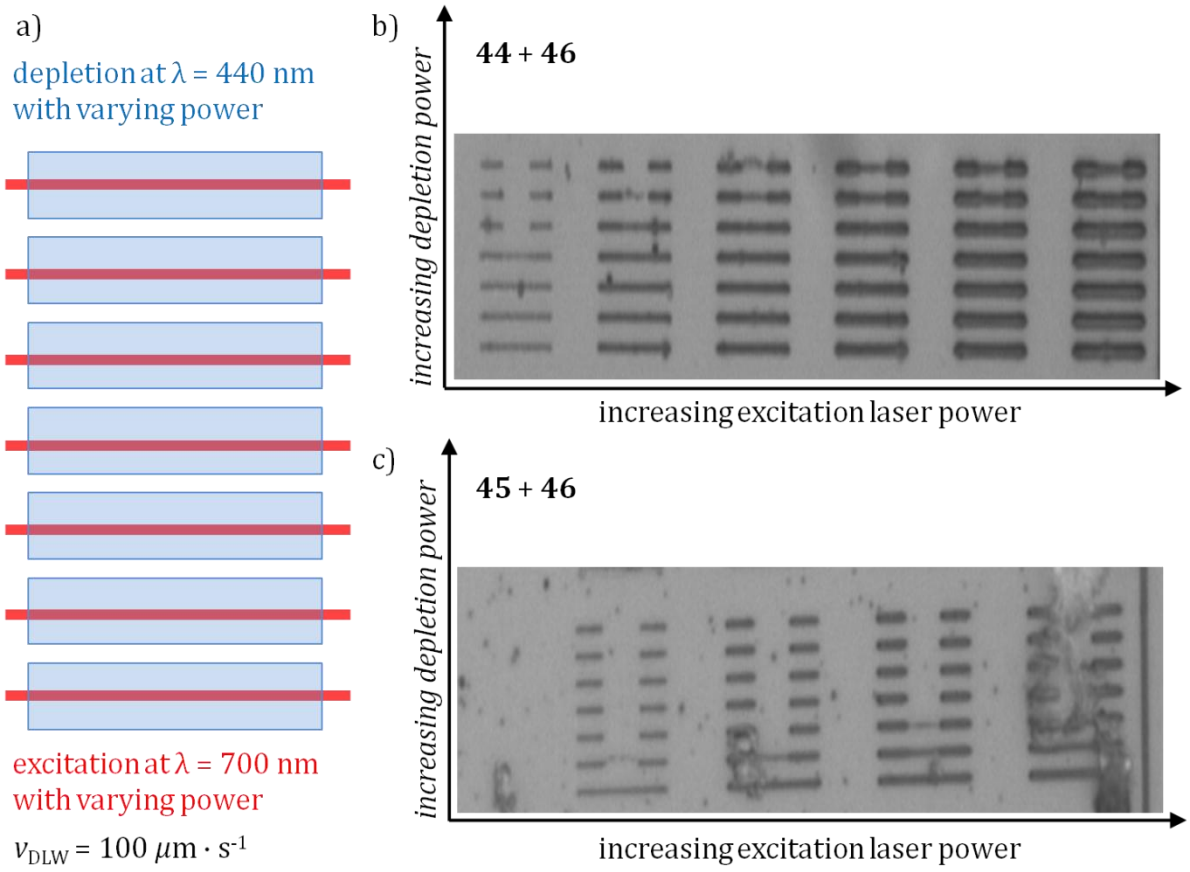

Figure 74: *a) The area of the DLW-threshold experiment (red) at λ = 440 nm with variable excitation powers is partially stimulated with a laser beam (blue) allowing depletion at λ = 440 nm with variable powers. b) The photo-depletion of the o-methyl benzaldehyde species **44** is efficient for low excitation powers and high depletion powers. c) The tetrazole species **45** shows an even more efficient depletion than **44**, since the depletion occurs also at high excitation powers and low depletion powers.*

The threshold experiments of the *o*-methyl benzaldehyde containing photoresist indicate that the photoenol depletion works very well for low excitation laser powers

(λ = 700 nm) and high depletion laser powers (λ = 440 nm) (refer to Figure 74b). Surprisingly, the DLW process of the diphenyl tetrazole species **45** in the other photoresists can be stopped by the diode-laser (λ = 440 nm). The diphenyl tetrazole deactivation even occurs at low depletion laser powers (λ = 440 nm) and high excitation laser powers (λ = 700 nm) (refer to Figure 74c). The fact that **45** and **46** can be used to write structures during the excitation at λ = 700 nm suggests that the obtained nitrile imine intermediate undergoes an irreversible relaxation at λ = 440 nm, since the nitrile imine cannot be retransformed into the tetrazole moiety ,in contrast to the photoenol, resulting in the formation of the *o*-methyl benzaldehyde compound. Therefore the inhibition of **45** is even more efficient than the photoenol depletion of **44**.

As a result, the second generation photoresist, based on side group functionalised copolymers, allows for the controlled writing of three-dimensional structures. Nevertheless, *o*-methyl benzaldehyde and diphenyl tetrazole cannot be employed for a λ-orthogonal photoresist because there is no appropriate excitation wavelength allowing the exclusive activation of one photoactive compound. In addition, the photochemical deactivation on the basis of the photoenol depletion via irradiation with a diode-laser at λ = 440 nm is also highly efficient for the diphenyl tetrazole. Presumably, the diphenyl tetrazole deactivation relies on the irreversible relaxation of the formed nitrile imine intermediate.

5.3.3. Investigation of a λ-orthogonal Photoresist on the Basis of a Tetrafunctional *o*-Methyl Benzaldehyde and a Pyrene Functionalised Tetrazole

The third generation of photoresists, used for the λ-orthogonal DLW investigations, substitutes diphenyl tetrazole with a pyrene functionalised tetrazole showing a significant red shifted absorption. Therefore, the pyrene functionalised tetrazole can be activated at significantly higher wavelengths than the *o*-methyl benzaldehyde species. The system utilised in the third photoresist generation consists of the tetrafunctional *o*-methyl benzaldehyde **48**, the copolymer **47** with a pMA backbone carrying pyrene

functionalised tetrazole side groups, and the copolymer **46** with a pMMA backbone carrying maleimide side groups (refer to Scheme 53).

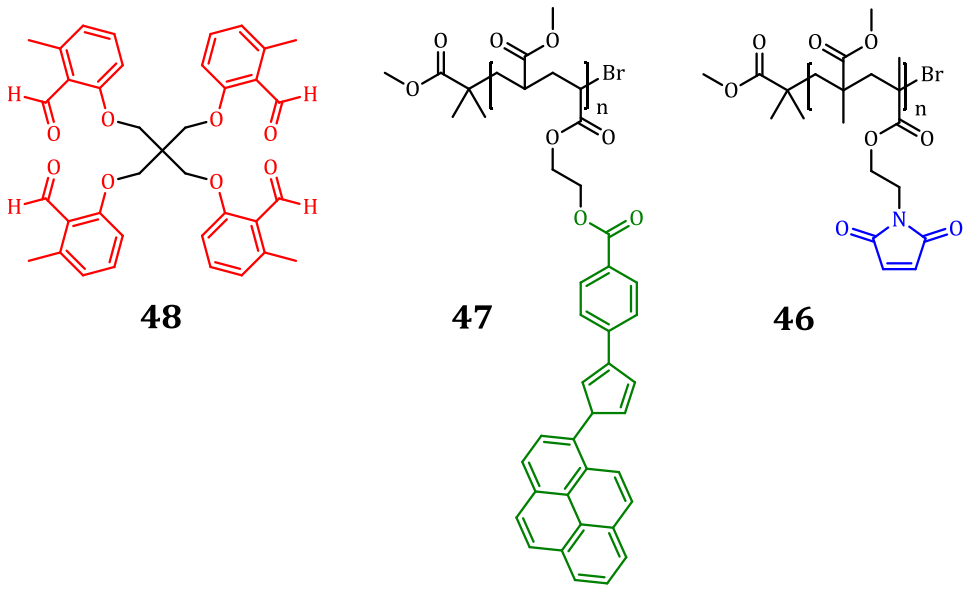

Scheme 53: *The third photoresist consists of the copolymer **44** carrying o-methyl benzaldehyde side groups, the copolymer **47** carrying pyrene functionalised tetrazole side groups, and the copolymer **46** carrying maleimide side groups.*

The cross-linking threshold test was performed for the photoresists containing *o*-methyl benzaldehyde and the pyrene functionalised tetrazole, respectively. The writing speed of the DLW process was always set to 100 μm·s^{-1}, whereas the excitation wavelength was varied between 700 nm and 780 nm.

The photoresist containing **44** and **46** in a 1:1 mixture of acetophenon and ***γ***-butyrolactone (GBL) (mass fraction: w_i = 18 %) allows for the controlled writing of structures at ***λ*** = 700 nm (corresponding to a one-photon process at ***λ*** = 350 nm) within a threshold power of 6-12 mW (refer to Figure 75a), whereas the threshold experiment at ***λ*** = 780 nm (corresponding to a one-photon process at ***λ*** = 390 nm) leads to uncontrolled structures within a power range of 20-40 mW (refer to Figure 75c). The photoresist containing **47** and **46** in a 1:1 mixture of acetophenon and ***γ***-butyrolactone (GBL) (mass fraction: w_i = 18 %) creates faint structures at ***λ*** = 700 nm within a threshold power of 10-12 mW (refer to Figure 75b), whereas the threshold experiment at ***λ*** = 780 nm leads to uncontrolled structures within a power range of 22-40 mW (refer to Figure 75d). In theory, the threshold experiments demonstrate that *o*-methyl benzaldehyde has the potential to be exclusively activated in the presence of pyrene functionalised tetrazole at an excitation wavelength of ***λ*** = 700 nm in a power range of 6-10 mW. The converse ***λ***-orthogonal reaction path, including the initial pyrene

functionalised tetrazole activation in the presence of *o*-methyl benzaldehyde at λ = 780 nm, is not possible as appropriate DLW parameters could not be identified. Instead, the relatively high excitation power of more than 20 mW prevents the generation of controlled structures and thus results in microexplosions.

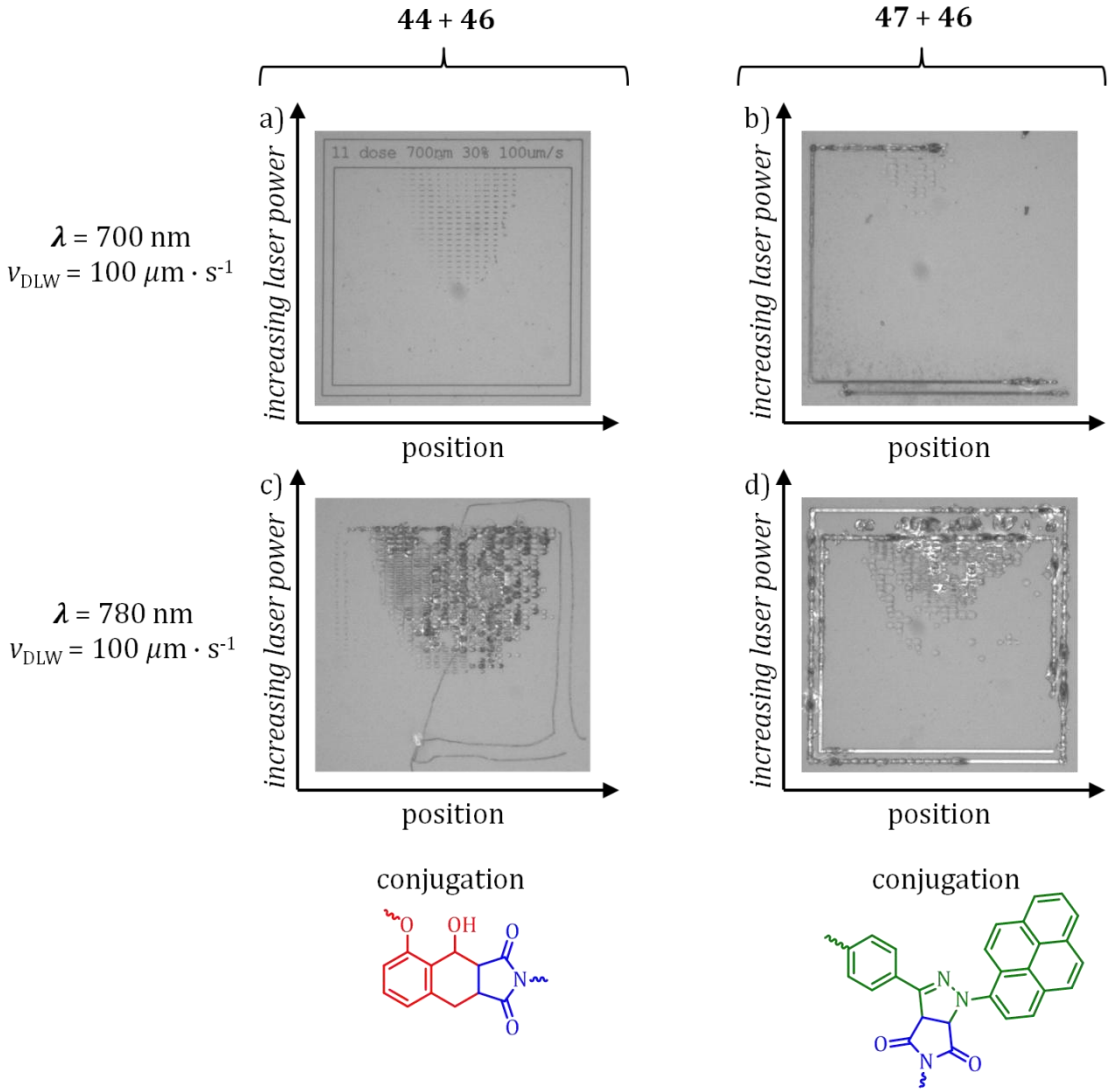

Figure 75: *The cross-linking threshold investigation was performed for a photoresist containing* ***44*** *and* ***46*** *as well as a photoresist containing* ***47*** *and* ***46*** *at varying wavelengths, respectively. The photoresist containing* ***44*** *and* ***46*** *yielded controlled structures at* λ *= 700 nm with a writing speed of 100* $\mu m \cdot s^{-1}$ *within a laser power range of 6-12 mW (a). The photoresist containing* ***47*** *and* ***46*** *yielded faint structures at* λ *= 700 nm with a writing speed of 100* $\mu m \cdot s^{-1}$ *within a laser power range of 10-12 mW (b). Therefore, the DLW parameters at* λ *= 700 nm should allow the exclusive o-methyl benzaldehyde activation in the presence of the pyrene functionalised tetrazole. The photoresist containing* ***44*** *and* ***46*** *afforded uncontrolled structures at* λ *= 780 nm with a writing speed of 100* $\mu m \cdot s^{-1}$ *within a laser power range of 20-40 mW (c). The photoresist containing* ***47*** *and* ***46*** *led to uncontrolled structures bearing microexplosions at* λ *= 780 nm with a writing speed of 100* $\mu m \cdot s^{-1}$ *within a laser power range of 22-40 mW (d).*

In the following, the initial *o*-methyl benzaldehyde activation in the presence of the pyrene functionalised tetrazole according to the **λ**-orthogonal principle was investigated. Therefore, a photoresist containing **44**, **47** and **46** in a 1:1 mixture of acetophenon and **γ**-butyrolactone (GBL) (mass fraction: w_i = 19 %) was employed for the writing of a three-dimensional block at **λ** = 700 nm by applying the **λ**-orthogonal principle in one direction allowing for the exclusive *o*-methyl benzaldehyde activation in the presence of the pyrene functionalised tetrazole. Therefore, the obtained block, based on Diels-Alder linkage, should not show any fluorescence. In addition, the photoresist was employed for the generation of a three-dimensional block at **λ** = 780 nm affording a fluorescent structure.

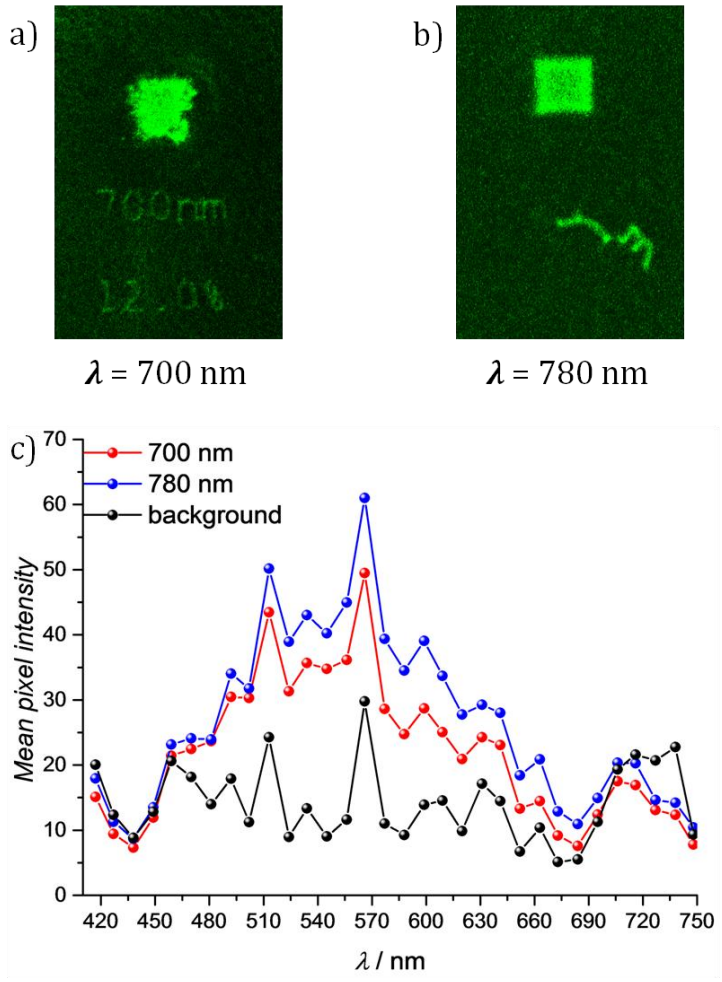

Figure 76: *The photoresist containing **44**, **47**, and **46** yielded a fluorescent block at **λ** = 700 nm with a writing speed of 10 µm·s^{-1} with an excitation laser power of 6 mW. The fluorescence indicates that o-methyl benzaldehyde was not exclusively cross-linked. Instead, the NITEC reaction of **47** and **46** was additionally operational (a). The photoresist containing **44**, **47**, and **46** yielded the expected fluorescent block at **λ** = 780 nm with a writing speed of 10 µm·s^{-1} with an excitation laser power of 10 mW (b). The fluorescence in relation to the activation wavelength was detected for the background, the block obtained at **λ** = 700 nm as well as the block obtained at **λ** = 780 nm (c).*

The photoresist containing both the *o*-methyl benzaldehyde and the pyrene functionalised tetrazole could only be processed with a reduced writing speed of 10 μm·s^{-1}. The DLW process at λ = 700 nm with a laser power of 6 mW led to a controlled structure. Surprisingly, the obtained block is fluorescent (refer to Figure 76a) indicating that **44** and **47** were activated although – in theory – the pyrene functionalised tetrazole should not be affected under the chosen conditions (refer to Figure 75b). In fact, the detectable fluorescence demonstrates that the pyrene functionalised tetrazole forms the fluorescent 4,5-dihydro pyrazole while the *o*-methyl benzaldehyde species is activated. The unexpected activation of the tetrazole species resembles the results of the network formation (refer to chapter 5.2.3) suggesting that energy transfer occurs between both photoactive compounds in concentrated solutions. The DLW process at λ = 780 nm with a laser power of 10 mW allowed the controlled writing of structures showing the expected fluorescence associated with the 4,5-dihydro pyrazole product of the NITEC reaction of **47** with **44** (refer to Figure 76b). The fluorescence of the blocks obtained at λ = 700 nm and λ = 780 nm was detected in the wavelength range between λ = 417-755 nm via a laser scanning microscope (LSM), respectively. The fluorescence increase of the structure obtained at λ = 700 nm is smaller than the fluorescence of the structure obtained at λ = 780 nm in comparison to the background measurement (refer to Figure 76c). Although the λ-orthogonal generation of DLW structures is not possible with the present photoresist, it appears that the pyrene functionalised tetrazole conversion is dependent on the excitation wavelength and the applied laser power.

In summary, DLW parameters such as the applied laser power and the excitation wavelength allow the wavelength selective generation of controlled structures for a photoresist containing either the *o*-methyl benzaldehyde or the pyrene functionalised tetrazole. A photoresist containing both photoactive compounds yields a mixture of both photochemical conjugation products.

5.4. Conclusions

Wavelength selective network formation is explored featuring *o*-methyl benzaldehyde, diphenyl tetrazole, and maleimide species. Therefore, a system containing a star polymer carrying *o*-methyl benzaldehyde end groups and a trifunctional maleimide is irradiated at λ_{max} = 375 nm yielding a Diels-Alder linked network. A system containing a star polymer carrying diphenyl tetrazole termini and a trifunctional maleimide is irradiated at λ_{max} = 315 nm resulting in a fluorescent 4,5-dihydro pyrazole linked network whereas the diphenyl tetrazole moiety cannot be activated at λ_{max} = 375 nm. Next, the network formation is investigated on the basis of the λ-orthogonal principle allowing the initial activation of the *o*-methyl benzaldehyde species at λ = 310-350 nm in the presence of the diphenyl tetrazole. A system containing the *o*-methyl benzaldehyde terminated star polymer, the diphenyl tetrazole terminated star polymer, and the trifunctional maleimide is irradiated at λ_{max} = 375 nm leading to the combined activation of the *o*-methyl benzaldehyde and the diphenyl tetrazole preventing a λ-orthogonal network formation.

The second aspect of the previous chapter explored the design and investigation of a photoresist, including stiff and flexible polymers carrying different photoactive compounds, enabling the λ-orthogonal design of three-dimensional structures in a DLW process. Therefore, the physical properties of the obtained structures may be adjusted by the applied laser wavelength. The first generation of λ-orthogonal photoresists is based on star polymers carrying either *o*-methyl benzaldehyde or the diphenyl tetrazole end groups as well as a trifunctional maleimide. The *o*-methyl benzaldehyde and the diphenyl tetrazole species lead to the formation of uncontrolled structures at various excitation wavelengths. The second generation of photoresists uses side chain functionalised polymers carrying either *o*-methyl benzaldehyde, diphenyl tetrazole or maleimide allowing for the writing of controlled DLW-structures. Nevertheless, the exclusive activation of one photoactive compound cannot be realised as no unique DLW parameters enabling λ-orthogonality could be determined. The depletion of *o*-methyl benzaldehyde with a diode-laser at λ = 440 nm also leads to depletion effects for the diphenyl tetrazole species which is inhibited in writing laser induced structures by the diode laser. The third generation of photoresists uses side chain functionalised polymers carrying either *o*-methyl benzaldehyde, pyrene functionalised tetrazole or maleimide. A

photoresist containing the *o*-methyl benzaldehyde species and the maleimide can be exclusively activated at λ = 700 nm with an excitation laser power range of 6-12 mW whereas a photoresist containing the pyrene functionalised tetrazole and the maleimide species cannot be employed for the design of controlled structures under the chosen conditions. The excitation of a photoresist containing both photoactive compounds at λ = 700 nm with an excitation laser power of 6 mW results in the activation of the *o*-methyl benzaldehyde and the pyrene functionalised tetrazole preventing the generation of a λ-orthogonal photoresist.

6

6. Outlook

The modular building-block concept based on *click* criteria is a versatile method for the orthogonal ligation of molecules in soft matter science. Especially, consecutive modification steps for polymers benefit from modular ligation chemistry since elaborate post-modification steps require the purification of the polymer after the first modification, restricting possible applications. In this context, photoreactions offer an accessible, efficient, and fast ligation method. The combination of light triggered reactions with modular building-block concepts enables a wavelength selective ligation protocol showing great potential in the field of synthetic polymer chemistry.

In chapter 3, a light activated reaction manifold is introduced allowing either a photochemical or a non-irradiative, thermally induced reaction path for *o*-methyl benzaldehyde species. The photoreaction is based on the light induced transformation of the *o*-methyl benzaldehyde into a highly reactive *o*-quinodimethane species (photoenol) which is able to undergo an irreversible Diels-Alder reaction with a maleimide compound. The non-irradiative reaction step relies on the reversible reaction between *o*-methyl benzaldehyde and hexylamine yielding a stable imine.
The strong kinetic preference of the light induced Diels-Alder reaction between *o*-methyl benzaldehyde and a maleimide species over the imine formation in polar solvents such

as acetonitrile was exploited to synthesise block copolymers via either the photoreaction path or the non-irradiative imine formation. Thus, the manifold system in acetonitrile offers the possibility to synthesise even more complex polymer architectures such as star polymers and networks using multifunctional compounds for future applications. In addition, the concept of the *o*-methyl benzaldehyde manifold system could be applied in an orthogonal step growth polymerisation in a one-pot system using bifunctional oligomers. Therefore, the irradiative reaction path thus offers an access route to non-degradable polymers on the basis of a Diels-Alder conjugation, whereas the non-irradiative reaction path would generate degradable polymers on the basis of the imine conjugation.

The second aspect of the reaction manifold relies on the true competition of the photoreaction and the imine formation in non-polar solvents such as dichloromethane as the photoreaction rate is herein significantly reduced. Semi-qualitative calculations as well as experimental data indicate that the light triggered equilibrium between *o*-methyl benzaldehyde and the photoenol species can be shifted by an increase of the maleimide concentration leading to a preference of the photoreaction during irradiation. Consequently, the reactivity of the aldehyde functionality could be exploited in order to implement novel non-irradiative reaction paths for the *o*-methyl benzaldehyde species, such as oxime formation using hydroxylamine or hydrazone formation using organic hydrazine derivatives. Both the oxime and the hydrazone reaction paths could be individually investigated in terms of reaction kinetics and product stability. Moreover, these substitution reactions could be performed as non-irradiative reaction path, such as the imine formation, in competition to the photoinduced step.

In chapter 4, the concept of the $\boldsymbol{\lambda}$-orthogonal pericyclic photoligation was implemented using the photoactive compounds *o*-methyl benzaldehyde and diphenyl tetrazole. The $\boldsymbol{\lambda}$-orthogonal principle rests on the different absorptivities – and thus reactivities – of both photoactive species allowing for the initial activation of *o*-methyl benzaldehyde in the wavelength range of $\boldsymbol{\lambda}$ = 310-350 nm in the presence of diphenyl tetrazole. The exclusive diphenyl tetrazole activation in the presence of *o*-methyl benzaldehyde is prevented due to the fact that the absorptivities of both moieties only overlap below $\boldsymbol{\lambda}$ = 310 nm (refer to chapter 4.2). Therefore, the insertion of *o*-methyl benzaldehyde, diphenyl tetrazole, and maleimide into polymers constitutes a one-pot system enabling polymer based

ligation protocols according to the ***λ***-orthogonal principle in one direction. Therefore, an *o*-methyl benzaldehyde terminated polymer, a diphenyl tetrazole terminated polymer, and maleimide was employed for wavelength selective end group modifications in order to determine the kinetic parameters for both photoreactions in a one-pot system. The design of an α,ω-functional oligomeric bilinker, carrying *o*-methyl benzaldehyde and tetrazole at each chain end, allows for the site-specific end group modification as well as the ***λ***-orthogonal formation of triblock copolymers. The exclusive diphenyl tetrazole activation in the presence of *o*-methyl benzaldehyde was realised by the initial transformation of *o*-methyl benzaldehyde into the photochemically inactive imine.
Although, the ***λ***-orthogonal principle based on *o*-methyl benzaldehyde and diphenyl tetrazole is a versatile system for phototriggered ligations in polymer chemistry, the development of novel photoreactions is necessary. These photoreactions should be employed according to the ***λ***-orthogonal concept, enabling the exclusive photochemical absorption of one compound within a distinct wavelength regime in the presence of the other photoactive compound. Moreover, the absorptivities of the present system based on the *o*-methyl benzaldehyde species and the diphenyl tetrazole moiety could be separated from each other more efficiently by red shifting the absorption of one species while the absorption of the other one is blue shifted via the modification of both compounds with appropriate functionalities. For instance, the red shifting of diphenyl tetrazole has been already reported by the insertion of a pyrene functionality (refer to chapter 2.4.2), yet but the absorption tuning requires further improvement.

In chapter 5, the wavelength selective network formation was demonstrated for two different photoresists. Thus, a photoresist containing an *o*-methyl benzaldehyde terminated star polymer and a trifunctional maleimide afforded a network after the irradiation with LEDs at $\lambda = 375$ nm whereas a photoresist containing a diphenyl tetrazole terminated star polymer and a trifunctional maleimide yielded a fluorescent network after the irradiation with a lamp at $\lambda = 315$ nm. The ***λ***-orthogonal principle based on the initial *o*-methyl benzaldehyde activation and the subsequent diphenyl tetrazole reaction could not be employed on a photoresist containing both photoactive compounds. In this case, a possible problem may be the highly concentrated solution inducing interactions between the *o*-methyl benzaldehyde and the diphenyl tetrazole. The implementation of novel photoreactions showing less overlapping in the

absorptivies could be of interest in the future. In addition, the broad emission of the applied light sources could be circumvented by either using UV filters in order to remove inadvertent wavelengths or by using a tuneable laser at a low power level.
The second application of a photoresist based on *o*-methyl benzaldehyde and a tetrazole species is focussed on the generation of three-dimensional structures via DLW in a wavelength selective fashion. The three presented generations of photoresists using different polymer architectures and different tetrazole species (refer to chapter 5.3) could not be employed according to the $\boldsymbol{\lambda}$-orthogonal principle. The main problem seems to be the energy transfer between both photoactive compounds during the laser excitation. Therefore, a strategy for the future might be to add small scavenger molecules into the photoresist which absorb the excess energy but do not undergo any reaction. Moreover, a future photoresist should contain photoactive compounds whose absorptivity/activation ranges differ immensely from each other. Therefore, the photoresist of the next generation could be based on a multifunctional diphenyl tetrazole, a photoinitiator absorbing visible light such as camphorquinone, and a tetrafunctional acrylate.

In summary, the present dissertation introduces the concept of $\boldsymbol{\lambda}$-orthogonality into polymer chemistry and investigates kinetic parameters of the photoreactions as well as mechanistic details. Moreover, the present dissertation demonstrates possible applications such as the wavelength selective design block copolymers, star polymers, and networks. In addition, it is shown that the $\boldsymbol{\lambda}$-orthogonal principle, based on *o*-methyl benzaldehyde and diphenyl tetrazole, is a versatile ligation tool in dilute solutions, yet faces challenges for highly concentrated solutions as well as highly energetic light sources such as femtosecond lasers.

7

7. Experimental Section

The synthesis of the tetrafunctional RAFT agents and the resulting polymers based on the RAFT agents in Chapter 7.3.2 were performed by M. Kaupp (Institute for Chemical Technology and Polymer Chemistry, KIT).

7.1. A Light Activated Reaction Manifold

7.1.1. Materials and Instrumentation

Materials

Acetonitrile (99.8%, anhydrous, Sigma-Aldrich), dichloromethane (DCM, HPLC grade, Acros), dichloromethane (DCM, 99.8%, extra dry, Acros), 1-(3-dimethylaminopropyl)-3-ethylcarbodiimide hydrochloride (EDC·HCl, 98+%, Acros), 4-dimethylaminopyridine (DMAP, 99%, abcr), 4-formyl benzoic acid (96%, Acros), hydrochloric acid (37%, Roth), maleic anhydride (≥ 99%, Sigma Aldrich), ethyl maleimide (99%, VWR), hexylamine (98%, Merck), N,N'-dicyclohexylcarbodiimide (DCC, 99%, Acros), mono-ethyl fumarate (97%, Alfa Aesar), poly(ethylene glycol) methyl ether (PEG, $M_n \approx 2200$ g·mol^{-1}, Sigma Aldrich), poly (L-lactide) (pL, $M_n \approx 5700$ g·mol^{-1}, Sigma Aldrich), poly(L-lactide) amine terminated (pL-Amine, $M_n \approx 5000$ g·mol^{-1}, Sigma Aldrich), poly(N-isopropylacrylamide) maleimide terminated (pNIPAAm-Mal-, $M_n \approx 5500$ g·mol^{-1}, Sigma Aldrich), tetrahydrofuran (THF, 99.85%, extra dry, Acros) were used as received.

NMR spectroscopy

^{1}H NMR spectroscopy was performed using a Bruker Ascend 400 at 400 MHz. All samples were dissolved in $CDCl_3$, deuterated dimethylsulfoxide (DMSO-d^6), or deuterated acetonitrile (MeCN-d^3) The δ-scale is referenced to the internal standard trimethylsilane (TMS, δ = 0.00 ppm).

Mass spectrometry

ESI-MS (Electrospray Ionization Mass Spectrometry) spectra were recorded on a Q Exactive (Orbitrap) mass spectrometer (ThermoFisher Scientific, San Jose, CA, USA) equipped with an HESI II probe. The instrument was calibrated in the m/z range of 74-1822 using a premixed standard comprising caffeine, Met-Arg-Phe-Ala acetate (MRFA), and a mixture of fluorinated phosphazenes (Ultramark 1621). A constant spray voltage of 4.6 kV and a dimensionless sweep gas flow rate of 5 were applied. The capillary temperature and the S-lens RF level were set to 320°C an 62.0, respectively. The samples

were dissolved with a concentration of 0.05 mg·mL^{-1} in a mixture of THF and MeOH (3:2) containing 100 μmol sodium trifluoracetate (NaTFA). The samples were infused with a flow of 5 μL·min^{-1}.

Gel Permeation Chromatography

Gel Permeation Chromatography (GPC) measurements were performed on a Waters gel permeation chromatography system equipped with a Waters 1515 isocratic HPLC pump comprising a Waters 2707 autosampler, three consecutive Waters Styragel columns (all 7.8 x 7.5 mm), preceded by a Waters Styragel guard column (4.6 x 30 mm) and a Waters 2487 dual wavelength absorbance detector (analysis in 254 nm) in series with a refractive index detector using THF as the eluent at 30°C with a flow rate of 1 mL min^{-1}. The present GPC system was calibrated using linear poly(styrene) standards ranging from 100 to 4·10^{6} g mol^{-1}. The resulting molar mass distributions were determined by universal calibration using Mark-Houwink parameters for polystyrene (K = 14.1·10^{-5} *d*L g^{-1}, α = 0.7).

Irradiation

The samples to be irradiated were placed on a metallic disc revolving in a custom-built photoreactor around a light source (refer to Figure S1).

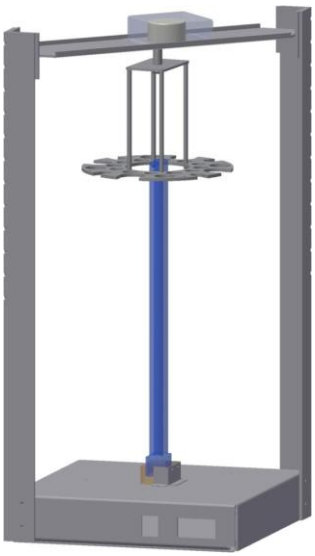

Figure S1: *Drawing of the custom-built photoreactor employed in the current study. The angular velocity is 0.5 rad·s^{-1}. The samples do not spin while revolving around the light source. The emitted intensity of the applied light sources are sufficient in order to guarantee a sufficient photon penetration of the samples.*

The utilised light sources are a compact low-pressure fluorescent lamp (Cleo PL-L, Philips Deutschland GmBH) emitting at λ_{max} = 365 nm (± 50 nm, 36 W) at a distance of 40-50 mm in the custom-built photoreactor or three UV-A LEDs (Avonec Online-Handel, Germany) emitting at λ_{max} = 375 nm (± 30 nm, each 3 W) at a distance of 5 mm. No bandpass filter was used for the irradiations with the PL-L lamp.

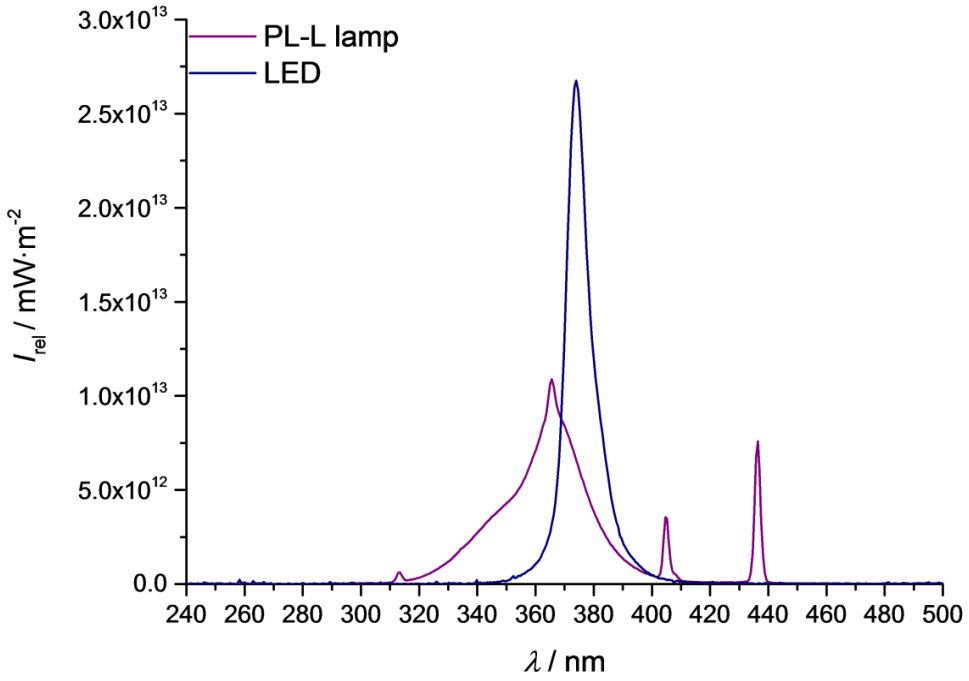

Figure S2: *Emission spectra of the previously employed compact low-pressure fluorescent lamp PL-L (36 W, λ_{max} = 365 nm) and the high power LEDs (3 W, λ_{max} = 375 nm). The emission spectra were recorded with a UV sensor (Opsytec Dr. Gröbel GmbH; Ettlingen, Germany). The image was modified from ref.*[297] *with permission from the American Chemical Society (ACS), 2016.*

7.1.2. Syntheses

o-Methyl benzaldehyde

The synthesis of 4-((2-formyl-3-methylphenoxy)methyl) benzoic acid (*o*-methyl benzaldehyde) was performed in four steps according to the appropriate literature procedures: step 1,[329] step 2,[184] step 3,[329] and step 4.[298]

^{1}H NMR (DMSO-d^6) δ/ppm 2.47 (s, 3H), 5.34 (s, 2H), 6.89 (d, 1H), 7.13 (d, 1H), 7.47 (t, 1H), 7.60 (d, 1H), 7.97 (d, 1H), 10.62 (s, 1H), 12.97 (s, 1H).

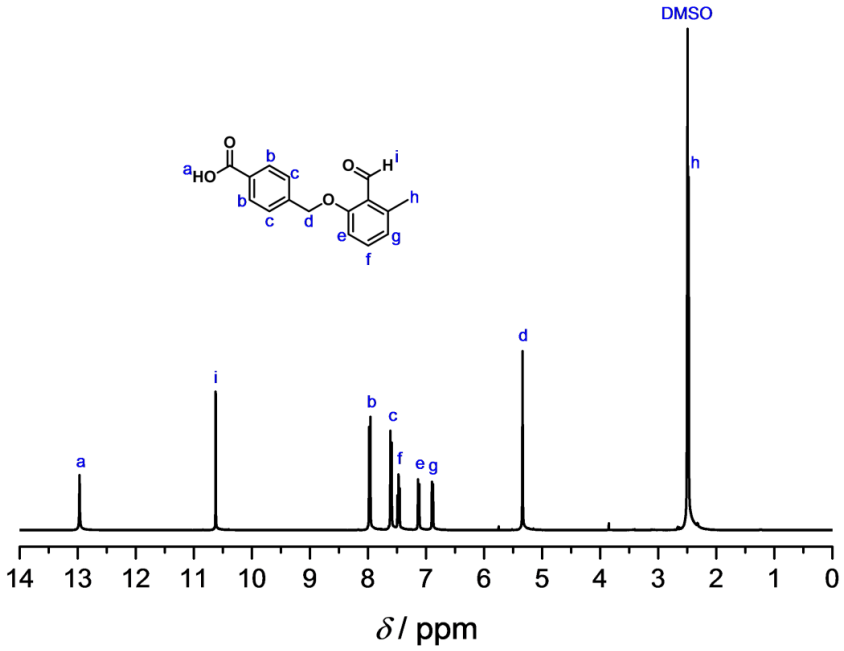

Figure S3: *^{1}H NMR spectrum of o-methyl benzaldehyde in DMSO-d^6.*

o-Methyl benzaldehyde terminated PEG 4

The synthesis of the *o*-methyl benzaldehyde terminated poly(ethylene glycol) was performed according to a literature procedure.[298]

^{1}H NMR ($CDCl_3$) δ/ppm 1.4-1.60 (m, 237H), 2.52 (s, 3H), 3.67 (s, 3H), 5.05-5.20 (m, 81 H), 6.77 (t, 2H), 7.29 (t, 1H), 7.44 (d, 2H), 7.60 (d, 1H), 8.02 (d, 2H), 10.69 (s, 1H).

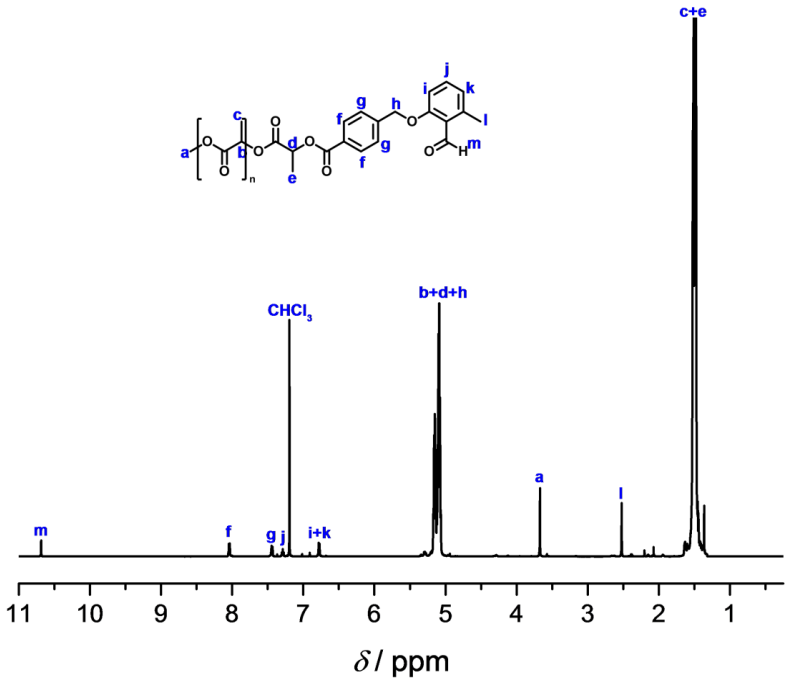

Figure S4: *^{1}H NMR spectrum of the o-methyl benzaldehyde terminated PEG in $CDCl_3$.*

o-Methyl benzaldehyde terminated pL 12

500.0 mg ($M_n \approx 5000$ g·mol^{-1}, 0.1 mmol, 1.eq.) of polylactide, 108.1 mg (0.4 mmol, 4 eq.) of *o*-methyl benzaldehyde acid, 12.2 mg (0.1 mmol, 1 eq.) of DMAP, and 383.4 mg (2.0 mmol, 20 eq.) of EDC·HCl were dissolved in 10 mL dry THF. The solution was stirred at ambient temperature for 3 days. Precipitated urea was filtered off. Afterwards, the solution was dialysed in a mixture of THF and methanol (1:1), followed by a dialysis in water yielding a slightly yellow powder.

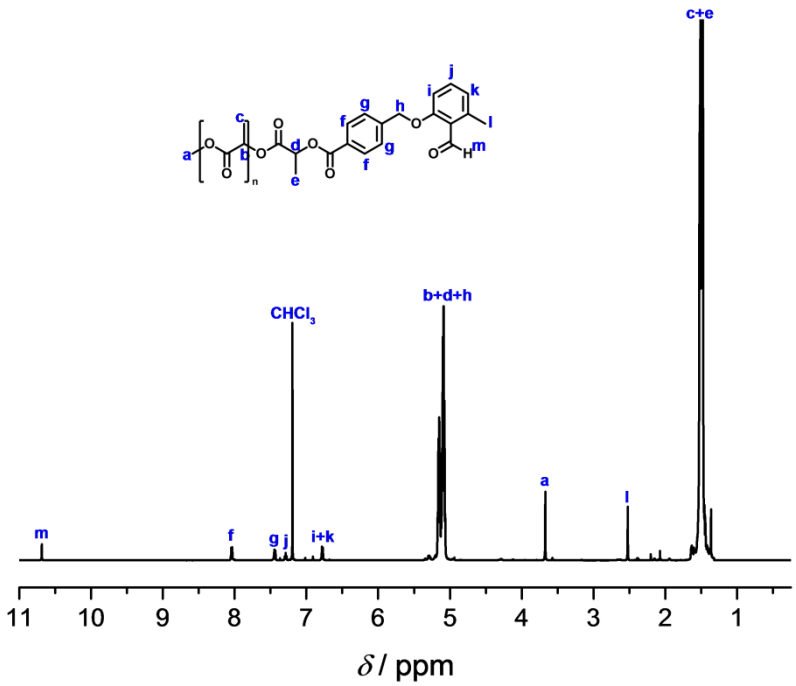

Figure S5: *^{1}H NMR spectrum of the o-methyl benzaldehyde terminated polylactide in $CDCl_3$.*

PEG-fumarate 14

500.0 mg ($M_n \approx 2000$ g·mol^{-1}, 0.25 mmol, 1.0 eq.) of poly(ethylene glycol) methyl ether, 72.1 mg (0.5 mmol, 2.0 eq.) of mono-ethyl fumarate, and 239.6 mg (1.0 mmol, 5.0 eq.) of EDC·HCl were dissolved in 6 mL dry THF. 22.9 mg (0.187 mmol, 0.75 eq.) of DMAP was added and the solution was stirred at room temperature overnight. Precipitated urea was removed by filtration and the solvent was removed under reduced pressure. The polymer was obtained via dialysis of the solution initially in MeOH/THF (1:1) and subsequently in water over 2 days.

^{1}H NMR ($CDCl_3$) δ/ppm 1.25 (t, 3 H), 3.31 (s, 3H), 3.45-3.65 (m, 200 H), 3.68 (t, 2H), 4.19 (q, 2H), 4.27 (t, 1H), 6.80 (d, 2H).

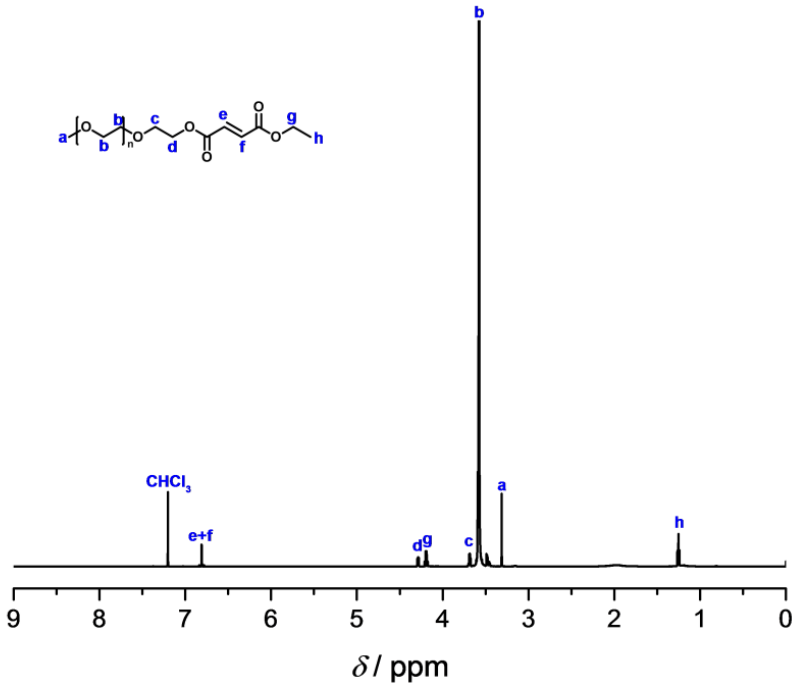

Figure S6: *^{1}H NMR spectrum of the fumarate terminated PEG in $CDCl_3$.*

Imine formation of *o*-methyl benzaldehyde yielding 3

20.0 mg (0.070 mmol, 1.0 eq.) of *o*-methyl benzaldehyde **1** and 7.7 μL (7.83 mg, 0.077 mmol, 1.1 eq.) of hexylamine **2** were stirred in 2 mL dry acetonitrile at room temperature for 20 min.

^{1}H NMR ($CDCl_3$) δ/ppm 0.81 (t, 3H), 1.16-1.38 (m, 6H), 1.63 (p, 2H), 2.43 (s, 3H), 3.56 (t, 2H), 3.85 (s, 3H), 5.08 (s, 2H), 6.68 (d, 1H), 6.78 (d, 1H), 7.11 (t, 1H), 7.41 (d, 2H), 7.99 (d, 2H), 8.63 (s, 1H).

Evidencing the versatility of hexylamine as a protection group for photoreactions including *o*-methyl benzaldehyde

I) 4.0 mg (1.4 μmol, 1 eq.) of the *o*-methyl benzaldehyde terminated PEG **4** and 0.5 mg (5.1 μmol, 3.6 eq.) of the hexylamine **2** were dissolved in 0.3 mL deuterated acetonitrile. The solution was left for 24 h.

II) 0.5 mg (5.5 μmol, 3.8 eq.) of the ethyl maleimide **8** was added to the previous solution (I). The solution was deoxygenated by purging the vial with argon for 5 min and irradiated subsequently for 30 min at λ_{max} = 365 nm. The inhibition of the light triggered Diels-Alder reaction due to the imine protection group was depicted by an *in-situ* ^{1}H NMR measurement.

III) 4.4 mg (222.0 μmol, 155.0 eq.) of D_2O and 2.1 mg (35.0 μmol, 24.5 eq.) of acetic acid was added to the previous solution (II). The solution was left for 5 min.
IV) The solution was deoxygenated by purging the vials with argon for 5 min and irradiated subsequently for 60 min at $\boldsymbol{\lambda}_{max}$ = 365 nm. The *in-situ* light triggered Diels-Alder product **9** was analysed via ^{1}H NMR measurement.

Determination of the kinetic data

The single charged range in the mass spectra was used for the kinetic study. Hereby, the absolute intensities of the first peak of the isotopic pattern regarding all product signals were determined. The absolute intensities of all polymers having the same repeating units in the m/z area of 2150 to 2600 were compared with each other in order to calculate the relative percentage of the products. The standard deviation was determined by calculating the average value of the repeating units n = 43, n = 44, n = 45, and n = 46.

Photoenol reaction kinetics

3.0 mg ($M_n \approx 2000$ g·mol^{-1}, 0.0015 mmol, 1.0 eq.) of the *o*-methyl benzaldehyde capped PEG **4** and 0.2 mg (0.0018 mmol, 1.2 eq.) of the ethyl maleimide **8** were dissolved in 1.5 mL DCM and the same amount of **4** and **8** was dissolved in 1.5 mL acetonitrile. Both samples were crimped air-tight in a headspace vial (Pyrex, diameter 20 mm) using SBR seals with PTFE inner liner. The solutions were deoxygenated by purging the vials with nitrogen for 5 min. The sample dissolved in DCM was irradiated for a) 45 s, b) 105 s, c) 180 s, d) 270 s, e) 360 s, and f) 450 s in the aforementioned photoreactor. The sample dissolved in acetonitrile was irradiated for a) 30 s, b) 60 s, c) 90 s, d) 120 s, e) 150 s, and f) 180s by revolving around a compact low-pressure fluorescent lamp (Cleo PL-L, Philips Deutschland GmbH) emitting at $\boldsymbol{\lambda}_{max}$ = 365 nm (±70 nm) with $I_{rel,max} = 1.1 \cdot 10^{13}$ mW·m^{-2}. After the irradiation procedure the samples were directly analysed via Orbitrap electrospray ionisation mass spectrometry (ESI-MS).

Imine formation reaction kinetics

3.00 mg ($M_n \approx 2000$ g·mol^{-1}, 0.0015 mmol, 1.0 eq.) of the *o*-methyl benzaldehyde capped PEG **4** and 0.7 μL (0.0054 mmol, 3.6 eq.) hexylamine **2** were dissolved in 1.5 mL DCM

and the same amount of **4** and **2** was dissolved in 1.5 mL acetonitrile. The samples dissolved in DCM and acetonitrile were stirred for a) 5 min, b) 10 min, c) 15 min, d) 20 min, e) 25 min, f) 30 min, g) 40 min, h) 50 min, i) 60 min, j) 80 min, and k) 90 min, respectively. The samples were directly analysed via Orbitrap electrospray ionisation mass spectrometry (ESI-MS) after all measurement points.

Switchable system in DCM (1.2 eq. ethyl maleimide)

3.00 mg (1.0 eq., 0.001 mol·L^{-1}) of the *o*-methyl benzaldehyde terminated PEG **4** and 0.23 mg (1.2 eq., 0.0012 mol·L^{-1}) of the ethyl maleimide **8** were dissolved in 1 mL dry DCM. The solution was deoxygenated by purging the vial with nitrogen for 5 min. A solution containing 0.71 μL (3.6 eq., 0.0036 mol·L^{-1}) of the hexylamine **2** in 0.5 mL dry DCM was deoxygenated following the same procedure and subsequently added to the first solution. Next, the combined solution was irradiated for 7 min.

Switchable system in DCM (2.4 eq. ethyl maleimide)

3.00 mg (1.0 eq., 0.001 mol·L^{-1}) of the *o*-methyl benzaldehyde terminated PEG **4** and 0.46 mg (2.4 eq., 0.0024 mol·L^{-1}) of the ethyl maleimide **8** were dissolved in 1 mL dry DCM. The solution was deoxygenated by purging the vial with nitrogen for 5 min. A solution containing 0.71 μL (3.6 eq., 0.0036 mol·L^{-1}) of the hexylamine **2** in 0.5 mL dry DCM was deoxygenated following the same procedure and subsequently added to the first solution. Next, the combined solution was irradiated for 7 min.

Block copolymer formation via the irradiation of a system containing 4, 10, and 2

3.0 mg (1.20 μmol, 1.00 eq.) of the *o*-methyl benzaldehyde terminated PEG **4** and 6.3 mg (1.26 μmol, 1.05 eq.) of the pNIPAAm-maleimide **10** were dissolved in 1.5 mL dry acetonitrile in a headspace vial (Pyrex, diameter 20 mm). The vial was crimped air-tight using SBR seals with PTFE inner liner and the solution was deoxygenated by purging the vial with nitrogen for 5 min. 0.23 mg (2.27 μmol, 1.89 eq.) of the hexylamine **2** was added subsequently. The flask was irradiated immediately for 1 h with three LEDs at λ_{max} = 375 nm. After the irradiation procedure, the solvent was evaporated under vacuum.

Block copolymer formation via the non-irradiative imine formation of a system containing 4, 10, and 2

3.0 mg (1.00 μmol, 1.20 eq.) of the benzaldehyde PEG **4**, 6.3 mg (1.26 μmol, 1.05 eq.) of the pNIPAAm-maleimide **10**, and 0.3 mg (2.86 μmol, 2.39 eq.) of the hexylamine **2** were dissolved in 1.5 mL dry acetonitrile in a headspace vial (Pyrex, diameter 20 mm). The vial was crimped air-tight using SBR seals with PTFE inner liner. The solution was stirred for 6 h at ambient temperature. Afterwards the solvent was evaporated under vacuum.

Block copolymer formation via the irradiation of a system containing 12, 13, and 14

6.0 mg (1.00 μmol, 1.00 eq.) of the *o*-methyl benzaldehyde terminated pL **12** and 2.2 mg (1.02 μmol, 1.02 eq.) of the PEG-fumarate **14** were dissolved in 1 mL dry acetonitrile in a headspace vial (Pyrex, diameter 20 mm). The vial was crimped air-tight using SBR seals with PTFE inner liner and the solution was deoxygenated by purging the vial with nitrogen for 5 min. 5.1 mg (1.02 μmol, 1.02 eq.) of the pL-amine **13** in 0.5 mL dry acetonitrile was added subsequently The flask was irradiated immediately for 1 h with three high power LEDs at λ_{max} = 375 nm. After the irradiation procedure, the solvent was evaporated under vacuum.

Block copolymer formation via the non-irradiative imine formation of a system containing 12, 13, and 14

6.0 mg (1.00 μmol, 1.00 eq.) of the *o*-methyl benzaldehyde terminated pL **12**, 2.2 mg (1.02 μmol, 1.02 eq.) of the PEG-fumarate **14**, and 5.1 mg (1.02 μmol, 1.02 eq.) of the pL-amine **13** were dissolved in 1.5 mL dry acetonitrile in a headspace vial (Pyrex, diameter 20 mm). The vial was crimped air-tight using SBR seals with PTFE inner liner. The solution was stirred for 2 days at ambient temperature.

7.2. λ-Orthogonal Photoligation

7.2.1. Materials and Instrumentation

Materials

Acrylic acid (99%, Sigma Aldrich), acetone (ACS grade, VWR), acetonitrile (99.9%, Fisher Scientific), aluminium chloride (99%, Acros),aniline (99%, Sigma Aldrich), 2-bromoisobutyryl bromide (98%, Sigma Aldrich), copper(I) chloride (99.99%, Sigma-Aldrich), copper sulfate pentahydrate (98%, Acros), 18-crown-6 (99%, Acros), dichloromethane (DCM, HPLC grade, Acros), dichloromethane (DCM, 99.8%, extra dry, Acros), diethyl ether (99%, VWR), 1-(3-dimethylaminopropyl)-3-ethylcarbodiimide hydrochloride (EDC·HCl, 98+%, Acros), 4-dimethylaminopyridine (DMAP, 99%, abcr), N,N-dimethylformamide (DMF, 99.8%, anhydrous), 2,3-dimethylanisole (97%, Sigma-Aldrich), 3,6-dimethyl-1,4-dioxane-2,5-dione (lactide, 99%, Acros), ethanol (99.8%, VWR), ethanolamine (≥ 99.5%, Sigma Aldrich), ethyl acetate (99.5%, VWR), 4-formyl benzoic acid (96%, Acros), fluorescein diacetate 5-maleimide (Sigma Aldrich), furan (98%, Sigma-Aldrich), hexylamine (98%, Merck), hydrochloric acid (37%, Roth), magnesium sulfate (≥ 99%, Roth), maleic anhydride (≥ 99%, Sigma Aldrich), maleimide (98+%, VWR), methanol (99.9%, VWR), methyl acrylate (99%, Sigma Aldrich),), methyl 4-(bromomethyl)benzoate (97%, TCI), N,N'-dicyclohexylcarbodiimide (DCC, 99%, Acros), n-hexane (99%, VWR), N,N,N',N',N''-pentamethyldiethylenetriamine (PMDTA, 99+ %, Acros), o-(2-azidoethyl)nonadecaetyhlene glycol (HO-PEG_{19}-N_3, ≥ 95%, Sigma Aldrich), petroleum ether (ACS reagent, Sigma-Aldrich), poly (ethylene glycol) methyl ether (PEG, $M_n \approx$ 2000 g·mol^{-1}, Sigma Aldrich), poly (L-lactide) N-2-hydroxyethylmaleimide terminated (pL, $M_n \approx$ 8000 g·mol^{-1}, Sigma Aldrich), potassium carbonate (99%, Alfa Aesar), propargyl alcohol (99 %, abcr), *p*-toluenesulfonyl hydrazide (99%, Merck), pyridine (99%, Alfa Aesar), sodium nitrite (≥ 97%, Sigma-Aldrich), tetrahydrofuran (THF, 99.85%, extra dry, Acros), tin(II) 2-ethylhexanoate (~ 95%, Sigma Aldrich), toluene (99%, Alfa Aesar), toluene (HPLC grade, Sigma Aldrich), triethylamine (≥ 99%, Sigma Aldrich), tris(2-aminoethyl)amine (96%, Sigma-Aldrich) were used as received.

N-α-Fmoc protected amino acids (Fmoc-Gly-OH, Fmoc-L-Ile-OH, Fmoc-L-Leu-OH, Fmoc-L-Ala-OH, Fmoc-L-Phe-OH, Fmoc-L-Met-OH, Fmoc-L-Ser(tBu)-OH, Fmoc-L-Glu(tBu)-OH, Fmoc-L-Lys(tBoc)-OH, Fmoc-L-His(tBoc)-OH), 2-(1H-benzotriazole-1-yl)-1,1,3,3-tertamethyluroniumhexafluorophosphate (HBTU) and TentaGel Rink-amide SRAM poly(styrene)resin (loading: 0.24 $mmol \cdot g^{-1}$) were used as received from IRIS Biotech GmbH (Marktredwitz, Germany). Benzotriazol-1-yloxyl) tripyrrolidinophosphonium-hexa-fluorophosphate (PyBOP) were used as received from novabiochem, Merck KGaA (Darmstadt, Germany). Piperidine (99%, Alfa Aesar) and diisopropylethylamine (99.96%, DIPEA; IRIS Biotech) were distilled from KOH prior to use. Triethylsilane (TES; 98+ %, Alfa Aesar), and 1,2-ethanedithiol (EDT; 99+%, Sigma Aldrich) have been used as received. *N*-methyl-2-pyrrolidone (NMP, 99.9+ %, peptide synthesis grade, IRIS Biotech) was purified by filtration through a column (10*60 cm) filled with aluminium oxide and silica gel at a rate of 1 $mL \cdot min^{-1}$. Trifluoracetic acid (TFA; IRIS Biotech, peptide grade) was distilled prior to use. Dichloromethane (DCM, IRIS Biotech GmbH, peptide grade) was distilled from CaH_2 prior to use. Maleimidopropionic acid (MPA) was synthesised as described by Philp et al.[330]

The synthesis of 4-((2-formyl-3-methylphenoxy)methyl) benzoic acid (*o*-methyl benzaldehyde) is performed in four steps according to the appropriate literature procedures: step 1,[329] step 2,[184] step 3,[329] and step 4.[298] The synthesis of the *o*-methyl benzaldehyde terminated poly(ethylene glycol) is performed according to a literature procedure.[298] N-(2-Hydroxyethyl)maleimide is synthesised according to a literature procedure.[331]

NMR spectroscopy

^1H NMR spectroscopy was performed using a Bruker Ascend 400 at 400 MHz. All samples were dissolved in $CDCl_3$, deuterated dimethylsulfoxide (DMSO-d^6), or deuterated tetrahydrofuran (THF-d^8). The δ-scale is referenced to the internal standard trimethylsilane (TMS, δ = 0.00 ppm).

Mass spectrometry

ESI-MS (Electrospray Ionization Mass Spectrometry) spectra of chapter 4.2 were recorded on a LXQ mass spectrometer (ThermoFisher Scientific) equipped with an atmospheric pressure ionization source operating in the nebulizer-assisted electrospray

mode. The instrument was calibrated in the m/z range of 195-1822 using a standard comprising caffeine, Met-Arg-Phe-Ala acetate (MRFA), and a mixture of fluorinated phosphazenes (Ultramark 1621, all Aldrich). A constant spray voltage of 4.5 kV, a dimensionless sweep gas flow rate of 2 and a dimensionless sheath gas flow rate of 12 were applied. The capillary voltage, the tube lense offset voltage, and the capillary temperature were set to 60 V, 110 V, and 300°C, respectively.

ESI-MS (Electrospray Ionization Mass Spectrometry) spectra of chapter 4.3 were recorded on a Q Exactive (Orbitrap) mass spectrometer (ThermoFisher Scientific, San Jose, CA, USA) equipped with an HESI II probe. The instrument was calibrated in the m/z range of 74-1822 using a premixed standard comprising caffeine, Met-Arg-Phe-Ala acetate (MRFA), and a mixture of fluorinated phosphazenes (Ultramark 1621). A constant spray voltage of 4.6 kV and a dimensionless sweep gas flow rate of 5 were applied. The capillary temperature and the S-lens RF level were set to 320°C an 62.0, respectively. The samples were dissolved with a concentration of 0.05 mg·mL^{-1} in a mixture of THF and MeOH (3:2) containing 100 μmol sodium trifluoracetate (NaTFA). The samples were infused with a flow of 5 μL·min^{-1}.

Gel Permeation Chromatography

Gel Permeation Chromatography (GPC) measurements were performed on a Polymer Laboratories (Varian) PL-GPC 50 Plus Integrated System, comprising an autosampler, a PLgel 5 mm bead-size guard column (50 x 7.5 mm), one PLgel 5mm Mixed E column (300 x 7.5 mm), three PLgel 5mm Mixed C columns (300 x 7.5 mm) and a differential refractive index detector using THF as the eluent at 35 °C with a flow rate of 1 mL·min^{-1}. The present GPC system was calibrated using linear poly(styrene) standards ranging from 476 to 2.5·10^{6} g mol^{-1} and linear poly(methyl methacrylate) standards ranging from 700 to 2·10^{6} g mol^{-1}. The molar mass distributions were determined by universal calibration using Mark-Houwink parameters for polystyrene (K = 14.1·10^{-5} dL·g^{-1}, α = 0.7).

UV/vis spectroscopy

UV/vis spectra were recorded on a Varian Cary 300 Bio spectrophotometer.

Irradiation

The samples to be irradiated were placed on a metallic disc revolving in a custom-built photoreactor around a light source (refer to Figure S1, chapter 7.1.1). The utilised light sources are a compact low-pressure fluorescent lamp (Cleo PL-L, Philips Deutschland GmBH) emitting at λ_{max} = 365 nm (± 50 nm, 36 W) at a distance of 40-50 mm or a compact low-pressure fluorescent lamp (Arimed B6, Cosmedico GmbH) emitting at λ_{max} = 315 nm (± 60 nm, 36 W) at a distance of 40-50 mm in the custom-built photoreactor. No bandpass filter was used for the irradiations with the PL-L lamp and the Arimed B6 lamp.

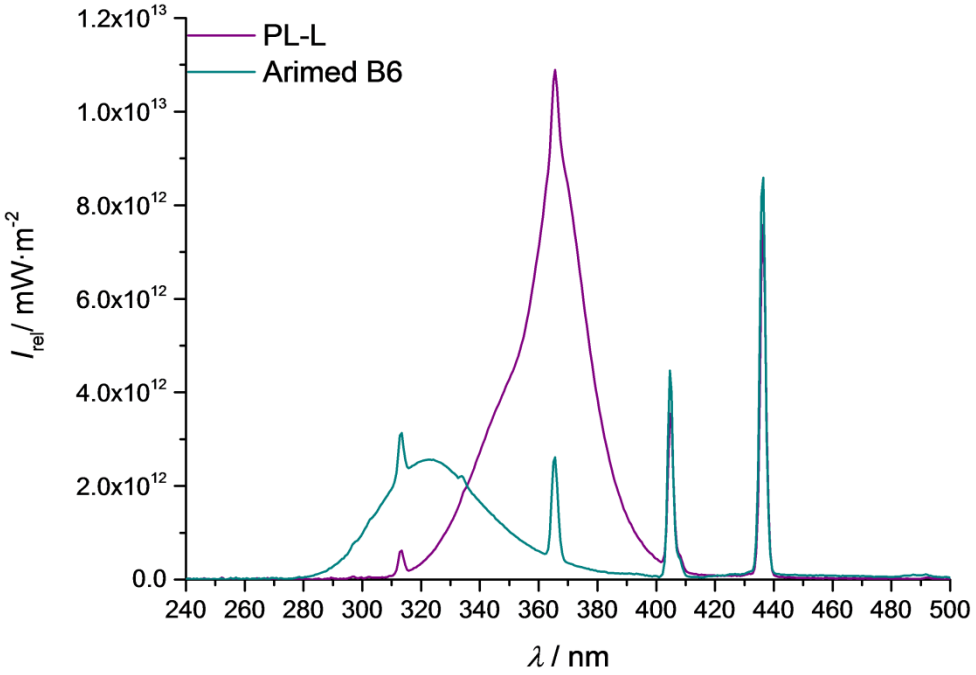

Figure S7: *Emission spectra of the previously employed compact low-pressure fluorescent lamps PL-L (36 W, λ_{max} = 365 nm) and Arimed B6 (36 W, λ_{max} = 315 nm). The emission spectra were recorded with a UV sensor (Opsytec Dr. Gröbel GmbH; Ettlingen, Germany). Reproduced with permission from the Royal Society of Chemistry (RSC).*

7.2.2. Syntheses

Diphenyl tetrazole

Step 1: 1.50 g (10.0 mmol, 1 eq.) of 4-formyl benzoic acid and 1.86 g (10.0 mmol, 1 eq.) of *p*-toluenesulfonyl hydrazide are dissolved in 25 mL ethanol. The solution was subsequently heated under reflux for 4 h. The obtained product was precipitated in water. 3.02 g (9.5 mmol, 95 %) of a yellow solid was obtained. The compound was used in the subsequent reaction without any further purification (yield: 95 %).

Step 2: 0.88 g (9.4 mmol, 1 eq.) of aniline was cooled to 0°C in a solution of 2.5 mL concentrated hydrochloric acid, 8 mL water and 8 mL ethanol. A cooled solution of 0.65 g (9.4 mmol, 1 eq.) of sodium nitrite in 4 mL water was added dropwise. The solution was stirred at 0°C for 10 min. The in-situ generated diazonium salt was added dropwise to the dissolved product of step 1 in 50 mL pyridine. After the complete addition, the solution was stirred overnight at ambient temperature. The diphenyl tetrazole was precipitated in water from the turbid red coloured solution and washed with water (yield: 80 %).

^{1}H NMR (DMSO-d^6) δ/ppm 7.65 (t, 1H), 7.72 (t, 2H), 8.18 (t, 4H), 8.31 (d, 2H), 13.25 (s, 1H).

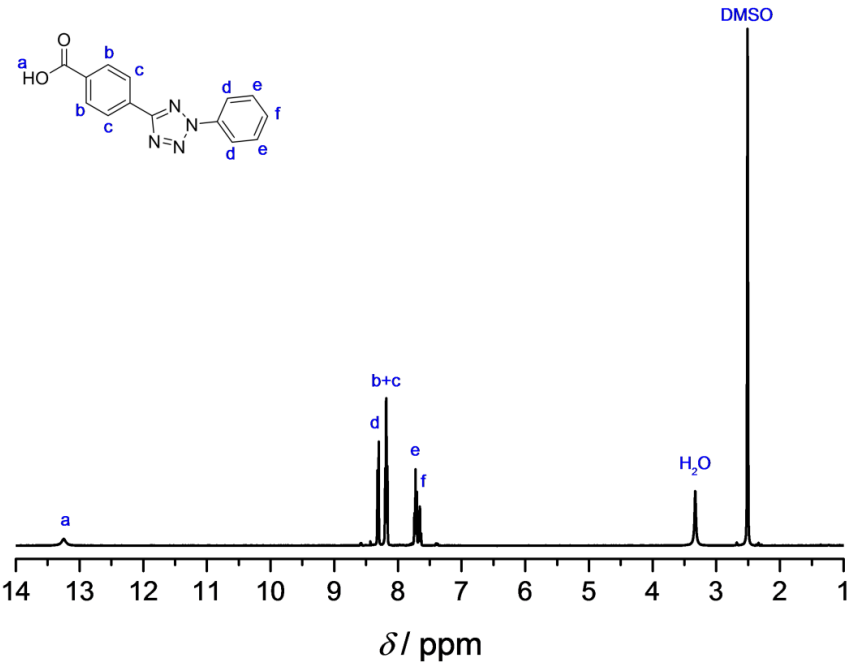

Figure S8: *^{1}H NMR spectrum of diphenyl tetrazole in DMSO-d^6.*

Diphenyl tetrazole terminated PEG 17

293 mg (1.1 mmol, 4.0 eq.) of the diphenyl tetrazole, 585 mg of the poly(ethylene glycol) methyl ether ($M_n \approx 2000$ g·mol^{-1}, 0.29 mmol, 1.0 eq.), and 120 mg (0.58 mmol, 2.0 eq.) of DCC were dissolved in a mixture of 10 mL dry DCM and 1 mL of DMF. 27 mg (0.22 mmol, 0.75 eq.) of DMAP was added and the solution was stirred overnight. Precipitated urea was removed by filtration and the solvent was removed under reduced pressure. The obtained polymer was dissolved in THF and purified by a two-fold precipitation in diethyl ether.

Propargyl tetrazolate

200 mg (0.75 mmol, 1 eq.) of the diphenyl tetrazole, 421.1 mg (7.51 mmol, 10 eq.) of propargyl alcohol, and 288.0 mg (1.50 mmol, 2 eq.) of EDC·HCl were dissolved in 10 mL dry THF. 68.8 mg (0.56 mmol, 0.75 eq.) of DMAP was added and the solution was stirred overnight. Precipitated urea was filtered off and the product was precipitated in water (yield: 97 %).

^{1}H NMR (THF-d^8) δ/ppm 2.93 (t, 1H), 4.86 (t, 2H), 7.44 (t, 1H), 7.52 (t, 2H), 8.11 (m, 4H), 8.25 (d, 2H).

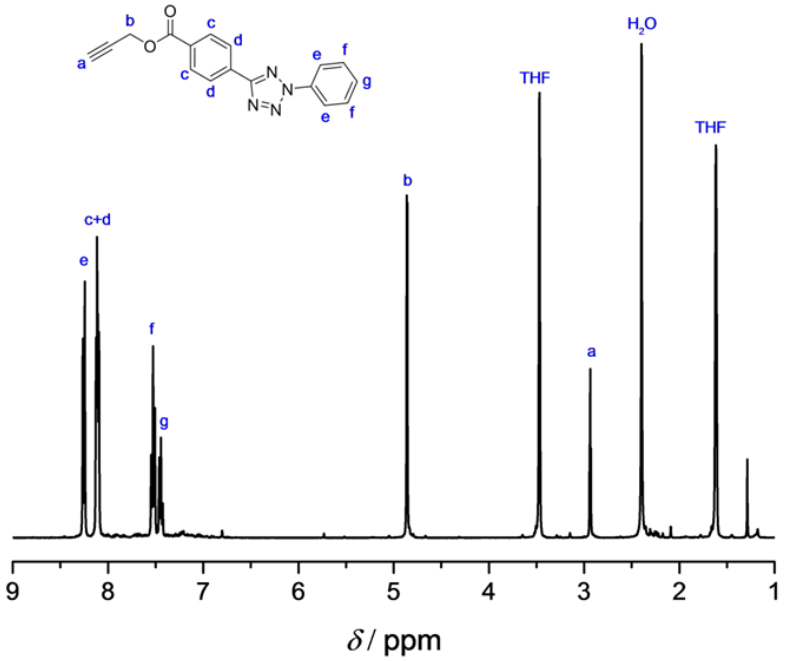

Figure S9: *^{1}H NMR spectrum of propargyl tetrazole in THF-d^8.*

α,ω-Functional bilinker 19

Step 1: 100 mg (0.11 mmol, 1.0 eq.) of O-(2-azidoethyl)nonadecaetyhlene glycol and 32.9 mg (0.11 mmol, 1.0 eq.) of the propargyl tetrazole were dissolved in 3 mL dry THF. In a seperate flask, 37.5 mg (0.22 mmol, 2.0 eq.) of N,N,N',N''-pentamethyldiethylenetriamine (PMDETA), and 24.1 mg (0.24 mmol, 2.25 eq.) of CuCl were dissolved in 1 mL dry THF and purged with N_2. The mixture was subsequently transferred into the O-(2-azidoethyl)nonadecaetyhlene glycol containing solution and stirred at ambient temperature for 24 h. After the reaction, the solution was passed through a column of neutral alumina and washed with a mixture of DCM and methanol (1:1). The resulting solution was dried under vacuum. The resulting solid was washed with n-hexane and was subsequently dried (yield: 98 %).
^{1}H NMR ($CDCl_3$) δ/ppm 3.50-3.65 (m, 74H), 3.65 (m, 2H), 3.82 (t, 2H), 4.28 (t, 1H), 4.50 (t, 2H), 5.44 (s, 2H), 7.46 (m, 1H), 7.53 (m, 2H), 7.86 (s, 1H), 8.11-8.18 (m, 4H), 8.26 (d, 2H).

Step 2: 50.0 mg (40.70 μmol, 1.0 eq.) of the obtained product from step 1, 22.0 mg (81.40 μmol, 2.0 eq.) of 4-((2-formyl-3-methylphenoxy)methyl) benzoic acid (*o*-methyl benzaldehyde), and 23.4 mg (0.12 mmol, 3.0 eq.) of EDC·HCl were dissolved in 4 mL dry THF. 3.7 mg (30.52 μmol, 0.75 eq.) DMAP was added and the solution was stirred for 3 days. Precipitated urea was filtered off and the product was dried under vacuum. The remaining solid was passed through a column of neutral alumina, washed with a mixture of DCM and methanol (1:1) and dried under vacuum (yield: 60 %).
^{1}H NMR ($CDCl_3$) δ/ppm 2.52 (s, 3H), 3.35-3.70 (m, 72H), 3.67 (t, 2 H), 3.77 (t, 2H), 3.83 (t, 2H), 4.41 (t, 2H), 4.50 (t, 2H), 5.16 (s, 2H), 5.45 (s, 2H), 6.76-6.83 (m, 1H), 7.26-7.33 (m, 1H), 7.39-7.57 (m, 6H), 7.86 (s, 1H), 7.99-8.07 (m, 2H), 8.11-8.17 (m, 4H), 8.26 (d, 2H), 10.68 (s, 1H).
^{13}C NMR ($CDCl_3$) δ/ppm 20.46 (CH_3), 49.35 (CH_2), 57.33 (CH_2), 63.23 (CH_2), 68.28 (CH_2), 68.91 (CH_2), 69.54 (CH_2), 109.31 ($CH_{arom.}$), 113.91 ($CH_{arom.}$), 122.65 ($C_{tert.}$), 123.68 ($CH_{arom.}$), 125.87 ($CH_{arom.}$), 128.74 ($C_{tert.}$), 129.11 ($CH_{arom.}$), 129.38 ($CH_{arom.}$), 130.52 ($C_{tert.}$), 133.40 ($C_{tert.}$), 135.71 ($C_{tert.}$), 141.27 ($CH_{arom.}$), 141.46 ($C_{tert.}$), 160.88 ($C_{tert.}$), 163.26 ($C_{tert.}$), 165.12 (COO), 199.98 (CHO).

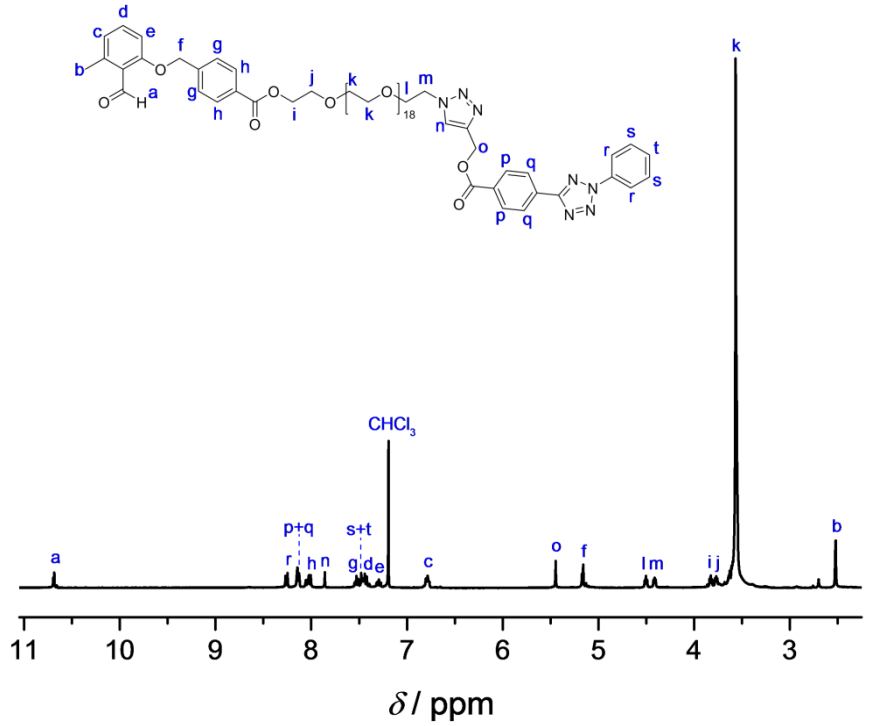

Figure S10: *^{1}H NMR spectrum of the α,ω-functional bilinker in $CDCl_3$.*

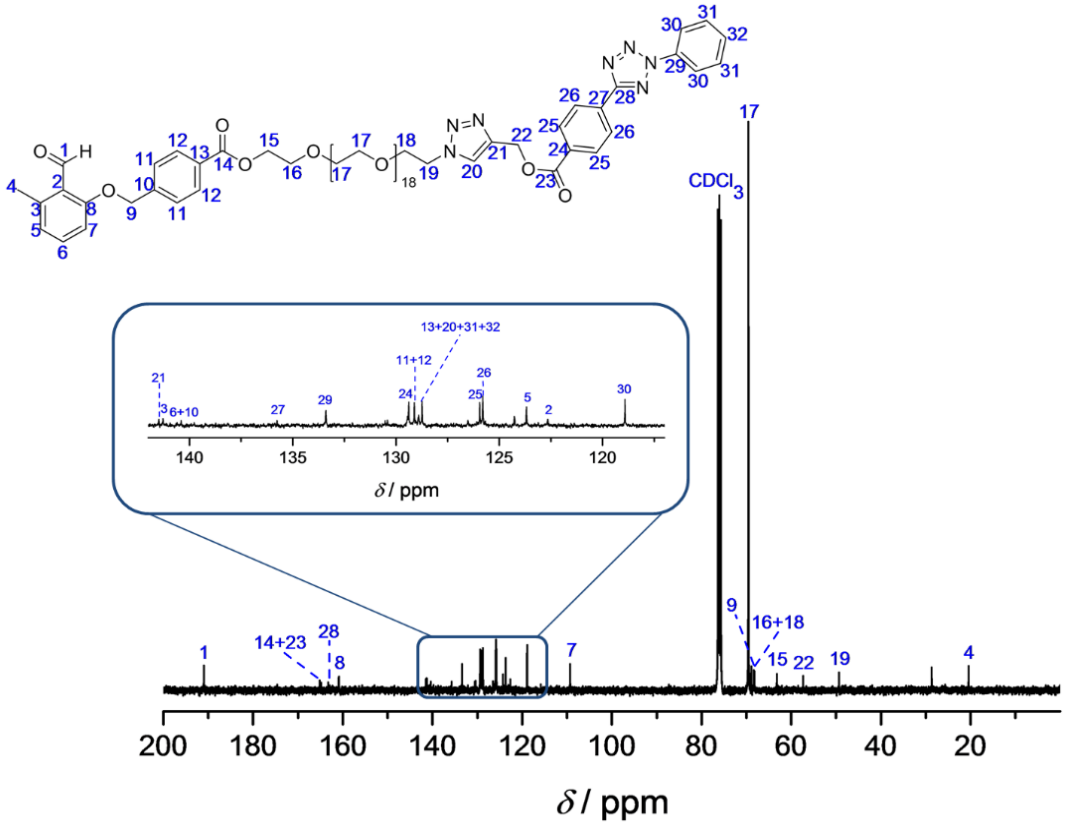

Figure S11: *^{13}C NMR spectrum of the α,ω-functional bilinker in $CDCl_3$.*

Maleimide terminated polylactide 25

50.0 mg (0.35 mmol, 0.04 eq.) of N-(2 hydroxethyl)maleimide and 1.28 g (8.86 μmol, 1.0 eq.) of lactide were dissolved in 2 mL dry toluene in an inert atmosphere (glove box). Tin(II) 2-ethylhexanoate dissolved in 2 mL dry toluene was added to the first solution. The combined solution was stirred at 100°C under argon atmosphere for approximately 5 h. Subsequently, the polymer was precipitated in cold n-hexane.

^{1}H NMR (Acetone-d^6) δ/ppm 1.34-1.50 (m, 294H), 3.59 (s, 1H), 3.65 (t, 2H), 4.12-4.28 (m, 2H), 4.96-5.16 (m, 97H), 6.77 (s, 2H).

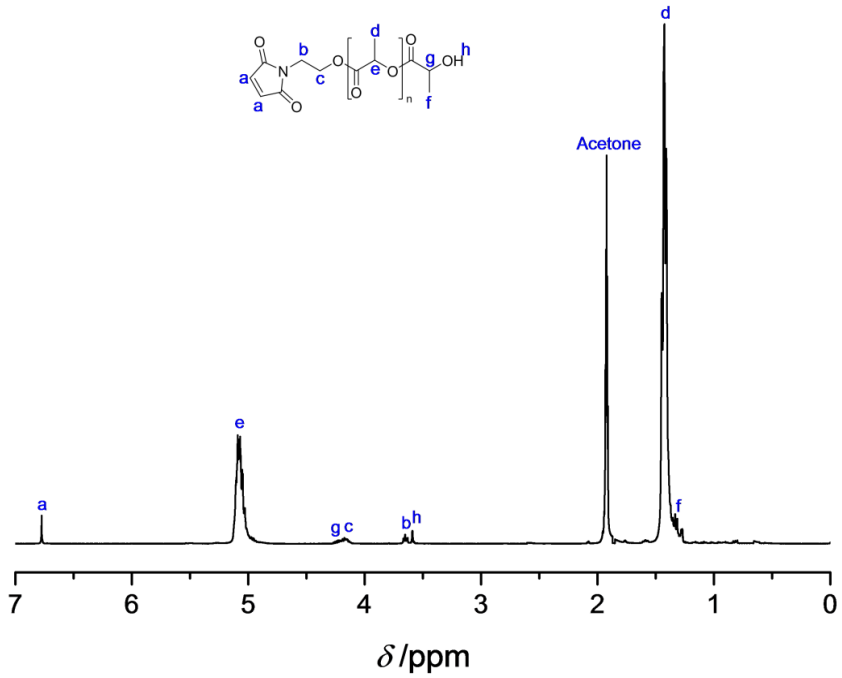

Figure S12: *^{1}H NMR spectrum of the maleimide terminated polylactide in acetone-d^6.*

Trifunctional maleimide 32

Step 1: 30.0 g (306 mmol, 1.0 eq.) of maleic anhydride was suspended in 150 mL toluene and the mixture was heated to 80 °C. 33.4 mL (459 mmol, 1.5 eq.) of furan was added and the turbid solution was stirred for 6 h. The mixture was subsequently cooled to ambient temperature. After 1 h, the resulting white crystals were collected by filtration and washed with 60 mL petroleum ether (yield: 87 %).

Step 2: 5.7 g (34 mmol, 5 eq.) of the product obtained in step 1 was dissolved in 150 mL methanol and the solution was cooled to 0 °C. A solution of 1.0 g (6.8 mmol, 1.0 eq.) tris(2-aminoethyl)amine in 50 mL methanol was added dropwise to the reaction mixture within 30 min. The solution was stirred at 0 °C for 5 min, 30 min at ambient

temperature and the solution was then refluxed for 4 h. After this time, the yellow solution was concentrated to ca. 75 mL and left to crystallize at 4 °C overnight. The obtained pale yellow crystals were filtered and washed with ethyl acetate. Residual solvent was evaporated under reduced pressure (yield: 24 %).

Step 3: 3.0 g (5.1 mmol, 1 eq.) of the product derived from step 2 was dissolved in 60 mL toluene and the solution was refluxed for 7 h. The solvent was removed subsequently under reduced pressure. The residual solid was dissolved in ethyl acetate and underwent flash chromatography (dichloromethane/ethyl acetate 60/40) (yield: 84 %). ^{1}H NMR ($CDCl_3$) δ/ppm 2.64 (t, 6H), 3.45 (t, 6H), 6.61 (s, 6H).

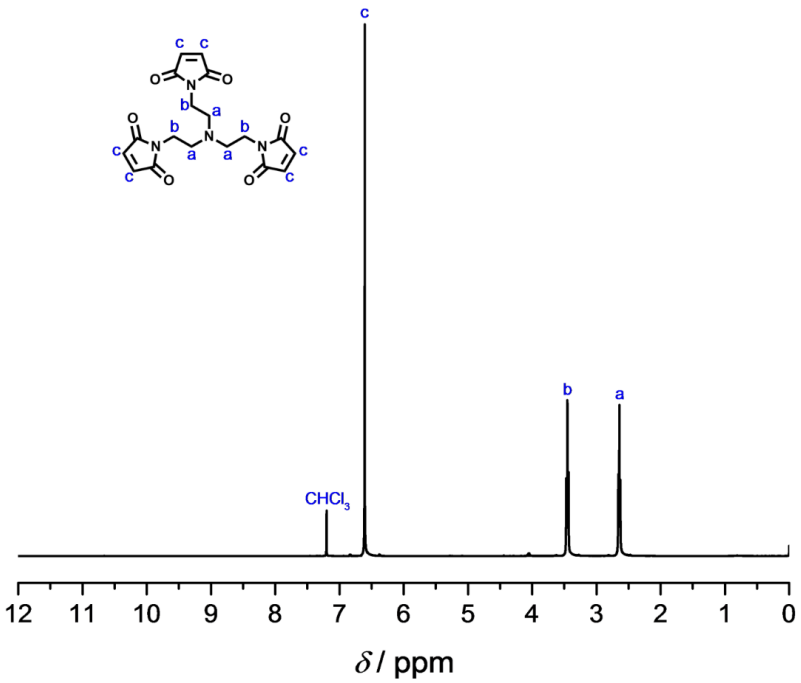

Figure S13: *^{1}H NMR spectrum of the trifunctional maleimide in $CDCl_3$.*

Determination of the kinetic data

The double-charged areas in the mass spectra of all samples were used for the kinetic study. Hereby, the relative intensities of all present polymers were determined by comparing the peak integrals of the polymers having the same repeating unit in the m/z area of 1040 to 1290. Since the signals of the *o*-methyl benzaldehyde terminated PEG **4** and the diphenyl tetrazole terminated PEG **17** overlapped in the double-charged mass spectrum region, the following assumptions were made:

1) For all samples with the repeating unit n at the irradiation time *t*, the combined integrals of **4** and **17** $I_{n,t}$(4+17) were set to the value 1. Within this integral, the value of **17** was considered to be constant over the irradiation time *t*.

2) The relative integrals of compound **4** $I_{n,t}^{rel}(4)$, compound **17** $I_{n,t}^{rel}(17)$, compound **7** $I_{n,t}^{rel}(7)$, and compound **18** $I_{n,t}^{rel}(18)$ were determined for every repeating unit n at the respective irradiation time *t* by the formula $I_{n,t}^{rel}(x) = \frac{I_{n,t}(x)}{I_{n,t}(4+17)}$.

3) The relative integrals $I_{n,t}^{rel}(x)$ with the same n values were standardised with regard to the ratio $I_{n,0}^{rel}(x) = \frac{I_{n,0}(x)}{I_{n,0}(4+17)}$.

4) Finally, an averaged value for all $I_{n,t}^{rel}(x)$ with the same t value was calculated resulting in intensity vs. time profiles.

Site-specific attachment maleimide to the α,ω-functional bilinker in a *λ*-orthogonal fashion

2.00 mg (1.35 μmol, 1.0 eq.) of the α,ω-functional bilinker **19**, and 0.33 mg (3.38 μmol, 2.5 eq.) of maleimide were dissolved in 8 mL DCM and aliquoted into 4 different headspace vials (2 mL in each one, Pyrex, diameter 20 mm), which were crimped air-tight using SBR seals with PTFE inner liner. The solutions were deoxygenated by purging the vials with nitrogen for 5 min. All flasks were irradiated for 15 min by revolving around the PL-L lamp emitting at λ_{max} = 365 nm yielding **20**. Two of the flasks were subsequently irradiated for 4 h by revolving around the Arimed B6 lamp emitting at λ_{max} = 315 nm leading to the formation of **21**. After the irradiation procedure, the solvent was evaporated under reduced pressure.

Site-specific attachment of fluorescein diacetate 5-maleimide and acrylic acid to the α,ω-functional bilinker in a *λ*-orthogonal fashion

2.00 mg (1.35 μmol, 1.0 eq.) of the α,ω-functional bilinker **19** and 0.35 mg (0.68 μmol, 1.1 eq.) of the fluorescein species **22** are dissolved in 1 mL DCM and are subsequently aliquoted into two headspace vials (2 mL in each one, Pyrex, diameter 20 mm), which are crimped air-tight using SBR seals with PTFE inner liner. The solutions are deoxygenated by purging the vials with nitrogen for 5 min. All flasks are irradiated for 20 min by revolving around the PL-L lamp emitting at λ_{max} = 365 nm leading to **23**. The

content of one flask is mixed with 0.72 mg (10.04 μmol, 20.0 eq.) of the acrylic acid and is subsequently irradiated for 4 h by revolving around the Arimed B6 lamp emitting at λ_{max} = 315 nm yielding **24**. After the irradiation procedure, the solvent was evaporated under reduced pressure.

Triblock copolymer formation via the site-specific attachment the maleimide terminated polylactide to the α,ω-functional bilinker in a -λ-orthogonal fashion

4.00 mg (2.70 μmol, 1.0 eq.) of the α,ω-functional bilinker **19** and 24.85 mg (6.21 μmol, 2.3 eq.) of the maleimide capped polylactide **25** were dissolved in 8 mL DCM and aliquoted into 4 different headspace vials (2 mL in each one, Pyrex, diameter 20 mm), which were crimped air-tight using SBR seals with PTFE inner liner. The solutions were deoxygenated by purging the vials with nitrogen for 5 min. All flasks were irradiated for 15 min by revolving around the PL-L lamp emitting at λ_{max} = 365 nm leading to the diblock polymer **26**. Two of the flasks were subsequently irradiated for 6 h by revolving around the Arimed B6 lamp emitting at λ_{max} = 315 nm leading to the triblock polymer **27**. After the irradiation procedure, the solvent was evaporated under reduced pressure.

Triblock copolymer formation via the site-specific attachment of the magainin maleimide and the maleimide terminated polylactide to the α,ω-functional bilinker in a -λ-orthogonal fashion

4.00 mg (2.70 μmol, 1.0 eq.) of the α,ω-functional bilinker **19** and 8.30 mg (3.24 μmol, 1.2 eq.) of the magainin maleimide **28** were dissolved in 4 mL dry DMF and aliquoted into two headspace vials (2 mL in each one, Pyrex, diameter 20 mm), which were crimped air-tight using SBR seals with PTFE inner liner. The solutions were deoxygenated by purging the vials with nitrogen for 5 min. All flasks were irradiated for 30 min by revolving around the PL-L lamp emitting at λ_{max} = 365 nm leading to the magainin-PEG diblock **29**. The content of one flask was mixed with 3.71 mg (3.24 μmol, 1.2 eq.) of the maleimide terminated polylactide **25** and subsequently irradiated for 6 h by revolving around the Arimed B6 lamp emitting at λ_{max} = 315 nm leading to the triblock polymer **31**. After the irradiation procedure, the solvent was evaporated under reduced pressure.

Photoenol centre attached star shaped precursor (diphenyl tetrazole terminated) 33

0.6 mg (1.5 μmol, 1 eq.) of the trifunctional maleimide **32** and 6.9 mg (4.7μmol, 3 eq.) of the α,ω-functional bilinker **19** were dissolved in 0.5 mL DCM and separated into two aliquots in headspace vials (0.25 mL in each one, Pyrex, diameter 7 mm). The vials containing the solution were crimped air-tight using SBR seals with PTFE inner line. The solutions were deoxygenated by purging the vials with nitrogen for 5 min. Both of the flasks were subsequently irradiated for 3 h by revolving around the PL-L lamp emitting at λ_{max} = 365 nm. After the irradiation, the solvent was evaporated under reduced pressure.

Photoenol centre attached star polymer 34

2.5 mg (0.5 μmol, 1 eq.) of the diphenyl tetrazole terminated star shaped precursor **33** and 8.1 mg (1.5 μmol, 3 eq.) of the pL-maleimide **30** were dissolved in 1.0 mL DCM and separated into two aliquots in headspace vials (0.5 mL in each one, Pyrex, diameter 7 mm). The vials containing the solution were crimped air-tight using SBR seals with PTFE inner line. The solutions were deoxygenated by purging the vials with nitrogen for 5 min. Both of the flasks were subsequently irradiated for 13 h by revolving around the Arimed B6 lamp emitting at λ_{max} = 315 nm. After the irradiation, the solvent was evaporated under reduced pressure.

Telechelic bilinker imine 35

10.0 g (6.8 μmol, 1 eq.) of the α,ω-functional polymer **19** and 2.49 μL (18.9 mmol, 2.8 eq.) of hexylamine **2** were dissolved in 1.5 mL dry THF. The solution was stirred for 3 h at ambient temperature (yield: 99 %).

^{1}H NMR ($CDCl_3$) δ/ppm 0.81 (t, 2H), 1.14-1.38 (m, 6H), 1.63 (p, 2H), 2.43 (s, 3H), 3.35-3.70 (m, 74H), 3.77 (t, 2H), 3.83 (t, 2H), 4.41 (t, 2H), 4.50 (t, 2H), 5.08 (s, 2H), 5.44 (s, 2H), 6.68 (d, 1H), 6.78 (d, ^{3}J = 7.6 Hz, 1H), 7.09 (t, 1H), 7.37-7.56 (m, 6H), 7.86 (s, 1H), 7.99 (d, 2H), 8.11-8.17 (m, 4H), 8.26 (d, 2H), 8.63 (s, 1H).

Tetrazole centre attached star shaped precursor (imine terminated) 36

0.5 mg (1.3 μmol, 1 eq.) of the trifunctional maleimide **32** and 6.1 mg (3.9 μmol, 3 eq.) of the telechelic bilinker **35** were dissolved in 0.5 mL dry DCM and separated into two aliquots in headspace vials (0.25 mL in each one, Pyrex, diameter 7 mm). The vials containing the solution were crimped air-tight using SBR seals with PTFE inner line. The solutions were then deoxygenated by purging the vials with nitrogen for 5 min. Both of the flasks were subsequently irradiated for 13 h by revolving around the Arimed B6 lamp emitting at λ_{max} = 315 nm. After the irradiation, the solvent was evaporated under reduced pressure.

Tetrazole centre attached star shaped precursor (*o*-methyl benzaldehyde terminated) 37

6.6 mg (4.2 μmol, 1 eq.) of **36** was dissolved in 2 mL THF containing wet molecular sieves (3 Å). The solution was left overnight at ambient temperature. After the imine deprotection, the molecular sieve was removed and the solvent was subsequently evaporated under reduced pressure.

Tetrazole centre attached star polymer 39

4.5 mg (0.9 μmol, 1 eq.) of the *o*-methyl benzaldehyde terminated star shaped precursor **37** and 6.5 mg (2.8 μmol, 3 eq.) of PEG-maleimide **38** were dissolved in 1.0 mL DCM and separated into two aliquots in headspace vials (0.5 mL in each one, Pyrex, diameter 7 mm). The vials containing the solution were crimped air-tight using SBR seals with PTFE inner line. The solutions were deoxygenated by purging the vials with nitrogen for 5 min. Both of the flasks were subsequently irradiated for 3 h by revolving around the PL-L lamp emitting at λ_{max} = 365 nm. After the irradiation, the solvent was evaporated under reduced pressure.

7.3. Selective Design of Networks and 3D-Structures

7.3.1. Materials and Instrumentation

Materials

Acetone (ACS grade, VWR), aluminium chloride (99%, Acros), aniline (99%, Sigma Aldrich), 1,4-bis(bromomethyl)benzene (99%, Sigma Aldrich), 2,2'-bipyridine (99%, Sigma Aldrich), 2-bromoisobutyryl bromide (98%, Sigma Aldrich), 4-(bromomethyl)benzoic acid (97%, Sigma Aldrich), carbon disulfide (99%, anhydrous, Sigma Aldrich), copper (II) bromide (99%, Sigma Aldrich), copper(I) chloride (99.99%, Sigma-Aldrich), copper sulfate pentahydrate (98%, Acros), 18-crown-6 (99%, Acros), cyclohexane (ACS grade, VWR), 4-dimethylaminopyridine (DMAP, 99%, abcr), N,N-dimethylformamide (DMF, 99.8%, anhydrous), 2,3-dimethylanisole (97%, Sigma-Aldrich), ethanol (99.8%, VWR), ethyl acetate (99.5%, VWR), ethylene glycol (99.8%, Sigma Aldrich), 4-formyl benzoic acid (96%, Acros), hydrochloric acid (37%, Roth), maleic anhydride (≥ 99%, Sigma Aldrich), methanol (99.9%, VWR), methyl 4-(bromomethyl)benzoate (97%, TCI), methyl 2-bromo-2-methylpropionate (99%, Sigma-Aldrich), N,N'-dicyclohexylcarbodiimide (DCC, 99%, Acros), pentaerythritol (96%, Sigma Aldrich), pentaerythritol tetrabromide (96%, Sigma Aldrich), pentaerythritol tetrakis(3-mercaptopropionate) (>95%, Sigma Aldrich), potassium carbonate (99%, Alfa Aesar), potassium phosphate (>98%, Sigma Aldrich), propargyl alcohol (99 %, abcr), *p*-toluenesulfonyl hydrazide (99%, Merck), pyridine (99%, Alfa Aesar), sodium azide (99%, Sigma Aldrich), sodium hydrogencarbonate (≥ 95%, Sigma-Aldrich), sodium nitrite (≥ 97%, Sigma-Aldrich), tetrahydrofuran (THF, 99.85%, extra dry, Acros), tin(II) 2-ethylhexanoate (~ 95%, Sigma Aldrich), triethylamine (≥ 99%, Sigma Aldrich), tris(2-aminoethyl)amine (96%, Sigma-Aldrich) were used as received.

2,2'-azobis(2-methylpropionitrile) (AIBN; 98%, Sigma Aldrich) was recrystallized twice from methanol and stored at -19°C. 4-vinylbenzyl chloride (90%, Sigma Aldrich) was distilled and stored at -19°C. 4-Bromostyrene (97%, Sigma Aldrich), 2-hydroxyethyl acrylate (HEA, 96%, Sigma Aldrich), 2-hydroxyethyl methacrylate (HEMA, 97%, Sigma

Aldrich), methyl acrylate (MA, 99%, Sigma Aldrich), methyl methacrylate (MMA, 99%, Sigma Aldrich) were passed through a column of basic alumina in order to remove inhibitor and subsequently stored at -19°C, respectively. The synthesis of 4-((2-formyl-3-methylphenoxy)methyl) benzoic acid (*o*-methyl benzaldehyde) was performed in four steps according to the appropriate literature procedures: step 1,[329] step 2,[184] step 3,[329] and step 4.[298] The synthesis of the pyrene functionalised tetrazole was performed according to the literature procedure.[210] The synthesis of the furan protected maleimide terminated ethyl methacrylate was performed according to the literature procedure.[334] The synthesis of the diphenyl tetrazole, the propargyl tetrazolate and the trifunctional maleimide were performed according to the procedure in chapter 7.2.2.

NMR spectroscopy

^{1}H NMR spectroscopy was performed using a Bruker Ascend 400 at 400 MHz. All samples were dissolved in $CDCl_3$, deuterated dimethylsulfoxide (DMSO-d^6), or deuterated tetrahydrofuran (THF-d^8). The δ-scale is referenced to the internal standard trimethylsilane (TMS, δ = 0.00 ppm).

Gel Permeation Chromatography

Gel Permeation Chromatography (GPC) measurements were performed on a Polymer Laboratories (Varian) PL-GPC 50 Plus Integrated System, comprising an autosampler, a PLgel 5 mm bead-size guard column (50 x 7.5 mm), one PLgel 5mm Mixed E column (300 x 7.5 mm), three PLgel 5mm Mixed C columns (300 x 7.5 mm) and a differential refractive index detector using THF as the eluent at 35 °C with a flow rate of 1 mL·min^{-1}. The present GPC system was calibrated using linear poly(styrene) standards ranging from 476 to 2.5·10^6 g mol^{-1} and linear poly(methyl methacrylate) standards ranging from 700 to 2·10^6 g mol^{-1}. The molar mass distributions were determined by universal calibration using Mark-Houwink parameters for polystyrene (K = 14.1·10^{-5} *d*L·g^{-1}, α = 0.7).

UV/vis spectroscopy

UV/vis spectra were recorded on a Varian Cary 300 Bio spectrophotometer.

X-ray photoelectron spectroscopy

X-ray photoelectron spectroscopy (XPS) investigations were performed on a K-Alpha spectrometer (Thermofisher Scientific, East Grinstead, UK) using a micro-focused, monochromated Al Kα X-ray source (400 μm pot size). The kinetic energy of the electron was measured by a 180° hemispherical energy analyser operated in the constant analyser energy mode (CAE) at 50 eV pass energy for elemental spectra. The photoelectrons were detected at an emission angle of 0° with respect to the normal of the sample surface. The K-Alpha charge compensation system was employed during analysis, using electrons of 8 eV energy and low-energy argon ions to prevent any localized charge build-up. The spectra were fitted with one or more Voigt profiles (BE uncertainty: ± 0.2 eV). The analyser transmission function, Scofield[332] sensitivity factors, and effective attenuation lengths (EALs) for photoelectrons were applied for quantification. EALs were calculated using the standard TPP-2 M formalism.[333] All spectra were referenced to the C 1s peak of hydrocarbon at 285.0 eV binding energy, controlled by means of the well-known photo-electron peaks of metallic Cu, Ag, and Au. Signals were divided by the maximum of the analysed peak without background subtraction.

Direct Laser Writing

3D polymer structures were fabricated on a home-made Direct Laser Writing (DLW) system by means of two-photon photopolymerisation. The system uses a Ti:Sa femtosecond laser source (Spectra-Physics MaiTai HP) which pumps an optical parametric oscillator (Spectra-Physics Inspire HF100) to generate femtosecond laser pulses with a selectable wavelength in the range of 540-700 nm. The laser beam is focused by an oil immersion objective lens with a magnification of 100x and a numerical aperture of 1.4 (Leica HCX PL APO 100x/1.4 CS). Relative 3D movement of sample and focal spot is realized by a 3D piezo stage. Standard microscopy cover slides were used as substrates. To remove excess photoresist after writing, the samples were developed in acetone for 15 min and rinsed with isopropanol.

Depletion experiments during the DLW processes

The home-built direct laser writing setup is based on a tunable Ti:sapphire oscillator (Coherent Chameleon Ultra II) delivering 150 fs pulses at a centre wavelength of 700nm. The depletion laser source is a cw laser-diode (Picoquant LDH) with an emission wavelength of 440 nm. The beam intensities are controlled by acousto-optical modulators (AA Optic-Electronic). The laser beams are focused through an oil immersion objective lens with an numerical aperture of 1.4 (Leica HCX PL APO 100x/1.4-0.7 OIL CS). The sample is held by a 3D piezo stage (Physik Instrumente) that allows for its relative translation with respect to the laser beam focus. An additional CCD camera is used for monitoring the writing process and sample alignment.

Irradiation

The samples to be irradiated were placed on a metallic disc revolving in a custom-built photoreactor around a light source (refer to Figure S1, chapter 7.1.1). The utilised light sources are a compact low-pressure fluorescent lamp (Arimed B6, Cosmedico GmbH) emitting at λ_{max} = 315 nm (± 60 nm, 36 W) at a distance of 40-50 mm in the custom-built photoreactor or three UV-A LEDs (Avonec Online-Handel, Germany) emitting at λ_{max} = 375 nm (± 30 nm, each 3 W) at a distance of 5 mm.

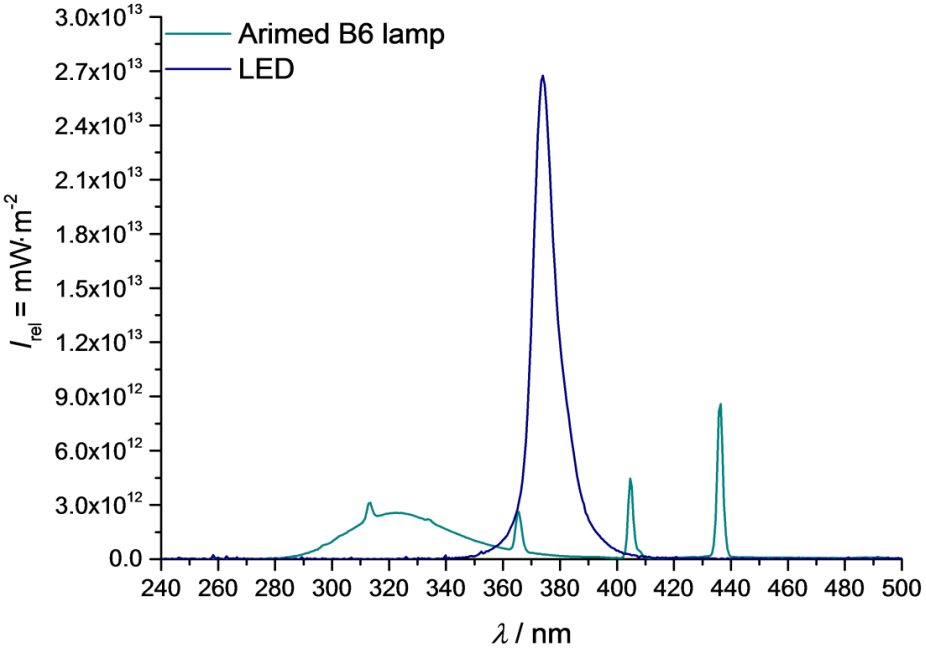

Figure S14: *Emission spectra of the previously employed compact low-pressure fluorescent lamp Arimed B6 (36 W, λ_{max} = 315 nm) and the high power LEDs (3 W, λ_{max} = 375 nm). The emission spectra were recorded with a UV sensor (Opsytec Dr. Gröbel GmbH; Ettlingen, Germany). The image was modified from ref.*[144] *with permission from the Royal Society of Chemistry (RSC), 2016.*

Fluorescence microscopy

Fluorescence micrographs of the three-dimensional DLW structures were recorded with a laser scanning microscope (Zeiss LSM 510 Meta) using a laser diode with an emission wavelength of λ = 405 nm as excitation source, an oil immersion objective lens with a magnification of 63x and a numerical aperture of 1.4.

7.3.2. Syntheses

Tetrafunctional RAFT agent with *o*-methyl benzaldehyde end groups

Step 1: 8.26 g (31.3 mmol, 3 eq.) of 1,4-bis(bromomethyl)benzene, 2.16 g (15.6 mmol, 1.5 eq.) of potassium carbonate, and 49 mg (0.2 mmol, 0.18 eq.) of 18-crown-6 were stirred in 100 mL of acetone at 40 °C. 1.41 g (10.4 mmol, 1 eq.) of 2-hydroxy-6-methylbenzaldeyhde (step 2 of the *o*-methyl benzaldehyde synthesis, refer to chapter 7.1.2) dissolved in 25 mL of acetone was added dropwise and the mixture was stirred at 40 °C over night. After filtration, the solvent was evaporated under reduced pressure. The solid was suspended in cold acetone, the residue was filtered off and washed with cold acetone. The solvent was again removed under reduced pressure and the crude product was purified via column chromatography (silica gel, cyclohexane/ethyl acetate 19:1) yielding a white solid (yield: 54 %).
^{1}H NMR ($CDCl_3$) δ/ppm 2.59 (s, 3H), 4.51 (s, 2H), 5.15 (s, 2H), 6.80 (m, 2H), 7.40 (m, 5H), 10.73 (s, 1H).

Step 2: 454 mg (0.9 mmol, 1 eq.) of pentaerythritol tetrakis(3-mercaptopropionate), 849 mg (11.1 mmol, 12 eq.) of carbon disulfide, and 1.19 g (5.6 mmol, 6 eq.) of potassium phosphate were stirred in 15 mL THF for 30 min. 1.78 g (5.6 mmol, 6 eq.) of the product of step 1 is added and the pale yellow liquid turned intensively yellow. After stirring at ambient temperature over night, the remaining potassium phosphate was filtered off and the solvent was removed under reduced pressure The crude product was purified via column chromatography (silica gel, cyclohexane/ethyl acetate 2:1) yielding a yellow solid (yield: 40 %).

^{1}H NMR ($CDCl_3$) δ/ppm 2.57 (s, 12H), 2.80 (t, 8H), 3.61 (t, 8H), 4.14 (s, 8H) 4.61 (s, 8H), 5.11 (s, 8H), 6.80 (m, 8H), 7.35 (m, 20H), 10.71 (s, 4H).

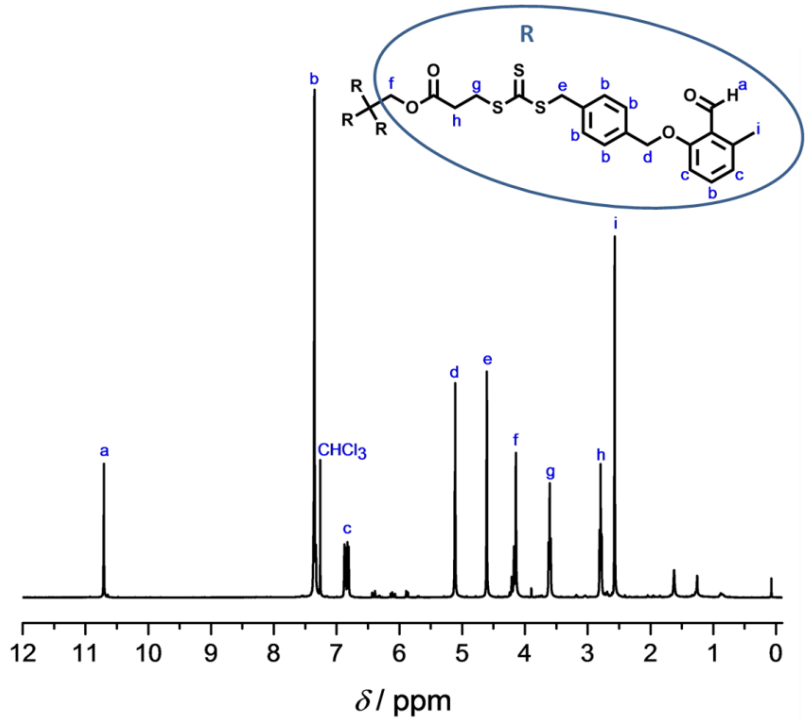

Figure S15: *^{1}H NMR spectrum of the tetrafunctional RAFT agent with o-methyl benzaldehyde end groups in $CDCl_3$.*

Polymerisation of 4-vinylbenzyl chloride with the tetrafunctional RAFT agent carrying *o*-methyl benzaldehyde end groups yielding 40

A solution of 7.6 mg (46 μmol, 0.4 eq.) of AIBN, 201.7 mg (115 μmol, 1.0 eq) of the tetrafunctional RAFT agent carrying *o*-methyl benzaldehyde end groups, and 1.41 g (9.2 mmol, 80 eq.) of 4-bromostyrene in 1.1 mL toluene was deoxygenated via three consecutive freeze-pump thaw cycles. Subsequently, the polymerisation was performed at 60 °C for 8 h. The polymer was isolated via precipitation in cold methanol and subsequent drying under reduced pressure yielding a yellow powder (M_n = 4400).

Tetrafunctional RAFT agent with diphenyl tetrazole end groups

Step 1: 3.0 g (14.0 mmol, 1 eq.) of 4-(bromomethyl) benzoic acid, 341 mg (2.8 mmol, 0.2 eq.) of DMAP, and 2.6 g (41.9 mmol, 3 eq.) of ethylene glycol are stirred in 50 mL dry THF. Subsequently, 3.17 g (15.4 mmol, 1.1 eq.) of DCC dissolved in 15 mL of dry THF was added dropwise. The reaction proceeded over night at ambient temperature. After

filtration, the solvent was removed under reduced pressure and the crude product was purified via column chromatography (silica gel, cyclohexane/ethyl acetate 1:1) yielding a white solid (yield: 66 %).

^{1}H NMR ($CDCl_3$) δ/ppm 3.95 (t, 2H), 4.46 (t, 2H), 4.49 (s, 2H), 7.45 (d, 2H), 8.02 (d, 2H).

Step 2: 526 mg (2.0 mmol, 1 eq.) of the product of step 1, 25 mg (0.2 mmol, 0.1 eq.) of DMAP, and 541 mg (2.0 mmol, 1 eq.) of the diphenyl tetrazole species were dissolved in 20 mL THF. Subsequently, 524 mg (2.5 mmol, 1.25 eq.) of DCC dissolved in 10 mL THF was added dropwise. The reaction proceeded over night at ambient temperature. After filtration, the solvent was removed under reduced pressure and the crude product was purified via column chromatography (silica gel, cyclohexane/ethyl acetate 4:1) yielding a slightly red solid (yield: 47 %).

^{1}H NMR ($CDCl_3$) δ/ppm 4.50 (s, 2H), 4.80 (s, 4H), 7.30-7.60 (m, 5H), 8.04 (d, 2H) 8.21 (d, 4H), 8.34 (d, 2H).

Step 3: 122.5 mg (0.25 mmol, 1 eq.) of pentaerythritol tetrakis(3-mercaptopropionate), 229.2 mg (3.0 mmol, 16 eq.) of carbon disulfide, and 319 mg (1.5 mmol, 8 eq.) of potassium phosphate were stirred in 10 mL THF for 30 min. 757 mg (1.5 mmol, 8 eq.) of the product of step 2 was added and the pale yellow liquid turned red. After stirring at ambient temperature over night, the remaining potassium phosphate was filtered off and the solvent was removed under reduced pressure The crude product was purified via column chromatography (silica gel, cyclohexane/ethyl acetate 3:1) yielding a slightly red solid (yield: 46 %).

^{1}H NMR ($CDCl_3$) δ/ppm 2.76 (m, 8H), 3.58 (m, 8H), 4.11 (s, 8H), 4.61 (m, 8H), 4.68 (s, 16H), 7.30-7.60 (m, 20H), 8.00 (m, 8H) 8.18 (m, 16H), 8.31 (m, 8H).

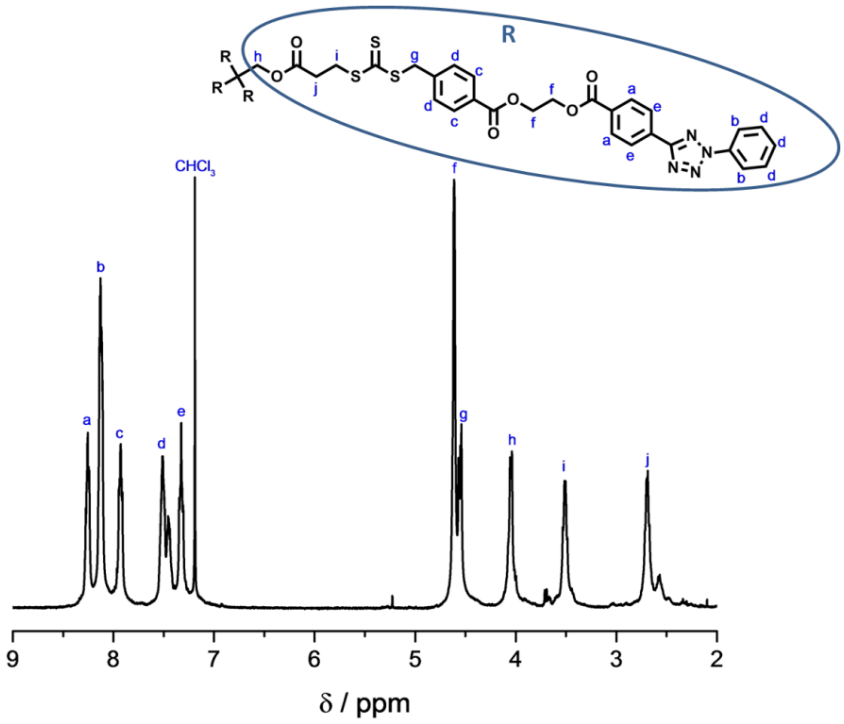

Figure S16: *^{1}H NMR spectrum of the tetrafunctional RAFT agent with diphenyl tetrazole end groups in $CDCl_3$.*

Polymerisation of 4-bromostyrene with the tetrafunctional RAFT agent carrying diphenyl tetrazole end groups yielding 41

A solution of 3.7 mg (23 μmol, 0.4 eq.) of AIBN, 140 mg (56 μmol, 1.0 eq) of the tetrafunctional RAFT agent carrying diphenyl tetrazole end groups, and 825 mg (4.5 mmol, 80 eq.) of 4-bromostyrene in 2.5 mL toluene was deoxygenated via three consecutive freeze-pump thaw cycles. Subsequently, the polymerisation was performed at 60 °C for 8 h. The polymer was isolated via precipitation in cold methanol and subsequent drying under reduced pressure yielding a yellow powder (M_n = 3800).

Pentaerythritol tetrakis(2-bromoisobutyrate)

41.0 g (178.5 mmol, 8.1 eq.) of 2-bromoisobutyryl bromide dissolved in 25 mL dry THF was added slowly to a solution containing 3.0 g (22.0 mmol, 1.0 eq.) of pentaerythritol and 17.6 g (174.4 mmol, 7.9 eq.) of triethylamine in 25 mL dry THF at 0 °C. The solution was stirred for 24 h at ambient temperature. Afterwards, the solution was transferred into 350 mL DCM and rinsed successively with hydrochloric acid (10 %), a solution of sodium hydrogencarbonate in water (5 %), and water. The organic phase was dried over magnesium sulfate and the solvent was removed under reduced pressure. The crude

product was dissolved in a small amount of DCM and recrystallized in methanol (yield: 80 %).

^{1}H NMR ($CDCl_3$) δ/ppm 1.87 (s, 24H), 4.26 (s, 8H).

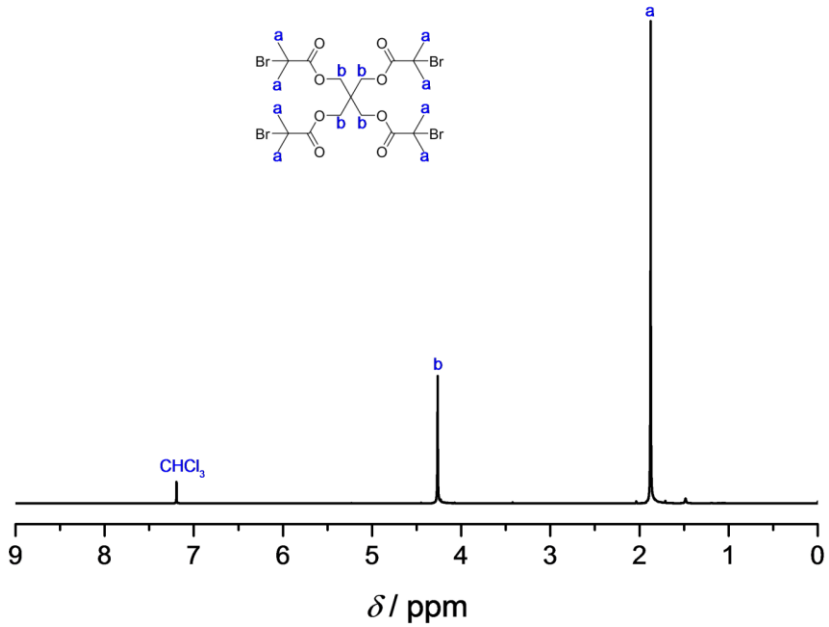

Figure S17: *^{1}H NMR spectrum of pentaerythritol tetrakis(2-bromoisobutyrate) in $CDCl_3$.*

Propargyl functionalised *o*-methyl benzaldehyde

1.0 g (3.7 mmol, 1 eq.) of *o*-methyl benzaldehyde acid, 2.1 g (37 mmol, 10 eq.) of propargyl alcohol, and 2.2 g (11.1 mmol, 3 eq.) of EDC·HCl were dissolved in 10 mL dry THF. 340 mg (2.8 mmol, 0.75 eq.) of DMAP was added and the solution was stirred overnight. Precipitated urea was filtered off and the product was precipitated in water (yield: 98 %).

^{1}H NMR ($CDCl_3$) δ/ppm 2.42 (s, 3H), 2.89 (s, 1H), 4.81 (d, 2H), 5.20 (s, 2H), 6.72 (d, 1H), 6.92 (d, 1H), 7.26 (t, 1H), 7.49 (d, 2H), 7.96 (d, 2H), 10.62 (s, 1H).

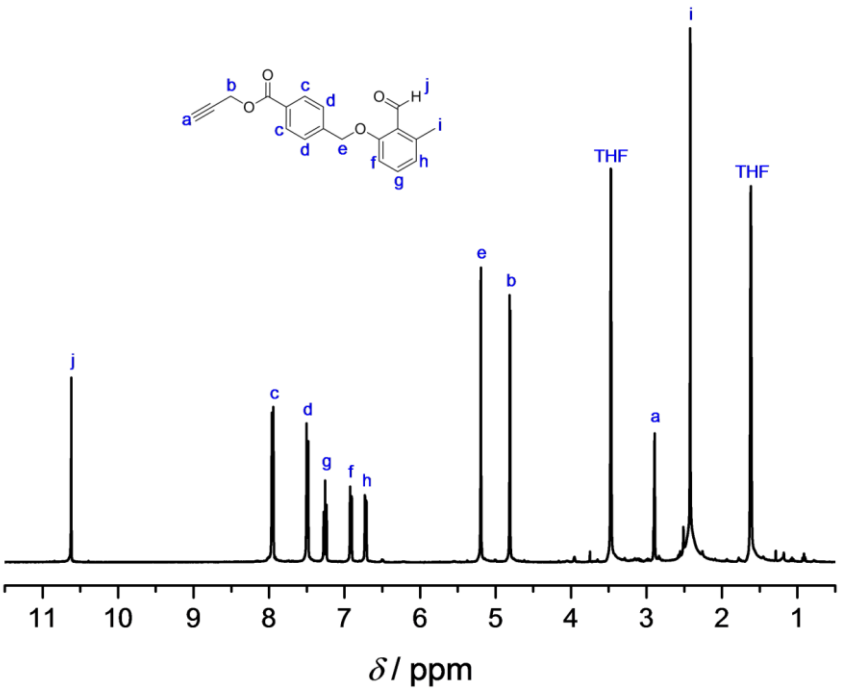

Figure S18: *^{1}H NMR spectrum of the propargyl functionalised o-methyl benzaldehyde in THF-d^{8}.*

o-Methyl benzaldehyde terminated pMMA star polymer 42

Step 1: 150.0 mg (418.7 μmol, 1 eq.) of pentaerythritol tetrakis(2-bromoisobutyrate), 9.4 mg (41.8 μmol, 0.1 eq) of copper(II) bromide, 32.7 mg (20.9 μmol, 0.5 eq) of 2,2'-bipyridine, and 3.27 g (23.0 mmol, 78 eq.) of MMA were dissolved in 6 mL dry DMF. The green solution was deoxygenated by performing three consecutive freeze-pump thaw cycles. Subsequently, 50.9 mg (125.6 μmol, 0.3 eq.) of tin(II) 2-ethylhexanoate was added on the surface of the freezed solution under a nitrogen atmosphere. After one additional freeze-pump thaw cycle, the polymerisation was performed at 60 °C for 30 min whereby the colour of the solution turned brown. After the polymerisation, the solution was cooled in an ice bath and quenched with oxygen. The solution was dialysed in a mixture of THF and methanol (1:1), followed by a dialysis in water yielding a white powder (M_n = 5900).

Step 2: 250.0 mg (42.5 μmol, 1 eq.) of the bromine terminated pMMA star polymer of step 1 and 220 mg (3.4 mmol, 80 eq.) of sodium azide were suspended in DMF and stirred over night. The polymer was purified via dialysis in water yielding a white powder (M_n = 5800).

Step 3: 200.0 mg (33 μmol, 1.0 eq.) of the azide terminated pMMA star polymer of step 2 and 45.2 mg (146 μmol, 4.4 eq.) of the propargyl functionalised *o*-methyl benzaldehyde

were purged with N_2. Subsequently, both compounds were dissolved in 5 mL dry THF. 46.2 mg (267 μmol, 8.0 eq.) of PMDETA and 29.7 mg (300 μmol, 9.0 eq.) copper(I) chloride were purged with N_2 in a seperate flask. The THF containing solution was transferred into the copper containing solution in the presence of a N_2 counterstream. The combined solution was stirred at ambient temperature for 24 h. Afterwards, the solution was dialysed in a mixture of THF and methanol (1:1), followed by a dialysis in water yielding a slightly yellow powder (M_n = 7000).

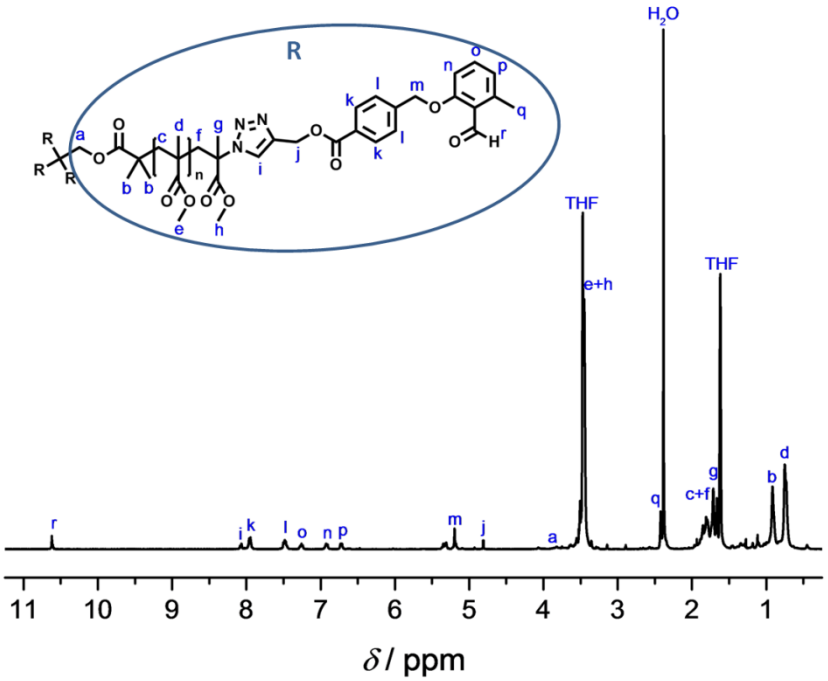

Figure S19: *^{1}H NMR spectrum of the o-methyl benzaldehyde terminated pMMA star polymer in THF-d^8.*

Diphenyl tetrazole terminated pMA star polymer 43

Step 1: 100.0 mg (279.2 μmol, 1 eq.) of pentaerythrithol tetrakis(2-bromoisobutyrate), 6.2 mg (27.9 μmol, 0.1 eq) of copper(II) bromide, 21.8 mg (14.0 μmol, 0.5 eq) of 2,2'-bipyridine, and 2.16 g (25.1 mmol, 90 eq.) of MA were dissolved in 6 mL dry DMF. The green solution was deoxygenated by performing three consecutive freeze-pump thaw cycles. Subsequently, 33.9 mg (83.8 μmol, 0.3 eq.) of tin(II) 2-ethylhexanoate was added on the surface of the freezed solution under a nitrogen atmosphere. After one additional freeze-pump thaw cycle, the polymerisation was performed at 60 °C for 70 min whereby the colour of the solution turned brown. After the polymerisation, the solution was cooled in an ice bath and quenched with oxygen. The solution was dialysed in a mixture

of THF and methanol (1:1), followed by a dialysis in water yielding a sticky elastic mass (M_n = 2900).

Step 2: 250.0 mg (86.2 μmol, 1 eq.) of the bromine terminated pMA star polymer of step 1 and 448 mg (6.9 mmol, 80 eq.) of sodium azide were suspended in DMF and stirred over night. The polymer was purified via dialysis in water yielding a sticky elastic mass (M_n = 2800).

Step 3: 200.0 mg (58.8 μmol, 1.0 eq.) of the azide terminated pMA star polymer of step 2 and 73.4 mg (241.1 μmol, 4.1 eq.) of propargyl tetrazolate (refer to chapter 7.2.2) were purged with N_2. Subsequently, both compounds were dissolved in 6 mL dry THF. 81.6 mg (470.1 μmol, 8.0 eq.) of PMDETA and 29.7 mg (529.4 μmol, 9.0 eq.) of copper(I) chloride were purged with N_2 in a seperate flask. The THF containing solution was transferred into the copper containing solution in the presence of a N_2 counterstream. The combined solution was stirred at ambient temperature for 24 h. Afterwards, the solution was dialysed in a mixture of THF and methanol (1:1), followed by a dialysis in water yielding a red powder (M_n = 3900).

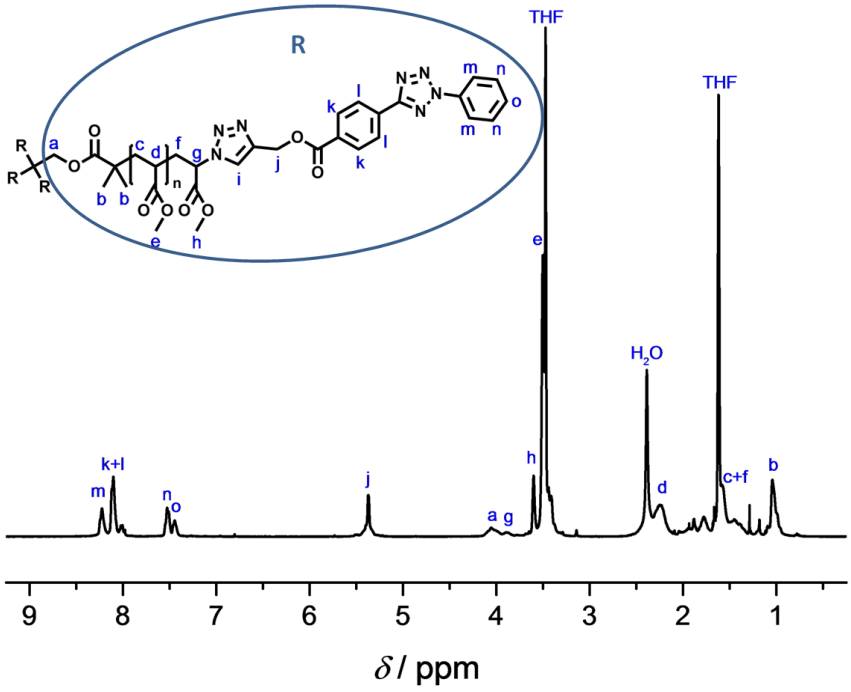

Figure S20: *^{1}H NMR spectrum of the diphenyl tetrazole terminated pMA star polymer in THF-d^8.*

o-Methyl benzaldehyde side chain functionalised pMMA 45

Step 1: 200.0 mg (1.1 mmol, 1 eq.) of methyl 2-bromo-2-methylpropionate, 24.7 mg (110.5 μmol, 0.1 eq) of copper(II) bromide, 86.3 mg (552.4 μmol, 0.5 eq) of 2,2'-bipyridine, 7.19 g (55.2 mmol, 50 eq.) of HEMA, and 5.53 g (55.2 mmol, 50 eq.) of MMA were dissolved in 8 mL dry DMF. The green solution was deoxygenated by performing three consecutive freeze-pump thaw cycles. Subsequently, 143.3 mg (331.4 μmol, 0.3 eq.) of tin(II) 2-ethylhexanoate was added on the surface of the freezed solution under a nitrogen atmosphere. After one additional freeze-pump thaw cycle, the polymerisation was performed at 60 °C for 40 min whereby the colour of the solution turned brown. After the polymerisation, the solution was cooled in an ice bath and quenched with oxygen. The solution was dialysed in a mixture of THF and methanol (1:1), followed by a dialysis in water yielding a white powder (M_n = 6000).

Step 2: 250.0 mg (41.7 μmol, 1 eq.) of the copolymer containing MMA and HEMA repeating units of step 1, 900.9 mg (3.3 mmol, 80 eq.) of *o*-methyl benzaldehyde acid, 1.3 g (6.6 mmol, 160 eq.) of EDC·HCl, and 6.1 mg (49.9 mmol, 1.2 eq.) of DMAP were dissolved in 20 mL dry THF. The solution was stirred for 3 days. Precipitated urea was filtered off and the crude product was dialysed in a mixture of THF and methanol (1:1), followed by a dialysis in water yielding a slightly yellow powder (M_n = 11000).

Diphenyl tetrazole side chain functionalised pMA 45

Step 1: 200.0 mg (1.1 mmol, 1 eq.) of methyl 2-bromo-2-methylpropionate, 24.7 mg (110.5 μmol, 0.1 eq) of copper(II) bromide, 86.3 mg (552.4 μmol, 0.5 eq) of 2,2'-bipyridine, 7.19 g (55.2 mmol, 50 eq.) of HEA, and 5.53 g (55.2 mmol, 50 eq.) of MA were dissolved in 8 mL dry DMF. The green solution was deoxygenated by performing three consecutive freeze-pump thaw cycles. Subsequently, 143.3 mg (331.4 μmol, 0.3 eq.) of tin(II) 2-ethylhexanoate was added on the surface of the freezed solution under a nitrogen atmosphere. After one additional freeze-pump thaw cycle, the polymerisation was performed at 60 °C for 40 min whereby the colour of the solution turned brown. After the polymerisation, the solution was cooled in an ice bath and quenched with oxygen. The solution was dialysed in a mixture of THF and methanol (1:1), followed by a dialysis in water yielding a white powder (M_n = 2900).

Step 2: 500.0 mg (172.4 μmol, 1 eq.) of the copolymer containing MA and HEA repeating units of step 1, 1.1 g (4.3 mmol, 25 eq.) of diphenyl tetrazole acid, 2.0 g (10.3 mmol, 60 eq.) of EDC·HCl, and 16.9 mg (137.9 μmol, 0.8 eq.) of DMAP were dissolved in 20 mL dry THF. The solution was stirred for 3 days. Precipitated urea was filtered off and the crude product was dialysed in a mixture of THF and methanol (1:1), followed by a dialysis in water yielding a red powder (M_n = 6000).

Maleimide side chain functionalised pMMA 46

Step 1: 20.0 mg (110 μmol, 1 eq.) of methyl 2-bromo-2-methylpropionate, 2.5 mg (11.5 μmol, 0.1 eq) of copper(II) bromide, 8.6 mg (55.2 μmol, 0.5 eq) of 2,2'-bipyridine, 1.2 g (5.5 mmol, 50 eq.) of furan protected maleimide terminated ethyl methacrylate, and 553 mg (5.5 mmol, 50 eq.) of MMA were dissolved in 4 mL dry DMF. The green solution was deoxygenated by performing three consecutive freeze-pump thaw cycles. Subsequently, 14.3 mg (33.1 μmol, 0.3 eq.) of tin(II) 2-ethylhexanoate was added on the surface of the freezed solution under a nitrogen atmosphere. After one additional freeze-pump thaw cycle, the polymerisation was performed at 60 °C for 50 min whereby the colour of the solution turned brown. After the polymerisation, the solution was cooled in an ice bath and quenched with oxygen. The solution was dialysed in a mixture of THF and methanol (1:1), followed by a dialysis in water yielding a white powder (M_n = 11000).

Step 2: 200.0 mg of the copolymer containing MMA and furan protected maleimide terminated ethyl methacrylate repeating units of step 1 heated at 80 C under reduced pressure over night. The polymer was obtained as a white powder (M_n = 10000).

Pyrene functionalised tetrazole side chain functionalised pMA 47

Step 1: 200.0 mg (1.1 mmol, 1 eq.) of methyl 2-bromo-2-methylpropionate, 24.7 mg (110.5 μmol, 0.1 eq) of copper(II) bromide, 86.3 mg (552.4 μmol, 0.5 eq) of 2,2'-bipyridine, 7.19 g (55.2 mmol, 50 eq.) of HEA, and 5.53 g (55.2 mmol, 50 eq.) of MA were dissolved in 8 mL dry DMF. The green solution was deoxygenated by performing three consecutive freeze-pump thaw cycles. Subsequently, 143.3 mg (331.4 μmol, 0.3 eq.) of tin(II) 2-ethylhexanoate was added on the surface of the freezed solution under a nitrogen atmosphere. After one additional freeze-pump thaw cycle, the polymerisation

was performed at 60 °C for 40 min whereby the colour of the solution turned brown. After the polymerisation, the solution was cooled in an ice bath and quenched with oxygen. The solution was dialysed in a mixture of THF and methanol (1:1), followed by a dialysis in water yielding a white powder (M_n = 2900).

Step 2: 500.0 mg (172.4 μmol, 1 eq.) of the copolymer containing MA and HEA repeating units of step 1, 1.7 g (4.3 mmol, 25 eq.) of diphenyl tetrazole acid, 2.0 g (10.3 mmol, 60 eq.) of EDC·HCl, and 16.9 mg (137.9 μmol, 0.8 eq.) of DMAP were dissolved in 20 mL dry THF. The solution was stirred for 3 days. Precipitated urea was filtered off and the crude product was dialysed in a mixture of THF and methanol (1:1), followed by a dialysis in water yielding a green powder (M_n = 6000).

Tetrafunctional *o*-methyl benzaldehyde 48

1.30 g (9.56 mmol, 7.0 eq) of 2-hydroxy-6-methylbenzaldeyhde (step 2 of the *o*-methyl benzaldehyde synthesis, refer to chapter 7.1.2), 0.53 g (1.37 mmol, 1.0 eq) of pentaerythritol tetrabromide, and 2.83 g (0.02 mol, 15.0 eq) of potassium carbonate were dissolved in 45 mL DMF The reaction mixture was refluxed at 120°C for 3 days. Afterwards, the solvent was removed under reduced pressure at 80°C. The crude product was purified via column chromatography (silica gel, hexane/ethyl acetate 7:3). The yellow solid was recrystallized in diethyl ether (yield: 50%).
^{1}H NMR ($CDCl_3$) δ/ppm 2.46 (s, 3H), 2.89 (s, 12H), 4.42 (d, 8H), 6.79 (dd, 8H), 7.31 (t, 4H), 10.64 (s, 4H).

ABBREVIATIONS

AIBN	2,2'-azobis(2-methylpropionitrile)
AllBr	allyl bromide
AGET	activator generated by electron transfer
ARGET	activators regenerated by electron transfer
ATRP	atom transfer radical polymerisation
BrBN	2-bromopropionitrile
CI	chemical ionisation
DCM	dichloromethane
DLW	direct laser writing
DMF	dimethylformamide
DMSO	dimethyl sulfoxide
DNA	deoxyribonucleic acid
EBPA	ethyl α-bromophenylacetate
ESI	electrospray ionisation
eV	electronvolt
FRP	free radical polymerisation
FT-ICR	fourier transform ion cyclotron resonance
GBL	$\boldsymbol{\gamma}$-butyrolactone
GPC	gel permeation chromatography
HEA	2-hydroxyethyl acrylate
HEMA	2-hydroxyethyl methacrylate
IC	internal conversion
ISC	inter system crossing
LED	light-emitting diode
MA	methyl acrylate

MADIX	macromolecular design by interchange of xanthates
MeCN	acetonitrile
MAO	methylaluminoxane
MBriB	methyl α-bromoisobutyrate
MMA	methyl methacrylate
MS	mass spectrometry
NITEC	nitrile imine-mediated tetrazole ene cycloaddition
NMR	nuclear magnetic resonance
PEG	poly(ethylene glycol)
pL	polylactide
pMA	poly(methyl acrylate)
PMDETA	N,N,N',N',N''-pentamethyldiethylenetriamine
pMMA	poly(methyl methacrylate)
pNIPAAm	poly(N-isopropylacrylamide)
ppm	parts per million
PTFE	polytetrafluoroethylene
RAFT	reversible addition-fragmentation chain transfer
SEC-ESI-MS	size-exclusion chromatography electrospray ionization mass spectrometry
SIMS	secondary ion mass spectrometry
THF	tetrahydrofuran
ToF	time-of-flight
TMEDA	N,N,N',N'-tetramethylethane-1,2-diamine
TMS	tetramethylsilane
TPMA	tris(2-pyridylmethyl)amine
TREN	tris(2-aminoethyl)amine
TPA	two-photon absorption
UV	ultraviolet
vis	visible
XPS	x-ray photoelectron spectroscopy

CURRICULUM VITAE

Personal Data

Name:	Kai Hiltebrandt
Date of Birth	17.05.1987
Place of Birth	Heilbronn, Germany
Nationality:	German

Education

10/2013-10/2016 **PhD Studies, Chemistry, Karlsruhe Institute of Technology (KIT)**
under supervision of Prof. Dr. Christopher Barner-Kowollik (Institute for Synthetic Macromolecular Chemistry)
Dissertation: "Implementation and Application of the λ-orthogonal photoligation principle in polymer science"

09/2015–12/2015 **Occupational Trainee, Queensland University of Technology (QUT), Brisbane, Australia**
Research stay under supervision of Dr. James Blinco
Project: "Light induced, orthogonal end group conversions of polymers and analytic investigation of block copolymers"

10/2008–08/2013 **Diploma, Chemistry, Karlsruhe Institute of Technology (KIT)**
Specialisation: Analytical and polymer chemistry
Thesis: "A systematic analysis into the electrospray ionisation behaviour of synthetic polymers"

09/1998–06/2007 **A-Levels, Elly-Heuss-Knapp-Gymnasium, Heilbronn**

Work Experience

10/2013-10/2016	**Research Assistant, Karlsruhe Institute of Technology (KIT)**
04/2008–08/2008	**Mail Carrier, Deutsche Post AG**
07/2007-03/2008	**Civilian Service, Retirement Home St. Elisabeth, Heilbronn**

Scholarships and Voluntary Work

03/2014-02/2016	**PhD scholarship, Verband der Chemischen Industrie (VCI)**
since 05/2015	**e-fellows.net scholarship**
03/2015-07/2016	**Arbeiterwohlfahrt (AWO), Karlsruhe** voluntary after-school homework supervision

Conferences and Summer School Participations

09/2014	**European Symposium of Photopolymer Science (ESPS), Vienna**
08/2016	**Participation at the 131st BAST Summer Course, Ludwigshafen**

REFERENCES

[1] W. Amass, A. Amass, B. Tighe, *Polym. Int.* **1998**, *47*, 89-144.
[2] R. A. Gross, B. Kalra, *Science* **2002**, *297*, 803-807.
[3] J. C. Middleton, A. J. Tipton, *Biomaterials* **2000**, *21*, 2335-2346.
[4] J. Luten, C. F. van Nostrum, S. C. De Smedt, W. E. Hennink, *J. Controlled Release* **2008**, *126*, 97-110.
[5] K. K. Oehlenschlaeger, J. O. Mueller, J. Brandt, S. Hilf, A. Lederer, M. Wilhelm, R. Graf, M. L. Coote, F. G. Schmidt, C. Barner-Kowollik, *Adv. Mater.* **2014**, *26*, 3561-3566.
[6] N. K. Guimard, K. K. Oehlenschlaeger, J. Zhou, S. Hilf, F. G. Schmidt, C. Barner-Kowollik, *Macromol. Chem. Phys.* **2012**, *213*, 131-143.
[7] P. Andersson, D. Nilsson, P. O. Svensson, M. Chen, A. Malmström, T. Remonen, T. Kugler, M. Berggren, *Adv. Mater.* **2002**, *14*, 1460-1464.
[8] A. Facchetti, *Chem. Mater.* **2011**, *23*, 733-758.
[9] L. Nyholm, G. Nyström, A. Mihranyan, M. Strømme, *Adv. Mater.* **2011**, *23*, 3751-3769.
[10] L. Yuan, B. Yao, B. Hu, K. Huo, W. Chen, J. Zhou, *Energy Environ. Sci.* **2013**, *6*, 470-476.
[11] D. R. Paul, L. M. Robeson, *Polymer* **2008**, *49*, 3187-3204.
[12] K. Pu, A. J. Shuhendler, J. V. Jokerst, J. Mei, S. S. Gambhir, Z. Bao, J. Rao, *Nat. Nano.* **2014**, *9*, 233-239.
[13] Q. Li, L. Chen, M. R. Gadinski, S. Zhang, G. Zhang, H. Li, A. Haque, L.-Q. Chen, T. Jackson, Q. Wang, *Nature* **2015**, *523*, 576-579.
[14] H. J. Ploehn, *Nature* **2015**, *523*, 536-537.
[15] T. F. A. de Greef, E. W. Meijer, *Nature* **2008**, *453*, 171-173.
[16] G. Ciamician, *Science* **1912**, *36*, 385-394.
[17] E. J. Park, G. T. Carroll, N. J. Turro, J. T. Koberstein, *Soft Matter* **2009**, *5*, 36-50.
[18] K. Hiltebrandt, T. Pauloehrl, J. P. Blinco, K. Linkert, H. G. Börner, C. Barner-Kowollik, *Angew. Chem. Int. Ed.* **2015**, *54*, 2838-2843.
[19] W. B. Jensen, *J. Chem. Educ.* **2008**, *85*, 624.
[20] A. Abdulshafi, K. E. Kaloush, DTIC Document, **1990**.
[21] H. Staudinger, *Ber. Deut. Chem. Ges.* **1920**, *53*, 1073-1085.
[22] H. Staudinger, J. Fritschi, *Helv. Chim. Acta* **1922**, *5*, 785-806.
[23] I. Eisenbach, in *English for Materials Science and Engineering*, Springer, **2011**, pp. 51-62.
[24] B. Ellis, R. Smith, *Polymers: a property database*, CRC Press, **2008**.
[25] R. C. Thompson, S. H. Swan, C. J. Moore, F. S. Vom Saal, *Phil. Trans. R. Soc. B* **2009**, *364*, 1973-1976.
[26] E. W. Flick, *Plastics Additives, Volume 1: An Industry Guide*, Elsevier, **2013**.
[27] M. Wensing, E. Uhde, T. Salthammer, *Sci. Total Environ.* **2005**, *339*, 19-40.

[28] J. Murphy, *The additives for plastics handbook: antioxidants, antistatics, compatibilisers, conductive fillers, flame-retardants, pigments, plasticisers, reinforcements: classification, data, tables, descriptions, market trends, suppliers/brand names*, Elsevier advanced technology, **1996**.
[29] M. Xanthos, *Functional fillers for plastics*, John Wiley & Sons, **2010**.
[30] J. A. Brydson, *Plastics materials*, Butterworth-Heinemann, **1999**.
[31] N. Stribeck, *X-Ray Scattering of Soft Matter* **2007**, 1-5.
[32] P. J. Flory, *Principles of Polymer Chemistry*, Cornell University Press, **1953**.
[33] H. G. Elias, *Macromolecules*, Springer US, **2012**.
[34] D. I. Bower, *An Introduction to Polymer Physics*, Cambridge University Press, **2002**.
[35] Y. Tezuka, H. Oike, *Prog. Polym. Sci.* **2002**, *27*, 1069-1122.
[36] J. K. Stille, *J. Chem. Educ.* **1981**, *58*, 862.
[37] K. Miki, Y. Washitake, K. Ohe, S. Uemura, *Angew. Chem. Int. Ed.* **2004**, *43*, 1857-1860.
[38] M. P. Stevens, *Polymer Chemistry, Vol. 2*, oxford university press New York, **1990**.
[39] N. Heymans, *Macromolecules* **2000**, *33*, 4226-4234.
[40] F. Garbassi, R. Po, in *Encyclopedia of Polymer Science and Technology*, John Wiley & Sons, Inc., **2002**.
[41] J. E. Mark, *Physical properties of polymers handbook*, Springer, **1996**.
[42] J. E. K. Schawe, *Thermochim. Acta* **1995**, *261*, 183-194.
[43] J. H. Gibbs, E. A. Di Marzio, *J. Chem. Phys.* **1958**, *28*, 373-383.
[44] Q. Guo, *Thermosets: Structure, properties and applications*, Elsevier, **2012**.
[45] M. G. Lu, M. J. Shim, S. W. Kim, *J. Appli. Polym. Sci.* **2000**, *75*, 1514-1521.
[46] K. Pielichowski, J. Njuguna, in *Structural Materials and Processes in Transportation*, Wiley-VCH Verlag GmbH & Co. KGaA, **2013**, pp. 237-252.
[47] C. L. Restuccia, C. Lofaro, Google Patents, **2013**.
[48] M. Morton, *Rubber technology*, Springer Science & Business Media, **2013**.
[49] G. Odian, *Principles of Polymerization*, Wiley, **2004**.
[50] K. Matyjaszewski, in *Controlled and Living Polymerizations*, Wiley-VCH **2010**, pp. 103-166.
[51] K. Matyjaszewski, T. P. Davis, *Handbook of Radical Polymerization*, Wiley, **2003**.
[52] T. Iwasaki, J.-I. Yoshida, *Macromolecules* **2005**, *38*, 1159-1163.
[53] R. Guerrero-Santos, E. Saldívar-Guerra, J. Bonilla-Cruz, in *Handbook of Polymer Synthesis, Characterization, and Processing*, John Wiley & Sons, Inc., **2013**, pp. 65-83.
[54] H. F. Gruber, *Prog. Polym. Sci.* **1992**, *17*, 953-1044.
[55] C. J. Hawker, *J. Am. Chem. Soc.* **1994**, *116*, 11185-11186.
[56] L. Rey, J. Duchet, J. Galy, H. Sautereau, D. Vouagner, L. Carrion, *Polymer* **2002**, *43*, 4375-4384.
[57] A. Lagos, J. Reyes, *J. Polym. Sci. Part A: Polym. Chem.* **1988**, *26*, 985-991.
[58] P. C. Deb, I. D. Gaba, *Makromol. Chem.* **1978**, *179*, 1549-1557.
[59] M. S. Matheson, E. E. Auer, E. B. Bevilacqua, E. J. Hart, *J. Am. Chem. Soc.* **1951**, *73*, 1700-1706.
[60] M. P. Tonge, A. Kajiwara, M. Kamachi, R. G. Gilbert, *Polymer* **1998**, *39*, 2305-2313.
[61] T. Junkers, M. Schneider-Baumann, S. S. P. Koo, P. Castignolles, C. Barner-Kowollik, *Macromolecules* **2010**, *43*, 10427-10434.
[62] A. P. Haehnel, M. Schneider-Baumann, L. Arens, A. M. Misske, F. Fleischhaker, C. Barner-Kowollik, *Macromolecules* **2014**, *47*, 3483-3496.

[63] R. A. Hutchinson, S. Beuermann, D. A. Paquet, J. H. McMinn, *Macromolecules* **1997**, *30*, 3490-3493.
[64] M. Buback, F.-D. Kuchta, *Macromol. Chem. Phys.* **1997**, *198*, 1455-1480.
[65] P. E. M. Allen, C. R. Patrick, *Makromol. Chem.* **1961**, *47*, 154-167.
[66] C. Barner-Kowollik, G. T. Russell, *Prog. Polym. Sci.* **2009**, *34*, 1211-1259.
[67] J. Krstina, G. Moad, E. Rizzardo, C. L. Winzor, C. T. Berge, M. Fryd, *Macromolecules* **1995**, *28*, 5381-5385.
[68] M. Buback, M. Egorov, R. G. Gilbert, V. Kaminsky, O. F. Olaj, G. T. Russell, P. Vana, G. Zifferer, *Macromol. Chem. Phys.* **2002**, *203*, 2570-2582.
[69] S. Beuermann, M. Buback, *Prog. Polym Sci.* **2002**, *27*, 191-254.
[70] F. R. Mayo, *J. Am. Chem. Soc.* **1943**, *65*, 2324-2329.
[71] M. J. Monteiro, N. Subramaniam, J. R. Taylor, B. T. T. Pham, M. P. Tonge, R. G. Gilbert, *Polymer* **2001**, *42*, 2403-2411.
[72] D. Kukulj, T. P. Davis, *Macromol. Chem. Phys.* **1998**, *199*, 1697-1708.
[73] J. Boissel, *J. Appl. Polym. Sci.* **1977**, *21*, 855-857.
[74] K. G. Suddaby, D. R. Maloney, D. M. Haddleton, *Macromolecules* **1997**, *30*, 702-713.
[75] Z. Szablan, T. Junkers, S. P. S. Koo, T. M. Lovestead, T. P. Davis, M. H. Stenzel, C. Barner-Kowollik, *Macromolecules* **2007**, *40*, 6820-6833.
[76] J. L. O'Brien, F. Gornick, *J. Am. Chem. Soc.* **1955**, *77*, 4757-4763.
[77] N. M. Ahmad, F. Heatley, P. A. Lovell, *Macromolecules* **1998**, *31*, 2822-2827.
[78] J.-S. Wang, K. Matyjaszewski, *J. Am. Chem. Soc.* **1995**, *117*, 5614-5615.
[79] N. V. Tsarevsky, B. S. Sumerlin, S. Craig, A. S. Abd-El-Aziz, J. Dong, T. Masuda, C. Weder, P. Vana, Y. Yagci, *Fundamentals of Controlled/Living Radical Polymerization*, Royal Society of Chemistry, **2012**.
[80] B. D. Coleman, T. G. Fox, *J. Am. Chem. Soc.* **1963**, *85*, 1241-1244.
[81] Y. Tezuka, *Topological Polymer Chemistry: Progress of Cyclic Polymer in Syntheses, Properties and Functions*, World Scientific Publishing Company Incorporated, **2012**.
[82] B. V. K. J. Schmidt, C. Barner-Kowollik, *Nat. Chem.* **2013**, *5*, 990-992.
[83] A. D. Jenkins, R. G. Jones, G. Moad, *Pure Appl. Chem.* **2010**, *82*, 483-491.
[84] M. Zhong, Y. Wang, P. Krys, D. Konkolewicz, K. Matyjaszewski, *Macromolecules* **2013**, *46*, 3816-3827.
[85] W. A. Braunecker, K. Matyjaszewski, *Prog. Polym. Sci.* **2007**, *32*, 93-146.
[86] K. Matyjaszewski, *Polym. Int.* **2003**, *52*, 1559-1565.
[87] K. Matyjaszewski, T. Shigemoto, J. M. J. Fréchet, M. Leduc, *Macromolecules* **1996**, *29*, 4167-4171.
[88] J. Nicolas, Y. Guillaneuf, C. Lefay, D. Bertin, D. Gigmes, B. Charleux, *Prog. Polym. Sci.* **2013**, *38*, 63-235.
[89] M. Kato, M. Kamigaito, M. Sawamoto, T. Higashimura, *Macromolecules* **1995**, *28*, 1721-1723.
[90] K. Matyjaszewski, S. G. Gaynor, J.-S. Wang, *Macromolecules* **1995**, *28*, 2093-2095.
[91] C. D. Borman, A. T. Jackson, A. Bunn, A. L. Cutter, D. J. Irvine, *Polymer* **2000**, *41*, 6015-6020.
[92] K. Matyjaszewski, *Macromolecules* **2012**, *45*, 4015-4039.
[93] S.-M. Jo, W.-S. Lee, B.-S. Ahn, K.-Y. Park, K.-A. Kim, I.-S. R. Paeng, *Polym. Bull.* **2000**, *44*, 1-8.
[94] Y. Wang, Y. Kwak, J. Buback, M. Buback, K. Matyjaszewski, *ACS Macro Lett.* **2012**, *1*, 1367-1370.
[95] W. Tang, K. Matyjaszewski, *Macromolecules* **2006**, *39*, 4953-4959.

[96] C. Ulbricht, C. R. Becer, A. Winter, D. Veldman, U. S. Schubert, *Macromol. Rapid Commun.* **2008**, *29*, 1919-1925.
[97] V. C. Gibson, R. K. O'Reilly, W. Reed, D. F. Wass, A. J. P. White, D. J. Williams, *Chem. Commun.* **2002**, 1850-1851.
[98] J. Xia, K. Matyjaszewski, *Macromolecules* **1997**, *30*, 7697-7700.
[99] K. Matyjaszewski, N. V. Tsarevsky, *Nat. Chem.* **2009**, *1*, 276-288.
[100] C. Boyer, A. H. Soeriyadi, P. J. Roth, M. R. Whittaker, T. P. Davis, *Chem. Comm.* **2011**, *47*, 1318-1320.
[101] V. Coessens, K. Matyjaszewski, *J. Macromol. Sci. A* **1999**, *36*, 667-679.
[102] W. Tang, *Coord. Chem. Rev.* **2005**, *249*, 1155-1184.
[103] L. Bai, L. Zhang, Z. Zhang, Y. Tu, N. Zhou, Z. Cheng, X. Zhu, *Macromolecules* **2010**, *43*, 9283-9290.
[104] W. Jakubowski, K. Matyjaszewski, *Macromolecules* **2005**, *38*, 4139-4146.
[105] L. Zhang, Z. Cheng, S. Shi, Q. Li, X. Zhu, *Polymer* **2008**, *49*, 3054-3059.
[106] K. Min, H. Gao, K. Matyjaszewski, *J. Am. Chem. Soc.* **2005**, *127*, 3825-3830.
[107] Y. Yamamura, K. Matyjaszewski, *J. Macromol. Sci., Part A: Pure Appl. Chem.* **2007**, *44*, 1035-1039.
[108] Z. Hu, X. Shen, H. Qiu, G. Lai, J. Wu, W. Li, *Eur. Polym. J.* **2009**, *45*, 2313-2318.
[109] K. Matyjaszewski, B. E. Woodworth, X. Zhang, S. G. Gaynor, Z. Metzner, *Macromolecules* **1998**, *31*, 5955-5957.
[110] H. Dong, K. Matyjaszewski, *Macromolecules* **2008**, *41*, 6868-6870.
[111] K. Min, W. Jakubowski, K. Matyjaszewski, *Macromol. Rapid Commun.* **2006**, *27*, 594-598.
[112] Q. Li, L. Zhang, Z. Zhang, N. Zhou, Z. Cheng, X. Zhu, *J. Polym. Sci. Part A: Polym. Chem.* **2010**, *48*, 2006-2015.
[113] A. C. C. Esteves, L. Bombalski, T. Trindade, K. Matyjaszewski, A. Barros-Timmons, *Small* **2007**, *3*, 1230-1236.
[114] F. Stoffelbach, B. Belardi, J. M. R. C. A. Santos, L. Tessier, K. Matyjaszewski, B. Charleux, *Macromolecules* **2007**, *40*, 8813-8816.
[115] J. K. Oh, K. Min, K. Matyjaszewski, *Macromolecules* **2006**, *39*, 3161-3167.
[116] D. C. H. McBrien, K. A. Hassall, *Physiol. Plant.* **1967**, *20*, 113-117.
[117] S. Meshitsuka, M. Ishizawa, T. Nose, *Experientia* **1987**, *43*, 151-156.
[118] N. V. Tsarevsky, K. Matyjaszewski, *J. Polym. Sci. Part A: Polym. Chem.* **2006**, *44*, 5098-5112.
[119] N. Jasinski, A. Lauer, P. J. M. Stals, S. Behrens, S. Essig, A. Walther, A. S. Goldmann, C. Barner-Kowollik, *ACS Macro Lett.* **2015**, *4*, 298-301.
[120] N. V. Tsarevsky, W. Tang, S. J. Brooks, K. Matyjaszewski, in *ACS Sym. Ser., Vol. 944*, Oxford University Press, **2006**, pp. 56-70.
[121] Y. Kwak, K. Matyjaszewski, *Polym. Int.* **2009**, *58*, 242-247.
[122] K. Min, H. Gao, K. Matyjaszewski, *Macromolecules* **2007**, *40*, 1789-1791.
[123] K. A. Payne, D. R. D'hooge, P. H. M. Van Steenberge, M.-F. Reyniers, M. F. Cunningham, R. A. Hutchinson, G. B. Marin, *Macromolecules* **2013**, *46*, 3828-3840.
[124] J. Chiefari, Y. K. Chong, F. Ercole, J. Krstina, J. Jeffery, T. P. T. Le, R. T. A. Mayadunne, G. F. Meijs, C. L. Moad, G. Moad, E. Rizzardo, S. H. Thang, *Macromolecules* **1998**, *31*, 5559-5562.
[125] S. Perrier, P. Takolpuckdee, *J. Polym. Sci. Part A: Polym. Chem.* **2005**, *43*, 5347-5393.
[126] C. Barner-Kowollik, *Handbook of RAFT Polymerization*, Wiley, **2008**.
[127] D. J. Keddie, *Chem. Soc. Rev.* **2014**, *43*, 496-505.

[128] A. Feldermann, A. Ah Toy, T. P. Davis, M. H. Stenzel, C. Barner-Kowollik, *Polymer* **2005**, *46*, 8448-8457.
[129] J. M. G. Cowie, J. M. K. G. Cowie, *Polymers: Chemistry and Physics of Modern Materials*, Stanley Thornes publishers, **1991**.
[130] R. T. A. Mayadunne, E. Rizzardo, J. Chiefari, Y. K. Chong, G. Moad, S. H. Thang, *Macromolecules* **1999**, *32*, 6977-6980.
[131] G. Moad, E. Rizzardo, S. H. Thang, *Austr. J. Chem.* **2009**, *62*, 1402-1472.
[132] C. Barner-Kowollik, M. Buback, B. Charleux, M. L. Coote, M. Drache, T. Fukuda, A. Goto, B. Klumperman, A. B. Lowe, J. B. McLeary, G. Moad, M. J. Monteiro, R. D. Sanderson, M. P. Tonge, P. Vana, *J. Polym. Sci. Part A: Polym. Chem.* **2006**, *44*, 5809-5831.
[133] D. J. Keddie, G. Moad, E. Rizzardo, S. H. Thang, *Macromolecules* **2012**, *45*, 5321-5342.
[134] J. T. Lai, D. Filla, R. Shea, *Macromolecules* **2002**, *35*, 6754-6756.
[135] C. Fortunatti, C. Sarmoria, A. Brandolin, M. Asteasuain, *Macromol. React. Eng.* **2014**, *8*, 781-795.
[136] T. Junkers, *J. Polym. Sci. Part A: Polym. Chem.* **2011**, *49*, 4154-4163.
[137] C. Barner-Kowollik, J. F. Quinn, D. R. Morsley, T. P. Davis, *J. Polym. Sci. Part A: Polym. Chem.* **2001**, *39*, 1353-1365.
[138] D. Konkolewicz, B. S. Hawkett, A. Gray-Weale, S. Perrier, *J. Polym. Sci. Part A: Polym. Chem.* **2009**, *47*, 3455-3466.
[139] M. J. Monteiro, H. de Brouwer, *Macromolecules* **2001**, *34*, 349-352.
[140] H. Willcock, R. K. O'Reilly, *Polym. Chem.* **2010**, *1*, 149-157.
[141] G. Moad, Y. K. Chong, A. Postma, E. Rizzardo, S. H. Thang, *Polymer* **2005**, *46*, 8458-8468.
[142] T. Gruendling, M. Dietrich, C. Barner-Kowollik, *Aust. J. Chem.* **2009**, *62*, 806-812.
[143] O. Altintas, K. Riazi, R. Lee, C. Y. Lin, M. L. Coote, M. Wilhelm, C. Barner-Kowollik, *Macromolecules* **2013**, *46*, 8079-8091.
[144] M. Kaupp, K. Hiltebrandt, V. Trouillet, P. Mueller, A. S. Quick, M. Wegener, C. Barner-Kowollik, *Chem. Comm.* **2016**, *52*, 1975-1978.
[145] L. Hlalele, D. R. D'hooge, C. J. Dürr, A. Kaiser, S. Brandau, C. Barner-Kowollik, *Macromolecules* **2014**, *47*, 2820-2829.
[146] D. Roy, J. T. Guthrie, S. Perrier, *Soft Matter* **2008**, *4*, 145-155.
[147] G. R. Fleming, J. Longworth, B. P. Krueger, Encyclopædia Britannica, **2015**.
[148] H. Trommsdorff, *Ann. Pharm. Chem.* **1834**, *11*, 190-207.
[149] H. Bouas-Laurent, A. Castellan, J.-P. Desvergne, R. Lapouyade, *Chem. Soc. Rev.* **2000**, *29*, 43-55.
[150] G. Ciamician, P. Silber, *Ber. Dtsch. Chem. Ges.* **1901**, *34*, 1530-1543.
[151] G. Ciamician, P. Silber, *Ber. Dtsch. Chem. Ges.* **1907**, *40*, 2415-2424.
[152] M. Planck, *Ber. Verh. Dtsch. Phys. Ges.* **1900**, *2*, 237.
[153] A. Einstein, *Ann. Physik* **1905**, *17*, 132.
[154] B. Feldman, *The Nobel Prize: a history of genius, controversy, and prestige*, Arcade Publishing, **2001**.
[155] M. Planck, *Nobel lecture* **1920**, *2*, 1-10.
[156] K. Dietliker, A. Braig, A. Ricci, in *Photochemistry: Vol. 38*, The Royal Society of Chemistry, **2010**, pp. 344-368.
[157] G. T. Wondrak, M. K. Jacobson, E. L. Jacobson, *Photochem. Photobiol. Sci.* **2006**, *5*, 215-237.
[158] A. Einstein, *Verh. Dtsch. Phys. Ges.* **1916**, *18*, 318-323.

[159] M. Bodenstein, F. Weigert, R. Luther, J. Franck, L. S. Ornstein, F. A. Lindemann, J. Rice, J. A. Christiansen, E. C. C. Baly, E. K. Rideal, A. J. Allmand, H. von Halban, P. Lasareff, E. J. Bowen, H. S. Taylor, D. L. Chapman, S. C. Roy, S. L. Langedyk, M. Padoa, F. I. G. Rawlins, *Trans. Faraday Soc.* **1926**, *21*, 515-524.
[160] L. Sun, J. R. Bolton, *J. Phys. Chem.* **1996**, *100*, 4127-4134.
[161] A. Jabłoński, *Z. Physik* **1935**, *94*, 38-46.
[162] J. Zimmermann, A. Zeug, B. Roder, *Phys. Chem. Chem. Phys.* **2003**, *5*, 2964-2969.
[163] A. S. Coolidge, H. M. James, R. D. Present, *J. Chem. Phys.* **1936**, *4*, 193-211.
[164] C. M. Marian, *WIRes: Comput. Mol. Sci.* **2012**, *2*, 187-203.
[165] D. E. Damschen, C. D. Merritt, D. L. Perry, G. W. Scott, L. D. Talley, *J. Phys. Chem.* **1978**, *82*, 2268-2272.
[166] G. G. Guilbault, *Practical fluorescence, Vol. 3*, CRC Press, **1990**.
[167] A. Samanta, *J. Phys. Chem. B* **2006**, *110*, 13704-13716.
[168] G. N. Lewis, M. Kasha, *J. Am. Chem. Soc.* **1944**, *66*, 2100-2116.
[169] K. A. Franz, W. G. Kehr, A. Siggel, J. Wieczoreck, W. Adam, in *Ullmann's Encyclopedia of Industrial Chemistry*, Wiley-VCH Verlag GmbH & Co. KGaA, **2000**.
[170] R. G. W. Norrish, C. H. Bamford, *Nature* **1936**, *138*, 1016.
[171] R. G. W. Norrish, C. H. Bamford, *Nature* **1937**, *140*, 195.
[172] Z. Wang, in *Comprehensive Organic Name Reactions and Reagents*, John Wiley & Sons, Inc., **2010**.
[173] J. Hutchison, A. Ledwith, *Polymer* **1973**, *14*, 405-408.
[174] D. Voll, A. Hufendiek, T. Junkers, C. Barner-Kowollik, *Macromol. Rapid Commun.* **2012**, *33*, 47-53.
[175] D. S. Esen, N. Arsu, J. P. Da Silva, S. Jockusch, N. J. Turro, *J. Polym. Sci. Part A: Polym. Chem.* **2013**, *51*, 1865-1871.
[176] R. S. Davidson, D. Goodwin, P. F. de Violet, *Tetrahedron Lett.* **1981**, *22*, 2485-2486.
[177] V. Ramamurthy, D. R. Corbin, L. J. Johnston, *J. Am. Chem. Soc.* **1992**, *114*, 3870-3882.
[178] P. J. Wagner, *Acc. Chem. Res.* **1971**, *4*, 168-177.
[179] J. C. Scaiano, E. A. Lissi, M. V. Encina, *Rev. of Chem. Intermed.* **1978**, *2*, 139-196.
[180] G. S. Hammond, W. M. Moore, *J. Am. Chem. Soc.* **1959**, *81*, 6334-6334.
[181] J. N. Pitts, R. L. Letsinger, R. P. Taylor, J. M. Patterson, G. Recktenwald, R. B. Martin, *J. Am. Chem. Soc.* **1959**, *81*, 1068-1077.
[182] N. C. Yang, C. Rivas, *J. Am. Chem. Soc.* **1961**, *83*, 2213-2213.
[183] P. G. Sammes, *Tetrahedron* **1976**, *32*, 405-422.
[184] K. K. Oehlenschlaeger, J. O. Mueller, N. B. Heine, M. Glassner, N. K. Guimard, G. Delaittre, F. G. Schmidt, C. Barner-Kowollik, *Angew. Chem. Int. Ed.* **2013**, *52*, 762-766.
[185] T. Gruendling, K. K. Oehlenschlaeger, E. Frick, M. Glassner, C. Schmid, C. Barner-Kowollik, *Macromol. Rapid Commun.* **2011**, *32*, 807-812.
[186] G. Porter, M. F. Tchir, *J. Chem. Soc. D: Chem. Comm.* **1970**, 1372-1373.
[187] G. Porter, M. F. Tchir, *J. Chem. Soc. A* **1971**, 3772-3777.
[188] L. Salem, C. Rowland, *Angew. Chem. Int. Ed.* **1972**, *11*, 92-111.
[189] S. M. Mellows, P. G. Sammes, *J. Chem. Soc. D: Chem. Commun.* **1971**, 21-22.
[190] R. M. Wilson, K. Hannemann, W. R. Heineman, J. R. Kirchhoff, *J. Am. Chem. Soc.* **1987**, *109*, 4743-4745.
[191] J. N. Moorthy, S. Samanta, *ARKIVOC* **2007**, *8*, 324-340.
[192] N. Zydziak, F. Feist, B. Huber, J. O. Mueller, C. Barner-Kowollik, *Chem. Comm.* **2015**, *51*, 1799-1802.

[193] B. Richter, T. Pauloehrl, J. Kaschke, D. Fichtner, J. Fischer, A. M. Greiner, D. Wedlich, M. Wegener, G. Delaittre, C. Barner-Kowollik, M. Bastmeyer, *Adv. Mater.* **2013**, *25*, 6117-6122.
[194] C. M. Preuss, T. Tischer, C. Rodriguez-Emmenegger, M. M. Zieger, M. Bruns, A. S. Goldmann, C. Barner-Kowollik, *J. Mater. Chem. B* **2014**, *2*, 36-40.
[195] L. Stolzer, I. Ahmed, C. Rodriguez-Emmenegger, V. Trouillet, P. Bockstaller, C. Barner-Kowollik, L. Fruk, *Chem. Comm.* **2014**, *50*, 4430-4433.
[196] M. Glassner, K. K. Oehlenschlaeger, T. Gruendling, C. Barner-Kowollik, *Macromolecules* **2011**, *44*, 4681-4689.
[197] S. Arumugam, V. V. Popik, *J. Am. Chem. Soc.* **2011**, *133*, 5573-5579.
[198] R. Huisgen, M. Seidel, J. Sauer, J. McFarland, G. Wallbillich, *J. Org. Chem.* **1959**, *24*, 892-893.
[199] J. S. Clovis, A. Eckell, R. Huisgen, R. Sustmann, *Chem. Ber.* **1967**, *100*, 60-70.
[200] P. Weinberg, U. W. Grummt, C. Csongar, *J. Prakt. Chem.* **1988**, *330*, 887-892.
[201] G. Bertrand, C. Wentrup, *Angew. Chem. Int. Ed.* **1994**, *33*, 527-545.
[202] M. Dietrich, G. Delaittre, J. P. Blinco, A. J. Inglis, M. Bruns, C. Barner-Kowollik, *Adv. Funct. Mater.* **2012**, *22*, 304-312.
[203] W. Song, Y. Wang, J. Qu, Q. Lin, *J. Am. Chem. Soc.* **2008**, *130*, 9654-9655.
[204] M. M. Madden, C. I. Rivera Vera, W. Song, Q. Lin, *Chem. Comm.* **2009**, 5588-5590.
[205] Z. Yu, R. K. V. Lim, Q. Lin, *Chem. Eur. J.* **2010**, *16*, 13325-13329.
[206] J. O. Mueller, N. K. Guimard, K. K. Oehlenschlaeger, F. G. Schmidt, C. Barner-Kowollik, *Polym. Chem.* **2014**, *5*, 1447-1456.
[207] Y. Sugawara, N. Jasinski, M. Kaupp, A. Welle, N. Zydziak, E. Blasco, C. Barner-Kowollik, *Chem. Comm.* **2015**, *51*, 13000-13003.
[208] Y. Wang, W. J. Hu, W. Song, R. K. V. Lim, Q. Lin, *Org. Lett.* **2008**, *10*, 3725-3728.
[209] S. Arndt, H.-A. Wagenknecht, *Angew. Chem. Int. Ed.* **2014**, *53*, 14580-14582.
[210] P. Lederhose, K. N. R. Wust, C. Barner-Kowollik, J. P. Blinco, *Chem. Comm.* **2016**, *52*, 5928-5931.
[211] W. Song, Y. Wang, J. Qu, M. M. Madden, Q. Lin, *Angew. Chem. Int. Ed.* **2008**, *47*, 2832-2835.
[212] H.-P. M. de Hoog, M. Nallani, B. Liedberg, *Polym. Chem.* **2012**, *3*, 302-306.
[213] M. Merkel, K. Peewasan, S. Arndt, D. Ploschik, H. A. Wagenknecht, *Chem. Bio. Chem.* **2015**, *16*, 1541-1553.
[214] Z. Li, L. Qian, L. Li, J. C. Bernhammer, H. V. Huynh, J.-S. Lee, S. Q. Yao, *Angew. Chem. Int. Ed.* **2016**, *55*, 2002-2006.
[215] T. Tischer, C. Rodriguez-Emmenegger, V. Trouillet, A. Welle, V. Schueler, J. O. Mueller, A. S. Goldmann, E. Brynda, C. Barner-Kowollik, *Adv. Mater.* **2014**, *26*, 4087-4092.
[216] C. Rodriguez-Emmenegger, C. M. Preuss, B. Yameen, O. Pop-Georgievski, M. Bachmann, J. O. Mueller, M. Bruns, A. S. Goldmann, M. Bastmeyer, C. Barner-Kowollik, *Adv. Mater.* **2013**, *25*, 6123-6127.
[217] E. Blasco, M. Piñol, L. Oriol, B. V. K. J. Schmidt, A. Welle, V. Trouillet, M. Bruns, C. Barner-Kowollik, *Adv. Funct. Mater.* **2013**, *23*, 4011-4019.
[218] J. O. Mueller, D. Voll, F. G. Schmidt, G. Delaittre, C. Barner-Kowollik, *Chem. Comm.* **2014**, *50*, 15681-15684.
[219] J. Willenbacher, K. N. R. Wuest, J. O. Mueller, M. Kaupp, H.-A. Wagenknecht, C. Barner-Kowollik, *ACS Macro Lett.* **2014**, *3*, 574-579.
[220] P. Lederhose, N. L. Haworth, K. Thomas, S. E. Bottle, M. L. Coote, C. Barner-Kowollik, J. P. Blinco, *J. Org. Chem.* **2015**, *80*, 8009-8017.

[221] J. P. Blinco, K. E. Fairfull-Smith, B. J. Morrow, S. E. Bottle, *Austr. J. Chem.* **2011**, *64*, 373-389.
[222] H. C. Kolb, M. G. Finn, K. B. Sharpless, *Angew. Chem. Int. Ed.* **2001**, *40*, 2004-2021.
[223] J. E. Moses, A. D. Moorhouse, *Chem. Soc. Rev.* **2007**, *36*, 1249-1262.
[224] H. C. Kolb, K. B. Sharpless, *Drug Discov. Today* **2003**, *8*, 1128-1137.
[225] E. Van der Eycken, K. U. Leuven, K. B. Sharpless, *QSAR & Comb. Sci.* **2007**, *26*, 1115-1115.
[226] C. Barner-Kowollik, A. J. Inglis, *Macromol. Chem. Phys.* **2009**, *210*, 987-992.
[227] W. H. Binder, R. Sachsenhofer, *Macromol. Rapid Commun.* **2007**, *28*, 15-54.
[228] S. Sinnwell, A. J. Inglis, M. H. Stenzel, C. Barner-Kowollik, *Macromol. Rapid Commun.* **2008**, *29*, 1090-1096.
[229] K. L. Killops, L. M. Campos, C. J. Hawker, *J. Am. Chem. Soc.* **2008**, *130*, 5062-5064.
[230] C. Barner-Kowollik, F. E. Du Prez, P. Espeel, C. J. Hawker, T. Junkers, H. Schlaad, W. Van Camp, *Angew. Chem. Int. Ed.* **2011**, *50*, 60-62.
[231] J.-F. Lutz, H. G. Börner, K. Weichenhan, *Macromol. Rapid Commun.* **2005**, *26*, 514-518.
[232] P. L. Golas, K. Matyjaszewski, *Chem. Soc. Rev.* **2010**, *39*, 1338-1354.
[233] R. Huisgen, *Angew. Chem. Int. Ed.* **1963**, *2*, 633-645.
[234] R. Huisgen, *Angew. Chem. Int. Ed.* **1963**, *2*, 565-598.
[235] C. W. Tornøe, C. Christensen, M. Meldal, *J. Org. Chem.* **2002**, *67*, 3057-3064.
[236] V. V. Rostovtsev, L. G. Green, V. V. Fokin, K. B. Sharpless, *Angew. Chem. Int. Ed.* **2002**, *41*, 2596-2599.
[237] F. Himo, T. Lovell, R. Hilgraf, V. V. Rostovtsev, L. Noodleman, K. B. Sharpless, V. V. Fokin, *J. Am. Chem. Soc.* **2005**, *127*, 210-216.
[238] J. McNulty, K. Keskar, *Eur. J. Org. Chem.* **2012**, *2012*, 5462-5470.
[239] B. C. Boren, S. Narayan, L. K. Rasmussen, L. Zhang, H. Zhao, Z. Lin, G. Jia, V. V. Fokin, *J. Am. Chem. Soc.* **2008**, *130*, 8923-8930.
[240] J. M. Baskin, J. A. Prescher, S. T. Laughlin, N. J. Agard, P. V. Chang, I. A. Miller, A. Lo, J. A. Codelli, C. R. Bertozzi, *Proc. Natl. Acad. Sci. USA* **2007**, *104*, 16793-16797.
[241] J. A. Codelli, J. M. Baskin, N. J. Agard, C. R. Bertozzi, *J. Am. Chem. Soc.* **2008**, *130*, 11486-11493.
[242] E. M. Sletten, C. R. Bertozzi, *Angew. Chem. Int. Ed.* **2009**, *48*, 6974-6998.
[243] O. Diels, K. Alder, *Liebigs Ann. Chem.* **1928**, *460*, 98-122.
[244] R. B. Woodward, R. Hoffmann, *Angew. Chem. Int. Ed.* **1969**, *8*, 781-853.
[245] M. J. S. Dewar, S. Olivella, J. J. P. Stewart, *J. Am. Chem. Soc.* **1986**, *108*, 5771-5779.
[246] K. N. Houk, *J. Am. Chem. Soc.* **1973**, *95*, 4092-4094.
[247] Y. A. Titov, *Russ. Chem. Rev.* **1962**, *31*, 267-283.
[248] K. C. Nicolaou, S. A. Snyder, T. Montagnon, G. Vassilikogiannakis, *Angew. Chem. Int. Ed.* **2002**, *41*, 1668-1698.
[249] J. G. Martin, R. K. Hill, *Chem. Rev.* **1961**, *61*, 537-562.
[250] L. R. Domingo, M. J. Aurell, P. Pérez, R. Contreras, *Tetrahedron* **2002**, *58*, 4417-4423.
[251] K. N. Houk, *Acc. Chem. Res.* **1975**, *8*, 361-369.
[252] T. Ernet, G. Haufe, *Tetrahedron Lett.* **1996**, *37*, 7251-7252.
[253] K. N. Houk, R. J. Loncharich, J. F. Blake, W. L. Jorgensen, *J. Am. Chem. Soc.* **1989**, *111*, 9172-9176.
[254] A.-C. Knall, C. Slugovc, *Chem. Soc. Rev.* **2013**, *42*, 5131-5142.
[255] M. Malinauskas, M. Farsari, A. Piskarskas, S. Juodkazis, *Phys. Rep.* **2013**, *533*, 1-31.
[256] M. Deubel, G. Von Freymann, M. Wegener, S. Pereira, K. Busch, C. M. Soukoulis, *Nat. Mater.* **2004**, *3*, 444-447.

[257] M. S. Rill, C. Plet, M. Thiel, I. Staude, G. Von Freymann, S. Linden, M. Wegener, *Nat. Mater.* **2008**, *7*, 543-546.
[258] W. Gao, N. Singh, L. Song, Z. Liu, A. L. M. Reddy, L. Ci, R. Vajtai, Q. Zhang, B. Wei, P. M. Ajayan, *Nat. Nano.* **2011**, *6*, 496-500.
[259] Y. Zhou, Q. Bao, B. Varghese, L. A. L. Tang, C. K. Tan, C.-H. Sow, K. P. Loh, *Adv. Mater.* **2010**, *22*, 67-71.
[260] A. Selimis, V. Mironov, M. Farsari, *Microelectron. Eng.* **2015**, *132*, 83-89.
[261] M. Göppert-Mayer, *Ann. Phys.* **1931**, *401*, 273-294.
[262] W. Kaiser, C. G. B. Garrett, *Phys. Rev. Lett.* **1961**, *7*, 229-231.
[263] R. W. Boyd, *Nonlinear Optics*, Elsevier Science, **2003**.
[264] N. V. Tkachenko, *Optical Spectroscopy: Methods and Instrumentations*, Elsevier Science, **2006**.
[265] S. M. Kuebler, M. Rumi, in *Encyclopedia of Modern Optics*, Elsevier, Oxford, **2005**, pp. 189-206.
[266] W. R. Zipfel, R. M. Williams, W. W. Webb, *Nat. Biotech.* **2003**, *21*, 1369-1377.
[267] J. Thomas, M. Heinrich, P. Zeil, V. Hilbert, K. Rademaker, R. Riedel, S. Ringleb, C. Dubs, J.-P. Ruske, S. Nolte, A. Tünnermann, *Phys. Status Solidi A* **2011**, *208*, 276-283.
[268] E. Hoffmann, *Mass spectrometry*, Wiley Online Library, **1996**.
[269] S. Weyer, J. B. Schwieters, *Int. J. Mass Spectrom.* **2003**, *226*, 355-368.
[270] H. Deutsch, K. Becker, S. Matt, T. D. Märk, *Int. J. Mass Spectrom.* **2000**, *197*, 37-69.
[271] R. Zenobi, R. Knochenmuss, *Mass Spectrom. Rev.* **1998**, *17*, 337-366.
[272] R. W. Howard, C. A. McDaniel, D. R. Nelson, G. J. Blomquist, *J. Chem. Ecol.* **1980**, *6*, 609-623.
[273] M. Mann, *Org. Mass Spectrom.* **1990**, *25*, 575-587.
[274] P. H. Dawson, *Quadrupole mass spectrometry and its applications*, Elsevier, **2013**.
[275] R. E. March, J. F. Todd, *Quadrupole ion trap mass spectrometry, Vol. 165*, John Wiley & Sons, **2005**.
[276] W. C. Wiley, I. H. McLaren, *Rev. Sci. Instrum.* **1955**, *26*, 1150-1157.
[277] M. Scigelova, A. Makarov, *Proteomics* **2006**, *6*, 16-21.
[278] A. G. Marshall, C. L. Hendrickson, G. S. Jackson, *Mass Spectrom. Rev.* **1998**, *17*, 1-35.
[279] T. Y. Kim, J. C. Schwartz, J. P. Reilly, *Anal. Chem.* **2009**, *81*, 8809-8817.
[280] A. S. Fomichev, I. David, S. M. Lukyanov, Y. E. Penionzhkevich, N. K. Skobelev, O. B. Tarasov, A. Matthies, H.-G. Ortlepp, W. Wagner, M. Lewitowicz, *Nucl. Instr. Meth. Phys. Res.* **1994**, *344*, 378-383.
[281] M. Dole, L. L. Mack, R. L. Hines, R. C. Mobley, L. D. Ferguson, M. B. Alice, *J. Chem. Phys.* **1968**, *49*, 2240-2249.
[282] M. Yamashita, J. B. Fenn, *J. Phys. Chem.* **1984**, *88*, 4451-4459.
[283] L. Q. Huang, A. Paiva, R. Bhat, M. Wong, *J. Am. Soc. Mass Spectrom.* **1996**, *7*, 1219-1226.
[284] J. B. Fenn, M. Mann, C. K. Meng, S. F. Wong, C. M. Whitehouse, *Science* **1989**, *246*, 64-71.
[285] M. S. Wilm, M. Mann, *Int. J. Mass Spectrom.* **1994**, *136*, 167-180.
[286] S. Banerjee, S. Mazumdar, *Int. J. Anal. Chem.* **2012**, *2012*, 40.
[287] M. Peschke, U. H. Verkerk, P. Kebarle, *J. Am. Soc. Mass Spectrom.* **2004**, *15*, 1424-1434.
[288] D. Schröder, *Angew. Chem. Int. Ed.* **2004**, *43*, 1329-1331.
[289] J. F. De La Mora, *Anal. Chim. Acta* **2000**, *406*, 93-104.

[290] Y. Yamashita, J. C. Tellis, G. A. Molander, *Proc. Natl. Acad. Sci.* **2015**, *112*, 12026-12029.
[291] A. Fürstner, C. Brehm, Y. Cancho-Grande, *Org. Lett.* **2001**, *3*, 3955-3957.
[292] J. Fickert, M. Makowski, M. Kappl, K. Landfester, D. Crespy, *Macromolecules* **2012**, *45*, 6324-6332.
[293] Y. Zeng, R. Zou, Z. Luo, H. Zhang, X. Yao, X. Ma, R. Zou, Y. Zhao, *J. Am. Chem. Soc.* **2015**, *137*, 1020-1023.
[294] C. A. DeForest, K. S. Anseth, *Nat. Chem.* **2011**, *3*, 925-931.
[295] F. Zeng, S. C. Zimmerman, *J. Am. Chem. Soc.* **1996**, *118*, 5326-5327.
[296] X. Deng, C. Friedmann, J. Lahann, *Angew. Chem. Int. Ed.* **2011**, *50*, 6522-6526.
[297] K. Hiltebrandt, K. Elies, D. R. D'hooge, J. P. Blinco, C. Barner-Kowollik, *J. Am. Chem. Soc.* **2016**, *138*, 7048-7054.
[298] T. Pauloehrl, G. Delaittre, V. Winkler, A. Welle, M. Bruns, H. G. Börner, A. M. Greiner, M. Bastmeyer, C. Barner-Kowollik, *Angew. Chem. Int. Ed.* **2012**, *51*, 1071-1074.
[299] R. M. Wilson, K. A. Schnapp, W. S. Patterson, *J. Am. Chem. Soc.* **1992**, *114*, 10987-10989.
[300] R. W. Redmond, J. C. Scaiano, *J. Phys. Chem.* **1989**, *93*, 5347-5349.
[301] A. Konosonoks, P. J. Wright, M.-L. Tsao, J. Pika, K. Novak, S. M. Mandel, J. A. Krause Bauer, C. Bohne, A. D. Gudmundsdóttir, *J. Org. Chem.* **2005**, *70*, 2763-2770.
[302] W. Brown, C. Foote, B. Iverson, E. Anslyn, *Organic Chemistry*, Cengage Learning, **2008**.
[303] K. Hiltebrandt, M. Kaupp, E. Molle, J. P. Menzel, J. P. Blinco, C. Barner-Kowollik, *Chem. Comm.* **2016**, *52*, 9426-9429.
[304] K. R. Huffman, M. Loy, E. F. Ullman, *J. Am. Chem. Soc.* **1965**, *87*, 5417-5423.
[305] V. San Miguel, C. G. Bochet, A. del Campo, *J. Am. Chem. Soc.* **2011**, *133*, 5380-5388.
[306] L. Xu, J. Farrell, R. G. Karunakaran, A. Honglawan, S. Yang, *J. Polym. Sci. Part A: Polym. Chem.* **2013**, *51*, 1215-1222.
[307] R. Franking, H. Kim, S. A. Chambers, A. N. Mangham, R. J. Hamers, *Langmuir* **2012**, *28*, 12085-12093.
[308] S. Murata, J. Kobayashi, C. Kongou, M. Miyata, T. Matsushita, H. Tomioka, *J. Org. Chem.* **2000**, *65*, 6082-6092.
[309] M.-A. Shafer, E. Vaughan, E. S. Lipkin, B. a. A. Moscicki, J. Schachter, *J. Pediatr.* **1986**, *108*, 779-783.
[310] N. Saruyama, Y. Sakakura, T. Asano, T. Nishiuchi, H. Sasamoto, H. Kodama, *Anal. Biochem.* **2013**, *441*, 58-62.
[311] V. Humblot, J.-F. Yala, P. Thebault, K. Boukerma, A. Héquet, J.-M. Berjeaud, C.-M. Pradier, *Biomaterials* **2009**, *30*, 3503-3512.
[312] N. A. Peppas, J. Z. Hilt, A. Khademhosseini, R. Langer, *Adv. Mater.* **2006**, *18*, 1345-1360.
[313] W. Lu, D. Yuan, D. Zhao, C. I. Schilling, O. Plietzsch, T. Muller, S. Bräse, J. Guenther, J. Blümel, R. Krishna, Z. Li, H.-C. Zhou, *Chem. Mat.* **2010**, *22*, 5964-5972.
[314] Y. Sun, Y. Peng, Y. Chen, A. J. Shukla, *Adv. Drug Deliv. Rev.* **2003**, *55*, 1201-1215.
[315] C. M. Soukoulis, M. Wegener, *Nat. Photon.* **2011**, *5*, 523-530.
[316] J. K. Gansel, M. Thiel, M. S. Rill, M. Decker, K. Bade, V. Saile, G. von Freymann, S. Linden, M. Wegener, *Science* **2009**, *325*, 1513-1515.
[317] G. Tillet, B. Boutevin, B. Ameduri, *Prog. Polym. Sci.* **2011**, *36*, 191-217.
[318] J. E. Elliott, C. N. Bowman, *Macromolecules* **2001**, *34*, 4642-4649.
[319] A. A. Askadskii, *Polym. Sci.* **1990**, *32*, 2061-2069.

[320] D. J. Broer, R. A. M. Hikmet, G. Challa, *Macromol. Chem. Phys.* **1989**, *190*, 3201-3215.
[321] C. R. Morgan, F. Magnotta, A. D. Ketley, *J. Polym. Sci. Polym. Chem.* **1977**, *15*, 627-645.
[322] G. T. Carroll, N. J. Turro, J. T. Koberstein, *J. Colloid Interface Sci.* **2010**, *351*, 556-560.
[323] G. T. Carroll, M. E. Sojka, X. Lei, N. J. Turro, J. T. Koberstein, *Langmuir* **2006**, *22*, 7748-7754.
[324] V. Kumbaraci, N. Talinli, Y. Yagci, *Macromol. Rapid Commun.* **2007**, *28*, 72-77.
[325] S. Kadłubowski, A. Henke, P. Ulański, J. M. Rosiak, L. Bromberg, T. A. Hatton, *Polymer* **2007**, *48*, 4974-4981.
[326] J. R. Jones, C. L. Liotta, D. M. Collard, D. A. Schiraldi, *Macromolecules* **2000**, *33*, 1640-1645.
[327] A. Quick, *Functional Microstructures via Direct Laser Writing*, KIT (Karlsruhe), **2015**.
[328] P. Mueller, B. Richter, A. Quick, J. Fischer, J. B. Mueller, L. Zhou, G. U. Nienhaus, M. Bastmeyer, C. Barner-Kowollik, M. Wegener, in *Conference on Lasers and Electro-Optics*, Optical Society of America, San Jose, California, **2016**, p. SW4L.3.
[329] D. M. Bauer, A. Rogge, L. Stolzer, C. Barner-Kowollik, L. Fruk, *Chem. Comm.* **2013**, *49*, 8626-8628.
[330] E. Kassianidis, R. J. Pearson, D. Philp, *Chem. Eur. J.* **2006**, *12*, 8798-8812.
[331] E. Daskalaki, B. Le Droumaguet, D. Gerard, K. Velonia, *Chem. Comm.* **2012**, *48*, 1586-1588.
[332] J. H. Scofield, *J. Electron Spectrosc. Relat. Phenom.* **1976**, *8*, 129-137.
[333] S. Tanuma, C. J. Powell, D. R. Penn, *Surf. Interface Anal.* **1994**, *21*, 165-176.
[334] T. Dispinair, R. Sanyal, A. Sanyal, *J. Polym. Sci. Part A: Polym. Chem.* **2007**, *45*, 4545-4551.

ACKNOWLEDGEMENTS

An dieser Stelle möchte ich den Personen danken, die mich während meiner dreijährigen Promotion begleitet und unterstützt haben.

Zuerst möchte ich mich bei Prof. Dr. Christopher Barner-Kowollik für die freundliche Aufnahme in die macroarc Gruppe und die sehr gute Betreuung herzlich bedanken. Insbesondere seine Ratschläge und die intensiven wissenschaftlichen Diskussionen bei gemeinsamen Besprechungen waren sehr hilfreich für mich. Desweitern bin ich sehr dankbar, dass ich von Prof. Dr. Christopher Barner-Kowollik darin unterstützt wurde einen Forschungsaufenthalt an der Queensland University of Technology (QUT) in Brisbane (Australien) durchzuführen.

Ein großes Dankeschön geht an meine Kooperationspartner Prof. Dr. Martin Wegener und Patrick Müller aus dem Institut für Angewandte Physik (KIT). Die Zusammenarbeit immer war immer angenehm und sehr professionell. Insbesondere danke ich Patrick Müller für die Durchführung zahlreicher DLW Experimente. Die gemeinsamen Besprechungen und die unterschiedliche Denkweise von Physikern und Chemikern im Rahmen einer komplexen Thematik führten hierbei zu sehr vielen guten Ideen. Insgesamt hat mir die Kooperation sehr darin geholfen meine interdisziplinäre Denkweise zu schulen.

Dr. James Blinco möchte ich herzlich für seine Unterstützung für meinen Forschungsaufenthalt in Australien, sowie seine Ratschläge bei Projekten in Deutschland und in Australien danken. Für eine unvergessliche und super Zeit in "down under" möchte ich mich bei Dr. James Blinco, meinen "Aussie Kollegen" Kai Anders Hansen, Liam Walsh, Hendrik Wöhlk, Komba Thomas, Rafael Da Silva, Anna Worthy, Nathan Boase, Christiane Lang, Jesse Alleen und Colin Schiemer am QUT, sowie meiner internationalen "Aussie WG" bestehend aus Corisco, Jogi, Marco und Timo, bedanken.

An dieser Stelle möchte ich auch dem Fonds der Chemischen Industrie (FCI) für die zweijährige Unterstützung in Form eines Doktorandenstipendiums danken.

Mein weiterer Dank gilt auch Dr. Anja Goldmann, Dr. Maria Schneider, Vincent Schüler und Evelyn Stühring. Alle vier haben immer dafür gesorgt, dass alles im Arbeitskreis so läuft wie es laufen sollte.

Ich möchte mich zudem bei allen meinen zahlreichen Kollegen in der macroarc Gruppe für eine tolle Atmosphäre, eine gute Zusammenarbeit und all die sommerlichen Grillfeiern nach Feierabend bedanken. Weiterhin möchte ich Michael Kaupp, Astrid Hirschbiel, Andrea Lauer, Janin Offenloch und Waldemar Konrad danken, die zusammen mit mir im Masseteam die oftmals kratzbürstigen Institutsmassenspektrometer am Laufen gehalten haben. Außerdem möchte ich innerhalb der Gruppe insbesondere Corinna Preuss, Astrid Hirschbiel und Nils Jasinski für eine tolle Freundschaft herausheben.

Weiterhin danke ich meinem Bachelorstudenten Edgar Molle und unserer damaligen Auszubildenden Katharina Elies für eine tolle Zusammenarbeit.

Für das Korrekturlesen dieser Arbeit und die damit einhergehenden Verbesserungsvorschläge danke ich Astrid Hirschbiel, Bryan Tuten, Dominik Voll und Patrick Müller.

Desweiteren danke ich meinen Kommilitonen Patrick Jäger, Johanna Becker, Benjamin Mutz, und Julia Eble für die gemeinsamen abendlichen Kochveranstaltungen.

Ich danke Dennis Gabeli, Michael Walch und Ute Schmidt für die langanhaltende und tolle Freundschaft.

Ich danke allen Mitgliedern des Yoshukai Karate Vereins in Karlsruhe für ein ausdauerndes Training und eine schöne Abwechslung zur Promotion.

Ein besonders großer Dank gebührt meiner Familie. Ich danke meinen Großeltern Klaus und Christa Hiltebrandt, sowie meiner Großmutter Betha Kern und meinem leider verstorbenen Großvater Hugo Kern für die finanzielle Unterstützung während meines gesamten Studiums und die schöne Zeit zusammen. Weiterhin möchte ich meine Mutter von ganzem Herzen dafür danken, dass sie mich in meinem Leben immer unterstützt hat und für mich da gewesen ist. Ein ganz großer Dank auch an meine Freundin Jennifer Kiefer, die ich sehr liebe und die mich sehr glücklich macht. Ich freue mich auf unsere

weitere gemeinsame Zukunft. Desweiteren möchte ich auch der Familie meiner Freundin – meinen zukünftigen Schwiegereltern Ulrich und Birgit Kiefer, sowie Daniel und Sandra Murr – für die herzliche Aufnahme und die schöne gemeinsame Zeit danken.